THE UNIVERSITY of EDINBURGH

This thesis has been submitted in fulfilment of the requirements for a postgraduate degree (e.g. PhD, MPhil, DClinPsychol) at the University of Edinburgh. Please note the following terms and conditions of use:

Metal mobility in sandstones and the potential environmental impacts of offshore geological CO_2 storage

Kit Carruthers

Thesis submitted for the degree of Doctor of Philosophy

School of GeoSciences

The University of Edinburgh

2016

Abstract

Geological carbon dioxide (CO_2) storage in the United Kingdom (UK) will likely be entirely offshore, which may lead to the production and disposal into the sea of reservoir waters to increase storage capacity, or through CO_2-Enhanced Oil Recovery (CO_2-EOR). These produced waters have the potential to contain significant concentrations of trace metals that could be of harm to the environment.

Batch experiments with CO_2, warm brines, and reservoir sandstones were undertaken for this thesis to determine concentrations of 8 trace metals (arsenic, cadmium, chromium, copper, mercury, nickel, lead, zinc) which could be leached during CO_2 storage in 4 UK North Sea hydrocarbon reservoirs. A sequential extraction procedure (SEP) was also used to determine the potential mobility of these metals under CO_2 storage from mineral phases making up the reservoir samples. The results broadly showed that mobilised trace metal concentrations were low (parts per billion, ppb) in the batch experiments, with the exceptions of nickel and zinc. These metals were associated with carbonate and some feldspar dissolution, with other metals apparently desorbed from mineral surfaces, probably clays. The results of the SEP, however, were a poor predictor of actual mobility with respect to the batch experiments, although useful in determining the distribution of trace metals within the defined mineral phases (water soluble, ion exchangeable, carbonate, oxide, sulphide, silicate).

In addition, fieldwork was carried out at Green River, Utah, to collect 10 CO_2-driven spring water samples and 5 local aquifer rock samples. This area was used as a natural analogue for CO_2-mobilised trace metals from sandstone aquifers. Trace metal concentrations in spring waters were very low (ppb) and batch experiments using Utah rock samples, spring water collected from Crystal Geyser, and CO_2 confirmed very low mobility of these metals. The SEP was repeated for the Utah reservoir rocks, but again was not a reliable predictor for actual mobility, other than to confirm that overall bulk concentrations of trace metals was low.

Comparison of trace metal concentrations from the batch experiments with data from UK North Sea oil and gas produced waters shows that overall, concentrations mobilised in batch experiments are within the range of concentrations across all North Sea fields reporting their data. However, on a field-by-field basis, some CO_2 mobilised concentrations exceeded those currently produced by oil and gas activities. Furthermore, average batch experiment trace metal loads are higher than average oil and gas produced waters, and in some cases exceed international guidelines. Therefore, while the majority of trace metals have low mobility and therefore low environmental impact, this should be assessed on a case-by-case basis. Regular monitoring of dissolved constituents in produced waters carried should also be carried out, particularly in the initial stages of CO_2 storage operations, with remedial action taken as required to reduce the environmental impact of offshore carbon capture and storage.

Author's Declaration

I declare that this thesis has been composed solely by myself and that it has not been submitted, either in whole or in part, in any previous application for a degree. Except where otherwise acknowledged, the work presented is entirely my own.

Kit Carruthers

May 2016

Acknowledgements

My name may grace the cover, but this thesis could not have been achieved without the gracious and patient support of many people. The past 4+ years have been a great personal battle with health and science, and I can only offer my thanks to the following who helped me get through to the end: EPSRC and Scottish Power for funding the project; my supervisors, Dr. Mark Wilkinson, Dr. Ian Butler and Prof. Stuart Haszeldine for their patience, understanding, support and guidance through challenging times; Dr. Lorna Eades for pushing the magic buttons on her ICP-MS and ICP-OES to produce the vast bulk of the data contained in this thesis (and it is a lot of data. . .); Georgios Lygkas, Ann Mennim, Alan Pike, Jimmy Smith, Dr. Katriona Edlmann, Dr. Bryne Ngwenya, Dr. Walter Geibert, all of (or formerly) the University of Edinburgh, for their invaluable help and advice, and lending of equipment and lab space and so without whom my experiments would not have been a success; Dr. Jiemin Lu, Dr. Pat Mickler, Dr. Staci Loewy, Dr. Nate Miller, and Dr. Toti Larson, all of the University of Texas, for their amazing support and work, and without whom I would not have achieved any fieldwork in Green River; and speaking of which, Jamie Stewart, thanks for a cracking time in the USA; and finally, to my fantastic friends and family, especially my Mum and Dad, for everything you've done for me since this journey began. Thank you.

> Roads go ever ever on,
>   Over rock and under tree,
> By caves where never sun has shone,
>   By streams that never find the sea;
> Over snow by winter sown,
>   And through the merry flowers of June,
> Over grass and over stone,
>   And under mountains in the moon.
>
> Roads go ever ever on
>   Under cloud and under star,
> Yet feet that wandering have gone
>   Turn at last to home afar.
> Eyes that fire and sword have seen
>   And horror in the halls of stone
> Look at last on meadows green
>   And trees and hills they long have known.

The Hobbit. J.R.R. Tolkein, 1892–1973

Contents

List of Figures

List of Tables

Introduction

1.1 Climate Change and Carbon Capture & Storage

Man-made emissions of 'greenhouse' gases (GHG) such as carbon dioxide (CO_2) and methane (CH_4) from our industrialisation activities have resulted in the warming of the surface of the Earth. The most recent report by the Intergovernmental Panel on Climate Change (IPCC) states that:

> *It is extremely likely that more than half of the observed increase in global average surface temperature from 1951 to 2010 was caused by the anthropogenic increase in GHG concentrations and other anthropogenic forcings together. The best estimate of the human-induced contribution to warming is similar to the observed warming over this period.* Intergovernmental Panel on Climate Change (2014).

In 2015, global average surface temperatures approached $1°C$ warmer than the 1951 - 1980 average, Figure 1.1, with this temperature increase since 1951 attributable to man-made emissions, mostly CO_2. We are already seeing some of the effects of climate change, for example rising sea levels, increased forest fires, changing timing of seasons, droughts, and the knock-on effects for ecosystems and societies (Intergovernmental Panel on Climate Change, 2014).
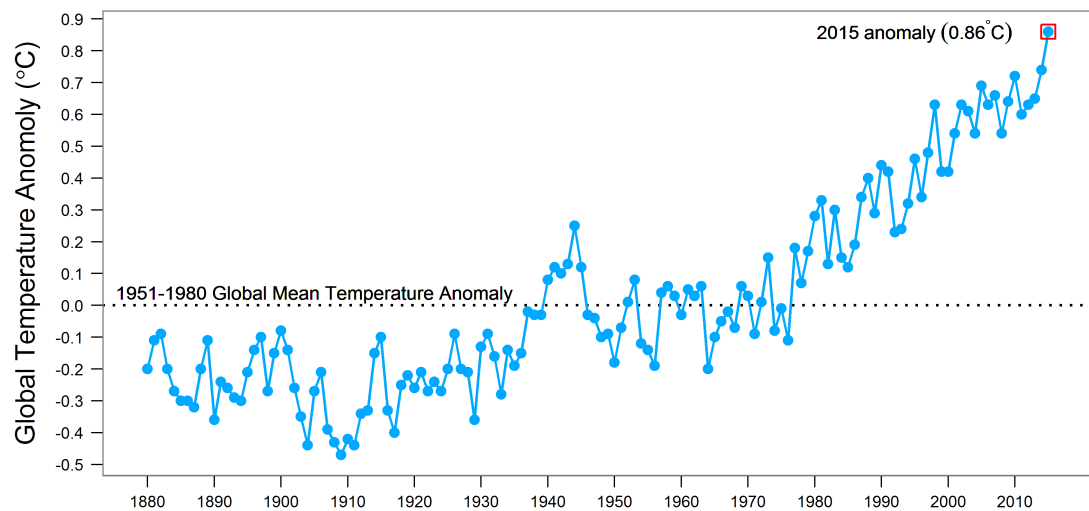
Figure 1.1: *Global annual mean temperature anomalies ($°C$) relative to the 1950 - 1980 baseline, showing warming of the late 20th Century. Data supplied by GISTEMP Team (2015). Annual mean values taken as January - December.*

In order that we limit CO_2 emissions, and therefore our impact on current and future generations, a range of options and technologies must be explored and deployed to mitigate climate change. According to the IPCC, CO_2 accounts for ~ 60% of our GHG emissions from fossil fuel use and industry since 1970 (Intergovernmental Panel on Climate Change, 2014). While these can be reduced through measures such as increased fuel efficiency and switching to other energy sources like renewables and nuclear, there would remain a need to reduce industrial CO_2 output, and to affordably mitigate emissions from fossil fuel power plants while a portfolio of alternatives is deployed.

Carbon capture and storage (CCS), a mitigation technology for removing CO_2 from large point source emitters such as coal-fired power plants and steel mills, could help reduce our CO_2 emissions by around 20% (Intergovernmental Panel on Climate Change, 2005). Carbon dioxide 'scrubbed' from power generators and industry is compressed and transported to long-term (> 10^4 years) storage in deep geological formations, which would be both onshore and offshore, depending on geographical location of the capture facilities.

The majority of suitable CO_2 storage sites are within sandstone formations from 800 m depth, with an impermeable caprock of mudstone/shale, and are saturated with saline waters. Some storage sites may be former and current hydrocarbon fields, with CO_2 used as an enhanced oil recovery (EOR) technique to extend the lifespan of these fields. Secure storage of CO_2 in these formations relies initially on the impermeable top seal, but other trapping mechanisms become more important with increasing storage time, including residual trapping of CO_2 bubbles in pores by water and/or oil, CO_2 dissolution in the formation waters, and mineralisation of CO_2 into an immobile solid (Intergovernmental Panel on Climate Change, 2005). Leakage of CO_2 is undesirable, not only from the point of view of releasing mitigated GHG back to the atmosphere, but there are also potential hazards to health and the environment.

1.2 Environmental Impacts of CO_2 storage

The unintended release of CO_2 from geological storage could have some environmental impact. CO_2 which escapes to the surface could accumulate and asphyxiate local residents and fauna (Kling *et al.*, 1987), damage vegetation (Krüger *et al.*, 2009) and poison marine organisms (e.g. Widdicombe *et al.* 2009). These risks are low, however, since CO_2 leaks tend to disperse rapidly in water (e.g. Blackford *et al.* 2013) and are much less likely to be fatal than other socially acceptable risks (Roberts *et al.*, 2011). Leaking CO_2 may, however, present environmental risks without reaching the surface, by dissolving into groundwaters and leaching potentially toxic metals from rocks and soils.

1.2.1 CO_2-water-rock chemistry

There is now a significant body of research focused on CO_2-water-rock interactions with respect to CO_2 storage, and the potential environmental impacts thereof. The published literature encompasses modelling, laboratory, and field experiments with earlier laboratory experimental research focussed mostly on porosity-permeability effects (e.g. Kaszuba *et al.* 2005; Pearce *et al.* 1996; Rosenbauer *et al.* 2005; Shiraki and Dunn 2000; Wandrey *et al.* 2011) and general fluid-mineral interactions (e.g. Gupta *et al.* 2000; Huq *et al.* 2012; Kaszuba *et al.* 2003; Wigand *et al.* 2008), with environmental impacts of CO_2 leakage on groundwater quality considered in more recent publications (e.g. Kharaka *et al.* 2010; Kirsch *et al.* 2014; Little and Jackson 2010; Lu *et al.* 2014, 2010; Smyth *et al.* 2009). Field studies have also focussed on the environmental impacts of CO_2 release into shallow potable waters (e.g. Cahill *et al.* 2013; Kharaka *et al.* 2006; Peter *et al.* 2012; Trautz *et al.* 2013) as an aid to understanding in-situ reactions, compared to often far-from-equilibrium laboratory experiments.

When CO_2 dissolves in water it lowers pH by the formation of a weak acid, carbonic acid (H_2CO_3), with subsequent dissociation to bicarbonate (HCO_3^-) and carbonate (CO_3^{2-}) ions, releasing protons (H^+) and increasing acidity, Equations 1.1 - 1.3.

$$CO_2 + H_2O \longleftrightarrow H_2CO_3 \tag{1.1}$$

$$H_2CO_3 \longleftrightarrow H^+ + HCO_3^- \tag{1.2}$$

$$HCO_3^- \longleftrightarrow H^+ + CO_3^{2-} \tag{1.3}$$
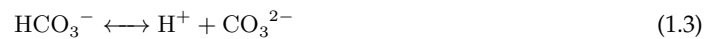
Lowered pH enhances the dissolution of rock-forming minerals in the presence of water, as protons substitute for metal cations in the mineral structure. The interaction of dissolved CO_2 in water with common mineral groups such as carbonates and feldspars can be generalised by Equations 1.4 and 1.5, and represent the common chemical weathering process of rocks on the Earth's surface.

Carbonate dissolution

$$CaMg(CO_3)_2 + 2\,H_2CO_3 \longleftrightarrow Ca^{2+} + Mg^{2+} + 4\,HCO_3^- \tag{1.4}$$

Potassium feldspar dissolution

$$2\,KAlSi_3O_8 + 2\,H_2CO_3 + 9\,H_2O \longrightarrow Al_2Si_2O_5(OH)_4 + 2\,K^+ + 4\,H_2SiO_4 + 2\,HCO_3^- \tag{1.5}$$
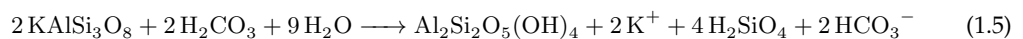
The theoretical effect of mineral dissolution is to increase pH through consumption of H^+ (mineral buffering), release metal cations such as calcium (Ca^{2+}) and potassium (K^+) into solution, increasing total dissolved solids (TDS), and increasing alkalinity. Alkalinity, defined here as carbonate alkalinity (HCO_3^-

$+ 2 \times CO_3^{2-}$) is dominated by HCO_3^- concentrations in solutions below pH 8.3 (Langmuir, 1997). From Equations 1.4 and 1.5, carbonate mineral dissolution generates twice the HCO_3^- as feldspars, for the same amount of carbonic acid.

Other sources of metal release into solution may be from desorption of metal ions adsorbed onto the surface of clay minerals or metal oxides, with clays being particularly important in this process due to their large surface areas (Langmuir, 1997); or degradation under oxidising conditions of organic matter which has complexed or bioaccumulated metals (Tessier *et al.*, 1979). Desorption from minerals and breakdown of organic matter may influence concentrations of dissolved 'trace metal' species such as mercury (Hg) and lead (Pb), which would otherwise be unidentified in the mineral assemblage of a rock.

1.2.2   Batch reaction studies

Laboratory experimental work under controlled conditions has been carried out to determine how water-saturated reservoir rocks and shallow aquifer soils react when CO_2 is introduced to the system. Table 1.1 shows the wide variety of temperature, pressure, time, and pore fluid conditions used in experimental studies. Conditions in the experiments are set either to replicate subsurface in-situ conditions, or to elucidate and measure a specific set of reactions.

Laboratory experiments usually comprise batch experiments which are often heated, sealed plastic (PTFE) containers with ports for introducing CO_2 and collecting aliquots of water for chemical measurements, and are capable of being pressurised (Kaszuba *et al.*, 2013). Rock or soil samples are sealed in with synthetic or actual formation waters, and CO_2 added after purging the batch reaction vessel with an inert gas. With a flow-through experiment, reaction fluids are periodically or continuously added to the reaction vessel, with displaced fluids collected for analysis. Core flood experiments comprise saturating an intact core of rock, rather than using ground/powdered/disaggregated samples, and usually have a flow-through component to study reactive pathways.

Batch and flow-through experiments have the benefit of allowing a high degree of control over the conditions of interest, for example observing the effects of changing pressures, redox conditions and temperature. However, it is important to acknowledge that these experiments are far-from-equilibrium and initial experimental conditions do not accurately represent reservoir condition, particularly with respect to the equilibrium between water and rock. Reaction rates are therefore orders of magnitude higher than field studies (Kampman *et al.*, 2009), but are nonetheless a useful tool for investigating how a reservoir rock, or overlying overburden, may react to CO_2.

For example, Lu *et al.* (2010) and Smyth *et al.* (2009) document a laboratory batch experiment where aquifer samples from the USA Gulf Coast were submersed in a weak saline solution and subjected to an argon gas flush for two weeks, followed by CO_2 gas flow for a further two weeks. Water samples were collected on hourly, then daily intervals following changes in gas type, and the samples analysed for thirty-three cations and pH. The results of their analysis showed a significant and rapid drop in water pH upon CO_2 flow, but which quickly rose due to mineral buffering (albeit to a lower level than initial conditions) and remained constant for the remainder of the experiment. Metal concentrations exhibited two broad trends: significant increases in concentration with CO_2 flow but then became constant; and concentrations which increased initially but then declined. pH was linked to reaction rates, showing that as pH increased due to mineral buffering, cation release rates decreased. Lu *et al.* (2010) and Smyth *et al.* (2009) also noted that minor mineral components of their samples had a major influence on cation concentrations and pH buffering, specifically the presence of carbonates. The role of carbonates, even at trace amounts, is acknowledged by many batch studies to heavily influence resulting fluid chemistry (Kaszuba *et al.*, 2013; Lions *et al.*, 2014).

Silicate mineral dissolution, such as potassium and plagioclase feldspars (e.g. Lions *et al.* 2014; Lu *et al.* 2014; Wandrey *et al.* 2011) also contributes to pH buffering and metal release into solution, albeit at a slower rate than carbonates such as calcite and dolomite (Kaszuba *et al.*, 2013; Lions *et al.*, 2014).

Authors	Provenance (Depth)	Fluids (*fluid:rock*)	T (°C)	P (bar)	t (days)	N$_2$ purge	Experiment
Pearce *et al.* (1996)	North Sea anhydrite, mudstone & sandstone	Synthetic seawater	80	200	60, 90, 240	N	Batch & core flood
Gupta *et al.* (2000)	USA shale, dolomite & sandstone (~850 - 1,845 m)	(Ca, K, Mg, Na)SO$_4$-NaCl synthetic brine	50 150 150	41.37 172.37 41.37	30 30 40	Y	Batch
Shiraki and Dunn (2000)	Tunsleep sandstone, USA (981 m & 1,208 m)	1. (Ca, Mg, Na)SO$_4$-NaCl 2. NaCl	80	166	7	N	Core flood
Kaszuba *et al.* (2003)	Synthetic arkose & New York shale	(Na, K, Mg)Cl synthetic brine (*18:1*)	200	200	80	N	Batch
Kaszuba *et al.* (2005)	Synthetic arkose & New York shale	NaCl	200	200	45	N	Batch
Rosenbauer *et al.* (2005)	Colorado limestone & Arizona sandstone	NaCl/CaSO$_4$ formation water (NaCa)Cl synthetic brine (*20:1*)	25 120	100 - 600	78	N	
Wigand *et al.* (2008)	Bunter Sandstone (1,500 - 2,000 m)	NaCl synthetic brine	60	150	62	N	Batch
Smyth *et al.* (2009) & Lu *et al.* (2010)	Texas & Gulf Coast shallow aquifers (9.1 - 86.3 m)	Deionised water (*5:1*) + ~40 ppm Cl$^-$	20	1	28	Argon	Batch
Little and Jackson (2010)	Shallow aquifers, USA (5 - 92.2 m)	Deionised water (*3:1*)	20	1	344 (max)	N	Batch
Fischer *et al.* (2010) & Wandrey *et al.* (2011)	Ketzin Triassic sandstone, Germany (627 - 633 m)	KCl/NaCl/CaCl$_2$/MgCl$_2$ synthetic brine	40	55	450, 630, 738	N	Batch
Kjöller *et al.* (2011)	Skagerrak, Bunter, Gassum, Haldagar (Danish)	(Na+Ca+Mg+K+Fe+Sr)Cl synthetic brine	70	200	13 months	Y	Batch
Lima *et al.* (2011)	Paraná Basin sandstone and shales, Brazil	NaCl	80	1	90-180	N	Batch
Lu *et al.* (2011)	Navajo Sandstone, USA	KCl (*10:1*)	200	250 - 300	58 (max)	N	Batch & flow through
Huq *et al.* (2012)	Altmark Rotliegend sandstone, Germany (~3,100 m)	NaCl (*1:1*)	125	50	3, 5, 9	N	Batch
Pudlo *et al.* (2012)	Altmark Rotliegend sandstone, Germany (~3,100 m)	KCl/NaCl/CaCl$_2$ synthetic brine	125	200	28 - 42	N	Core flood
Humez *et al.* (2013)	Albian sands, France (outcrop & borehole)	Ca$-$HCO$_3$ aquifer waters (*10:1*)	20	2	1 - 30	Y	Batch
Varadharajan *et al.* (2013)	Sands, clays and organic-rich sediments, USA	(Na+K+Ca)Cl, NaHCO$_3$, Na-acetate	25	1 - 5	25	Y	Flow through
Kirsch *et al.* (2014)	Mesaverde sandstones, Colorado	Pure water (*7.5:1*)	22	0.01 & 1	27	Y	Batch
Lu *et al.* (2014)	Sandstones - USA: offshore Texas, Mississippi Canada: Alberta (1,458 - ~3,040 m)	NaCl synthetic brine (*34:1*)	70 - 100	200	4 - 19	Helium	Batch
Purser *et al.* (2014)	Entrada Formation sandstones, Utah, USA	Synthetic (Na+Ca+Sr)Cl brine (*10:1*)	40	50	6 months	Y	Batch

Table 1.1: *Summary of literature CO$_2$-water-rock batch experiment conditions currently in the literature.*

1.2.3 Field studies

While laboratory batch experiments are useful tools for assessing the effect of CO_2 on samples, they are limited by the fact that they are simulations only of reservoir or aquifer conditions. Work carried out in-situ at field scale provide the best data on a specific site basis, however this can be a costly exercise; impossibly so in the UK North Sea context.

A number of field studies have now been carried out, Table 1.2. One such study was that undertaken by Kharaka *et al.* (2006) where supercritical CO_2 was injected at a depth of around 1,500 m into the Frio Formation, Texas, and water samples collected from an observation well some 30 m laterally up dip of the injection point. A novel sample retrieval system was utilised to maintain pressure in the sampling vessel as it was brought to the surface, to minimise degassing of CO_2 and subsequent changes in chemistry (Freifeld, 2005). Samples were analysed for pH, alkalinity and number of metal cations over a four month injection and sampling period. On CO_2 breakthrough at the monitoring well, pH declined and alkalinity increased. Both changes occurred rapidly.

Concentrations of dissolved metals also increased, from the dissolution of calcite and oxyhydroxides (Kharaka *et al.*, 2006). However, samples collected between 20 days and 6 months after CO_2 injection showed that pH has risen and metal concentrations had returned back to pre-injection levels, indicating mineral buffering of pH as well as potential precipitation of carbonate minerals had occurred.

The effect of CO_2 leakage on shallow groundwater (< 60 m depth) has been investigated in the field by a number of other studies. Kharaka *et al.* (2010), Peter *et al.* (2012) and Trautz *et al.* (2013), investigating sands in Germany and the USA found that pH declines with an increase in total inorganic carbon (TIC) and dissolved metal loads.

1.2.4 Experimental trace metals release

The impact of CO_2 mobilisation of metals is to release into the environment a variety of potentially toxic trace metals such as arsenic, chromium and mercury. These can affect potable groundwater quality, in the context of assessing the potential impact of a CO_2 leak from a geological storage site. The responses of trace metals to the addition of CO_2 in the experiments cited in Tables 1.1 and 1.2 are variable. Little and Jackson (2010) showed that CO_2 was capable of leaching metals such as nickel (Ni) and arsenic (As) from shallow aquifer soils at concentrations significant enough to breach US water quality standards, however these were often for

Authors	Target	Depth (m)	Fluid	T (°C)	P (bar)	t (days)	CO_2
Kharaka *et al.* (2006) & Freifeld (2005)	Frio sandstone, USA	1,500	(NaCa)Cl formation brine	-	146	3 - 180	Supercritical
Assayag *et al.* (2009)	Palisades dolerite/Newark Basin sediments contact zone, USA	232 - 240	Formation water with 160 ppm NaCl spike	14.7 - 17.3	1	24 - 28	Gas
Kharaka *et al.* (2010)	Sands and gravels, ZERT site, Montana, USA	2 - 2.3	Potable Water	-	-	29	Gas
Peter *et al.* (2012)	Sand aquifer, Germany	18	Potable water	-	-	10	Gas
Cahill and Jakobsen (2013)	Glacial sand, Denmark	10	Potable water	-	-	56	Gas
Trautz *et al.* (2013)	Sand aquifer, Mississippi, USA	46.9 - 54.6	Potable Water	-	-	157	Gas
Paterson *et al.* (2013) & Kirste *et al.* (2014)	Paaratte sandstone Formation CO2CRC site, Otway, Australia	1,392 - 1,399	Saline formation water	-	140	77	Supercritical

Table 1.2: *Summary of CO_2 injection field experiments reported in the literature. - Data not supplied.*

aquifers where waters were already higher than the water
quality standards.

Other trace metals such as cadmium (Cd), chromium (Cr) and lead (Pb) were considered in many of the studies cited above, and were often shown to be mobilised during the experiments and field studies (Humez *et al.*, 2013; Little and Jackson, 2010; Lu *et al.*, 2010; Trautz *et al.*, 2013). Trace metals are mobilised mainly through either mineral dissolution or desorbtion mechanisms (Lions *et al.*, 2014), however the mobility of these elements tends to be weak and concentrations in field and laboratory studies rarely exceed water quality guidelines (Lions *et al.*, 2014; Trautz *et al.*, 2013).

Despite similar conditions in a number of experiments, the conclusions made have large variations. Clearly a one-size-fits-all conclusion can't be drawn from the broad range of studies conducted. With the wide variation of rock and soil types being the strongest control on resulting fluid chemistry, the response of groundwaters to CO_2 injection or migration will depend on local conditions. However, a very broad set of conclusions can be drawn from the experimental work and field studies:

- pH decreases rapidly with CO_2 injection with a subsequent increase due to mineral buffering

- An increase in total inorganic carbon (TIC), largely in the form of HCO_3^-

- Concentrations of cations, both major and trace, initially increase with dissolution of a variety of minerals e.g. quartz, feldspars, anhydrite, calcite and dolomite. Carbonate dissolution is particularly important in influencing fluid chemistry of major cations with CO_2 injection, while trace metals have a variety of sources e.g. ion exchange, desorbtion, mineral dissolution.

- Cation concentrations often level off or decrease with time, or with distance from CO_2 injection, due to precipitation of minerals e.g. dolomite, calcite, siderite and clays

1.2.5   The UK offshore context

The research on CO_2-water-rock interactions with regard to environmental issues has so far focussed on onshore CO_2 storage and therefore potential risks to potable waters and human health. UK CO_2 storage is likely to be entirely offshore, with North Sea saline formations and depleted oil and gas fields having the potential to store over 200 years' worth of CO_2 (Scottish Centre for Carbon Storage, 2009). There is, however, currently no literature which considers the environmental impacts of CO_2-water-rock interactions in offshore storage. While North Sea offshore storage would not affect drinking water supplies, CO_2-modified formation waters could be brought to the surface and dumped ('overboarded') into the sea.

There are several reasons why this could happen. Firstly, one challenge of CO_2 storage in reservoirs is that storage capacity is limited by the fracture pressure of the reservoir (Chadwick *et al.* 2008). In the Central North Sea, for example, this pressure is $\sim$ 90% of the lithostatic pressure, Figure 1.2; if this pressure is exceeded by increasing the pore fluid pressure away from the normal hydrostatic gradient, then fracturing of the reservoir and/or caprock (seal) may occur, thereby reducing the security of the reservoir and ultimately allowing CO_2 to migrate vertically upward away from the storage site. By artificially removing brines from the reservoir through pressure relief wells and overboarding these produced waters to the North Sea, hydraulic pressure is reduced and CO_2 storage increases (Lindeberg *et al.*, 2009; Neal *et al.*, 2011; Scottish Carbon Capture & Storage, 2011).

Secondly, production waters could also enter the North Sea through CO_2-Enhanced Oil Recovery (CO_2-EOR), either as a by-product of oil production or through the WAG (water alternate gas) injection method, which alternates between CO_2 and water to enhance oil production in ageing or tight reservoirs (Blunt *et al.*, 1993). Residual trapping of CO_2 means this is a viable storage method in addition to simple CO_2 injection into a storage site.

Both techniques of pressure relief and WAG have the potential to generate waters which are modified by CO_2-water-rock reactions within the reservoir, with the result being to increase the dissolved trace
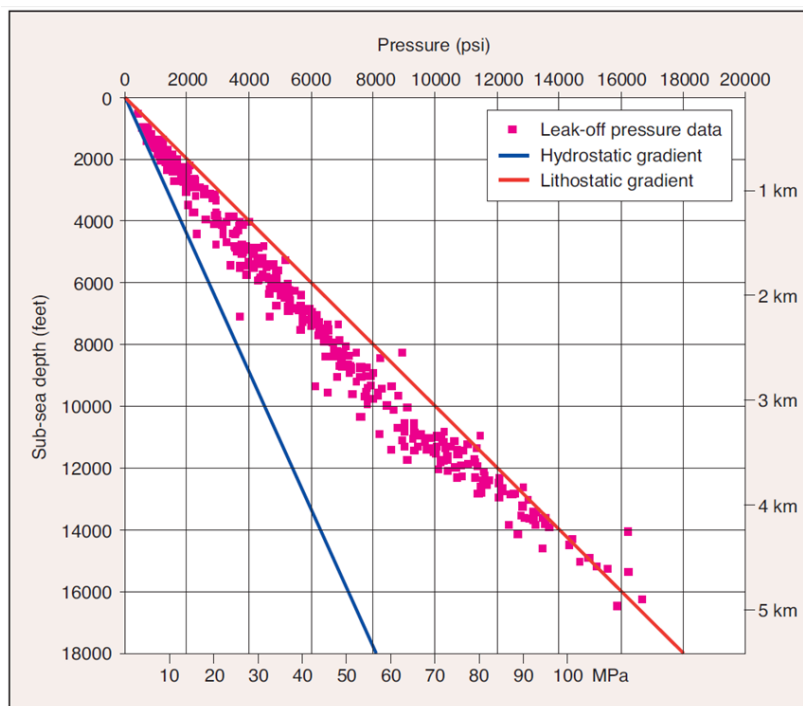
Figure 1.2: *Central North Sea fracture gradient, from Moss* et al. *(2003)*

metal load in overboarded produced waters. This could have a negative environmental impact to the offshore marine environment. The current analogy for future UK offshore CO_2 storage is the existing oil and gas industry; operators have been producing hydrocarbons from the North Sea since the late-1960's, with associated emissions, including produced waters.

In order to prevent serious environmental damage from current oil and gas operations in the UK North Sea, statutory regulations and acts, as well as voluntary agreements, have been set at local (e.g. Scotland), national (UK) and international (European Union) levels. Provision for CO_2 storage within the UK Continental Shelf (UKCS) has already entered the legislation, with The Energy Act 2008 (2008), and its subsequent modifications of existing regulations. However, the Act (2008) refers to minimising the impacts of a CO_2 leak offshore, rather than being concerned with modified production waters. Natural substances typically occurring in produced waters include hydrocarbons (benzene, toluene, ethylbenzene, and xylenes (BTEX), napthalenes, PAHs, alkyl phenols), trace metals and naturally occurring radioactive materials (NORM).

Offshore regulations currently in place cover UK Territorial Waters, which are all marine waters within the 12 nautical mile limit from the low tide line, and all areas within the UK Continental Shelf (UKCS), Figure 1.3. These regulations do not specifically cover Welsh and Scottish Controlled Waters, which are regulated by the Welsh Assembly and Scottish Government, respectively, however the regulations of the devolved national governments contain essentially the same guidance. In any case, these Scottish and Welsh water bodies include only coastal waters up to 3 nautical miles offshore of Scotland and Wales. Generally oil and gas fields, and future CO_2 storage, will be beyond the 3 mile limit.

1.2.6   Environmental impacts of trace metals

Produced water from North Sea oil and gas operations is routinely disposed of to the sea, with around 20 - 25% reinjected into the reservoir with seawater (Department of Energy & Climate Change, 2015). The total produced water volume for the UK North Sea in 2014 was 189×10^9 litres and has been dropping steadily since the maximum in 2003 of 317×10^9 litres as oil and gas production declines (Department
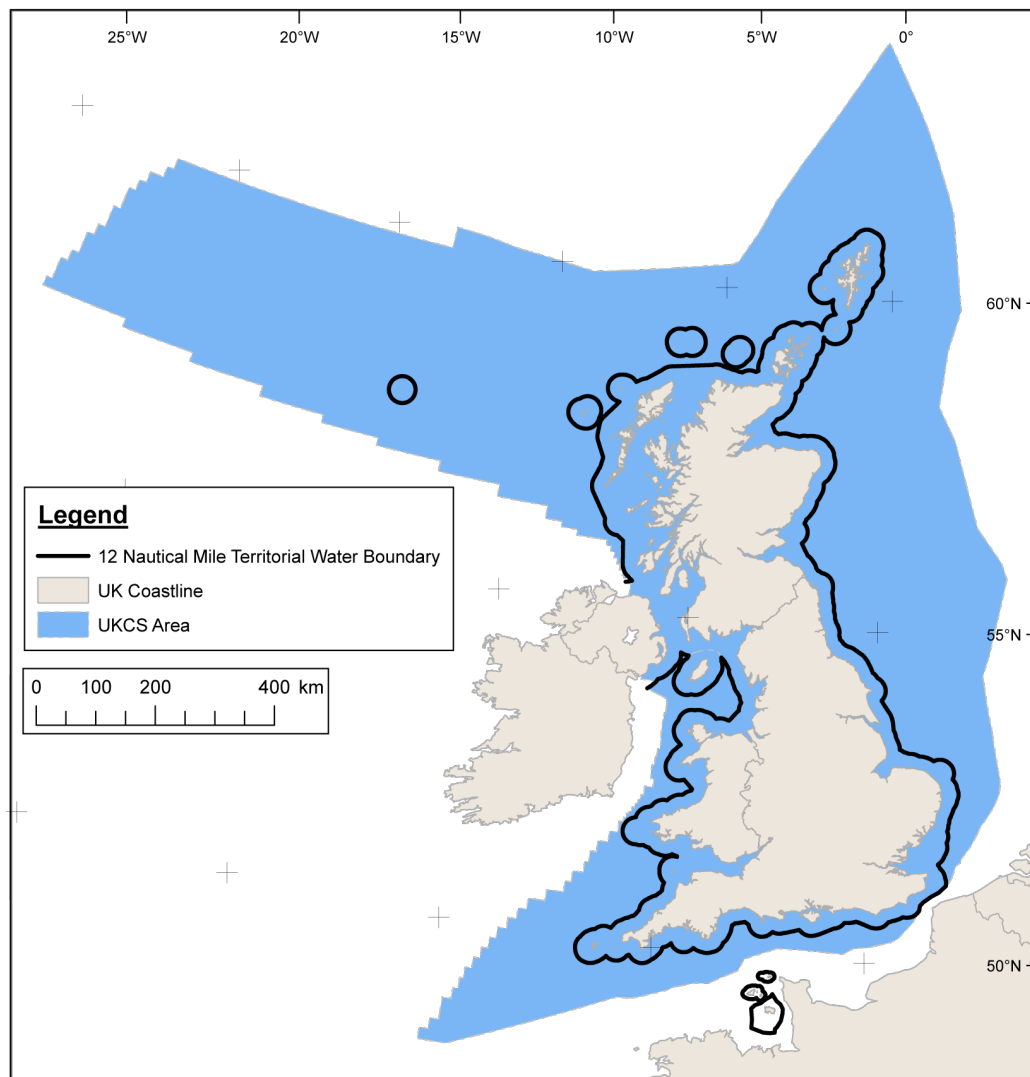
Figure 1.3: *United Kingdom Continental Shelf extent and the 12 mile territorial sea boundary.*

of Energy & Climate Change, 2015). However, while produced water volumes are decreasing, net production (produced minus injected) is on an upward trend, Figure 1.4.

Produced waters contain varying concentrations of major and trace elements, depending on the producing field (see Chapter 5 for examples), and include a variety of potentially toxic trace metals. Currently the concentrations of these trace metals are not regulated by the UK Government, although since 2006 the oil and gas industry have been required under certain permit conditions to bi-annually report trace metal concentrations in produced water of the following eight metals to the Environmental and Emissions Monitoring System (EEMS, Chapter 5): arsenic (As), cadmium (Cd), chromium (Cr), copper (Cu), lead (Pb), mercury (Hg), nickel (Ni) and zinc (Zn).

These 8 metals are List 1 and 2 prioritised metals under EC Directive 2006/11/EC (European Parliament, 2006) and therefore are considered to have a negative impact on both marine life and the human populations who feed on them. Typical background concentrations in uncontaminated seawater are given in Table 1.3.

While some of these metals are micronutrients, for example copper and zinc (Vanegas *et al.*, 1997), they are also known to be toxic to marine vertebrates and invertebrates, with effects such as: reduced growth and reproduction, and increased mortality rates (Eisler and Hennekey, 1977; Florence *et al.*, 1994;
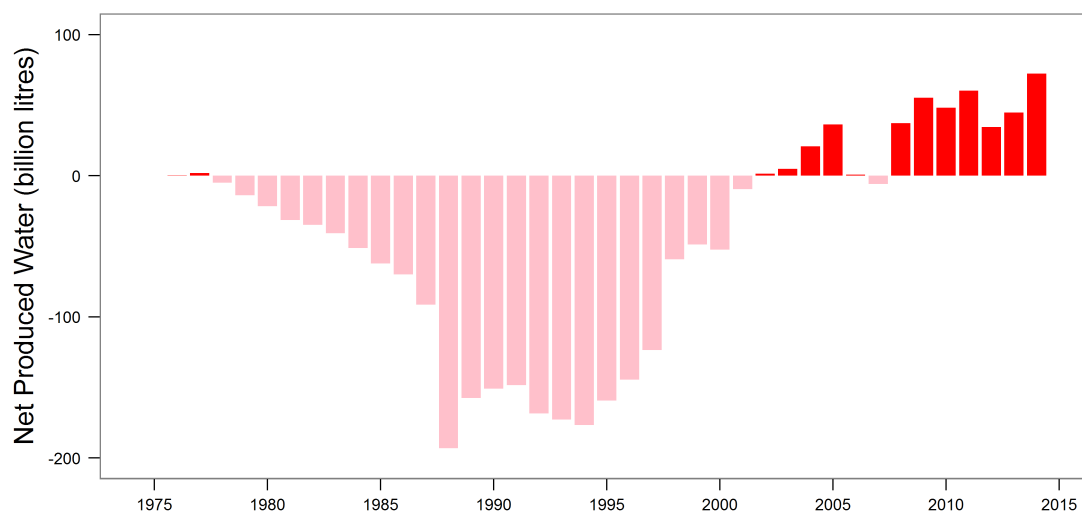
Figure 1.4: *Net UK North Sea water production (10^9 litres) 1976 - 2014. Pink bars represent negative net production, red bars represent positive net production. Net production is calculated as produced minus injected water, therefore negative net production still has a component of produced water. 2013 does not include September data.*

Mearns *et al.*, 1976; Neff, 1997); respiratory problems (Engel and Fowler, 1979; Taylor *et al.*, 1985); skin discolouration, unusual behaviours and balance problems in fish (Taylor *et al.*, 1985); and increased disease susceptibility (Pipe *et al.*, 1999).

Generally, marine invertebrates are more sensitive than vertebrates, possibly by one to two orders of magnitude (Taylor *et al.*, 1985) with the toxicity of these 8 trace metals to vertebrates being in the following order (adapted from Eisler and Hennekey (1977) & Taylor *et al.* (1985)):

$$Hg^{2+} > Cr^{6+} > Cu^{2+} > Cd^{2+} > Pb^{2+} > Zn^{2+} = As^{3+} >> Ni^{2+} \qquad (1.6)$$
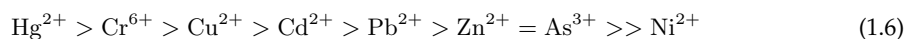
This toxicity order is not fixed, though, and depends on the species of the affected organism; for example crustaceans display a higher sensitivity to Zn^{2+}, while polychaete annelids (worms) are more sensitive to Cr^{6+} (Eisler and Hennekey, 1977; Guthrie *et al.*, 1979). Mercury is widely agreed as the most toxic and nickel as the least of these metals, however.

The toxicity of an element also varies depending on the speciation of that particular element. Notably, arsenic can have any of four valence states (-III, 0, III, V) (Phillips, 1990) and therefore can speciate into As^{3-}, As, As^{3+} and As^{5+}, forming both inorganic and organic compounds. Organic forms of arsenic are not generally toxic to marine life (Francesconi and Edmonds, 1996). Elemental arsenic (As) is rare, while As^{3-} is found only in highly reducing (anoxic) environments (Neff, 1997). Arsenite (As^{3+}) and arsenate (As^{5+}) are then the dominant inorganic forms of the element in the marine environment (Fattorini *et al.*,

Metal	Background Seawater (μg/L)	Source
As	$1 - 3$	Hem (1985); Neff (1997)
Cd	$0.004 - 0.110$	Beiras *et al.* (2003); Ferreira *et al.* (2004); Hem (1985); Laslett (1995); Ray (1986)
Cr	0.05 - 0.5	Hem (1985); Mearns *et al.* (1976)
Cu	$0.11 - 3.00$	Balls (1985); Beiras *et al.* (2003); Hem (1985); Laslett (1995)
Hg	$0.002 - 3$	Klein and Goldberg (1970); Matsunaga *et al.* (1979)
Ni	$0.1 - 20$	Beiras *et al.* (2003); Laslett (1995); Preston *et al.* (1972)
Pb	$0.013 - 0.500$	Balls (1985); Beiras *et al.* (2003); Laslett (1995)
Zn	$0.01 - 10$	Bruland *et al.* (1978); Hem (1985); Laslett (1995)

Table 1.3: *Background seawater concentrations of selected metals in uncontaminated seawater*

2004; Neff, 1997; Phillips, 1990), with arsenite being more bioavailable than arsenate and so is more toxic. Concentrations of As^{3+} with negative biological effects, such as reduced growth, reproduction and mortality in micro- and macroalgae range from 13 – 1,000 μg/L, while larger marine animals such as scallops, crabs and shrimp can tolerate up to 25,000 μg/L (Neff, 1997). Their tolerance appears to be related to the ability to convert toxic inorganic arsenic to non-toxic organic forms within their tissues (Fattorini *et al.*, 2004).

Chromium has two valencies: Cr^{3+} and Cr^{6+}. Cr^{3+} is fairly insoluble, while Cr^{6+} is very soluble and so the latter is responsible for most toxic effects in the aquatic environment (Mearns *et al.*, 1976; Taylor *et al.*, 1985). Cr^{6+} affects brood size and reproduction in benthic organisms at 10^{-5} g/L, with lethal effects in the ranges of $10^{-2} – 10^{-1}$ g/L for fish, and $10^{-5} – 10^{-3}$ g/L for invertebrates (Mearns *et al.*, 1976).

While the bioavailability of some elements depends on their speciation, the toxicity of other metals such as cadmium and copper is dependent on whether they exist as free metal ions (e.g. Cd^{2+} or Cu^{2+}) or bound to anionic species (e.g. chloride, Cl^-). Therefore the total dissolved cadmium or copper concentrations may not simply be an indication of toxicity. Engel and Fowler (1979) found that free ion concentration of cadmium decreased with salinity, due to complexation with chloride, and that the toxicity of cadmium on the grass shrimp *Palaemonetes pugio* was inversely proportional to salinity i.e. as salinity increased, toxicity decreased (also Phillips (1976) & Ray (1986)). Engel and Fowler (1979) also found that respiratory function of oysters was inhibited at dissolved cadmium concentrations of 300 - 600 μg/L at seawater chloride concentrations. Copper concentrations in the order of 10^{-5} g/L resulted in a toxic response from the *Mytilus edulis* mussel (Pipe *et al.*, 1999). Lead uptake was likewise found by Phillips (1976) to decrease with increasing salinity, possibly due to decreased filtration (feeding) rates or lowered solubility of lead in salt waters (Taylor *et al.*, 1985), while zinc toxicity increases with decreased salinity (Eisler and Hennekey, 1977).

Observed bioaccumulation factors (concentration in organism divided by concentration in environment) of cadmium were given by Ray (1986) as:

Plankton 10^4; Seaweed $10^2 – 10^3$; Mollusc $10^3 – 10^4$; Crustacean 10^3; Fish 10^2

The bioaccumulation factor for chromium in phytoplankton has been observed to be lower than cadmium, in the order of 10^2, with this being larger than higher trophic marine organisms (Mearns *et al.*, 1976). Mercury bioaccumulation is larger than cadmium, in the order of $10^3 – 10^4$ for marine fish, with strong enrichment in algae too (Klein and Goldberg, 1970). There is, then, a high storage capacity for cadmium and mercury in marine organisms, likely linked to 'metallothionein' proteins which act as a detoxifying guard against essential and non-essential trace elements. Metals bound to this protein are not available to the rest of the organism's functions (Ray, 1986) although they may reach saturation and cause mortality, as noted by the Engel and Fowler (1979) experiments.

The uptake of metals, and therefore potential toxicity, can also vary depending on other conditions. Examples include: exposure to other trace metals, which can modify uptake (Ray, 1986); increased temperature, which increases metabolic rate and so increases uptake in organisms (Eisler and Hennekey, 1977; Ray, 1986); seasonal variations (Blossom, 2006; Phillips, 1990; Ray, 1986); water column depth and the impact of freshwater inputs increasing concentrations of trace elements in shallow waters (Bruland *et al.*, 1978; Phillips, 1976); and body size. However there is often no apparent universal trends, which would indicate species specific responses only (Phillips, 1976; Ray, 1986).

While metals may not induce toxicity directly in marine organisms, the biomagnification of these trace elements up the food chain is of consequence to human diets, for instance cadmium, lead and mercury (Guthrie *et al.*, 1979; Neff, 1997; Ray, 1986; Renzoni *et al.*, 1998; Yamamoto *et al.*, 1994) are of particular concern. ^{210}Pb may account for 8% of internal radiation dose in humans consuming seafood (Yamamoto *et al.*, 1994). Inorganic mercury undergoes methylation in the aquatic environment to form methyl mercury, which is easily absorbed in organisms and enriches up the food chain (Renzoni *et al.*, 1998). The severe toxicity of bioaccumulated mercury to human populations was discovered in the 1960's

when the Japanese communities of Minimata Bay suffered neurological disorders due to the disposal of mercury waste in the bay waters (Klein and Goldberg, 1970).

1.2.7 Guidance on trace metals in produced waters

Concentrations of trace metals in produced waters are, so far, not specifically regulated by the UK in the offshore marine environment. The European Union Water Framework Directive (European Parliament, 2000) sets out targets for groundwater, freshwater and coastal pollution, which have been adopted by the various national UK environment agencies. Trace metal concentrations are set at legal limits throughout the UK for these environments. CO_2 storage activities in the UK will operate away from these areas on the UKCS, therefore the limits set by the regional agencies of the Scottish Environmental Protection Agency (SEPA), the Environment Agency (EA), and the Northern Ireland Environment Agency (NIEA) would not apply.

The UK, however, is a member of OSPAR (Oslo Paris Conventions) and therefore committed to meeting the recommendations set out by this trans-national agreement, to reduce the environmental impact of polluting activities. The recommendations emphasise the use of best environmental practice (BEP) and best available technology (BAT) when carrying out activities within the North Sea. The most recent recommendation with regard to produced water, OSPAR Recommendation 2012/5 for a risk-based approach to the Management of Produced Water Discharges from Offshore Installations (OSPAR Commission, 2012a), and the accompanying OSPAR Guidelines in support of the Recommendation 2012/5 (OSPAR Commission, 2012b) set out the framework for encouraging North Sea operators to reduce their environmental impact.

OSPAR Recommendation 2012/5 therefore outlines the approach that operators should take to calculating the risk to the environment of their activities. The heart of this risk based approach (RBA) is to calculate a ratio of modelled predicted concentration in the environment (PEC) to the predicted no-effect concentrations of those substances (PNEC). If PEC:PNEC ≤ 1 then the risk is controlled. If PEC:PNEC > 1 then this may present an unacceptable or uncontrolled risk and operators should revise their management and handling of produced waters. Appendix 5 of the OSPAR supporting guidelines provide calculated PNEC for naturally occurring substances in produced waters (including trace metals) which are repeated below in Table 1.4.

Metal	PNEC Concentration (μg/L)	
As	To be decided	
Ni	8.60	
Cd	0.21	$+ C_b$
Cr	0.60	$+ C_b$
Cu	2.60	
Hg	0.047	$+ C_b$
Pb	1.30	
Zn	3.00	$+ C_b$

Table 1.4: *Predicted no effect concentrations (PNEC, μg/L) from OSPAR Guidelines in support of Recommendation 2012/5 (OSPAR Commission, 2012b) for selected metals. C_b Background concentration (μg/l).*

Therefore, the absolute concentrations of trace metals measured in produced waters, from either existing oil and gas operations or future CCS projects, are not a reliable metric on the environmental impact of these waters. Many factors may be considered to influence the PEC, depending on conditions local to the production facility, such as water depth, current strength, salinity, etc. It is also not clear how operators are encouraged by DECC to adopt the RSA and whether operators are penalised for disposing of produced waters where their calculated PEC:PNEC is > 1. The assessment of whether future CO_2 storage will present an addition environmental risk depends on what current practices are for the oil and gas industry. Rather than calculate absolute environmental concentrations for any given project, the

relative concentrations of trace metals between potential CO_2 storage and existing oil and gas activities is the important metric, which is relatively straightforward to assess.

1.3   Thesis Outline

The overview presented above is that trace metals can be mobilised from brine-saturated sandstones with dissolved CO_2. These mobilised metals, if brought to the surface in produced waters during offshore CO_2 storage have the potential to negatively impact a variety of organisms spanning the entire food chain, depending on the concentrations of the metal encountered and the local conditions into which water is overboarded. The exact nature of the impact may vary by organism and metal, however the general effect is to potentially negatively impact marine and human populations.

Currently, there is no research which addresses the potential of UK North Sea reservoir sandstones to leach trace metals upon CO_2 injection and how this compares with current offshore oil and gas activities. The key questions that this thesis therefore seeks to address are:

- Does CO_2 mobilise trace metals from a variety of North Sea reservoir rocks?

- If so, can sources of mobilised trace metals be identified and used to predict future consequences of CO_2 injection?

- How does CO_2 leaching of trace metals from North Sea sandstones compare to a natural analogue site?

- How do concentrations of CO_2-mobilised trace metals from experiments compare with existing offshore oil and gas produced waters?

This thesis aims to address these research questions by reporting on the results of multiple experiments conducted for this study, fieldwork, and an examination of data from UK North Sea oil and gas operations. A comparison of the experimental results with the North Sea data should enable conclusions to be drawn on the potential for future CO_2 storage to negatively impact the offshore environment.

Simple batch experiments (Chapter 2) were carried out at The University of Edinburgh on a variety of available sandstones from UK North Sea oil fields (Chapter 3) and sandstones collected during fieldwork from Utah, USA (Chapter 4), using flowing CO_2 in brine-rock batch reactors, to determine the concentrations of the 8 trace metals of interest (As, Cd, Cr, Cu, Hg, Ni, Pb, Zn) which could be leached under experimental conditions. Data on trace metal concentrations in natural waters collected from CO_2-driven springs in Utah, USA (Chapter 2) was also obtained for comparison.

To complement the batch experiments, a sequential extraction procedure was designed to determine the mineral phases associated with these trace metals, and therefore the susceptibility of these metals to be mobilised under enhanced-CO_2 conditions (Chapters 3 & 4).

The comparison of data from these experiments provides information on how the presence of the 8 trace metals in solution with CO_2 leaching might be predicted, based on the known mineralogy of a CO_2 storage reservoir. The batch experiment concentrations are compared with UK North Sea production water data (Chapter 5), to determine similarities or differences between experimentally mobilised concentrations and current offshore activities. This allows an assessment of whether future CO_2 storage would negatively impact the environment, compared with what is currently permitted under existing guidance.

A summary of conclusions drawn from the experiment and fieldwork results chapters (Chapters 3 & 4), and comparison with EEMS (Chapter 5) are given in Chapter 6.

Laboratory & Field Methods

2.1 Utah Fieldwork

Field sampling of rock and water samples was carried out 4 - 6 [th] October 2013 in desert areas west-southwest and south, respectively, of Green River, Utah, Figure 2.1. Water samples collected from springs in this area were analysed for a suite of elements, including the 8 trace metals of interest (As, Cd, Cr, Cu, Hg, Ni, Pb, Zn) since data for these do not exist in the literature. Rock samples were collected in order that batch experiments could be carried out at the University of Edinburgh to investigate trace metal mobility, Section 2.2.

2.1.1 Rock sampling

A total of five rock samples, *S1 - S5*, were collected on 4 [th] October, 2013, adjacent to Interstate Route 70 from a cutting through the eastern limb of the San Rafael Swell anticlinal feature, around 18 kilometers west-southwest of Green River, Table 2.1 and Figure 2.1. With the aid of the 1980 edition of the Geologic Map of Utah (1:500,000 scale) and accompanying sheet of representative stratigraphic columns and cross sections, a number of locations were selected to examine rocks belonging to the *Entrada*, *Navajo* and *Wingate* sandstone formations.

Sample	Latitude	Longitude	Formation	Description
S1	38.9217500	-110.4300278	Entrada	*Upper portion*: mottled red/dark pink and white, medium grained, massive SANDSTONE. *Lower portion*: Mottled white/pale cream and pink, fine grained, subrounded, well sorted, SANDSTONE with occasional small (< 1 mm) dark feldspars. Friable surface, otherwise well cemented (calcite).
S2	38.9217500	-110.4300278	Entrada	Red, well sorted, well cemented (calcite), massive SANDSTONE.
S3	38.9230547	-110.4437193	Wingate	Pink/light red on surface crust, white underneath crust, fine-medium, well sorted SANDSTONE with mm-scale cross-bedding. Friable.
S4	38.9224444	-110.4404722	Navajo	Pink and white, fine-medium, well sorted, friable SANDSTONE with mm-scale cross bedding and 1 - 2 mm dark flecks throughout.
S5	38.9208056	-110.4375000	Navajo	Pink and white, fine-medium, well sorted, friable SANDSTONE with mm-scale cross bedding.

Table 2.1: *Grid co-ordinates, sampled formation, and field descriptions of rock samples S1 - S5 collected from the San Rafael Swell, Utah. See Figure 2.1 for mapped outcrop locations.*

The *Entrada*, *Wingate* and *Navajo* sandstones were chosen to be sampled as the CO_2-driven spring waters emanating at locations south of Green River originate from these formations. As the *Entrada*, *Wingate* and *Navajo* sandstones are not co-present together at the surface with the spring waters, they were sampled at the San Rafael Swell, located to the west-southwest of Green River. Here, the formations outcrop as the limbs on a large and spectacular weathered antiform, before dipping eastwards into first a syncline and then a shallow anticline beneath the Green River spring locations. Sampling was straightforward, since the outcrops were roadside, adjacent to Interstate 70.

Samples of approximately 10 x 10 x 10 cm in size were removed from the outcrops using a geological hammer, bagged and labelled for transport back to Edinburgh. Sample *S1* was chosen to include both a red/pink and white sandstone, and the boundary between them, Table 2.1. Since the observed sandstones at each location appeared well sorted and relatively homogenous, sample selection was dictated by practicality of obtaining the sample (i.e. height from the ground, ease of hammering, etc.). Sample *S3* included a thin (mm-scale) weathered 'crust' of red/pink sandstone, with an underlying white sandstone.
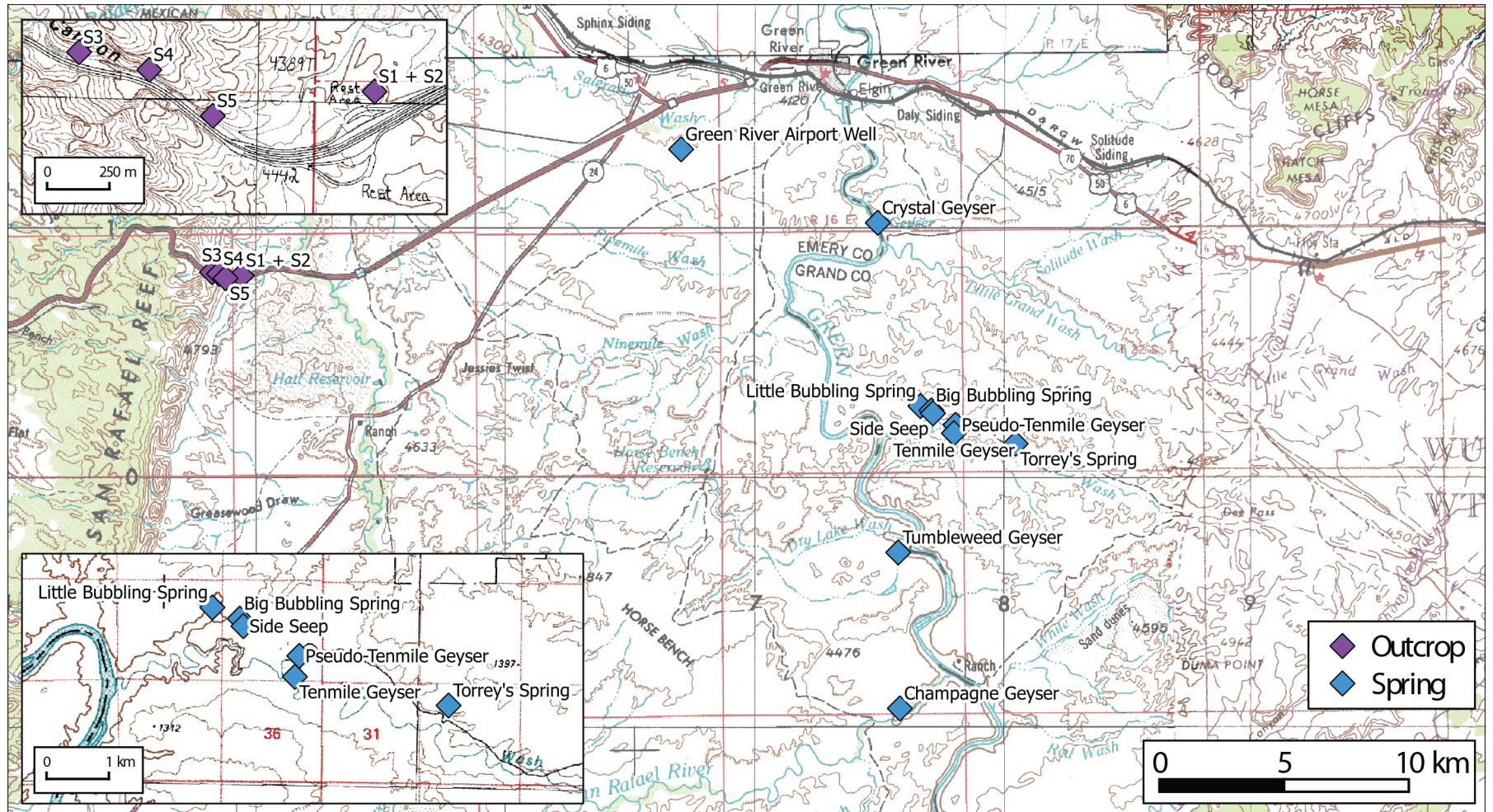
Figure 2.1: *Location map of outcrop and spring water sampling areas in the San Rafael Desert, near Green River, Utah. Clustered samples are expanded for clarity, top left and bottom left for outcrop rock samples and spring samples, respectively. Grid co-ordinates of outcrop samples are supplied in Table 2.1, and of spring samples in Table 2.2. Supplementary interactive maps with photographs of the outcrops and springs are available online at: https://goo.gl/wLpE1C (outcrops) and https://goo.gl/a6D9un (springs).*

Field notes were made, and location photographs taken of each sampling location. Sampling location photographs are provided in Figure 2.2.

Figure 2.2: *Photos of the exposures from which samples S1 - S5 were collected.*

2.1.2 Water sampling

Sampling of waters from 10 cold water springs was carried out 4 - 6 th October, 2013. The locations of the springs are given in Table 2.2 and Figure 2.1.

Spring Name	Latitude	Longitude	Remarks
Green River Airport Well	38.9661800	-110.2262400	50cm spring aperture surrounded by reeds on ochre travertine, slight sulphurous smell, warm water
Crystal Geyser	38.9390000	-110.1355000	Drill casing forms spring aperture. Occasional (> 12 hr) strong eruptions of water + gas
Little Bubbling Spring	38.8726500	-110.1166200	Water and gas bubble through < 10 cm fractures in ochre travertine
Big Bubbling Spring	38.8710700	-110.1115400	5m wide pond with vigorous gas bubbling
Side Seep	38.8699800	-110.1108600	Slight gas bubbling in stagnant creek
Tenmile Geyser	38.8627200	-110.1012500	20 cm wide spring aperture, bubbling gas
Pseudo-Tenmile Geyser	38.8657400	-110.1004600	Drill casing in ponded stagnant water. Occasional water + gas eruptions (not witnessed)
Torrey's Spring	38.8587300	-110.0727700	30 cm spring aperture, vigorous bubbling, ochre travertine mound
Tumbleweed Geyser	38.8198400	-110.1275300	Wide (10-15 m) pond, vigorous bubbling, turbid water
Champagne Geyser	38.7635000	-110.1274400	Occasional violent eruptions through < 5 cm aperture, ochre travertine

Table 2.2: *Grid co-ordinates and notable features of the 10 cold water springs located in the San Rafael desert, south of Green River, Utah. Spring locations are mapped in Figure 2.1.*

At each spring location, 8 discrete water samples were collected and treated as detailed in Table 2.3. Sampling kits were provided by Dr. Pat Mickler and Dr. Staci Loewy of the Jackson School of Geo-

Container	Volume (mL)	Analysis Type	Additives
Amber glass VOA[†]	40	Alkalinity	-
Amber glass VOA	40	Mercury	2% v/v 1M $K_2Cr_2O_7$ + 2% v/v 1N H_2SO_4
Amber glass VOA	20	Dissolved Inorganic Carbon	-
Amber glass VOA	20	H, C, O Isotopes	-
Polypropylene bottle	30	Trace elements	2% v/v 7N HNO_3
Polypropylene bottle	30	Major cations & anions	-
Polypropylene bottle	60	Archive	2% v/v 7N HNO_3
Polypropylene bottle	1,000	Fluid for batch experiments	-

Table 2.3: *Spring sampling bottle types, volumes, type of subsequent analysis, and chemical additives as supplied by the University of Texas (UT). All sample containers were supplied pre-cleaned with acid.* [†]*Volatile organic analysis vial.*

sciences, University of Texas (UT). All samples were syringe filtered through a 0.45 μm filter membrane prior to chemical treatments, and bottles were sealed with Parafilm™ for later analysis.

The sample containers, syringes and filters were pre-cleaned by UT using the following regime:

- Polypropylene bottles for cations and isotopes

    - Rinsed with deionised (D.I.) water then soaked in micro for 2 days

    - Rinsed with D.I. water then soaked in 30% trace metal grade HNO_3 for 2 days

    - Rinsed in D.I. water then soaked in 18 MΩ D.I. water for 2 days

    - Dried

- Polypropylene bottles for anions, glass VOA vials and syringes

    - Rinsed with D.I. then soaked in micro for 2 days

    - Rinsed with D.I. then soaked in 18 MΩ D.I. water for 2 days

    - Dried

- Filters

    - Rinsed with D.I. water

    - Filled with 18 MΩ D.I. water and soaked for 2 days

The sampling procedure was a standard field sampling method, as follows for small (< 60 mL) bottles and vials:

1. Draw full syringe of water from the geyser, as close to CO_2 bubbling as possible, then:

    (a) pass through filter onto the ground. Repeat three times

    (b) pass through filter into each sample container, rinse and discard. Repeat three times

    (c) pass through filter to fill each sample container, leaving no headspace

2. Add acids and reagents using a pipettor, to the volumes and concentrations as per Table 2.3

3. Seal container with cap and Parafilm™

4. Label container

For the 1,000 mL bottle, if the geyser pool was large enough, the bottle was filled by submerging it and the fluid discarded to the ground three times, before filling to the brim and capping it a final time. The cap was sealed with Parafilm™. If the geyser was small, for example *Little Bubbling Spring*, then the bottle was filled to the brim using the syringe (unfiltered) instead of submerging it.

The sampling for mercury (Hg) was carried out based on the method outlined in the Department for Energy and Climate Change (DECC) sampling guidance issued to North Sea oil and gas operators

(Department of Energy & Climate Change, 2014). Samples were therefore collected in glass vials, and preserved using 1M sulphuric acid (H_2SO_4) and 1M potassium dichromate ($K_2Cr_2O_7$). Cold Vapour Atomic Fluorescence Spectroscopy (CV-AFS) Hg analysis was subsequently carried out in the UK by a commercial laboratory, Scientific Analysis Laboratories Ltd (SAL) (see Section 2.5.2.3).

Nitrile gloves were worn throughout the sampling, and each time the pipettor was used for a different reagent the tip was rinsed three times with the reagent before adding to the sample bottle. A summary of the analysis carried out on the collected spring samples is provided in Table 2.4.

Spring	pH[‡]	Alkalinity[§]	Cations & anions	Trace Elements	Mercury
Green River Airport Well	Y	Y	IC[†]	ICP-MS[††]	ICP-MS[†††]
Crystal Geyser					
Little Bubbling Spring					
Big Bubbling Spring					
Tenmile Geyser					
Pseudo-Tenmile Geyser					
Torrey's Spring					
Tumbleweed Geyser					
Champagne Geyser					
Side Seep		N			

Table 2.4: *Summary of analysis carried out on spring water samples collected in Utah. [‡]Section 2.4.2. [§]Section 2.4.4. [†]Ion Chromatography at University of Texas (UT), Section 2.7. [††]Inductively Coupled Plasma Mass Spectroscopy (ICP-MS) at UT, Section 2.5.1. [†††]ICP-MS at University of Edinburgh, Section 2.5.2. See Table 2.2 and Figure 2.1 for sample location details.*

2.2 CO$_2$-Water-Rock Batch Experiments

To test whether adding CO$_2$ to reservoir formation waters will enhance the mobility of the reservoir rocks' constituent elements, batch reaction experiments were conducted at the School of Geosciences, University of Edinburgh. These comprised, at a general level, of reacting warm saline waters and gaseous bubbled CO$_2$ at atmospheric pressure (1 atm) with sandstones which could represent either potential CO$_2$ reservoir rocks (North Sea) or rocks which have already naturally reacted with CO$_2$ (Utah).

At reservoir depths suitable for storage, however, CO$_2$ would be in its supercritical phase i.e. at pressures > 72.9 atm. Clearly the proposed batch experiments are at a much lower pressure, however as pressure cells were not available to conduct these experiments, then the batch experiments were undertaken at realistic reservoir temperatures to see if mobilisation of elements could be induced without requiring large reservoir pressures. A clear positive result would be a strong driver for further elevated pressure experiments, after investing in the appropriate equipment.

These experiments were carried out on sandstone samples obtained for the North Sea hydrocarbon fields *Captain*, *Cormorant North*, *Thistle* (Table 2.5), which represent potential CO$_2$ storage reservoirs, and on outcrop sandstone samples obtained in the San Rafael Desert, Utah, which represent sandstones which may have already naturally reacted with CO$_2$ rich groundwaters (see Section 2.1 for Utah sampling details). A summary of the batch experiments undertaken, including sample names used through this thesis, is provided in Table 2.6.

A fourth North Sea sandstone was also used in the experiments, supplied for research undertaken by this author as part of the Scottish Carbon Capture and Storage (SCCS) Joint Industry Project (JIP), which has been published by SCCS on their website (http://www.sccs.org.uk/). Due to commercial reasons the field from which the rock came cannot be named, and is hereafter referred to as "*Field X*", Table 2.5. The batch experiment using the *Field X* data was published in the SCCS JIP report, however this has not been peer reviewed or submitted for degree assessment. The experimental method and results are therefore detailed here in full.

The *Captain* sandstone batch experiment method and results were previously submitted by this author for Masters degree assessment in August 2011, and so the detailed method is not included directly in the text of this chapter. However, a copy of the method taken from the Masters is included as Appendix A.

Cormorant North and *Thistle* sandstones were reacted in a batch experiment to provide data for this thesis, and for inclusion into a Masters thesis submitted by Georgios A. Lygkas in August 2012. The experimental design and setup was this author's own, with Georgios assisting in sample collection and the laboratory measurement of pH and alkalinity. The samples collected by Georgios were analysed separately by Inductively Couple Plasma Optical Emission Spectroscopy (ICP-OES) by this author, and so the concentration data collected is distinct from those already submitted by Georgios for assessment. This author acknowledges that the pH and alkalinity data used in this thesis was collected by Georgios. The experiment is described in full in this chapter.

Batch experiments using samples collected from Utah were entirely for the purposes of this Ph.D., and are outlined in full in this thesis.

2.2.1 Sample preparation

2.2.1.1 Captain, Cormorant and Thistle sandstones

UK Continental Shelf (UKCS) well bores from which the sandstone samples originally came are provided in Table 2.5. Please refer to Appendix A for the detailed batch experiment method for the *Captain* sandstone samples. A summary of the experimental work is given through this section, however, and a map of the location of the *Captain* field is given as Figure 2.3.

North Sea Field	Well Bore	Sample Depth(s) (m)	Formation	Hydrocarbon Type
Captain	13/24a-4	1,620 & 1,656	Captain	Condensate
Cormorant North	211/21-CN40	3,442	Brent	Oil
Thistle	211/19-6	3,253	Brent	Oil
Field X*	-	-	-	Oil

Table 2.5: *Locations and details of North Sea samples. *Due to commercial sensitivity, identifying reservoir details have been omitted.*

Cormorant and *Thistle* sandstone samples were chosen from archive material originally supplied by the companies operating the respective fields, and now held at the sample store at the Grant Institute, School of Geosciences, University of Edinburgh (see Table 2.5 for original well bores) The first sample, *Cormorant North*, was a core plug obtained from well 211/21-N40 at 11,294 ft (3,442 m). Well 211/21-N40 lies in a cluster of wells in the centre of the *Cormorant North* field, targeting the Brent Group of the Northern North Sea, northeast of Shetland in the UKCS area, Figure 2.4.

The second sandstone sample, *Thistle*, was a core slice from well 211/19-6 at 10,671 ft (3,252 m), which also lies within the Brent Group, Figure 2.4. Both samples were broken into chips measuring roughly 1 × 1 × 1 cm using a geological hammer and mortar and pestle. The weights of sample used in each batch flask are given in Table 2.6.

Reservoir temperatures for *Cormorant* and *Thistle* are given in the literature as 90.5 - 107.2°C (Taylor and Dietvorst, 1991) and 104.4°C (Brown *et al.*, 2003), respectively. However, since the experiment was undertaken at atmospheric pressure, the maximum temperature achievable in the batch flask is 100°C as the fluids then begin to boil. The fluid temperature for these fields was therefore set slightly lower at 95°C, Table 2.6. Reservoir fluid salinities are also given by Taylor and Dietvorst (1991), and Brown *et al.* (2003), and these were selected to make up synthetic NaCl solutions to the concentrations in Table 2.6.
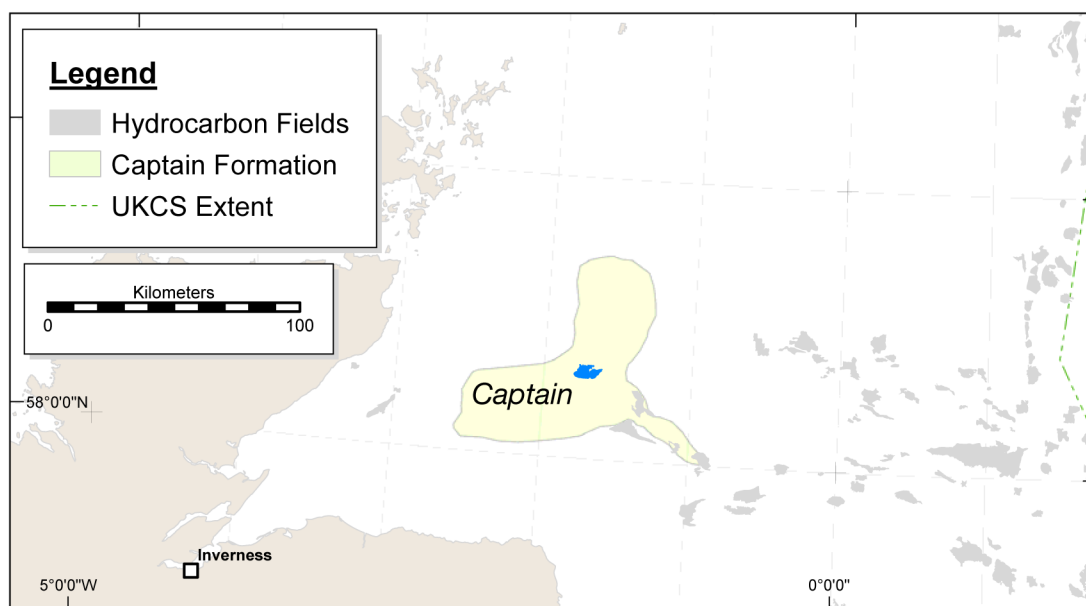
Figure 2.3: *Location of Captain UKCS field within Captain sandstone formation of the North Sea.*

2.2.1.2   Field X sandstones

The location of samples for the *Field X* experiment cannot be disclosed due to commercial confidentiality. Two core samples were supplied by Kirk Petrophysics; these were named "*8518*" and "*8579*", cut into

blocks with a rock saw, and the centre pieces of each core set aside for the experiment. The centres of the cores were anticipated to be less affected by drilling muds, which may have affected the batch experiment results, in particular barium (Ba) concentrations. Each centre piece was lightly disaggregated into sand-sized ($\sim$ < 2 mm) grains with a mortar and pestle for use in the batch experiments, being careful not to grind the sample in order to preserve as best as possible any mineral overgrowths and to avoid exposing fresh mineral surfaces. Pieces of the remaining core were set aside for thin sections, X-ray diffraction (XRD) and X-ray fluorescence (XRF) analysis. Both samples contained hydrocarbons, as evidenced by a distinctive odour and staining.

The formation water salinity of the field from which the core was obtained was not supplied at the time of the experiment, therefore an estimate was taken of salinity from nearby fields of the same geological age. Salinity was calculated to be approximately 80,000 ppm NaCl equivalent (field data supplied at a later date gave an average salinity of 81,200 ppm). The field formation water chemistry was also not supplied prior to undertaking the experiments, therefore the saline solution used was a simple NaCl solution only.

Synthetic NaCl solutions used in all the North Sea batch experiments were made up from 13.5 g (*Captain*), 16 g (*Cormorant*), 23.5 g (*Thistle*) and 80.00 g (*Field X*) $\pm$ 0.01 g of Fisherbrand 'SLR' grade NaCl solid reagent per 1,000 mL of 18 MΩ D.I. water (from a Milli-Q water system) to give the required NaCl concentrations.
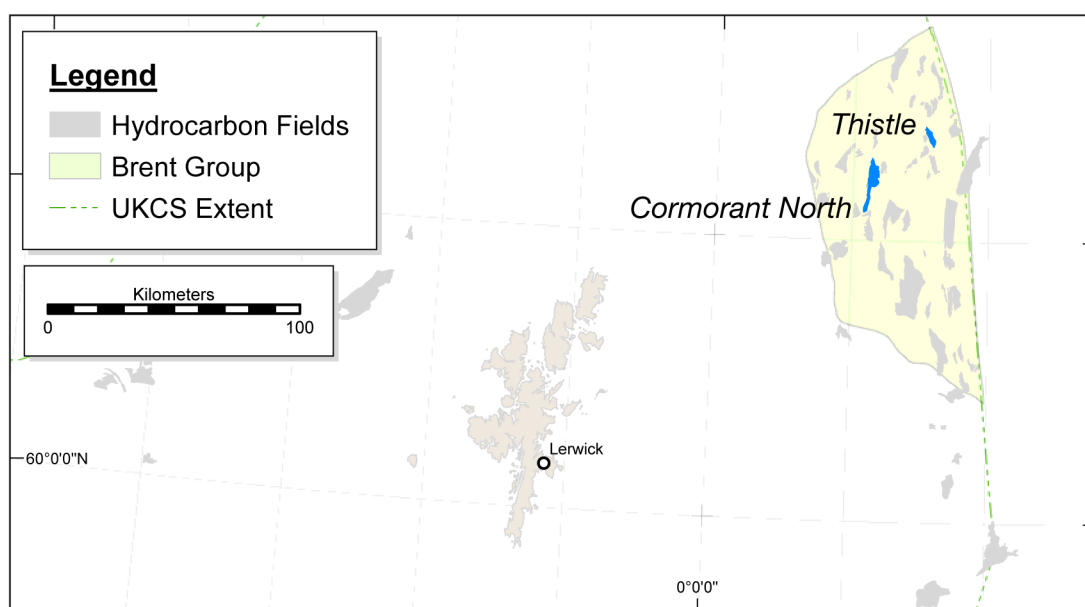
Figure 2.4: *Locations of Cormorant North and Thistle UKCS fields within the Brent Group of the North Sea.*

2.2.1.3 Utah sandstones

Pieces of sandstone were broken off the original field samples using a geological hammer, and these pieces reduced to chips with a jaw crusher. The chips were then disaggregated with a mortar and pestle, being careful not to grind the sample in order to preserve as best as possible any mineral overgrowths and to avoid exposing fresh mineral surfaces. Once disaggregated, approximately 30 g of each loose sample, Table 2.6, was weighed out with an electronic balance, accurate to $\pm$ 0.1 g, and added to each flask. Fluids collected from the *Crystal Geyser* spring were used in the Utah sandstone batch experiments.

Flask	Sample Name	Sample Weight (g)	Grain/Chip[‡]	Brine Concentration (mg/L)	Temperature (°C)	CO_2 Flow (Yes/No)	Duration (Days)	pH[†]	Alkalinity[††]	Cations[†††]
Captain (MSc Project)										
F1	Blank			13,500	58	Y	30	Y	Y	ICP-MS
F2	SA7	3.36	Chip							
F3	SA7	2.75	Grain							
F4	SA10	3.36	Chip			↓				
F5	SA10	2.64	Grain							
B1	Blank					N				
B2	SA7	3.17	Chip							
B3	SA7	2.75	Grain							
B4	SA10	3.18	Chip	↓	↓	↓	↓	↓	↓	↓
B5	SA10	2.85	Grain							
Cormorant										
F1	Cormorant	8.99	Chip	16,000	95	N	15	Y	Y	ICP-OES
F2	Cormorant	9.39	Chip	16,000	95	Y	15	Y	Y	ICP-OES
Thistle										
F3	Thistle	15.91	Chip	23,500	95	N	15	Y	Y	ICP-OES
F4	Thistle	15.25	Chip	23,500	95	Y	15	Y	Y	ICP-OES
Field X (JIP Project)										
F1	8579	17.10	Grain	80,000	80	Y	21	Y	Y	ICP-MS
F2	8579	18.80				N				
F3	8518	18.20	↓	↓	↓	Y	↓	↓	↓	↓
F4	8518	18.40				N				
Utah										
S1	Entrada	29.80	Grain	~ 15,000[§]	21	Y & N	159	Y	N	ICP-MS
S2	Entrada	29.60								
S3	Wingate	31.00	↓	↓	↓	↓	↓	↓	↓	↓
S4	Navajo	30.10								

Table 2.6: *Summary table of batch experiment conditions and measurements. All measurements taken at the University of Edinburgh. [‡]'Chip' refers to ~1 cm³ pieces, 'Grain' refers to disaggregated sample. [†]Section 2.4.1. [††]Section 2.4.3. [†††]Sections 2.5.2 & 2.6.1. [§]Approximation based upon sum of cation analysis by IC at University of Texas, Section 2.7. See Tables 2.1 & 2.5 for sample location details.*

2.2.2 Experiment setups

The experiment setup comprised of Quickfit[TM] 250 mL round bottomed, three necked borosilicate flasks, set in a fume cupboard each on a heating mantle to control temperature (where necessary), with a Liebig condenser, thermometer and hollow glass tube for CO_2 injection, Figure 2.5. The flask names and set ups for CO_2 are given in Table 2.6.
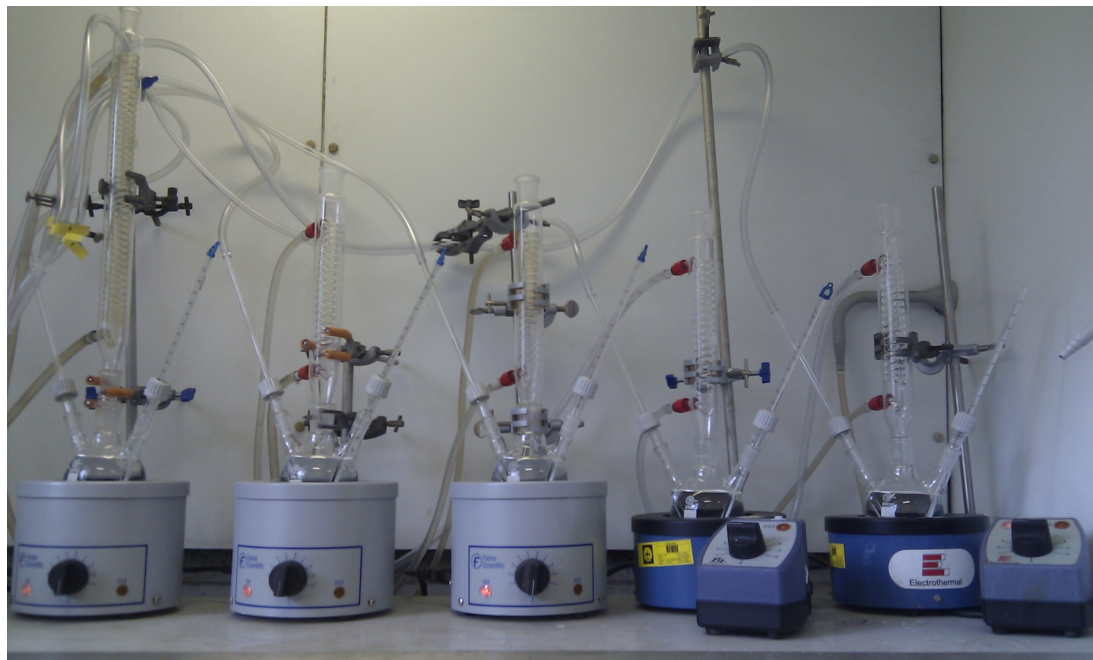
Figure 2.5: *General setup of sandstone batch experiments.*

Prior to set up, all glassware and sampling vessels were soaked in a 10% nitric acid (HNO_3) bath for at least 12 hours, before being rinsed four times with distilled water and twice with D.I. water, and dried in a drying cupboard.

For all of the North Sea sandstones (*Captain*, *Cormorant*, *Thistle*, *Field X*), 250 ± 1 mL of synthetic NaCl solution was added to each flask with an acid cleaned 50 mL measuring cylinder and heated to the appropriate temperature (Table 2.6) prior to adding the sandstone samples. Utah samples were added to the flasks before 250 ± 1 mL of *Crystal Geyser* spring water was added, and were not heated since Crystal Geyser fluid temperatures were measured in-situ as around $17°C$, and therefore slightly colder than room temperature.

After the North Sea sandstone samples were added, dry CO_2 gas was fed to each flask in the configuration in Table 2.6 from a BOC supplied vapour withdrawal CO_2 bottle with attached 2 bar regulator, through stainless steel piping and rubber tubing to the glass rods. PTFE tape at joints ensured a leak-free system until the point of delivery in the flasks. CO_2 flow was regulated using Hoffman tubing clamps and although flow was not measured, a pressure of 1.4 bar was maintained to bubble CO_2 into the batch fluids. The concentration of total CO_2 this pressure equates to in solution, assuming no reactions other than CO_2 + water, was modelled using PHREEQC v3.3.3.10424 and the results for each batch experiment are given in Table 2.7. The commencement of CO_2 flow was taken as the start of the experiments, 0hrs/0days.

The four samples used in the Utah experiment, *S1 - S4* were allowed to react with the *Crystal Geyser* brine before CO_2 was added. CO_2 bubbling in the Utah batch experiment began approximately 3 months into the experiment. This was much later than was planned due to problems obtaining replacement hardware to connect the regulator on the CO_2 bottle to the tubing supplying gas to the flasks. The

Batch	T	Na$^+$	Cl$^-$	Density	log P$_{CO2}$	Modelled Total CO$_2$		
	°C	(mg/L)	(mg/L)	(kg/L)	(bar)	(mol/kg)	(mol/L)	(g/L)
Captain	58	6,750	6,750	1.054	0.146§	0.026	0.024	1.05
Cormorant	95	8,000	8,000	1.064		0.014	0.015	0.67
Thistle	95	11,750	11,750	1.094		0.014	0.015	0.66
Field X	80	40,000	40,000	1.160		0.013	0.015	0.64
Utah	21	3,271†	3,966†	1.045		0.052	0.054	2.39

Table 2.7: *Initial batch experiment conditions data total CO$_2$ output as modelled with PHREEQC v3.3.3.10424. §P = 1.4 bar CO$_2$ pressure in batch experiments. †Concentrations as determined by Ion Chromatography at the University of Texas, Section 2.7.*

experiment was therefore extended from a planned 2 months (1 month each of equilibration and CO$_2$ bubbling) to 6 months (3 months each).

2.2.3 Fluid sampling

Fluid samples were drawn from the batch flasks with either a pipettor (*Captain*, Utah *S1 - S4*) and transferred to a disposable sterile syringe, or drawn directly with a disposable syringe and a short piece of rubber tubing (*Cormorant*, *Thistle*, *Field X*). Fluid in the syringe was then passed through a Millex GP 33 mm PES 0.22 μm filter into an acid cleaned borosilicate vial. From here, samples were pipetted into a plastic (PTFE) sample container, acidified with 2% v/v analytical grade 69% HNO$_3$ and refrigerated for later analysis. *Captain* and Utah samples were diluted at this stage with D.I. water, at the dilution factors given later in this chapter (Table 2.9).

2.2.4 CO$_2$ flow issues

CO$_2$ flow to the flasks stopped intermittently during *Captain*, *Field X* and Utah experiments due to the CO$_2$ bottle emptying. This occurred 4 times for the *Captain* experiment (faulty regulator), 2 times during the *Field X* experiment (leakage at joints in CO$_2$ delivery tubing) and once during the long duration Utah experiment when the CO$_2$ bottle emptied through constant use. CO$_2$ flow was also restricted, but not blocked, by salt precipitation in the tips of the glass rods used to inject CO$_2$ in the *Field X* experiment. A stainless steel needle was used to regularly clear the salt blockages. Salt precipitation indicates loss of water from the experiments, perhaps due to the condenser system not being as effective as it should have been.

2.2.5 Other comments

Captain, *Cormorant*, *Thistle* and Utah experiments withdrew fluids from the batch flasks, reducing the volume of experimental fluid in the flask to react with the rock samples. Due to the high temperature of the *Cormorant* and *Thistle* experiments, fluid volumes in flasks *F2* and *F4* became too low to sample on days 5 and 10, respectively, due to evaporation. 100 mL of synthetic NaCl solution was added to each flask on these days to top them up. During the *Field X* experiment, fluid volumes were kept topped up in the flasks by adding fresh NaCl solution of the same volume as that removed for analysis. The experimental metal concentrations and alkalinities are corrected for these dilutions for *Cormorant*, *Thistle* and *Field X*, using the method described in Appendix B.

2.2.6 Critical analysis of batch experiments

The experimental apparatus used in the batch experiments, Section 2.2.2, was originally intended for a different experiment but was appropriated for use in the MSc (*Captain* sandstone) experiments. With a

limited Ph.D. project budget, the apparatus was re-used for experiments conducted for this study (*Cormorant*, *Thistle*, *Field X* and Utah). However, as well as being inexpensive which allowed for a relatively large amount of chemical data to be collected over the duration of this study, a consistent experimental method allowed the results of each experiment to be compared with each other in a straightforward manner.

There are, however, issues with the experimental design which may affect the confidence with which the data is assessed. The most obvious problem is that the experiment set up was not capable of being pressurised to simulate CO_2 reservoir conditions, similar to experiments conducted by, for example Kaszuba *et al.* (2005), Lu *et al.* (2011), Pudlo *et al.* (2012) and Varadharajan *et al.* (2013). While a non-pressurised system may be considered wholly appropriate when looking at shallow sediments from 10's metres below ground level (e.g. Kirsch *et al.* 2014; Little and Jackson 2010; Smyth *et al.* 2009), the rock samples used for these experiments are considerably deeper, Table 2.5. This has a two-fold effect.

Firstly, more CO_2 dissolves in water at higher pressures, which reduces pH further than at the atmospheric pressure of the experiments. For example, dissolving CO_2 at the reservoir conditions for *Cormorant North* (Taylor and Dietvorst, 1991) of 90.5 - 107.2°C, 332 - 363 bar, and 16,000 ppm NaCl equivalent reservoir fluids, PHREEQC v3.3.3.10424 gives pH values in the range 2.86 - 2.95. These compare to PHREEQC modelled pH values of around pH 4.0, if the experimental CO_2 pressure of 1.4 bar is substituted into the model. An enhanced reduction in pH at reservoir pressures could affect mobilisation of elements by, for example, dissolution of mineral phases resistant at higher pH's. Secondly, above 31.1°C and 73.9 bar, CO_2 is in it's supercritical state (sc-CO_2). Water dissolves into sc-CO_2, effectively desiccating the formation brine and leading to precipitation of minerals where elements are close to saturation in the brine (Kaszuba *et al.* 2003; Rosenbauer *et al.* 2005). Trace metals may co-precipitate leading to reduced mobility. Precipitation of new minerals reduces porosity (Rosenbauer *et al.*, 2005), and therefore potentially leading to a reduction in reaction surfaces.

In addition to the experiments not being pressurised, water loss was a problem due to the condenser system not working efficiently. This was particularly noticeable in flasks which had CO_2 bubbled into them: the agitation of the brines appeared to enhance water loss through evaporation. The net result was that the salinities of the batch fluids would have increased over time, increasing the ionic strength gradually of the solutions. An increase in ionic strength can then increase the effect of any reactions in which Na^+ ions are substituting for other cations in mineral structures, potentially liberating more elements such as Ca and K with time. The batch fluids were also simple NaCl solutions, with the exception of the Utah experiments, primarily because detailed formation water chemistry of the North Sea fields was not known. Simulating fluids of a similar composition to the reservoirs could have resulted in fluids which were closer to equilibrium with the rock (e.g. because of the presence of Mg, K, etc.), than simple NaCl. Batch fluids were therefore potentially more aggressive under bubbled CO_2 conditions than reservoir fluids would have been (Kaszuba *et al.*, 2013), exaggerating the effect of CO_2 (if any).

An open system, such as the experimental set up described here (Section 2.2.2), is not free of oxygen (O_2) and therefore the experiments were conducted under oxidising conditions. Again, this may be suitable for investigation of shallow reactions (Little and Jackson, 2010), however deep geological CO_2 storage reservoirs would likely be under reducing conditions. Depending on the mineralogy of the experiment samples, element mobility may be prohibited or enhanced. Several authors purged their batch experiments with nitrogen, in order to reduce the effect of O_2 (e.g. Gupta *et al.* 2000; Lu *et al.* 2014; Purser *et al.* 2014; Smyth *et al.* 2009), and were able to maintain these conditions using closed vessel systems, such as those summarised by Kaszuba *et al.* (2013). Lu *et al.* (2014) demonstrated that the presence of O_2 can considerably increase reactions in these batch experiments and mobilise increased concentrations of some elements (e.g. Ca, Si, Zn) compared with low-O_2 experiments, while other elements such as Fe were largely immobile under increased O_2 conditions. Purser *et al.* (2014) confirmed the effect of the presence of O_2 with respect to Fe by demonstrating that the addition of a reducing agent (H_2S produced from thioacetamide) significantly increased Fe^{2+} in batch experiments.

However, despite these deficiencies (low pressure, water loss, oxidising conditions), there is confidence that this experimental approach is good enough for the purposes of this study. While not an ideal set up, the experiments attempted to simulate both the reservoir fluids and temperatures. Temperature overall can have a greater effect on reaction rates of mineral dissolution across all experiments than an increase in pressure (Kaszuba *et al.* 2013; Lu *et al.* 2014), since reaction rates will be different for each mineral depending on pH, but not dependent on temperature (reaction rates generally double for each $10°C$ increase in temperature). Therefore, since temperatures were simulated as close to reservoirs as possible, this could be a bigger control than pressure, and so the experiments may have captured the more important variable.

The simple NaCl solutions, and increasing ionic activity with time, would probably exaggerate reaction rates. The purpose of this study was to determine whether trace metals could be leached from sandstones under enhanced CO_2 conditions, therefore any exaggeration in mobility provides a potential 'worst case' set of data, in terms of informing industry and regulators what may be expected with offshore CO_2 storage. The study was not concerned initially with reaction rate data, although were these experiments to be repeated at reservoir pressures, then this data would be collected.

Overall, the batch experimental design could be improved, in line with previous studies. However, the batch experiments were inexpensive and simple to run, and likely captured the significant CO_2-water-rock reactions. While accurate transferral of the data obtained for this study to full-scale, pressurised CO_2 storage will be challenging, the data will at least provide some indication of likely issues and provide the platform for further research, based on improved experimental design.

2.3 Sequential Extraction Procedure (SEP)

Sequential extraction procedures (SEP) are a useful analytical tool for determining the relative mobility of elements from soils and rocks (e.g. Kirsch *et al.* 2014; Maskall and Thornton 1998; Rao *et al.* 2008; Tessier *et al.* 1979; Wigley *et al.* 2013b). More specifically, the analysis seeks to apportion the distribution of elements to a series of phases in the soil/rock, defined by mineral groups. A sequence of increasingly aggressive chemical leaches is performed on the rock or soil of choice, with their effectiveness depending on the chosen soil/rock and the chemistry used in the extraction.

The SEP chosen was a modified version of that presented by Wigley *et al.* (2013b), which was a method used for the sequential extraction of trace and major elements from Utah sandstones in the context of CO_2 leaching. In fact, some of the samples collected (*S1* & *S2*) for the extraction procedure are from the same *Entrada* formation as those selected by Wigley *et al.* (2013b), albeit from an outcrop located some 30 km to the west-southwest, Figure 2.1.

By selecting the same SEP as Wigley *et al.* (2013b), two advantages are conferred: i) as a published method with results applicable to carbon capture and storage (CCS), the SEP is considered a valid method for the testing of sandstones in the context of CCS in the North Sea; and ii) the experiment undertaken by Wigley *et al.* (2013b) can be replicated for Utah sandstones to confirm the validity - or otherwise - of the results obtained here.

The SEP was applied not only to samples from Utah, but also to North Sea sandstones. As such, the method was amended prior to being carried out, to allow for an additional step to target the sulphide mineral phase. This step was not in the original SEP devised by Wigley *et al.* (2013b) due to no sulphide minerals being identified in the mineralogy of the *Entrada* samples collected during that investigation. North Sea samples investigated for this Ph.D., however, do contain sulphide minerals (Chapter 3) and so this step was added to ensure potential leaching from this phase was captured. This step replaced the hydrochloric acid step in Wigley *et al.* (2013b).

Other details of the method were omitted from the Wigley *et al.* (2013b) publication, notably the mass of sample used in the SEP and the volume of reagent at each step. Wigley's method was already a modification of an original SEP devised by Tessier *et al.* (1979) and this paper was referred back to in order to decide the masses and volumes required. Some differences in timings of the SEP steps was observed between the Tessier *et al.* (1979) and Wigley *et al.* (2013b) methods; where this was the case, the timings from the Wigley paper were used.

2.3.1 Sample preparation

Samples from *Captain*, *Cormorant*, *Thistle* and Utah (*S1* - *S5*) were used in the SEP. 10 g each of sample were crushed with a mechanical jaw crusher and the resulting chips ground to a powder with a tungsten-carbide mill. Samples were homogenised and $1,000 \pm 2$ mg weighed out into 50 mL centrifuge tubes. Reagents were added to the centrifuge tubes in the steps listed below. A sample of SiO_2 was also run through the mill to determine concentrations of cations which may have been transferred from the crushing step, by comparing to a sample of SiO_2 which wasn't put through the mill. However after whole rock analysis (Section 2.6.2) both SiO_2 samples were found to contain high concentrations of a variety of cations and were therefore not a reliable indicator of transferred material.

2.3.2 SEP methodology

The method used to investigate the leaching of trace and major elements from North Sea and Utah sandstones was as follows:

1. **Water rinse**: 8 mL 18.2 MΩ de-ionized (D.I.) water with continuous agitation for 2 hrs.

2. **Exchangeable fraction**: 8 mL 1 M sodium acetate solution ($C_2H_3O_2Na$) at pH 8.2, with continuous agitation for 3 hrs.

3. **Carbonates**: 8 mL 1 M $C_2H_3O_2Na$ adjusted to pH 5 with acetic acid ($C_2H_4O_2$), with continuous agitation for 7 hrs, repeated 3 times with fresh reagent.

4. **Oxides**: 8 mL 0.1 M ammonium oxalate ($C_2H_8N_2O_4$) buffer adjusted to pH 3 with oxalic acid ($C_2H_2O_4$). Occasional agitation for 54 hrs, repeated 3 times with fresh reagent.

5. **Sulphides**: 3 mL 0.02 M nitric acid (HNO_3) + 5 mL of 30% hydrogen peroxide (H_2O_2), adjusted to pH 2 with concentrated HNO_3, heated to 85°C in a water bath for 2 hrs with occasional agitation. Added 3 mL H_2O_2, adjusted to pH 2 with HNO_3, and heated again for 3 hrs. After cooling to approximately room temperature, 5 mL of 3.2 M ammonium acetate ($C_2H_3O_2NH_4$) in 20% (v/v) HNO_3 was added and the whole mixture diluted to 20 mL with D.I. water before continuous agitation for 30 mins.

6. **Bulk digestion/Silicates**: Microwave digestion of residue with 4 mL concentrated hydrofluoric acid (HF), 3 mL concentrated HNO_3, 2 mL 20% hydrochloric acid (HCl) at 200°C and the resulting dry salt taken up in 2% HNO_3 (see detailed method below).

All continuous agitation was carried out by means of a rotating 'end-over-end' shaker connected to a voltage controller to adjust rotating speed, Figure 2.6. With the exception of Step 5, all SEP steps were carried out at a room temperature of ∼ 21°C.
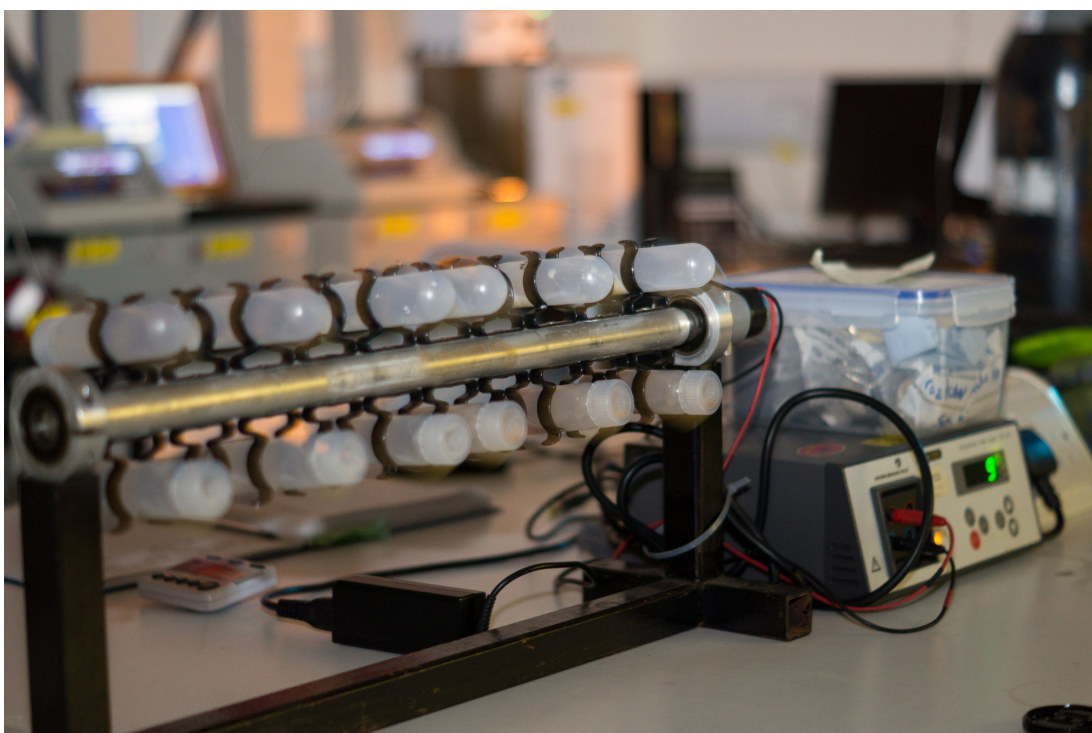
Figure 2.6: *Rotating shaker and voltage (speed) controller for sequential extraction continuous agitation.*

After each extraction period (2 - 54 hrs) the samples and supernatants were centrifuged at 12,000 rpm for 20 minutes, and the supernatants removed from the centrifuge tubes by carefully pouring out into an acid cleaned vial. The centrifugal speed was higher than the Wigley *et al.* (2013b) method as their speed was not high enough to ensure that any clays in suspension in the supernatant 'plate out' during centrifugation. However, although the clays plated out at the higher centrifugal speed used in this work, nonetheless when the supernatants were removed, some of the finest solid material was re-suspended

and transferred into the sub-sampling vial. This was most pronounced after the first step using D.I. water and became less apparent throughout the remainder of the steps. Each supernatant was, however, filtered through a 0.22 μm filter into the final sampling vessel to ensure no fine suspended solids were present in the final sample for analysis. Each sample was acidified with 2% HNO_3 and refrigerated for preservation until analysis.

2.3.3 Microwave digestion

The material remaining in the centrifuge tubes from Step 5 of the SEP was rinsed into an acid cleaned borosilicate vial using D.I. water and the samples allowed to dry. The resultant powder was homogenised and approximately 400 ± 1 mg weighed out onto weighing paper and transferred to 55 mL Teflon (TFM) digestion vessels, pre-cleaned with > 30% HNO_3. Whole rock samples not used in the SEP were also weighed out to compare the sum of the SEP steps with the bulk concentrations of elements.

The following microwave-assisted digestion procedure was carried out: 4 mL concentrated HF, 3 mL concentrated HNO_3 and 2 mL 30% HCl, all trace-metal grade, were added. In a CEM Mars Xpress system, a set of 24 samples including procedural blanks and 2 soil standard reference reference materials (NIST[1] SRM2710a and SRM2711a, see Section 2.10) was digested in closed vessels at 200°C and held for at least 30 minutes. The digested samples were evaporated to near dryness in the microwave system, using a MicroVap accessory. Samples were then taken up in the microwave in 10.5 ± 0.3 mL 2% HNO_3, at 180°C, prior to analysis by ICP-OES in the School of Geosciences, University of Edinburgh and by ICP-MS in the School of Chemistry, University of Edinburgh.

2.3.4 Procedural blanks

Blanks were run throughout the experiment, which were reaction vessels containing no sample and instead only the reagents used at each step. The blanks were subject to the exact same procedures as the samples. The concentrations of the elements of interest in the procedural blanks was assumed to be possible contamination from the experimental procedure and reagent assay background concentrations. On analysis by ICP-MS (Section 2.5.2) and ICP-OES (Section 2.6.2), values obtained for the procedural blanks - where above analytical detection limits - were subtracted from the concentrations obtained for the rock samples.

---

[1]National Institute of Standards and Technologies

2.4 pH & Alkalinity Measurements

2.4.1 Laboratory pH measurements

pH was measured during the batch experiments for *Captain*, *Cormorant*, *Thistle*, *Field X* and Utah sandstones by drawing 5 mL of fluid from the batch flasks with a disposable sterile syringe (*Cormorant*, *Thistle*, *Field X*) or a pipettor (*Captain*, Utah) and transferring to an acid cleaned vial. The North Sea samples were allowed to cool in air to ~26 - 27°C, while the Utah samples were measured immediately.

The measurements were then taken with a Hanna HI9125 pH meter with attached glass VWR ceramic junction pH electrode, calibrated with Hanna HI7007 (pH 7.01) and HI7004 (pH 4.01) NIST traceable buffer solutions, accurate to $\pm$ 0.01 pH.

Samples were allowed to cool to nearly room temperature since pH is temperature dependent: the samples initially cool very quickly from their experimental temperature (Table 2.6) to ~ 26 - 27°C. During this rapid cooling period, pH values constantly changed and therefore a precise reading was impossible. Furthermore, during this time any dissolved CO_2 may have degassed, affecting the accuracy of results. Nonetheless the data for cooled and degassed samples were used since this is not an uncommon method for pH determination of batch fluids in the peer-reviewed literature[2].

2.4.2 Field pH measurements

The pH and temperature of the water in each spring was measured after sampling by dipping a combined pH and temperature probe into the geyser, connected to a Thermo Scientific Orion 3 Star pH meter, accurate to $\pm$ 0.01 pH and $\pm$ 0.1°C, pre-calibrated at the University of Texas.

2.4.3 Laboratory alkalinity measurements

Alkalinity, as $CaCO_3$, HCO_3^- and CO_3^{2-} in mg/L was measured during the *Captain*, *Cormorant*, *Thistle* and *Field X* batch experiments using a Palintest Photometer 7100, with a claimed accuracy of $\pm$ 5 mg/L. Measurements were taken by crushing a Palintest alkophot 'M' reagent tablet in 10 mL of sample, immediately after removal from the batch flask with a disposable syringe or pipettor and placing in the photometer for an immediate reading. The photometer was calibrated with a blank of 10 mL of NaCl solution of the same concentration as the synthetic batch fluids.

To determine the accuracy and precision of the photometer, a solution of sodium bicarbonate ($NaHCO_3$) was prepared in Milli-Q D.I. water with a concentration of 500 mg/L. The pH and temperature were measured (8.27, 21.1°C), and the alkalinity (as HCO_3^-) calculated with PHREEQC v3.3.3.10424. HCO_3^- was then measured with the photometer and the average of five readings compared with the PHREEQC modelled value. The average photometer value of 582 $\pm$ 33 mg/L compared with the calculated value of 740 mg/L. The measured value therefore had a 2*s* precision of 5.7%, but the average measured value was 21% less than the calculated value. This test was carried out some 2 years after the final North Sea batch experiment and therefore this bias towards lower HCO_3^- values may possibly be because of equipment accuracy degradation over time, use of a different batch of reagent tablets, or an accurate reflection in measurement bias. Recorded values are presented un-corrected for this bias, with uncertainty in the values taken as the 2*s* precision of 5.7%.

Alkalinity measurement using the Palintest method was not included in the Utah sandstone batch experiment method in favour of retaining sample fluids in the batch vessels. With 10 mL required for the analysis, this would have more than doubled the volume of fluid removed from each flask, presenting

---

[2]pH data for Mickler *et al.* (2013) was obtained in this way (Jeimin Lu, University of Texas, personal communication, October 2013).

problems with running out of fluid before the experiment ended and the need to correct measurements for dilution.

2.4.4   Field alkalinity measurements

After sample collection, alkalinity was measured by adding 1.6N HNO_3 to the 40 mL sample collected in the field using a digital titrator, and titrating to an endpoint pH of 4.50 ± 0.02. The starting pH and temperature, and start and end readings on the titrator were recorded, and these data were entered into the USGS online alkalinity calculator using the fixed endpoint method (http://or.water.usgs.gov/alk/) to calculate the alkalinities of each sample.

2.5 Inductively Coupled Plasma Mass Spectroscopy (ICP-MS)

2.5.1 ICP-MS at the Jackson School of Geosciences, University of Texas

Cation concentrations (Ag, Al, As, B, Ba, Bi, Ca, Cd, Co, Cr, Cs, Cu, Fe, K, Li, Mg, Mn, Mo, Na, Ni, P, Pb, Rb, Sb, Se, Si, Sn, Sr, Th, Ti, Tl, U, V, Zn & Zr) of spring samples collected in Utah (Table 2.2) were determined using an Agilent 7500ce ICP-MS at the University of Texas (UT), operated by Dr. Nathan Miller. The instrument was optimised for sensitivity across the atomic mass unit (AMU) range, while minimising oxide production ($< 0.96\%$). The instrument set up provided by Dr. Miller at UT is presented in Table 2.8.

ICP-MS Instrument	Agilent 7500ce ICP-Q-MS
	(Jackson School of Geosciences, University of Texas)
Plasma Conditions	
Nebuliser	PFE microflow with 90 μL/min uptake rate
Nebuliser pump (rps)	0.1
Spray Chamber	Scott-type (quartz) with Peltier cooling (2°C)
Sampling Depth (mm)	8
RF power (W)	1600
RF Matching (V)	1.7
Carrier gas flow (L/min)	1
Make-up gas flow (L/min)	0.25
Cones	Ni
Reaction cell (ORS) modes and masses measured	
He mode (4.5 mL/min)	23, 24, 27, 39, 43, 44, 45, 51, 52, 53, 72, 75
H$_2$ mode (3.7 mL/min)	28, 40, 45, 56, 72, 78
No gas mode	7, 9, 11, 23, 24, 26, 27, 29, 31, 39, 43, 44, 45, 47, 51, 55, 57, 59, 60, 63, 66, 68, 72, 85, 88, 90, 95, 107, 111, 114, 115, 118, 121, 125, 133, 137, 175, 205, 206, 207, 208, 209, 232, 238
Internal stds	9, 45, 72, 115, 125, 175
Detection system	Dual stage (pulse & analog) discrete dynode electron multiplier
Data Acquisition	
Scan mode	Peak hopping
Points across peak	3
Integration per mass (sec)	0.100
Replicates	3

Table 2.8: *Jackson School of Geosciences, University of Texas ICP-MS operating conditions and instrument parameters.*

The analytical method employed an octopole reaction system (ORS), operated in helium (collision-mode) and hydrogen (reaction-mode) for removal of polyatomic interferences. Internal standards, mixed into unknowns via in-run pumping, were used to compensate for instrumental drift. Analytical limits of detection reported by UT, based upon the population of blank 2% HNO$_3$ analyses (n = 10 - 12) interspersed throughout the analytical sequence were typically better than 0.378 μg/L (median = 0.168 μg/L).

Analyte recoveries obtained for 5 replicates of an NIST standard reference material SRM1643e were typically within 2% of certified values. Relative precisions (n = 2 - 5) obtained for these quality control standards were typically within the range 0.04% to 1.16% (median = 0.35%) of replicate averages. Matrix spikes, performed on a randomly selected sample (*Side Seep*), had analyte recoveries of generally better than 97% (median = 100%) indicating that the saline matrices of diluted samples ionised comparable to calibration and quality control standards.

2.5.2 ICP-MS at the School of Chemistry, University of Edinburgh

2.5.2.1 Instrument setup and calibration

Batch fluid samples collected for the *Captain*, *Cormorant*, *Field X*, Utah sandstone, Utah spring samples and SEP experiments were analysed by ICP-MS at the University of Edinburgh for the elements given in Table 2.10 using an Agilent 7500ce (with octopole reaction system), employing an RF forward power of 1540 W, reflected power of 1 W, argon gas flows of 0.82 L/min and 0.2 L/min for carrier and makeup flows, respectively, and nickel skimmer and sample cones, with a Micro mist nebuliser and peristaltic pump providing a solution uptake rate of approximately 1.2 mL/min. The instrument was operated in spectrum multi-tune acquisition mode and three replicate runs per sample were employed, Table 2.10.

Sample	Dilution Factor
Captain	20
Cormorant	30
Field X	100
Utah	10
SEP 1	100
SEP 2	100
SEP 3	100
SEP 4	10
SEP 5	100
SEP 6	5

Table 2.9: *ICP-MS sample dilution factors.*

Calibration was with Merck VI multi-element ICP standard for all metals listed in Table 2.10 with the exception of Hg, which was calibrated with a BDH 'SpectrosoL' ICP-MS standard, and Cs, P, Sb, Si, Sn, Th, Ti and Zr which were calibrated with SPEX Certiprep® or Fisherbrand ICP-MS standards. All standards were made up in the same solution matrix as the samples to be analysed.

ICP-MS Instrument	Agilent 7500ce ICP-Q-MS (School of Chemistry, University of Edinburgh)
Plasma Conditions	
Nebuliser	Micro mist
Nebuliser peristaltic pump (mL/min)	1.2
Spray Chamber	Scott-type (quartz) with Peltier cooling (15°C)
Sampling Depth (mm)	8.4
RF Forward Power (W)	1540
RF Reflected Power (W)	1
RF Matching (V)	1.76
Carrier gas	Ar
Carrier gas flow (L/min)	0.82
Make-up gas flow (L/min)	0.20
Cones	Ni
Calibration standards and masses measured	
Merck VI multi-element	^{7}Li, ^{11}B, ^{23}Na, ^{24}Mg, ^{26}Mg, ^{24}Al, ^{39}K, ^{43}Ca, ^{44}Ca, ^{51}V, ^{52}Cr, ^{53}Cr, ^{55}Mn, ^{56}Fe, ^{57}Fe, ^{59}Co, ^{60}Ni, ^{62}Ni, ^{63}Cu, ^{65}Cu, ^{66}Zn, ^{68}Zn, ^{75}As, ^{82}Se, ^{85}Rb, ^{88}Sr, ^{92}Mo, ^{95}Mo, ^{97}Mo, ^{98}Mo, ^{107}Ag, ^{111}Cd, ^{114}Cd, ^{137}Ba, ^{205}Tl, ^{209}Pb, ^{238}U
Spex Certiprep single element	^{28}Si, ^{29}Si, ^{30}Si, ^{31}P, ^{47}Ti, ^{49}Ti, ^{90}Zr, ^{118}Sn, ^{121}Sb, ^{133}Cs, ^{232}Th
BDH SpectrosoL single element	^{200}Hg, ^{202}Hg
Internal standards (Spex Certiprep)	^{45}Sc, ^{103}Rh, ^{115}In, ^{209}Bi
Data Acquisition	
Scan mode	Spectrum multi-tune
Points across peak	3
Integration per mass (sec)	0.3
Replicates	3

Table 2.10: *School of Chemistry, University of Edinburgh ICP-MS operating conditions and instrument parameters.*

Where the total dissolved solids (TDS) of samples was considered to be > 0.1% then samples were diluted to ensure TDS < 0.1%, using the dilution factors given in Table 2.9. Rather than calculate dilution factors on a sample-by-sample basis, a dilution factor was chosen to apply to all samples analysed for

each run. Data received from the instrument was later corrected for the dilutions.

2.5.2.2 Instrumental limits of detection (LOD)

The instrumental limit of detection (LOD) for each element analysed by ICP-MS was calculated with essentially the same method for all of the analysis outlined above (Section 2.5.2). Blank aliquots of sample matrix and 2% HNO_3 solutions were analysed, and instrumental LOD for each element of interest was calculated as $3s$ of the blanks' ICP-MS counts per second (CPS) divided by the slope of calibration line (Vandecasteele and Block, 1993). LODs calculated for *Captain*, *Cormorant*, *Field X*, Utah Sandstones, and all SEP steps are summarised in Table 2.11. The number of blank samples used in calculating LODs (n) is also given.

If blank aliquots were considered to have anomalously high CPS values compared to other blanks, these were removed from the LOD calculation. An example of this would be for Hg where, due to the difficulty in washing out Hg from the instrument, high concentrations of Hg in the samples analysed prior to the blanks carried through to the blanks. This so-called 'washout' problem is evident as declining concentrations of Hg in blank samples, and so are easy to spot and discard from the LOD calculations, Figure 2.7.
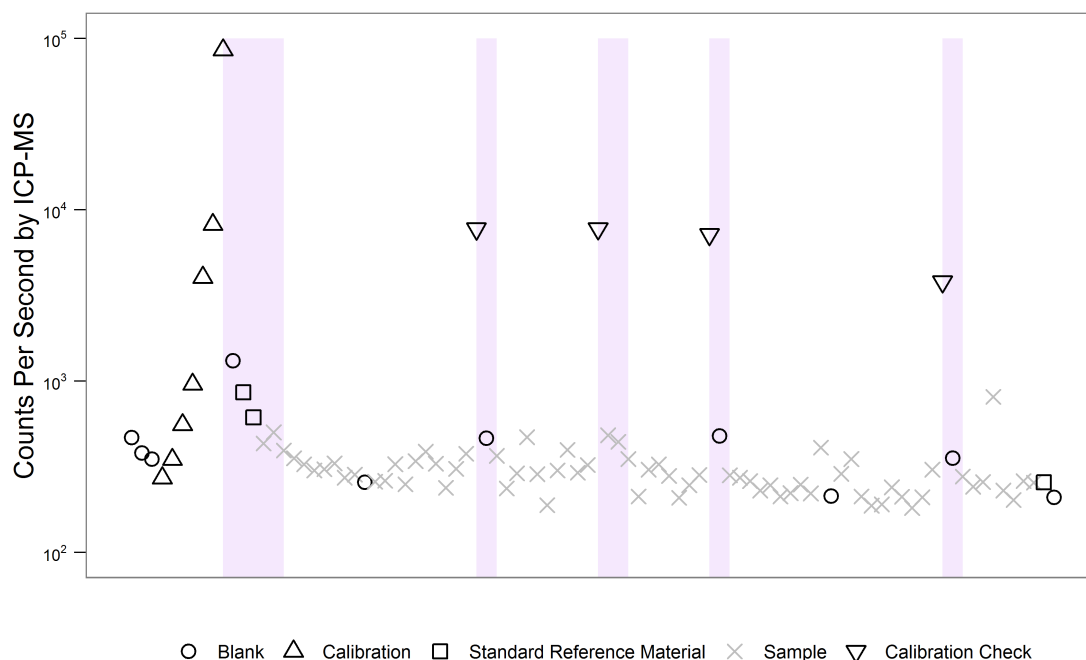
Figure 2.7: *Example of continuous sequence of aliquots analysed by ICP-MS for Hg, units in counts per second on $\log_{10}$ scale. Highlighted areas indicate periods of Hg washout following high concentration Hg samples, with a long washout period particularly following the calibration standards.*

Further examples of outliers would be CPS recorded consistently high across several elements in a blank, where CPS may be a factor of 2 - 40 higher than the other blanks. Removal of outliers in all cases reduced calculated LODs, although on the whole by less than an order of magnitude. The slope of the calibration line, a basic measure of instrument sensitivity (i.e. the greater the slope, the higher the sensitivity), had a greater effect on determining LODs than removal of outliers from blanks.

Where several isotopes for elements were analysed (e.g. ^{56}Fe and ^{57}Fe), the lowest calculated LOD was chosen and the data subsequently used for that element in later chapters.

Element	Captain	n	Cormorant	n	Field X	n	Utah	n	SEP 1	n	SEP 2	n	SEP 3	n	SEP 4	n	SEP 5	n	SEP 6	n
Al	5.02	10					6.22	10	19.1	10	6.98	12	5.61	5*	3.42	19	3.81	12		
As	0.255	10			3.67	11	1.17	10	2.09	10	3.45	12	2.70	19	1.48	19	2.98	12		
Ba	0.377	10			0.182	11	0.191	9	0.552	9	0.141	12	0.964	19	0.303	14	0.109	11		
Ca	130	10			3.92	11	63.0	10	35.4	9	92.5	12	36.2	19	34.2	19	49.0	12		
Cd	0.005	10	0.012	3	0.007	10	0.025	10	0.021	10	0.009	12	0.017	4*	0.154	19	0.028	12	0.008	10
Cr	0.080	10	0.074	6	0.453	11	0.090	10	0.524	10	0.184	12	0.268	19	0.551	19	0.948	12		
Cu	2.87	10			0.697	11	0.100	9	0.325	9	2.63	11	8.79	17	0.425	19	0.177	12		
Fe	1.43	10			1.75	11	0.468	10	1.14	10	5.36	11	1.69	4*	1.24	19	0.769	11		
Hg	0.023	10			0.038	9	0.043	10	0.037	10	0.017	10	0.031	16	0.042	16	0.053	10	0.090	10
K	14.0	10			32.6	11	21.9	10	76.5	9	65.2	12	139	19	25.9	19	133	12		
Li					3.50	11	0.895	8	0.667	10	1.24	12	0.352	19	0.461	19	0.407	12		
Mg	1.14	10			2.71	11	3.36	6	2.99	9	1.56	12	0.887	5*	1.65	19	1.87	12		
Mn	0.066	10			0.151	11	0.062	10	0.344	10	0.079	11	0.120	5*	0.362	19	0.241	12		
Na	119	10							90.4	10					218	19				
Ni	0.041	10			0.220	11	0.171	9	0.462	9	0.098	12	0.174	19	0.219	19	0.093	12		
Pb	0.125	10			0.676	11	0.033	10	0.035	9	0.068	12	0.013	5*	0.180	19	0.063	12		
Ti	0.710	10					2.87	10	0.155	10	0.282	11	0.153	19	0.090	19	0.179	12		
U	0.001	10					0.017	10	0.013	10	0.015	12	0.003	19	0.005	19	0.006	12		
V	0.026	10					0.051	10	0.057	10	0.018	12	0.038	19	0.027	19	0.046	12		
Zn	1.80	10			1.08	11	1.93	10	1.28	8	1.99	12	4.59	19	2.03	19	0.791	11		

Table 2.11: *ICP-MS (School of Chemistry, University of Edinburgh) analytical limits of detection (LOD) for elements of interest (μg/L). n is the number of blank aliquots used to calculate 3s. *LOD calculated using matrix blanks only since 2% HNO_3 blanks were significantly higher counts per second (CPS).*

The LOD values were substituted for any values less than the LODs in the sample data. For the majority of the matrix blanks, concentrations were less than the LODs. Some notable exceptions were Fe in the 1st step of the sequential extraction procedure (SEP), and Cu in the 3rd SEP step, where in both cases the blank concentrations were higher than their LODs by a factor of $\sim$ 10.

Where procedural blanks had values higher than the LODs, then the mean value of procedural blanks above the LOD was subtracted from the concentrations of the samples. Where this subtraction resulted in a negative concentration, this value was replaced with the LOD for that element. Some concentrations, corrected for the blanks, were occasionally much smaller that the LOD.

2.5.2.3 Comparing mercury analysis by ICP-MS and CV-AFS

Field samples were collected for Hg analysis at Green River, Utah, using the recommended method outlined by DECC (Department of Energy & Climate Change, 2014), which is that samples are preserved by 2% v/v H_2SO_4 and 2% v/v $K_2Cr_2O_7$ and analysed by cold vapour atomic fluorescence spectroscopy (CV-AFS). Once returned to the UK, the samples were sent to a commercial laboratory for analysis, as neither University of Texas nor University of Edinburgh were set up for the recommended cold vapour analysis.

The samples were analysed by Scientific Analysis Laboratories (SAL), Manchester, by CV-AFS, and reported all samples to be less than the detection limit of 0.01 μg/L. Archive samples, acidified with 2% v/v HNO_3, collected at Green River for possible cation analysis, were analysed by ICP-MS at the University of Edinburgh for Hg. The LOD of this analysis was 0.02 μg/L, similar to CV-AFS analysis by SAL (0.01 μg/L). During this analysis at Edinburgh, a method was developed for further ICP-MS analysis of samples for Hg, which involved running the Hg standard solution at the end of the analysis to prevent high concentrations of Hg propagating through later samples (see 'washout' problem in Figure 2.7), as well as using adding 2% v/v HCl to the instrument rinses carried out between samples.

Both sets of analyses of Green River spring samples by SAL and the University reported Hg concentrations less than their respective analytical detection limits. Since standard reference materials were not analysed by either method for Hg, neither the accuracy nor precision of these methods was determined.

Given the significant additional expense of CV-AFS analysis by an external lab, and without any indication of its accuracy, the decision was made to continue with samples preserved with 2% HNO_3 and analysed by ICP-MS at the University of Edinburgh, using the amended method described in the previous paragraph. Given that the DECC required instrumental detection limit for Hg is 0.5 μg/L by their recommended method, the method used at Edinburgh at least meets the criteria of being sensitive enough to resolve expected concentrations in waters reacting with North Sea reservoir sandstones. Any future work which included analysis for Hg should consider more detailed investigations into the most accurate Hg determination available, including sample preparation, storage and analysis.

2.6 Inductively Coupled Plasma Optical Emission Spectroscopy (ICP-OES)

2.6.1 ICP-OES at the School of Chemistry, University of Edinburgh

2.6.1.1 Instrument setup and calibration

Samples collected during the *Cormorant* and *Thistle* field batch experiments were analysed by ICP-OES at the School of Chemistry, University of Edinburgh. Cation concentrations (Table 2.12) were determined using a a Perkin Elmer Optima 5300DV, employing an RF forward power of 1400W, with argon gas flows of 15, 0.2 and 0.75 L/min for plasma, auxiliary and nebuliser flows respectively, Table 2.13. An autosampler system with peristaltic pump introduced sample solutions into a Gem Tip cross-Flow nebuliser and Scotts spray chamber at a rate of 1.50 mL/min. The selected wavelengths for each element were analysed in full quant mode (three points per unit wavelength). Three replicate runs per sample were employed. Cd and Cr were mistakenly not included in the analysis of *Cormorant* samples, and were subsequently analysed by ICP-MS (Section 2.5.2).

The instrument was calibrated with Merck IV multi-element ICP standard for the majority of elements, with As, Hg, S, Rb, Sc, Si, Ti and V calibrated using a custom multi-element standard made from Fisherbrand single-element ICP calibration standards. Two sets of standards were made using NaCl solutions of the same salinities as the two experimental fluids (Table 2.6) diluted by a factor of 3 with 2% HNO_3, in order that the ICP-OES calibration was corrected for the matrix of the samples.

Element	Cormorant (µg/L)	n	Thistle (µg/L)	n
Ag	3.91	8	0.814	7
Al	2.27	10	1.64	8
As	9.21	10	6.61	10
Ba	0.041	8	0.042	8
Ca	2.79	8	3.35	8
Cd	-	-	0.145	3
Cr	-	-	0.200	3
Cu	1.22	8	0.547	8
Fe	2.13	8	1.06	9
Hg	1.89	8	2.81	9
K	12.3	8	15.2	9
Li	0.108	8	0.094	9
Mg	0.547	8	4.64	8
Mn	0.236	8	0.068	9
Ni	0.604	10	0.950	9
Pb	2.597	8	4.20	9
S	58.3	8	-	-
Si	3.87	8	4.94	9
Sr	0.110	8	0.043	8
Ti	0.393	10	0.353	9
V	1.03	8	1.26	9
Zn	0.396	8	0.944	8

Table 2.12: *ICP-OES (School of Chemistry) analytical limits of detection for elements of interest. n is the number of blank aliquots used to calculate 3s.*

Samples were diluted by a factor of 3 with 2% HNO_3 to ensure that total dissolved solids (TDS) were sufficiently low prior to introduction to the instrument. Undiluted samples would cause problems with salt precipitation on the instrument cone and in the peristaltic tubing, eventually leading to loss of sensitivity and possible blockages.

2.6.1.2 Instrumental limits of detection (LOD)

Ten blank aliquots each of 16,000 ppm (*Cormorant*) and 23,500 ppm (*Thistle*) experimental NaCl solutions (diluted by a factor of 3 with 2% HNO_3) were analysed for the calculation of the instrumental LOD. Instrumental LOD for each element of interest was calculated as 3s of the blank OES intensity values (n = 10) divided by the slope of calibration line (Vandecasteele and Block, 1993).

A number of the blank intensity values were considered outliers and unrepresentative of blank solution values, being either anomalously high or low for Cu, Hg, Pb and Zn. These blanks were discarded from the LOD calculation for these elements concerned. ICP-OES analytical LOD's are given in Table

ICP-OES Instrument	Perkin Elmer Optima 5300DV ICP-OES
	(School of Chemistry, University of Edinburgh)
Plasma Conditions	
Nebuliser	Gem Tip Cross-Flow
Nebuliser peristaltic pump (mL/min)	1.5
Spray Chamber	Scotts
Sampling Depth (mm)	-3
RF Forward Power (W)	1400
Carrier gas	Ar
Plasma gas flow (L/min)	15
Auxiliary gas flow (L/min)	0.20
Nebuliser gas flow (L/min)	0.75
Cones	
Calibration standards and wavelengths measured	
Merck IV multi-element (nm)	206.204, 213.866, 217, 220.361, 221.657, 231.614, 232.244, 233.527, 238.204, 239.575, 257.612, 259.377, 279.084, 279.482, 285.22, 308.211, 315.892, 317.944, 324.759, 327.406, 328.077, 330.237, 338.299, 393.369, 396.159, 407.791, 455.426, 460.307, 460.733, 610.394, 670.798
Fisherbrand single element (nm)	180.678, 181.983, 188.984, 193.7, 194.168, 212.415, 251.615, 253.655, 270.093, 290.886, 309.31, 310.238, 334.945, 336.116, 357.256, 361.391, 404.656, 766.501, 780.071
Data Acquisition	
Scan mode	Full quantitative
Points across peak	3
Replicates	3

Table 2.13: *School of Chemistry, University of Edinburgh ICP-OES operating conditions and instrument parameters.*

2.12.

2.6.2 ICP-OES at the School of GeoSciences, University of Edinburgh

2.6.2.1 Instrument setup and calibration

Sequential Extraction Procedure (SEP) Step 6 samples prepared by microwave acid digestion (Section 2.3.3) were analysed by ICP-OES at the School of Geosciences, University of Edinburgh. Cation concentrations (Al, As, Ba, Ca, Cd, Cr, Cu, Fe, K, Li, Mg, Mn, Na, Ni, Pb, Ti, U, Zn) were determined using a Varian Vista Pro axial ICP-OES with enhanced sensitivity, using an APEX E desolvation system. Typical sample uptake rates were 400 µL/min. The RF power was set at 1200 W.

The ICP-OES was calibrated for the elements of interest with an in-house multi-element mixture of variable concentrations, using 200 ppm yttrium (Y) and scandium (Sc) solutions as internal standards in a 2% HNO_3 matrix. As was calibrated separately using an ICP tuning solution, also using Y and Sc in 2% HNO_3.

All samples for analysis were prepared with Y as an internal standard and, with the exception of the procedural blanks, were prepared as 25 µL Y solution, 100 µL sample and 2 mL of 2% HNO_3, giving a dilution factor of 21.25. Concentrations reported by the ICP-OES were subsequently corrected for this dilution. Procedural blanks were not diluted as they were expected to be low concentrations, and therefore prepared as 25 µL Y solution and 2 mL sample.

2.6.2.2 Instrumental limits of detection (LOD)

Six blank aliquots of 2% HNO_3 and 1 aliquot of HNO_3 instrument 'rinse' were analysed for the calculation of the instrumental LOD. Instrumental LOD for each element of interest was calculated as 3s of

the blank OES intensity values ($n = 7$) divided by the slope of calibration line (Vandecasteele and Block, 1993), Table 2.14

2% HNO_3 blanks were numbered 1 - 6. Blanks 3 - 6 were analysed after a sample of SiO_2 which turned out to be particularly high in some elements, therefore during the following two acid blanks (3 & 4), Al, Ba, Fe, Sr and Ti were still washing out of the instrument. These two blanks were discarded from the LOD calculation for these elements as concentrations were considered outliers and not deemed representative of blank acid concentrations.

Element	SEP 6 LOD ($\mu g/L$)	n
Al	8.28	5
As	1.41	7
Ba	0.0623	5
Ca	16.0	7
Cd	0.0590	7
Cr	0.585	7
Cu	0.264	7
Fe	6.31	5
K	7.52	7
Li	0.0750	7
Mg	14.6	7
Mn	0.160	7
Na	20.8	7
Ni	0.35	7
Pb	0.412	7
Ti	0.453	5
U	0.164	7
Zn	1.25	7

Table 2.14: *ICP-OES (School of Geosciences) analytical limits of detection for elements of interest. n is the number of 2% HNO_3 aliquots used to calculate 3s.*

2.7   Ion Chromatography

Major cations and anions of water samples were analysed on two Dionex ICS-1100 Ion Chromatography systems equipped with an AS-AP auto sampler at the Bureau of Economic Geology, University of Texas (UT) laboratories. Samples were diluted by a factor of 10 after collection, in order that Ca and SO_4^{2-} concentrations did not exceed 500 mg/L.

Repeat analysis of calibration standards ($n = 4$) gives the precision of the instrument, $1s$, as between 0.08% and 5.83% (median = 0.65%). Accuracy data was not provided by UT for the IC analysis. Cation concentration data obtained from ICP-MS and IC at UT were compared for 5 elements (Ca, K, Li, Mg, Na) to determine the accuracies of the methods employed. The comparison is shown in Figure 2.8.

It can be seen that once corrected for dilutions, cross-plotted ICP-MS and IC values have a good 1:1 relationship and therefore confirm the accuracy of both analyses. There are two obvious discrepancies: firstly, Ca concentrations for *Champagne Geyser*, Figure 2.8 are much higher by ICP-MS than IC. Secondly, *Little Bubbling Spring* ICP-MS data for all the elements considered here are all higher than the IC data. This is due to a discrepancy in diluting this particular sample and has been corrected for in the ICP-MS data for this spring.
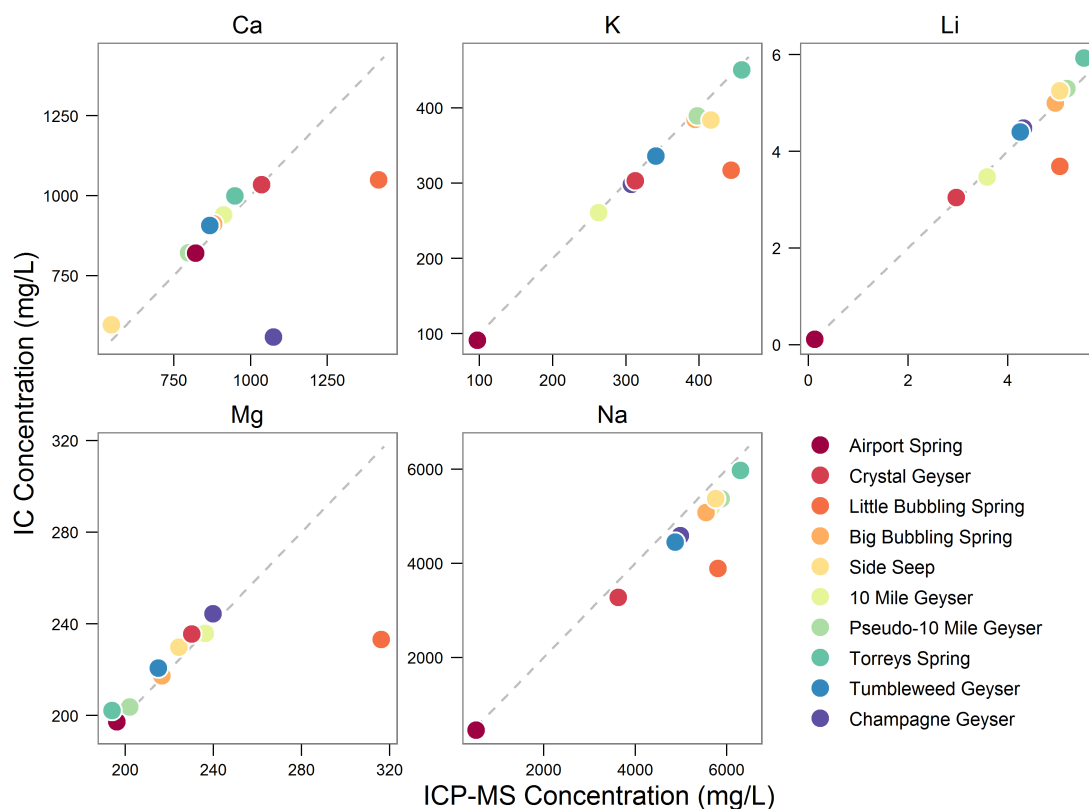
Figure 2.8: *Comparison concentration data for 10 spring water samples, obtained from of ICP-MS and IC analysis at the University of Texas. Error bars plot smaller than data points. Dotted grey line is 1:1; concentrations will plot on or close to this line when analyses are in good agreement. Little Bubbling Spring data consistently higher in ICP-MS data due to a dilution error; a further dilution correction was applied for this spring in all ICP-MS data. Discrepancy in Champagne Ca data of unknown cause.*

2.8 X-Ray Diffraction (XRD)

Samples of *Cormorant*, *Thistle*, *Field X* and Utah outcrop samples *S1 - S5* were prepared for XRD by grinding with an agate mortar and pestle, transferring to a plastic disk and bulk mineral analysis was carried out using a Bruker D8-Advance X-ray Diffractometer, employing a 2-theta (2θ) configuration, with X-rays generated by a Cu-anode X-ray tube operating at 40 kV, and a tube current of 40 mA. *Field X* samples had an additional preparatory step of heating overnight at 400°C to volatise off hydrocarbons prior to any other preparation for XRD or XRF (Section 2.9). 1.51% and 1.48% of sample mass (presumed hydrocarbons) was lost for *Field X* samples *8518* and *8579*, respectively, following overnight heating.

Diffracted X-rays were detected using a Sol-X energy dispersive detector, scanning from 2° to 60° 2θ at a scan rate of 0.01°/second and the resultant diffractograms compared with the 2008 issue of the International Centre for Diffraction Data (ICDD) diffractogram database library using the EVA analysis package. The detection limit for crystalline phases is approximately 1 wt.%.

XRD analysis had already been carried out for *Captain* samples by a former University of Edinburgh masters student and so these data were used (Antonelli, 2010).

2.9   X-Ray Fluorescence (XRF)

Major (Al, Ca, Fe, K, Mg, Mn, Na, P, Si, Ti) and trace (Ba, Cr, Cu, Ni, Pb, Rb, Sc, Sr, Th, U, V, Zn) element analysis by XRF was performed for *Cormorant*, *Thistle* and *Field X* samples by a Philips PW2404 wavelength-dispersive, sequential X-Ray fluorescence spectrometer fitted with an Rh anode end-window X-Ray tube.

For major element analysis, the samples were dried in an oven at 110°C for 2 hours. 1 g of dried sample was then weighed and Spectroflux® added to the sample in the ratio 5:1. The sample and flux were then heated at 1100°C for 20 minutes and the resulting molten mixture cast on a hotplate at around 220°C and flattened with an aluminium plunger to form a glass disk for analysis by the XRF spectrometer. For trace element analysis, a pressed-powder disk of sample was formed in a pressurised tungsten carbide mould at 8 tonnes pressure for 3 minutes and analysed with the spectrometer.

2.10   Analytical Uncertainties in Cation Determination

In order to assess the accuracy and precision of the analytical techniques used to determine concentrations of elements in experimental fluids, repeat analysis of aliquots of standard reference materials (SRMs) with known element concentrations was carried out. Two types of SRMs were used: water and soil. The water SRMs were not part of the experimental method and used only to check the calibration and set up of the ICP-MS and ICP-OES instruments for analysis. The soil SRMs were used during the final whole rock digestion step in the sequential extraction procedure (SEP).

The water SRMs therefore determine whether there are any analytical biases present in the instrumental analysis affecting accuracy, as well as determining the precision of the instrument. Both analytical accuracy and precision are dependent on the elements analysed due to a number of factors including, but not limited to, element stability, sample build-up/washout in instrument, ionisation efficiency, and interference. The water SRMs used were National Institute of Standards and Technologies (NIST) SRM1643e and SRM1640a, and National Research Council Canada (NRC) SLRS-5. The total number of analyses (n) for each SRM was 7 - 17 (SRM1643e), 2 - 21 (1640a) and 5 (SLRS-5).

The soil SRMs were used to check the accuracy of the whole rock SEP step (Step 6), and involved the weighing of soils NIST SRM2710a and SRM2711a for microwave acid digestion (see Section 2.3.3 for detailed method). Three samples of each were used.

Accuracy for the SEP step, and ICP-MS and ICP-OES analysis was determined by analysing aliquots of the SRMs and comparing the mean values ($\bar{x}$) obtained for each element by these methods with the certified mean values supplied with the SRMs. Bias, a measurement of accuracy, is then calculated as a percentage difference between the means. The larger the bias (positive or negative) the more inaccurate the analysis or method. However, in order to determine whether a large (or small) bias is statistically significant in terms of deviation from the 'true' certified value, a t-test was applied for each analysis. The bias and t-test calculations are as described in Gill *et al.* (1997), using a 2-sided test at the 95% confidence interval. Calculated t values exceeding the 95% confidence interval, based on t values given in Gill *et al.* (1997), represent a statistically significant bias in either sample analysis or SEP method.

Precision is simply calculated as 1 standard deviation (s) of the mean of the analysed SRM values. The mean certified and analysed values for each element analysed, together with the precision, biases, and significance test results are given in Tables 2.15 and 2.16 for all the SRMs used.

Accuracy varies between water SMRs and anlytical technique. ICP-MS analysis of SRM1643e is better than ICP-OES, for example, with only Cd determination considered to have a statistical bias to lower values than the SRM, compared with statistically significant biases for 10 of the 16 elements analysed by ICP-OES. Biases are particularly strong for Cd, Cu, Fe and V, Table 2.15. 8 out of 18 elements for SRM1640a analysed by ICP-MS, and 6 out of 7 elements for SLRS-5 show statistically significant biases. However, for SRM1643e, SRM1640a and SLRS-5 there is no apparent consistently high/low bias, as demonstrated by Figure 2.9, which plots certified SRM mean values against the mean analysed values for each element analysed, for each analytical technique. Comparing in this way, plotted data should appear as a 1:1 relationship on a $\log_{10}$ scale, within the precision of the analysis. Most data appears in this way, Figure 2.9, however the significant biases of ICP-OES analysis for SRM1643e are visually apparent.

The ICP-OES and ICP-MS were calibrated for samples with high total dissolved solids (TDS, i.e. > 0.1%), and most often for NaCl solutions. Given that the water SRMs are fresh/spring waters and therefore a different solution matrix than the calibrations, it is unsurprising that, statistically, the analysis exhibits significant bias for many elements. The comparison, therefore, between high-TDS calibrated instruments and the low-TDS SRMs is therefore considered to be quite good, particularly with reference to Figure 2.9.

SRM[†]	1643e*					1643e*					1640a*				
Technique:	Perkin Elmer Optima 5300DV ICP-OES					Agilent 7500ce ICP-MS					Agilent 7500ce ICP-MS				
Samples:	Batch: Cormorant, Thistle					Batch: Captain, Field X					Batch: Utah; SEP Step 1-6: All; Bulk: Utah				
	Certified	$\overline{x}$	s	Bias (%)	95% CL	Certified	$\overline{x}$	s	Bias (%)	95% CL	Certified	$\overline{x}$	s	Bias (%)	95% CL
Al	142	159	8	12.2	Y	142	133	20	-6.1	N	53.0	47.2	13.9	-11.0	N
As						60.5	61.3	9.0	1.4	N	8.08	10.49	4.85	29.9	Y
Ba	544	536	12	-1.6	N	544	535	23	-1.7	N	152	152	10	0.0	N
Ca	32000	30668	678	-4.2	Y	32000	30259	2858	-5.4	N	5570	7299	925	31.0	Y
Cd	6.57	9.80	0.44	49.3	Y	6.57	6.26	0.36	-4.6	Y	3.99	3.27	0.67	-18.2	Y
Cr	20.4	22.0	2.5	7.8	N	20.4	21.9	3.7	7.3	N	40.5	41.7	5.3	3.0	N
Cu	22.8	36.5	6.6	60.2	Y	22.8	24.0	2.2	5.3	N	85.8	106.7	49.7	24.4	N
Fe	98.1	255	35	160.4	Y	98.1	100.4	15.1	2.4	N	36.8	33.3	8.2	-9.4	N
Hg															
K	2034	1593	125	-21.7	Y	2034	2001	206	-1.6	N	575	619	207	7.7	N
Li	17.4	18.7	0.7	7.4	Y	17.4	26.6	6.6	52.6	N					
Mg	8037	8001	167	-0.4	N	8037	7718	813	-4.0	N	1050	1123	97	7.0	Y
Mn	40.0	39.7	1.1	-0.7	N	40.0	40.4	3.7	1.0	N	40.4	39.1	2.4	-3.2	Y
Na											3112	3184	100	2.3	N
Ni	62.4	65.5	4.2	4.9	N	62.4	62.5	2.8	0.1	N	25.3	27.2	8.2	7.4	N
Pb	19.6	22.2	12.2	13.1	N	19.6	19.5	1.7	-0.5	N	12.1	11.0	1.3	-9.0	Y
Sr	323	302	6	-6.4	Y						126	112	1	-11.3	Y
Ti															
U											25.4	22.6	2.3	-10.7	Y
V	37.9	64.7	4.2	70.9	Y	37.9	37.7	3.6	-0.4	N	15.1	15.0	1.4	-0.4	N
Zn	78.5	85.9	4.3	9.5	Y	78.5	84.4	13.4	7.5	N	55.6	56.8	16.7	2.0	N

Table 2.15: *Analytical precision and bias reporting for ICP-OES and ICP-MS techniques at the University of Edinburgh, Part I. Concentration values are in μg/L. Certified = published mean values for the Standard Reference Materials listed; $\overline{x}$ = mean values of analysed samples; s = standard deviation of analysed samples, representing analytical precision; Bias (%) = the difference between Certified and $\overline{x}$, as %; 95% CL = assessment of statistical significance of bias based on a 2 tailed t-test comparing, based on n - 1 samples at the 95% confidence limit, where Y represents statistically significant bias. † Standard Reference Material. * SRM supplied by National Institute of Standards and Technologies (NIST).*

SRM[†]	SLRS-5**					2710a*					2711a*				
Technique: Samples:	Varian Vista Pro Axial ICP-OES SEP Step 6 & Bulk: Captain, Cormorant, Thistle					Varian Vista Pro Axial ICP-OES Bulk: 2710a					Varian Vista Pro Axial ICP-OES Bulk: 2711a				
	Certified	$\bar{x}$	s	Bias (%)	95% CL	Certified $\bar{x}$	Sample $\bar{x}$	Sample s	Bias (%)	95% CL	Certified $\bar{x}$	Sample $\bar{x}$	Sample s	Bias (%)	95% CL
Al						2279	2234	108	-2.0	N	2522	2119	93	-16.0	Y
As						59.0	57.7	2.1	-2.2	N	4.02	3.85	0.45	-4.0	N
Ba	14	15.7	0.1	12.4	Y	30.3	23.7	1.2	-21.9	Y	27.4	19.4	0.9	-29.4	Y
Ca	10500	10688	56	1.8	Y										
Cd						0.471	0.450	0.025	-4.5	N	2.03	1.97	0.25	-2.9	N
Cr											1.96	1.76	0.15	-10.2	N
Cu	17.4	19.2	0.1	10.1	Y	131	124	6	-5.2	N	5.25	5.19	0.30	-1.3	N
Fe						1654	1813	75	9.6	N	1058	1247	108	17.8	N
Hg						0.378	0.102	0.004	-73.1	Y	0.278	0.031	0.005	-88.9	Y
K	839	930	18	10.8	Y	831	898	26	8.0	N	950	968	25	1.9	N
Li															
Mg	2540	2684	12	5.7	Y	281	255	13	-9.2	N	402	314	12	-21.7	Y
Mn						82.0	80.5	3.5	-1.8	N	25.3	24.1	2.0	-5.0	N
Na	5380	5397	56	0.3	N										
Ni											0.814	0.844	0.080	3.7	N
Pb						211	208	9	-1.8	N	52.5	52.6	5.0	0.1	N
Sr	53.6	52.9	0.3	-1.3	Y	9.77	9.45	0.46	-3.3	N	9.08	7.26	0.42	-20.1	Y
Ti						119.11	121.00	4.67	1.6	N	118.98	125.26	8.60	5.3	N
U						0.349	2.158	0.108	518.4	Y	0.113	1.481	0.069	1210.9	Y
V															
Zn						160	162	6	1.3	N	15.5	16.2	2.3	4.5	N

Table 2.16: *Analytical precision and bias reporting for ICP-OES and ICP-MS techniques at the University of Edinburgh, Part II. Concentration values are in µg/L. Certified = published mean values for the Standard Reference Materials listed; $\bar{x}$ = mean values of analysed samples; s = standard deviation of analysed samples, representing analytical precision; Bias (%) = the difference between Certified and $\bar{x}$, as %; 95% CL = assessment of statistical significance of bias based on a 2 tailed t-test comparing, based on n - 1 samples at the 95% confidence limit, where Y represents statistically significant bias. *SRM supplied by National Institute of Standards and Technologies (NIST). **SRM supplied by National Research Council Canada (NRC).*
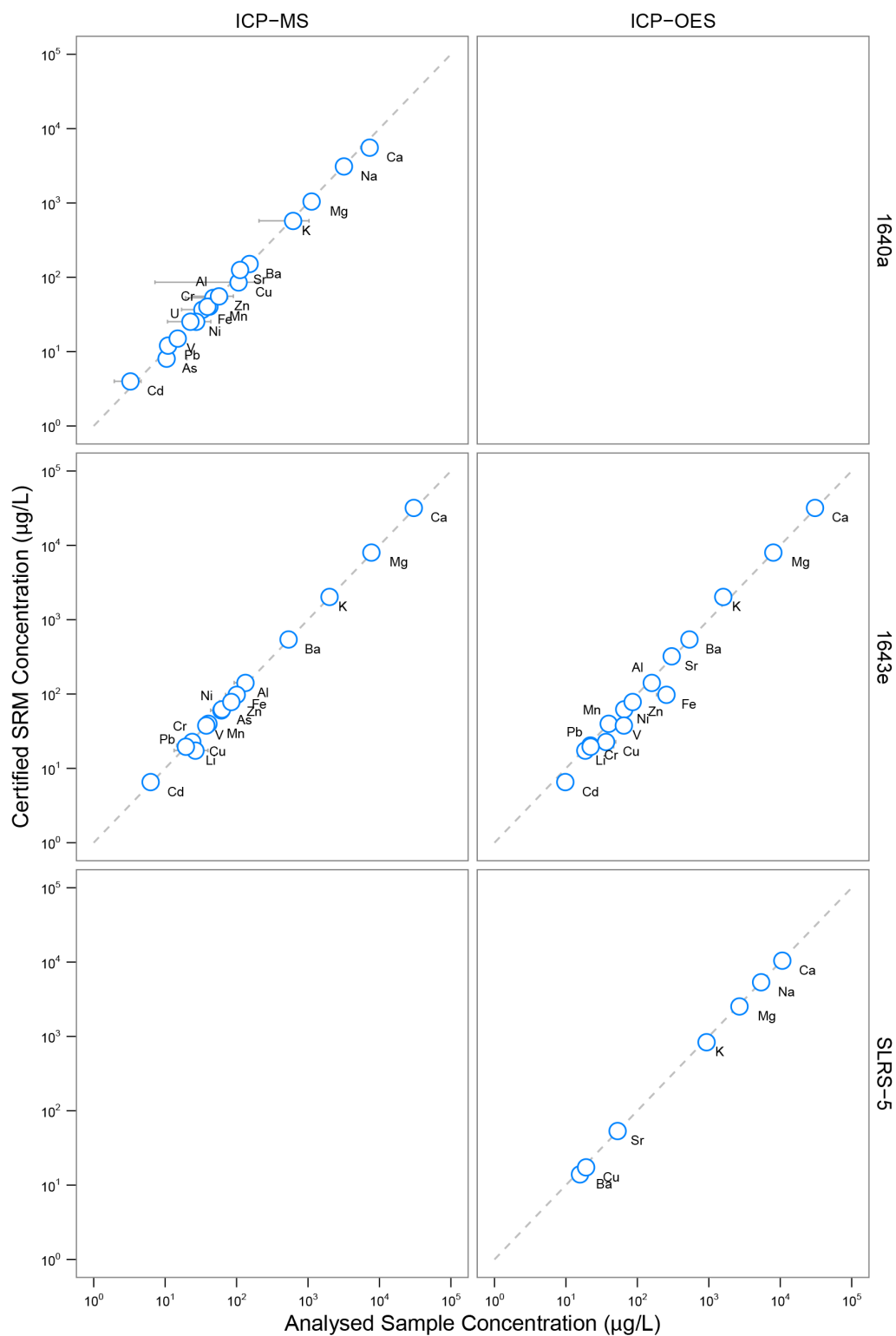
Figure 2.9: *Comparison of Standard Reference Material (SRM) mean concentration values (y-axis, $\log_{10}$ scale) for National Institute of Standards and Technologies (NIST) SRM 1640a, SRM 1643e and National Research Council Canada (NRC) SRM SLRS-5 with mean concentration values of repeat analysis by ICP-OES and ICP-MS at the University of Edinburgh (x-axis, $\log_{10}$ scale). Error bars are 2s from the mean. Dashed grey line represents 1:1 relationship, therefore more accurate analysis are closer to the line. Data and statistical significance of accuracy are provided in Tables 2.15 & 2.16.*

Since the accuracies are considered acceptable due to the mismatch between calibration and SRM matrices, data were not rejected based on the statistical test. However, large biases should be noted when evaluating the experimental data further. In future work, a saline standard would be more appropriate to use, such as the High Purity Standard CRM-SW which has a salinity of approximately 32,000 mg/L, comparable to seawater. This standard also includes Hg, which was not present in SRMs 1640a, 1643e or SLRS-5.

Lowest precision was noted for the SRM1640a samples analysed, since this SRM was used during SEP sample analysis and the SEP steps consisted a wide variety of matrices, which were calibrated for over a period of several sample runs. The precision (and accuracy) for these samples is therefore an aggregate of several very different calibrations.

The accuracy of the whole rock dissolution step, as determined by running SRM2710a and SRM2711a through the method and analysing the 3 repeat aliquots for each, is generally good. Hg was expected to have poor accuracy, due to the element volatising during the digestion and the results of the bias and t-test assessment bear this out. Concentrations of Hg are significantly lower than the reference materials, Figure 2.10. The SRM concentrations were low anyway, which can strongly influence analytical bias since determining the analytical signal from noise becomes more difficult.
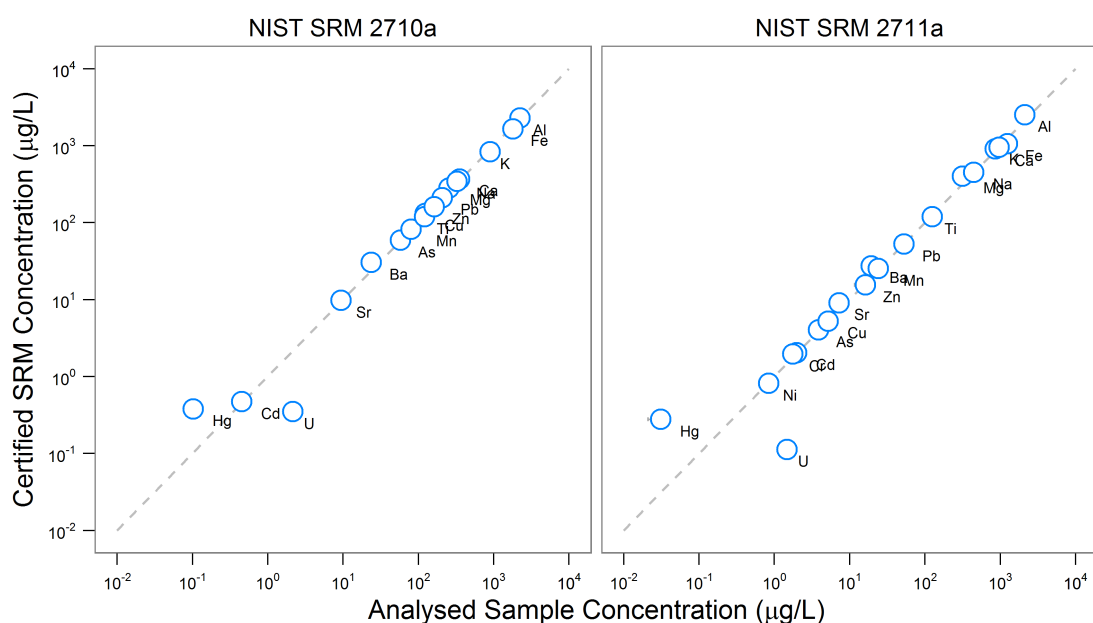
Figure 2.10: *Comparison of Standard Reference Material (SRM) mean concentration values (y-axis, $\log_{10}$ scale) for National Institute of Standards and Technologies (NIST) SRM 2710a and 2711a with mean concentration values of repeat analysis by ICP-OES and ICP-MS at the University of Edinburgh (x-axis, $\log_{10}$ scale). Sample Hg concentrations measured by ICP-MS, all other metals by ICP-OES. Error bars are 2s from the mean. Dashed grey line represents 1:1 relationship, therefore more accurate analysis are closer to the line. Data and statistical significance of accuracy are provided in Table 2.16.*

Error bars on batch experiment data presented in Chapters 3 and 4 (i.e. precision) were taken as two standard deviations ($\pm 2s$) of the SRM means, as a percentage, and depending on the relevant SRM for the samples analysed. The calculated $2s$ % for each batch experiment carried out are presented in Table 2.17. Where an element was analysed for, but no value was present in the SRM, the mean $2s$ value of the other elements was used.

| SRM[†]: | SRM1643e | | SRM1640a |
| Batch Experiment: | Cormorant, Thistle | Captain, Field X | Utah |
	2s (%)	2s (%)	2s (%)
Al	10.0	30.5	33.8
As		29.4	33.8
Ba	4.4	8.6	8.3
Ca	4.4	18.9	20.3
Cd	9.0	11.6	32.6
Cr	23.0	33.5	10.9
Cu	36.4	18.2	4.7
Fe	27.3	30.2	40.7
Hg	18.6*	23.0*	18.0*
K	15.7	20.6	37.6
Li	7.4	49.7	18.0*
Mg	4.2	21.1	11.0
Mn	5.5	18.2	9.0
Na			5.6
Ni	12.7	9.1	13.2
Pb	110.0	17.7	17.4
Sr	4.0		1.0
Ti		23.0*	
U			8.5
V	13.1	18.9	2.4
Zn	10.1	31.6	33.7

Table 2.17: *Analytical uncertainties of batch experiment fluid samples analysed by ICP-OES and ICP-MS, taken as 2s (%) of the mean of repeat analysis of standard reference materials.* [†] *Standard Reference Material, supplied by National Institute of Standards and Technologies (NIST).* *calculated as mean of 2s of other elements.*

2.10.1 Other sources of uncertainty

Analytical uncertainty (accuracy and precision) account for the large majority of error in reported values. Uncertainties due to the experimental methods were estimated, but considered small enough to, effectively, have negligible detectable effect on experimental results for cation analysis.

The experimental sources of error essentially comprise of experimental solid sample masses, and pipetted volumes of reagents and samples. While not every measurement can be checked for accuracy and precision, a general estimate of accuracy and precision can be made from limited data. Samples were weighed precisely prior to beginning the sequential extraction experiments and the resulting supernatants from each step were diluted gravimetrically. This meant that fluid weights in the dilutions (and, hence, volumes) were recorded.

Pipetting accuracy can be determined by comparing the volume set on the pipettor with the pipetted volume, as measured by taking the mass of pipetted fluid and assuming a fluid density of 1kg/L. Where these data were available (525 samples), pipetting accuracy is estimated to have a mean bias of 3.15%, with mean precision of $\pm$ 0.44%. All solid and fluid sample masses were measured on internally calibrated balances with quoted accuracies to at least $\pm$ 0.0001 g. The mean precision of 41 solid samples was $\pm$ 0.25%.

These uncertainties are therefore very small, with a combined uncertainty of less than 1% and a small positive bias.

2.11 Other Calculations

2.11.1 Calculating SEP released mass

Using the blank corrected concentrations, which are in µg/L (except Ca, in mg/L), the mass in µg (Ca, mg) was calculated by multiplying the concentration by the volume of extractant used i.e. 0.008 L (8 mL). Then, to express the mass released as mass of element per mass of solid sample, the mass in µg (Ca, mg) was divided by the weighed mass (g) of sample used in each extraction. This then gave a value of each element in each procedural repeat in µg/g, with Ca at this stage converted to µg. Three repeats of each sample were carried out, so the mean and $1s$ of each element was calculated, and the $1s$ used as the uncertainty in the values for the purposes of plotting error bars.

2.11.2 Total SEP digestion error

Determination of whole rock (bulk) concentrations of *Captain*, *Cormorant*, *Thistle* and Utah (*S1 - S5*) samples was carried out on only one sample of each. The precision of the values obtained was calculated from the average variation of the NIST soil standard reference materials (SRMs), Section 2.10. Three repeats each of the two NIST soil SRMs were analysed, with the mean $2s$ calculated as a percentage for each SRM based on the elements analysed. This percent uncertainty was then applied to the bulk concentration to give two standard deviation ($2s$) precision.

Li was one element analysed for throughout the extractions, but does not have a certified value in either SRMs. Therefore the percentage uncertainty was calculated by simply taking the mean of the $2s$ of the other elements. Two standard deviations ranged from 5.4% (K) to 15.4% (As), with the mean being 11.2%.

North Sea Results & Discussion

3.1   Introduction

The following chapter describes the data collected for UK North Sea sandstones for the *Captain*, *Cormorant*, *Thistle* and *Field X* fields, using the methods described in the preceding Methods chapter (Chapter 2). Following data presentation, the data is analysed and conclusions drawn here within the chapter. CO_2-water-rock batch experiments were used to determine concentrations of a suite of major elements and trace metals which could be leached from these sandstones. A sequential extraction procedure (SEP) was conducted on *Captain*, *Cormorant* and *Thistle* samples to determine the distributions within these sandstones of trace metals which could be leached from various mineral phases.

Data obtained for these experiments include: mineralogy by X-ray diffraction (XRD), batch fluid pH, batch fluid alkalinity, and cation concentrations by Inductively Coupled Plasma Mass Spectroscopy (ICP-MS) and Inductively Coupled Plasma Optical Emission Spectroscopy (ICP-OES) for batch experiments and the SEP, and whole rock composition.

The focus of the data analysis is the mobilisation of the suite of 8 trace metals of interest (As, Cd, Cr, Cu, Hg, Ni, Pb, Zn), with major cations such as Ca and Mg used as potential fingerprints for mobilisation mechanisms. These data are combined with the SEP to assess how predictable trace metal concentrations are, based on information on their distribution in 'mobile' phases of the rocks. Simple geochemical modelling was also carried out using PHREEQC to aid with data interpretation. The chapter conclusions are summarised on pg. 120, with overall thesis conclusions found in Chapter 6, pg. 199.

3.2 Captain Bulk Analysis

3.2.1 X-ray diffraction

The results of X-ray diffraction (XRD) analysis carried out on *Captain* samples *SA7* and *SA10* (Section 2.8) are given in Table 3.1, as the mineral assemblage by weight % (wt.%). Values < 1 wt.% are trace concentrations and are considered semi-quantitative only, therefore their values should not be taken as accurate but indicative only of their presence in the sample.

Mineral	Type	Captain SA7 wt.%	±	Captain SA10 wt.%	±
Halite	Water Sol	2.2	0.1	-	-
Calcite	Carbonate	1.6	0.4	0.37	0.06
Anatase	Oxide	-	-	0.9	0.1
Corundum	Oxide	-	-	0.66	0.09
Albite	Silicate	2.0	0.3	0.2	0.2
Anorthite		-	-	1.0	0.2
Chlorite		0.3	0.3	3.0	0.5
Illite		3.3	0.5	2.1	0.5
Kaolinite		2.8	0.6	0.9	0.2
Microcline		6.5	0.4	2.8	0.3
Orthoclase		-	-	0.4	0.2
Quartz		81	1.0	88	1

Table 3.1: *Results of XRD of Captain samples SA7 and SA10 as wt.% of mineral. Type refers to the mineral types targeted by the sequential extraction procedure (Section 2.3.2). - Not detected in sample.*

The minerals identified in samples *SA7* and *SA10* have been broadly grouped in Table 3.1 by mineral type, as per the SEP method outlined in Section 2.3.2 noting, however, that the SEP oxide step targets only Fe and Mn oxides, therefore corundum (Al_2O_3) and anatase (TiO_2) would not be affected by this step of the SEP. Summing the values of the grouped minerals and plotting them as a bar plot produces Figure 3.1.
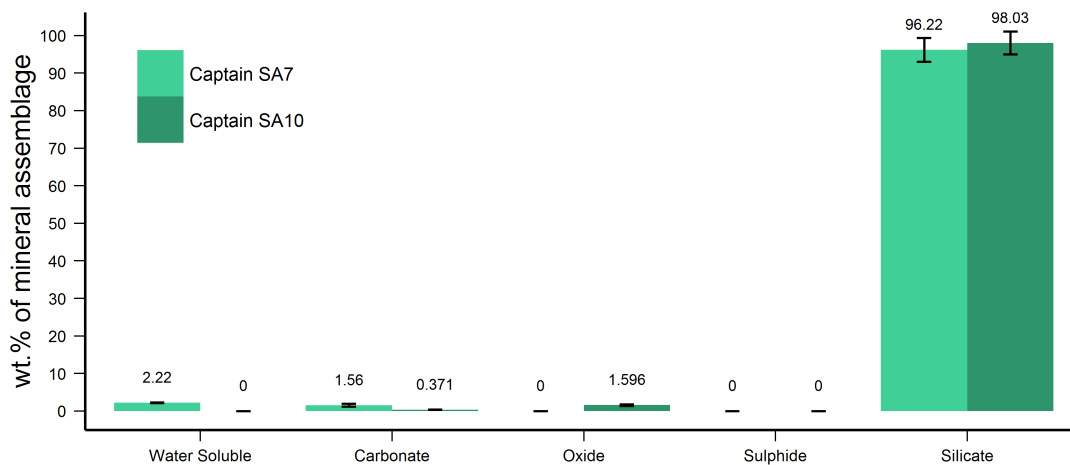
Figure 3.1: *Results of XRD analysis of Captain samples SA7 and SA10 grouped by mineral type, as wt.% of mineral. Summed values are given above each bar.*

Silicate minerals dominate the *Captain* samples, with *SA7* and *SA10* containing essentially the same silicate content, within error, Figure 3.1. Clays and feldspars make up 15 ± 2 wt.% of silicates in *SA7*, and 10 ± 2 wt.% in *SA10*. Some 3.8 ± 0.5 wt.% of *SA7* is made up of halite (likely residual from pore fluids at the time of coring) and calcite. No oxides were detected in *SA7*, however the oxides anatase and

corundum account for ~ 1.6 ± 0.2 wt.% of *SA10*.

3.2.2 Microwave digestion

Bulk chemical analysis was carried out by complete dissolution of sample *SA7* (insufficient *SA10* material) by microwave acid digestion, Section 2.3.3. The resulting solution was analysed by Inductively Coupled Plasma Optical Emission Spectroscopy (ICP-OES) for all elements listed in Table 3.2, except Cd and Hg which were analysed by Inductively Coupled Plasma Mass Spectroscopy (ICP-MS). The results of the bulk chemical analysis are given in Table 3.2 as parts per million (ppm) of each element analysed. Due to the microwave digestion method employed, Si volatises as hexafluorosilicic acid and therefore Si was not analysed for.

The dominant elements in *SA7* are Al and K, followed by Na. These are likely predominately the result of the presence of microcline ($KAlSi_3O_8$), albite ($NaAlSi_3O_8$) and kaolinite ($Al_2Si_2O_5(OH)_4$), Table 3.1. Ca is also a present in significant quantities due to the presence of calcite ($CaCO_3$).

Of the 8 trace metals of interest, concentrations are generally < 10 ppm, with Cr and Zn being the (slight) exceptions. Cadmium concentrations are very low at 0.029 ppm (29 ppb).

Element	ppm	$\pm$
Al	20,000	2,000
As	4.3	0.7
Ba	640	60
Ca	5,600	800
Cd[†]	0.029	0.001
Cr	24	3
Cu	7.8	0.8
Fe	5,400	700
Hg[†]	5.9	1.2
K	14,100	800
Li	14	2
Mg	940	80
Mn	54	7
Na	6,200	500
Ni	5.9	0.7
Pb	6.6	0.9
Ti	1,500	200
U	7.5	0.7
Zn	16	2

Table 3.2: *Concentration data (ppm) for microwave acid digestion and analysis by ICP-OES ([†]ICP-MS) for Captain sample SA7. Uncertainties are 2s of the mean of repeat analysis (n = 3).*

3.3 Captain Batch Reaction Experiments

3.3.1 pH

pH was measured throughout the experiment, on days 1 - 7, 9 - 11, 13, 14, 16, 22 & 30. The instrument used to measure pH was changed on day 9 to a more suitable and accurate type (Appendix A), indicated by the vertical dashed line in Figure 3.2. Values recorded from this point on are more accurate and preceding values should be interpreted with caution. The days on which the CO_2 bottle was replaced due to running out of CO_2 (days 3, 11, 22, 26) are indicated by the vertical dotted lines, Figure 3.2.

After the change in pH meter, the data indicate that the addition of CO_2 to the flasks overall has the effect of decreasing pH with respect to the controls (no bubbled CO_2), as would be expected. pH values in the Blank, *SA7* and *SA10* flasks which did not have CO_2 added are generally higher than those flasks with bubbled CO_2, although by the end of the experiment pH in the *SA7* and *SA10* control flasks are lower than those with rock, Figure 3.2. pH values in the flasks containing rock samples, regardless of whether they have CO_2 added, are consistently higher than the two Blank controls which have no rock samples. This is likely due to pH buffering by mineral dissolution, Equations 1.4 & 1.5 (Introduction).

Modelled pH values using PHREEQC v3.3.3.10424 are shown on Figure 3.2, using the experimental conditions given in Table 2.6 (Methods) and the carbonate quantities obtained by XRD in Table 3.1. The saturation indices for CO_2 were taken as the $\log_{10}$ of 400 ppm atmospheric CO_2 (controls) and 1.4 bar (bubbled CO_2). The model included only calcite for simplicity and because calcite was considered the most reactive mineral to CO_2 in the composition of the Captain samples. The PHREEQC model output gives equilibrium conditions, and so are unlikely to be consistent with the kinetic system in batch experiment, which is far from equilibrium, at least initially. However, modelled values give an envelope of values within which experimental data may fit, to aid interpretation.

Examining the more reliable pH data from day 9 onwards, there is a good fit with the modelled pH for the control +CO_2 flask, although instrument drift may account for later values in the experiment differing from the model. This gives some confidence that the bubbling of CO_2 is sufficient to dissolve in the saline batch fluids and reduce pH at this pressure.

Modelling the effect of calcite in the system for *SA7* and *SA10* raises the equilibrium pH and brackets the experimental data for these samples. The pH values for the +CO_2 experiments are higher than the modelled equilibrium pH with calcite, indicating firstly that pH is controlled by the buffering capacity of the rock at this stage of the CO_2-brine-rock interaction, and secondly that calcite alone is not responsible for all of the pH buffering. Other mineral dissolution, such as that of silica, feldspars and clays, as well as sorption/desorption from mineral surfaces are most likely contributing to buffering within the complex system of the batch experiment.

The effect of running out of CO_2 is noticeable only at day 11, where an increase of $\sim$ 0.80 pH is observed in both *SA7* and *SA10* flasks with CO_2 added, although this is probably only noticeable due to a lack of data at later stages of the experiment. This would also indicate mineral buffering of pH, which has a stronger effect without the addition of CO_2. pH values for the flasks without CO_2 added are largely constant throughout the experiment, however flasks with *SA7* and *SA10* samples show an increase in pH of $\sim$ 2 pH units between days 13 and 30, resulting in final pH values above the *SA7* and *SA10* control flasks without added CO_2. This is possibly related to replacing the CO_2 bottle twice during this period, allowing mineral buffering to dominate control on pH.
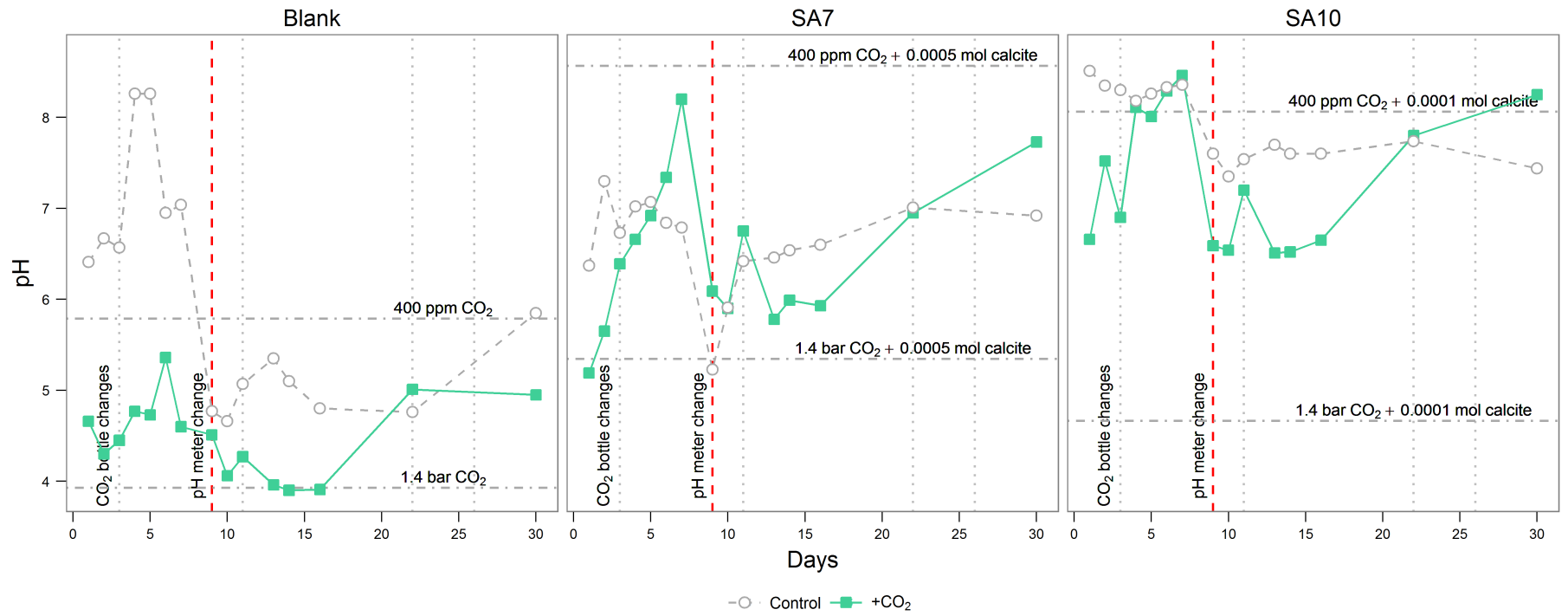
Figure 3.2: *pH values for the batch reaction experiment using samples of the Captain field. Vertical dashed line at day 9 represents change of pH meter. Vertical dotted lines at days 3, 11, 22 and 26 indicate replacement of CO_2 bottle. Horizontal dashed lines show PHREEQC modelled equilibrium pH values for atmospheric (400 ppm) CO_2 and bubbled (1.4 bar) CO_2 for the concentrations of calcite in the samples (Table 3.1).*

3.3.2   Alkalinity

Concentrations of bicarbonate (HCO_3^-) were measured on days 1-7, 9, 11, 14, 22 and 30 (Section 2.4.3). At the pH values obtained for the experiment, HCO_3^- concentrations are assumed to be the dominant carbonate species and therefore equal to total alkalinity, which is usually calculated from a titration of solution with an acid to determine the capacity of the solution's bases (e.g. HCO_3^-, CO_3^{2-}, OH^-, PO_4^{3-}, $SiO(OH)_3^-$) to neutralise H^+ ions. The results are shown in Figure 3.3 for samples *SA7* and *SA10*, and the Blank controls.

Alkalinity values for the two blank flasks show no effect of the addition of CO_2, with values pretty much constant through the duration of the experiment at 25 - 65 mg/L (CO_2) and 20 - 70 mg/L (control). *SA7* alkalinity values without the addition of CO_2 are only slightly higher than the blanks at a range of 45 - 95 mg/L, while *SA10* values without the addition of CO_2 increase from 80 mg/L to 165 mg/L. The addition of CO_2, however, increases alkalinity concentrations for both flasks with rock samples *SA7* and *SA10*, with *SA7* values increasing from 105 mg/L to 290 mg/L, and *SA10* increasing from 135 mg/L to 500 mg/L.

The increase in alkalinity with the addition of CO_2 shows that some dissolution of minerals is occurring, releasing neutralising bases into solution. PHREEQC v3.3.3.10424 modelled HCO_3^- values are marked on Figure 3.3 for bubbled CO_2 and show that the more calcite in the sample, the higher the equilibrium alkalinity concentration will be. With carbonate alkalinity dominated by bicarbonate and carbonate ions, one would suspect dissolution of carbonates detected by XRD to be the source, however no carbonate minerals were detected for *SA10* (Table 3.1) which elicited the strongest increase in carbonate alkalinity with the addition of CO_2. It is possible, however, that due to sample heterogeneity or the 'nugget' effect (a single/small number of undetected grain(s) influencing the results) that adding CO_2 has promoted dissolution of a carbonate mineral which wasn't detected by XRD. The dissolution of an additional 1 wt.% (the XRD detection limit) carbonate would produce alkalinity values closer to the experimental data, based on the PHREEQC model, however still requires some addition explanation, such as silicate dissolution.

The dissolution of silicates (e.g. feldspars) also contributes to alkalinity, by releasing the $SiO(OH)_3^-$ ion into solution. The difference in alkalinity between samples *SA7* and *SA10* may be due to differences between silicates in these samples, for example differences in grain size or the diagenetic history of the feldspars, such that smaller and more 'weathered' grains would be expected to more reactive than larger, fresher grains, or that different feldspars are reacting.
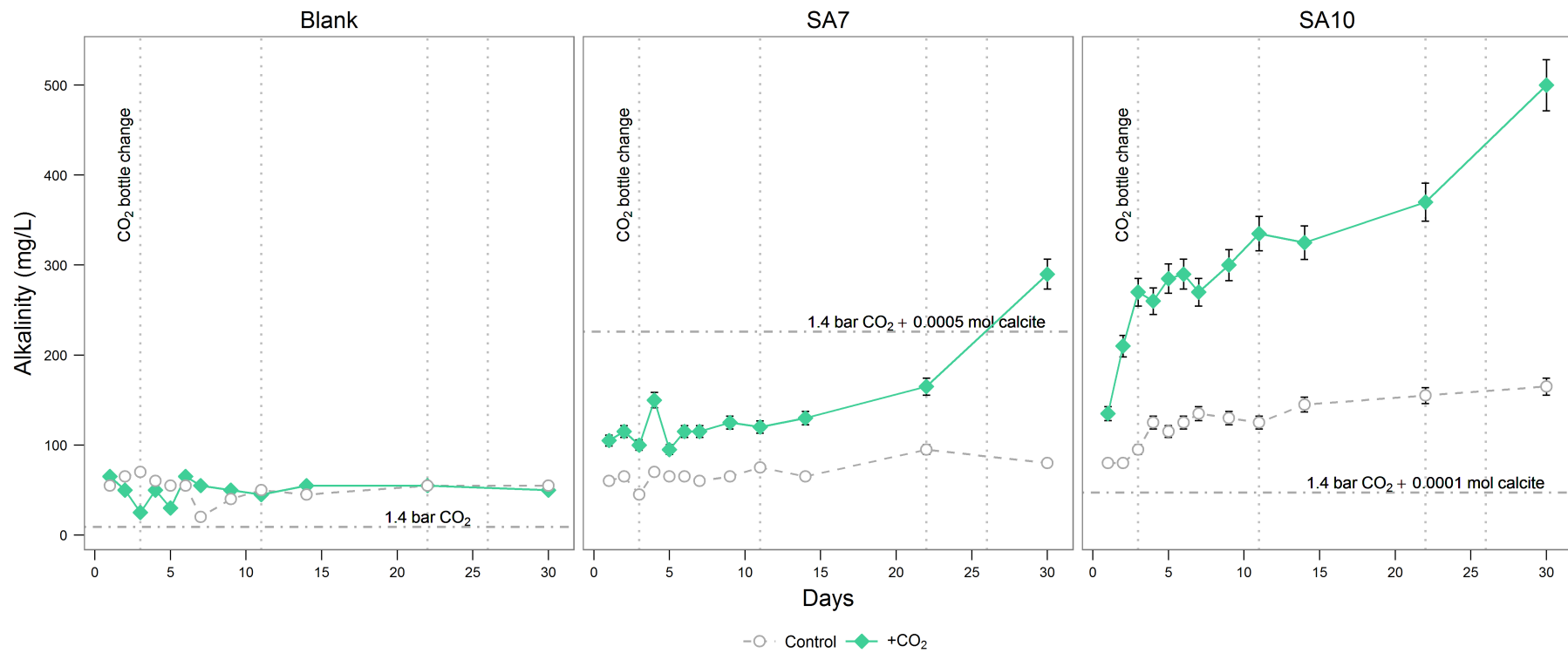
Figure 3.3: *Alkalinity values, as HCO_3^- (mg/L) for the batch reaction experiment using samples of the Captain field. Vertical dotted black line at days 3, 11, 22 and 26 indicate replacement of CO_2 bottle. Horizontal dashed lines show PHREEQC modelled equilibrium alkalinity values (as HCO_3^-) for bubbled (1.4 bar) CO_2 for the concentrations of calcite in the samples (Table 3.1).*

3.3.3 Trace metals of interest

Concentrations of the 8 trace metals of interest (As, Cd, Cr, Cu, Hg, Ni, Pb, Zn) were determined by ICP-MS for the $+CO_2$ and control Blank, *Captain SA7* and *Captain SA10* flasks (Section 2.5.2), Figure 3.4.

The concentrations of elements in the Blank flasks (which had no rock samples) are assumed to be representative of any background concentrations of elements present in the fluid samples. These might be due to the saline matrix assay, leaching from batch glassware and sampling equipment, and/or any other mode of introducing contamination to the samples. Zinc is particularly susceptible to affecting background concentrations since it is a common element in laboratory gloves, shampoo (e.g. Ullah *et al.* 2013), etc.

It is assumed that these background concentrations will be present in all samples, therefore the concentration data for the $+CO_2$ and control Blank flasks were subtracted from the $+CO_2$ and control *SA7* and *SA10* flasks, respectively, to give 'blank corrected' data for the leaching of elements from the *SA7* and *SA10* samples (Appendix C).

Concentrations of the 8 trace metals are, for the most part, very low. Arsenic, Cd, Hg and Pb concentrations in most cases without the addition of CO_2 are lower than the analytical detection limits, Figure 3.4. Where detectable, the highest concentrations for As, Cd, Cr and Hg tend to be within the first 5 - 15 days of the experiment, before tailing off, and with no obvious correlation of enhanced concentrations with the addition of CO_2 to the flasks.

Chromium concentrations peak at day 5 at $\sim 4.0 \pm 0.8$ µg/L in both the *SA7* and *SA10* $+CO_2$ flasks, before decreasing to < 1 µg/L, similar to the control flasks. Mercury concentrations in the *SA10* control flask increase with the experiment duration to a final maximum value of 6.6 ± 1.0 µg/L.

Nickel concentration spikes are evident on days 11 (*SA7* $+CO_2$, 376 ± 38 µg/L) and 14 (*SA10* control, 480 ± 48 µg/L), likely the result of some contamination since they are at least 10 times higher than prevailing concentration values, and occur only once. These spikes slightly mask the overall increased concentrations of the $+CO_2$ flasks for both *SA7* and *SA10* samples over the last half of the experiment. Final concentrations are 39.6 ± 3.9 µg/L and 20.0 ± 2.0 µg/L, respectively.

Concentrations of Pb for the *SA7* $+CO_2$ flask are elevated about the control, exhibiting a saw-tooth pattern of increasing/decreasing concentrations, but generally > 100 µg/L, with a final recorded value of 464 ± 46 µg/L.

There is no discernible difference between the control and $+CO_2$ flasks for *SA10* Cu concentrations, with both averaging $\sim 270 \pm 50$ µg/L. There is an increase in average concentrations for *SA7* $+CO_2$ (70 ± 13 µg/L) compared with average *SA7* control concentrations (20 ± 4 µg/L), although like Pb the $+CO_2$ concentrations fluctuate throughout the experiment.

Zinc concentrations increase steadily with time for both *SA7* and *SA10* $+CO_2$ samples, and are enhanced with respect to the controls, Figure 3.4. *SA7* control concentrations are $< $ LOD for all days except the last, however *SA7* $+CO_2$ concentrations increase from 124 ± 33 µg/L (day 1) to 450 ± 122 µg/L (day 30). There is not such a large difference with the *SA10* sample, but nonetheless the $+CO_2$ flask concentrations increase from 64 ± 17 µg/L (day 1) to 351 ± 95 µg/L (day 30).
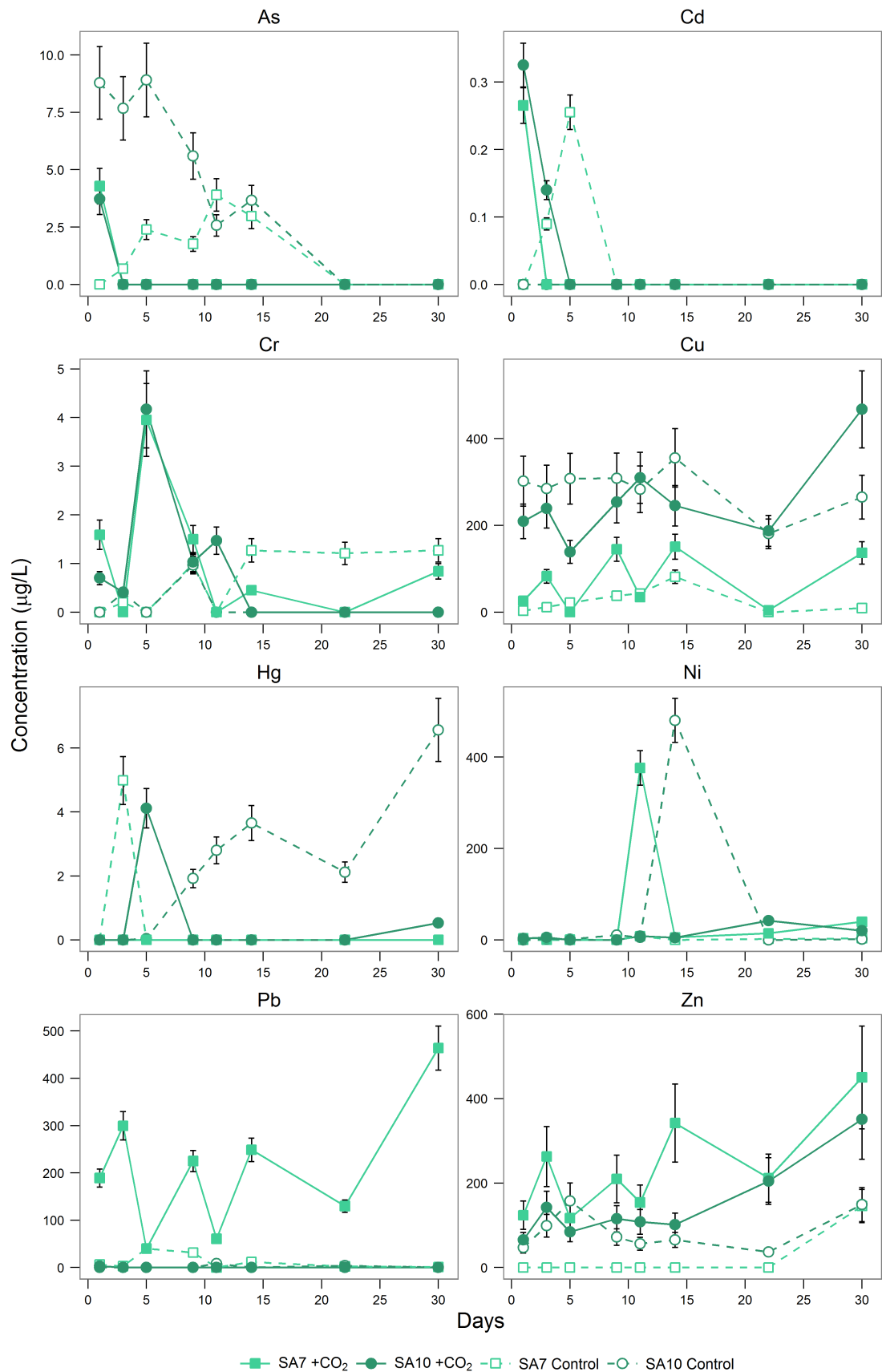
Figure 3.4: *Concentrations of the 8 trace metals of interest for the Captain SA7 and SA10 samples obtained by ICP-MS (μg/L). Error bars are 2s of the mean of standard reference material values, Section 2.10.*

3.3.4 Major elements

Concentration data for eight other elements analysed by ICP-MS (Al, Ba, Ca, Fe, K, Mg, Mn and Ti) are plotted in Figure 3.5. U concentrations all fell below the analytical limit of detection (LOD) and are therefore not reported here.

Aluminium concentrations are for the most part < LOD for the majority of the experiment for both *SA7* and *SA10* +CO_2 flasks, with the exception of day 5 when values of 0.14 ± 0.04 mg/L and 0.015 ± 0.004 mg/L, respectively were recorded. Concentrations were generally only detectable above the LOD for the *SA10* control flask, with concentrations in the range of 0.07 ± 0.02 mg/L to 0.10 ± 0.03 mg/L on 4 separate days, Figure 3.5.

Concentrations of Fe in the *SA7* and *SA10* control batch fluids are, for the most part, < LOD. A maximum concentration of 0.12 ± 0.02 mg/L was recorded on day 1 for the *SA10* control. The addition of CO_2 leached Fe at concentrations above the LOD in both *SA7* and *SA10*, with the *SA10* flask recording a peak concentration of 0.8 ± 0.2 mg/L on day 2, before declining to < LOD by day 22. *SA7* +CO_2 also peaks on day 2 at 0.9 ± 0.2 mg/L but otherwise values fluctuate between ~ 0.05 and 0.33 mg/L, Figure 3.5.

Titanium concentrations do not have any apparent trend, with no clear relationship between samples or the addition of CO_2. The highest concentration recorded was on day 11 in the *SA10* +CO_2 flask, at 36.8 ± 5.5 µg/L.

Barium, Ca, K, Mg and Mn all show similar trends for both *SA7* and *SA10* samples, Figure 3.5. For both samples, the +CO_2 batch fluids have higher concentrations than the controls, with *SA10* concentrations generally higher than *SA7*. The highest concentrations were recorded for Ca (maximum of 180 ± 22 mg/L), followed by K and Ba. The majority of these metals show an increase then plateauing of concentrations to day 14 with a steady increase thereafter, although some values are low e.g. Ba concentrations in *SA7* control do not exceed ~ 0.22 mg/L, compared with the *SA7* +CO_2 flask which reaches a maximum of 5.9 ± 0.4 mg/L. Of these metals, K does not appear to be significantly affected by the addition of CO_2, Figure 3.5. Concentrations for both *SA7* and *SA10* are similar for +CO_2 and ontrol flasks, although *SA10* +CO_2 flask increases over the ontrol from day 22, reaching a maximum concentration of 28 ± 6 mg/L.
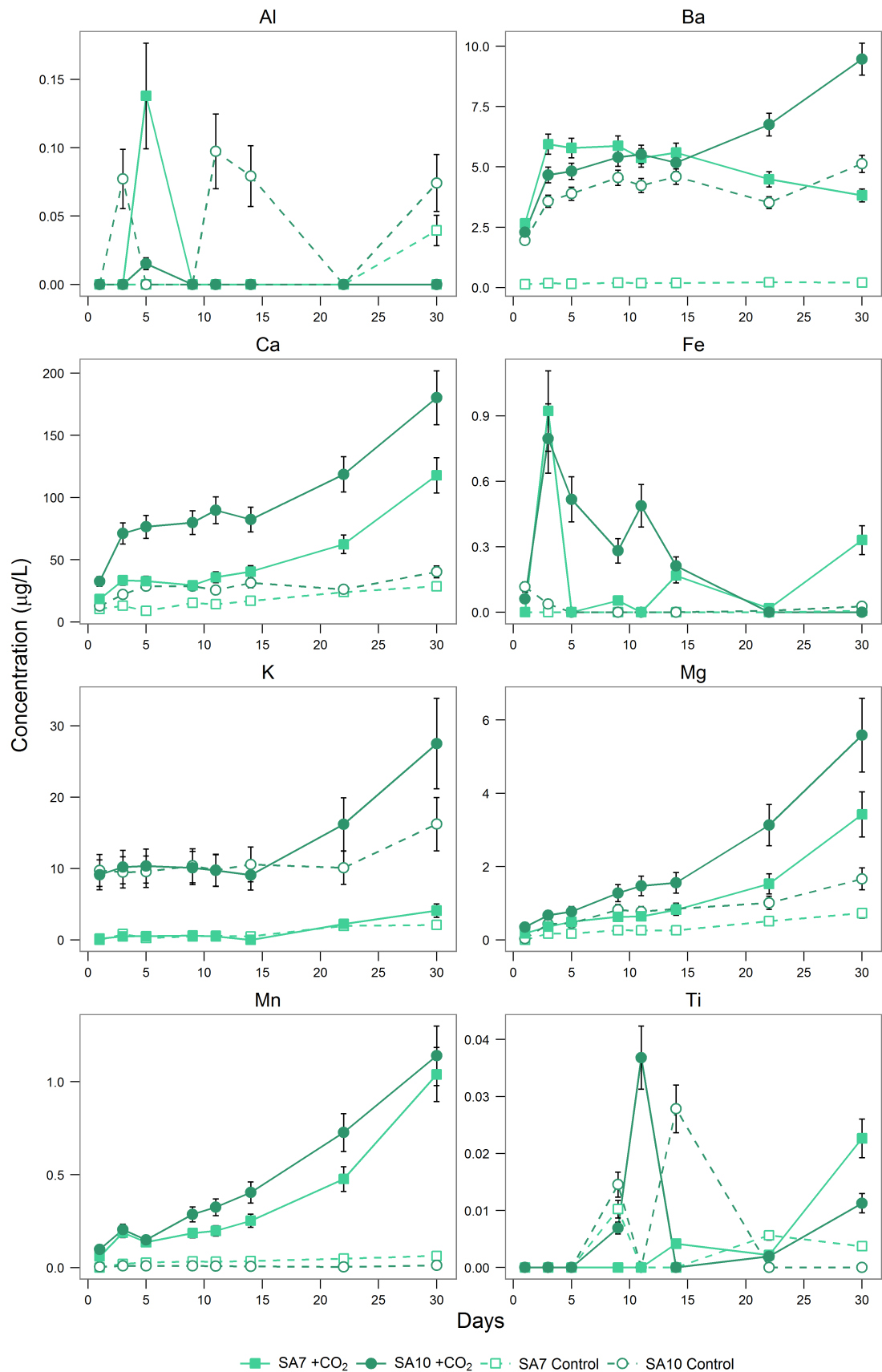
Figure 3.5: *Concentrations of major elements obtained by ICP-MS (mg/L) for Captain field samples SA7 and SA10. Error bars are 2s of the mean of standard reference material values, Section 2.10.*

3.4 Captain Sequential Extraction Procedure

In order to better determine the origin of the metals leached during batch reactions, a sequential extraction procedure (SEP) was carried out on sandstone samples from the North Sea. The experimental rationale and method are described in Chapter 2 (Methodology).

The sum of the concentrations obtained from each SEP step for each element analysed was compared with the bulk (whole rock) concentrations for the *Captain SA7* sample, Figure 3.6 (data: Table 3.3). Data are not available for *SA10* since there was not enough sample available for bulk or SEP analysis.
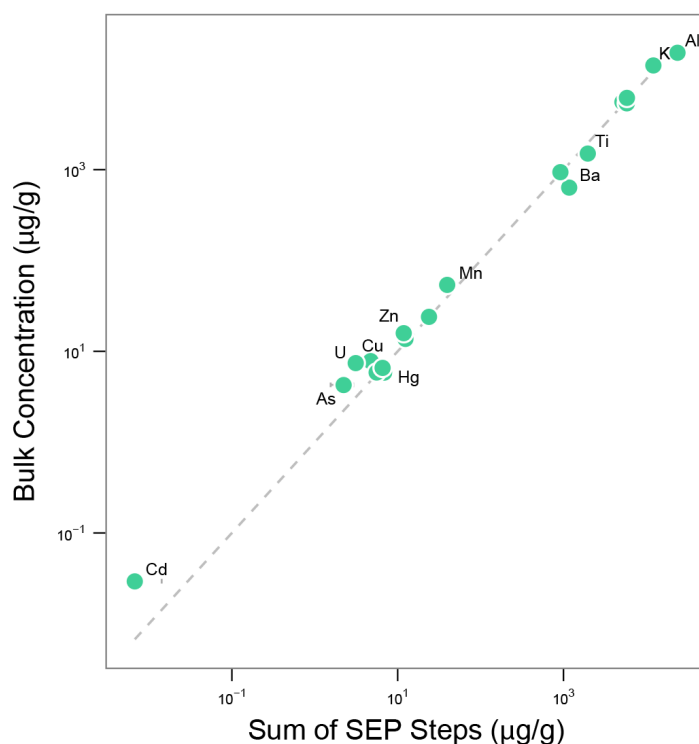
Figure 3.6: *Concentrations of SEP steps summed compared with bulk/whole rock concentrations for 19 elements (µg/g), obtained by ICP-MS and ICP-OES. Error bars are 2s.*

For 10 of the 19 elements analysed (Ca, Cr, Fe, K, Li, Mg, Na, Ni, Pb, Zn), there is good agreement (within 2s) between the concentrations obtained from the sum of all of the SEP steps and the bulk digestions value. For elements Al, As, Hg, Mn and Ti there is reasonable agreement, while the remaining elements Ba, Cd, Cu and U have poor agreement between the SEP sum and the bulk concentration. Summed SEP concentrations of Cd, Cu and U are lower than the bulk concentrations, possibly due to material losses during the SEP experiment, although why these elements are preferentially lower (instead of a systematic lowering of all other elements) is unclear.

Bulk concentrations would be considered more accurate than the summed SEP values, since the sample has not been previously reacted and can therefore rule out inaccuracies due to losses/accumulations of sample material and/or individual elements across each SEP step. Bulk concentrations are used further in this chapter to compare with other data, rather than use the summed SEP concentration data.

The results of the 6 SEP steps (water soluble, exchangeable, carbonate, oxide, sulphide and silicate (Section 2.3.2)) for the 8 trace metals of interest are given in Figure 3.7a. Concentrations are generally low, at < 10 µg/g, with the exception of Cr which reaches a maximum concentration of 18.4 ± 0.1 µg/g. Cd concentrations are very low at parts per trillion levels, Figure 3.7a.

Most elements are present in some quantity across each of the SEP steps. For the *Captain SA7* sample,

Element	Whole rock		Sum of SEPs	
	ppm	±	ppm	±
Al	20,000	2,000	23,700	700
As	4.3	0.7	2.2	0.7
Ba	640	60	1,270	40
Ca	5,600	800	5,100	200
Cd	0.029	0.001	0.007	0.007
Cr	24	3	23.9	0.3
Cu	7.8	0.8	4.7	0.3
Fe	5,400	700	5,800	200
Hg	5.9	1.2	6.9	0.6
K	14,100	800	12,100	600
Li	14	2	12.4	0.7
Mg	940	80	900	30
Mn	54	7	40	2
Na	6,200	500	5,800	300
Ni	5.9	0.7	5.6	0.7
Pb	6.6	0.9	6.6	0.6
Ti	1,500	200	1,960	30
U	7.5	0.7	3.1	0.1
Zn	16	2	11.8	2.5

Table 3.3: *Concentration data (ppm) for microwave acid digestion and analysis by ICP-OES/ICP-MS for Captain sample SA7. Uncertainties are 2s.*

elements are most concentrated in the silicate portion of the sample (quartz, feldspars, clays), with the exceptions of Cu, Ni and Zn. The largest concentrations of Cu and Zn are in the water soluble (2.49 ± 0.02 μg/g) and sulphide (8.9 ± 1.2 μg/g) fractions, respectively, while approximately 55% of Ni is found in water soluble, carbonate and oxide fractions. Elements aren't present above the analytical limits of detection (LODs) for the exchangeable fraction for these trace metals, with the exception of Hg. The exchangeable fraction represents concentrations of those elements occurring on mineral surfaces.

Cadmium is only present above the analytical LOD in the water soluble and silicate dissolution steps, and concentrations are very low (0.75 x 10^{-3} μg/g and 6.0 x 10^{-3} μg/g, respectively) and with large 2s uncertainty for the silicate concentration.

Concentrations of Al, Ca, Ba, Fe, K, Mg, Mn and Ti were also determined for each of the 6 SEP steps, Figure 3.7b. Maximum values of these elements are significantly higher than the 8 trace metals, with 7 of the 8 elements in the range of ∼ 500 - 23,000 μg/g. The lowest concentrations determined were for Mn, where the maximum concentration recorded is 18.7 ± 0.2 μg/g, similar to maximum trace metal concentrations (Cr, 18.4 ± 0.1 μg/g).

Aluminium and K are significantly concentrated in the silicate step, as would be expected from these elements which are both the primary mineral forming elements in the feldspar mineral microcline (6.5 ± 0.4 wt.% of *SA7*), as well as the clay minerals illite (Al, K) and kaolinite (Al) which are both present in this sample. Barium concentrations are highest in carbonate (212 ± 7 μg/g) and silicate (708 ± 10 μg/g) fractions. Ba is a common carbonate forming element, and is also associated with feldspars, with the concentration in the silicate fraction comparable to terrestrial feldspars (Smith and Brown, 1988).

Concentrations of Ca are highest in the carbonate fraction (2,950 ± 50 μg/g), which is to be expected given the presence of calcite. Ca concentrations are also significant in the feldspar fraction (1,560 ± 17 μg/g). Although the Ca-feldspar end member anorthite was not detected by XRD, Ca will readily substitute into other feldspars and so these are probably the source of Ca in the silicate fraction, rather than the clays chlorite and illite (Table 3.1). The carbonate fraction also contains comparatively small amounts of Al (92 ± 4 μg/g), Fe (223 ± 4 μg/g), Mg (62.5 ± 0.4 μg/g) and Mn (14.8 ± 0.1 μg/g), which may be attributable carry over from other mineral fractions in the SEP. Given the small amount of Mg, the carbonate mineral assemblage is confirmed to be dominated by calcite, rather than dolomite.

Mg is, however, concentrated in oxides (301 ± 3 μg/g) and silicates (482 ± 8 μg/g), similar to Fe (2,670 ± 30 μg/g, 2,650 ± 60 μg/g, respectively). The presence of chlorite in the *SA7* sample, which is an
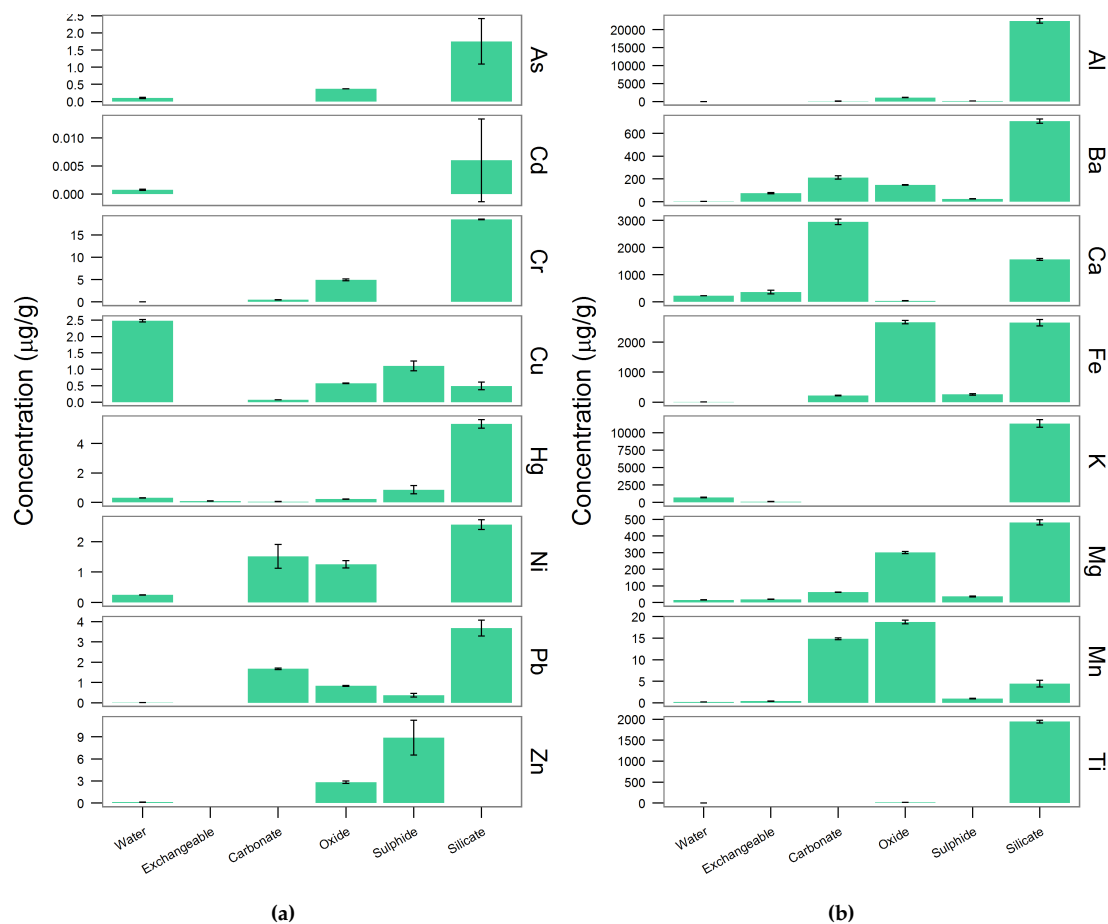
Figure 3.7: *Results of SEP experiments on Captain sample SA7. Concentrations in μg/g, analysed by ICP-OES and ICP-MS. Error bars are 2s of repeat analysis (n = 3) (a) Trace metal concentrations (b) Major element concentrations*

Fe and Mg-rich group of clays, could account for Fe and Mg concentrated partially in the silicate fraction. No oxide phases were detected by XRD (Table 3.1) however the presence of significant concentrations of Fe and Mg in the oxide fraction, together with Al ($1,100 \pm 9$ μg/g), Ba (148 ± 1 μg/g), Ca (40 ± 3 μg/g), Mn (18.7 ± 0.2 μg/g) and Ti (18.0 ± 0.1 μg/g) clearly indicates their presence, albeit at concentrations below the XRD detection limit. Total oxide concentrations are ∼ 0.7 wt.%, confirming that this is likely the case if it assumed that separate oxides form for each element represented here.

The highest concentration of Ti is within the silicate fraction, and given the relatively high concentrations ($1,945 \pm 15$ μg/g) are most likely associated with clays (e.g. González and del C. Ruiz 2006), although Ti is also present in feldspars but in low concentrations (Smith and Brown, 1988), Figure 3.8.

The general distribution trend is for elements to be present in greatest concentrations in oxide, sulphide and silicate associated fractions, and in least concentrations in the water, exchangeable and carbonate fractions, with some exceptions (e.g. Ca, Mn, Cu). Kirsch *et al.* (2014) carried our similar SEP analysis on samples from Colorado, classifying the SEP steps based on susceptibility to leach metals during enhanced CO_2, low O_2 and short duration experimental conditions (similar to batch experiments described above), into "mobile" and "immobile". Metals capable of being leached by water, ion exchange and carbonate dissolution were classified as "mobile", while oxide, sulphide and silicate dissolution were classified as "immobile" (Kirsch *et al.* 2014). This same classification was applied to the data collected for the *Captain SA7* sample, and mobile and immobile fractions calculated as a percentage for each element, Table 3.4 and Figure 3.9.
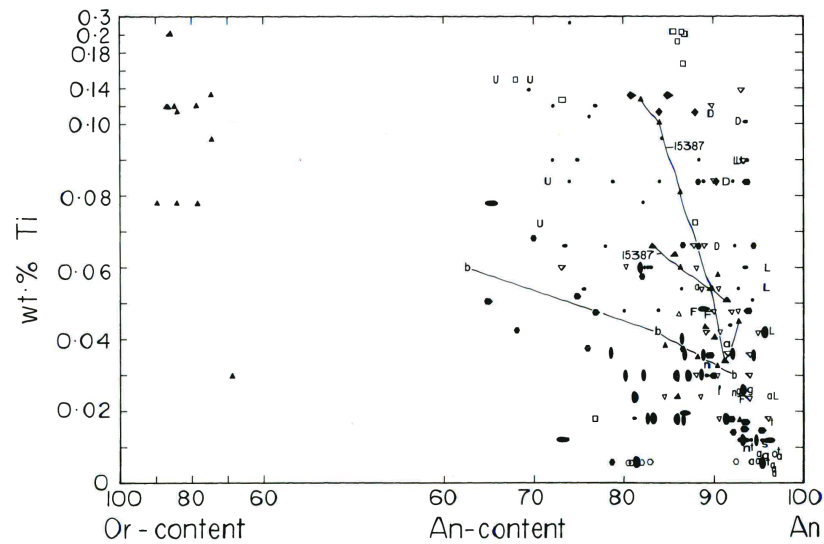
Figure 3.8: *Titanium content (wt.%) of orthoclase (Or) and anorthite (An) feldspars measured in lunar basalts. Figure from Smith and Brown (1988) pg. 332, their Figure 14.13.*

While one would expect these conditions (enhanced CO_2, low O_2) to apply to a CO_2 storage reservoir, they are not necessarily representative of experimental conditions. This therefore may not be an ideal classification when comparing the results of the batch experiments for *Captain*, *Cormorant* and *Thistle* for several reasons: (i) the batch experiments conducted for this thesis were not oxygen-free. Other batch studies such as Kirsch *et al.* (2014) and Lu *et al.* (2014) purged their reaction vessels of O_2 prior to the experiments being conducted. Therefore readily oxidised minerals, such as sulphides, which are present in the *SA7* and *SA10* samples could leach metals under weak CO_2 acid conditions in the experiments, despite perhaps being classified as immobile, although would be expected to remain relatively immobile within a CO_2 storage reservoir where anoxic conditions prevail; (ii) while silicates are, on the whole, far more resistant to weak-CO_2 acid dissolution, nonetheless minerals such as feldspars can be readily 'weathered' with CO_2. Classifying all silicates (and associated elements) as being susceptible only to strong acid digestions is therefore not necessarily accurate.

Element	Mobile (%)	Immobile (%)
Al	0.4	99.6
As	4.5	95.5
Ba	24.8	75.2
Ca	68.9	31.1
Cd	11.1	88.9
Cr	2.1	97.9
Cu	54.1	45.9
Fe	3.9	96.1
Hg	6.6	93.4
K	6.7	93.3
Li	3.8	96.2
Mg	10.7	89.3
Mn	38.9	61.1
Ni	31.7	68.3
Pb	25.6	74.4
Zn	0.9	99.1

Table 3.4: *Calculated percentages of "mobile" and "immobile" elements for the Captain SA7 sample, as per Kirsch et al. (2014), following analysis by sequential extraction procedure. Data plotted in Figure 3.9.*

However, this classification scheme does give some impression overall of how likely elements are to be leached, although caution needs to be exercised with regard to the calculated values attributed each to mobile and immobile categories.

This classification shows that the bulk of trace metal concentrations are classified as immobile under potential reservoir conditions of enhanced CO_2 and low O_2, with immobile concentrations accounting for > 90% of *Captain SA7* for Al, As, Cr, Fe, Hg, K, Li and Zn, and > 50% for Ba, Cd, Mg, Mn, Ni and Pb. The exceptions are Ca and Cu, where the majority of these elements (68.9% and 54.1%, respectively) are potentially mobile with enhanced CO_2. One cannot say for definite with regard to Cd, however, since

Figure 3.9: *Percentage of 16 elements classified as "mobile" and "immobile" as per Kirsch et al. (2014). Data in Table 3.4.*

the 2s uncertainty on the silicate concentration value is so large (Figure 3.7a).

By calculating the masses (µg) of the 16 elements considered earlier for the batch experiments (Figures 3.4 and 3.5) for sample *SA7*, and normalising them as concentrations per gram of sample (µg/g), one can compare these with the whole rock and mobile concentrations to determine the extent of leaching under experimental conditions. The concentrations of elements released from the batch experiments, Table 3.5, were calculated by:

- Multiplying the concentration of each element (µg/L) by the volume removed for element analysis (L), for each time step sampled except the final volume

- Multiplying the final concentration of each element (µg/L) by the final volume remaining (L) at the end of the experiment

- Summing the calculated masses (µg) for all time steps, and dividing by the mass of sample *SA7* used in the experiment (Table 2.6)

The results are given in Table 3.5, and visualised in Figure 3.10. The addition of CO_2 appears to increase the mass released during the batch experiments for Ba, Ca, Cu, Fe, Mg, Mn, Ni, Pb, Ti and Zn, compared with the controls, as also shown in Sections 3.3.3 and 3.3.4.

In terms of µg per gram of sample, 14 of the 16 elements leached less during the batch experiments with CO_2 than was determined to be mobile by the SEP, with mobilised concentrations of the major elements (e.g. Al, K) being particularly low compared with the bulk composition. Maximum mobilised Al, As, Cr, Cu, Fe, Hg, K and Ti from the batch experiments are < 0.5% of bulk concentrations, Table 3.5. Cd and Mg are also low compared with bulk composition (< 2%). Approximately 10%, 14%, 10% and 11% of bulk Ba, Ca, Mn and Ni, respectively, were mobilised by CO_2, Table 3.3.

Comparing mobilised elements with just the mobile fraction, one sees again that Al and Fe mobility is low, with maximum mobilised concentrations of either element in the batch experiments only 1.26% of the mobile fraction. Mobilised K is also low at ∼ 4% of the mobile fraction. Barium, Ca, Mg and Mn, which have the largest mobile fractions (as %), are mobilised to the greatest extent during the batch experiments. Maximum mobilised values from the batch experiments are for the +CO_2 flask. These values are 21.4%, 21.6%, 19.0% and 37.3% of the mobile fraction for Ca, Ba, Mg and Mn, respectively.

CO_2 mobilised half of the total Pb in the *SA7* sample, which is approximately twice that determined
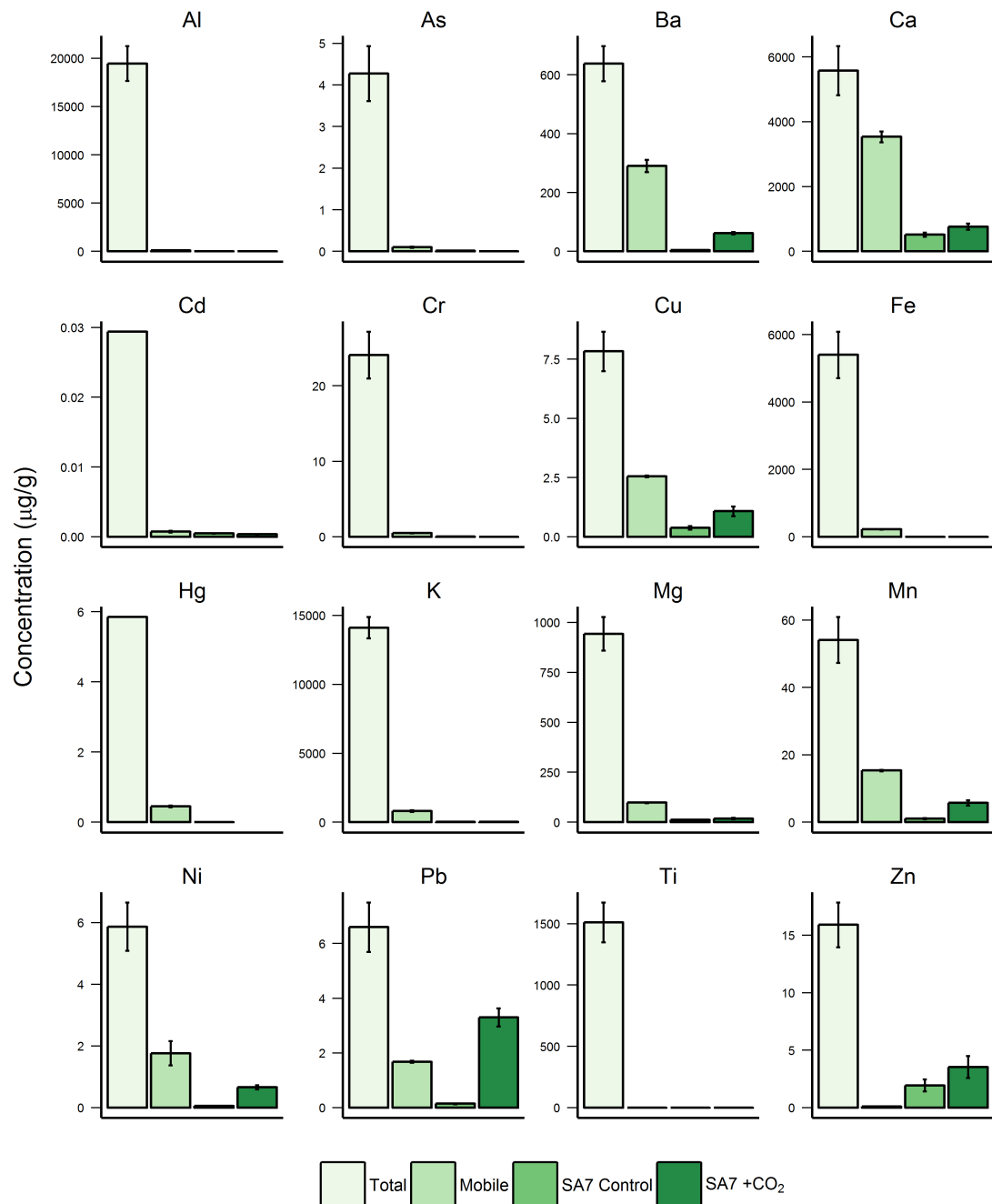
Figure 3.10: *Concentrations of 8 trace metals leached (μg/g) from Captain sample SA7 during batch experiments, compared with the whole rock and mobile fraction determined by the sequential extraction procedure. Error bars are 2s. Data provided in Table 3.5.*

to be mobile by the SEP. Zinc concentrations mobilised in both control and $+CO_2$ experiments also exceed the mobile fraction, although concentrations are still around 25% of bulk Zn, Figure 3.10.

Lead concentrations with the addition of CO_2 are within $2s$ of the mobile fraction, therefore it is possible that all Pb has leached from the mobile fraction of the sample. Equally, however, some Pb may be dissolving from an oxide, sulphide or silicate even though neither oxides or sulphides were detected by XRD. Pb may be present in oxide or sulphide form, but in trace quantities only, below the detection limit of XRD.

Leached Zn in the batch experiments is significantly higher than the theoretical mobile fraction, indicating that Zn is very likely dissolving from either an oxide or sulphide minerals (Figure 3.7a). Neither type of mineral was detected by XRD. Given that XRD is only accurate to 1 wt.%, and whole rock zinc concentrations are $\sim 0.0015\%$ then the detection of any significant zinc-containing minerals is challenging. XRD, therefore, does not appear to capture the complete picture of the mineralogy of this sample and so cannot be relied upon in this instance as a prediction of zinc leaching under enhanced CO_2 conditions.

Element	Total		Mobile		Captain SA7 Control		Captain SA7 +CO_2	
	µg/g	±	µg/g	±	µg/g	±	µg/g	±
Al	20,000	2,000	95	9	0.52	0.15	0.20	0.06
As	4.3	0.7	0.10	0.01	0.015	0.003	0.006	0.001
Ba	640	60	290	20	4.5	0.3	62	4
Ca	5,600	800	3,500	200	520	60	770	90
Cd	0.029	0.001	0.0007	0.0001	0.0005	0.0001	0.0003	0.0001
Cr	24	3	0.50	0.02	0.022	0.004	0.014	0.002
Cu	7.8	0.8	2.56	0.02	0.38	0.07	1.1	0.2
Fe	5,400	700	230	8	0.083	0.017	2.9	0.6
Hg	5.9	1.2	0.45	0.01	0.007	0.001	< LOD[†]	
K	14,100	800	815	57	34	8	21	5
Mg	940	80	98	3	12	2	19	3
Mn	54	7	15.4	0.2	1.1	0.2	5.8	0.8
Ni	5.9	0.7	1.7	0.2	0.058	0.006	0.66	0.07
Pb	6.6	0.9	1.68	0.02	0.15	0.02	3.30	0.33
Ti	1,500	200	0.39	0.03	0.07	0.01	0.09	0.01
Zn	16	2	0.112	0.002	2.0	0.5	4.0	1.0

Table 3.5: *Table of concentrations comparing masses of trace metals released during batch experiments with total masses in sample, and masses theoretically mobile with CO_2 based on the SEP "Mobile" classification.* [†]*Values less than the analytical detection limit.*

3.5 Cormorant & Thistle Bulk Analysis

3.5.1 X-ray diffraction

The results of X-ray diffraction (XRD) analysis carried out on *Cormorant* and *Thistle* samples (Section 2.8) are given in Table 3.6 as the mineral assemblage by weight % (wt.%). Values < 1 wt.% are trace concentrations and are considered semi-quantitative only, therefore their values should not be taken as accurate but indicative only of their presence in the sample.

Mineral	Type	Cormorant wt.%	±	Thistle wt.%	±
Halite	Water Sol	0.6	0.1	0.30	0.09
Dolomite	Carbonate	-	-	0.31	0.07
Siderite	Carbonate	0.9	0.1	0.03	0.06
Albite	Silicate	3.9	0.3	3.2	0.2
Chlorite		2.7	0.4	0.9	0.3
Kaolinite		6.6	0.5	3.5	0.3
Microcline		4.2	0.3	5.0	0.2
Orthoclase		6.0	0.3	4.8	0.2
Quartz		75	1	82	1

Table 3.6: *Results of XRD of Cormorant and Thistle samples as wt.% of mineral. Type refers to the mineral types targeted by the sequential extraction procedure (Section 2.3.2). - Not detected in sample.*

The minerals identified in *Cormorant* and *Thistle* samples have been broadly grouped in Table 3.6 by mineral type, as per the sequential extraction procedure (SEP) method outlined in Section 2.3.2. As already outlined, this classification is based on dissolution only of the mineral and not any other mechanism of element release. Summing the values of the grouped minerals and plotting them as a bar plot produces Figure 3.11.
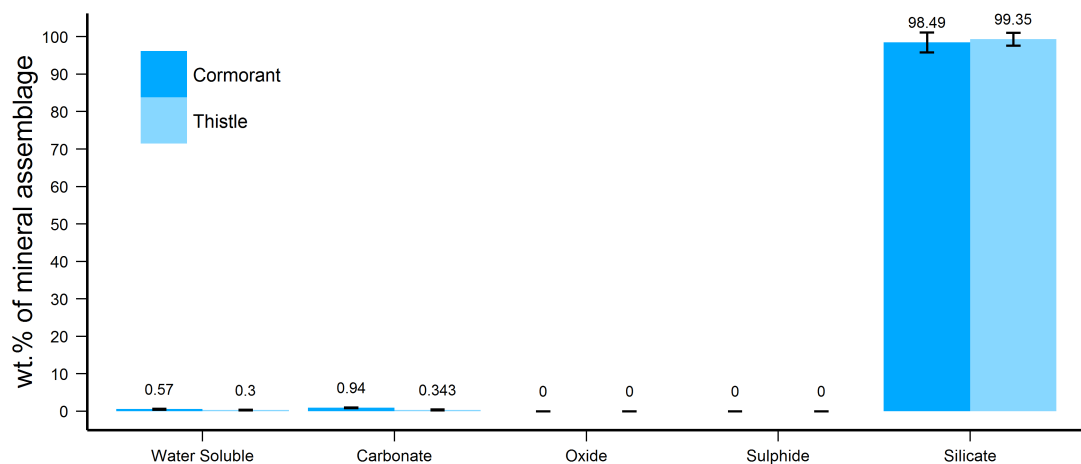
Figure 3.11: *Results of XRD analysis of Cormorant and Thistle samples grouped by mineral type, as wt.% of mineral. Summed values are given above each bar.*

Silicate minerals again dominate the *Cormorant* and *Thistle* sandstone samples, as would be expected, roughly equal silicate content in both samples, Figure 3.11. Clays and feldspars make up 23 ± 2 wt.% of silicates in *Cormorant*, and 17 ± 1 wt.% in *Thistle*, with the difference made up by increased quartz content in *Thistle*. Twice as much clay material was found in *Cormorant*, compared with *Thistle*. Trace amounts of water soluble (halite) and carbonate minerals were detected in both samples, with slightly greater carbonate content present in *Cormorant* (but still < 1 wt.%).

3.5.2 X-ray fluorescence & microwave digestion

Cormorant and *Thistle* powdered samples were analysed by X-ray fluorescence (XRF) for an MSc project submitted in August 2012 to give bulk element data for the samples (Section 2.9). In July 2014 a different set of powdered *Cormorant* and *Thistle* samples were analysed for bulk element composition by microwave acid digestion with ICP-OES analysis. The results of both sets of analyses are in Table 3.7 and plotted in Figure 3.12.

Element	Cormorant				Thistle			
	ICP-OES		XRF		ICP-OES		XRF	
	ppm	±	ppm	±	ppm	±	ppm	±
Al	32,000	3,000	21,100	1,000	18,800	1,700	10,500	500
As	1.70	0.30	-	-	3.4	0.5	-	-
Ba	520	50	790	-	620	60	1,700	
Ca	1,100	100	500	80	630	80	-	-
Cd	0.08	0.00	-	-	0.06	0.00	-	-
Cr	55	7	82	-	30	4	34.4	-
Cu	7.5	0.8	9.6	-	3.4	0.4	4.0	-
Fe	12,000	1,600	9,330	90	3,200	400	1,550	14
Hg	1.6	0.3	-	-	15	3	-	-
K	16,200	900	8,200	200	13,500	700	6,700	200
Mg	2,700	200	3,000	400	370	30	900	100
Mn	290	36	270	20	62	8	47	3
Na	4,800	390	2,000	300	4,500	400	1,900	300
Ni	19	2	23	-	4.6	0.6	2.4	-
Pb	10	1	12	-	15	2	16	-
Ti	3,900	400	5,000	100	2,000	200	2,130	40
Zn	41	5	39	-	15	2	8.7	-

Table 3.7: *Concentration data (ppm) for microwave acid digestion/ICP-OES, and XRF, for Cormorant and Thistle samples. - Not detected in sample.*
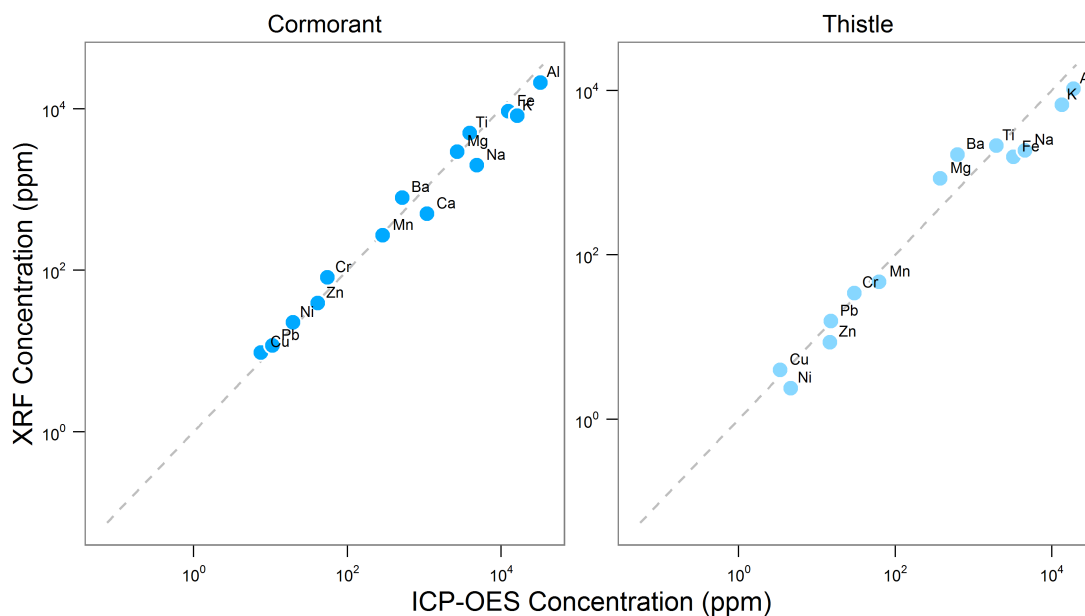
Figure 3.12: *Comparison of whole rock concentration data by microwave acid digestion with ICP-OES, and XRF (ppm, on log_{10} scale). Error bars on ICP-OES data are 2s of the average values obtained for Montana SRM2710A and SRM2711A (n = 6, Section 2.10). Error bars on XRF are 2s of repeat analysis (2004 - 2011, n = 133) of Shap Granite reference material.*

While XRF is a more straightforward method for determining bulk element concentrations, the instrumentation available at the University of Edinburgh was not able to analyse for three of the trace

metals of interest: As, Cd, Hg. Bulk chemical analysis by microwave acid digestion with ICP-OES undertaken after the SEP experiments allowed for the full suite of elements to be analysed, and facilitated the comparison of whole rock data with the sum of the SEP steps to determine inaccuracies in the methods used.

The whole rock analysis by ICP-OES can also be compared with the XRF data, where both methods analysed for the same elements. Figure 3.12 plots ICP-OES and XRF concentrations of the 14 of the 17 elements listed in Table 3.7 for *Cormorant* and 13 of the 17 for *Thistle*. The plots are on $\log_{10}$ axis to cover the entire range of concentrations on single plots.

Concentrations between the two methods compare reasonably well for most elements. The largest differences are for major elements such as Al, K and Na. Ca concentrations are at the 0.05% (500 ppm) detection limit of the instrument, hence the discrepancy in the *Thistle* sample between analytical techniques.

Concentrations of the 8 trace metals of interest are low, ranging from 0.08 ± 0 ppm (Cd) to 55 ± 7 ppm (Cr) in the *Cormorant* sample, and 0.06 ± 0 ppm (Cr) to 30 ± 4 ppm (Cr) in the *Thistle* sample. Concentrations of As and Pb are slightly higher in *Thistle* than they are in *Cormorant*, and Hg is a factor of 10 higher in the *Thistle* sample, Figure 3.13.
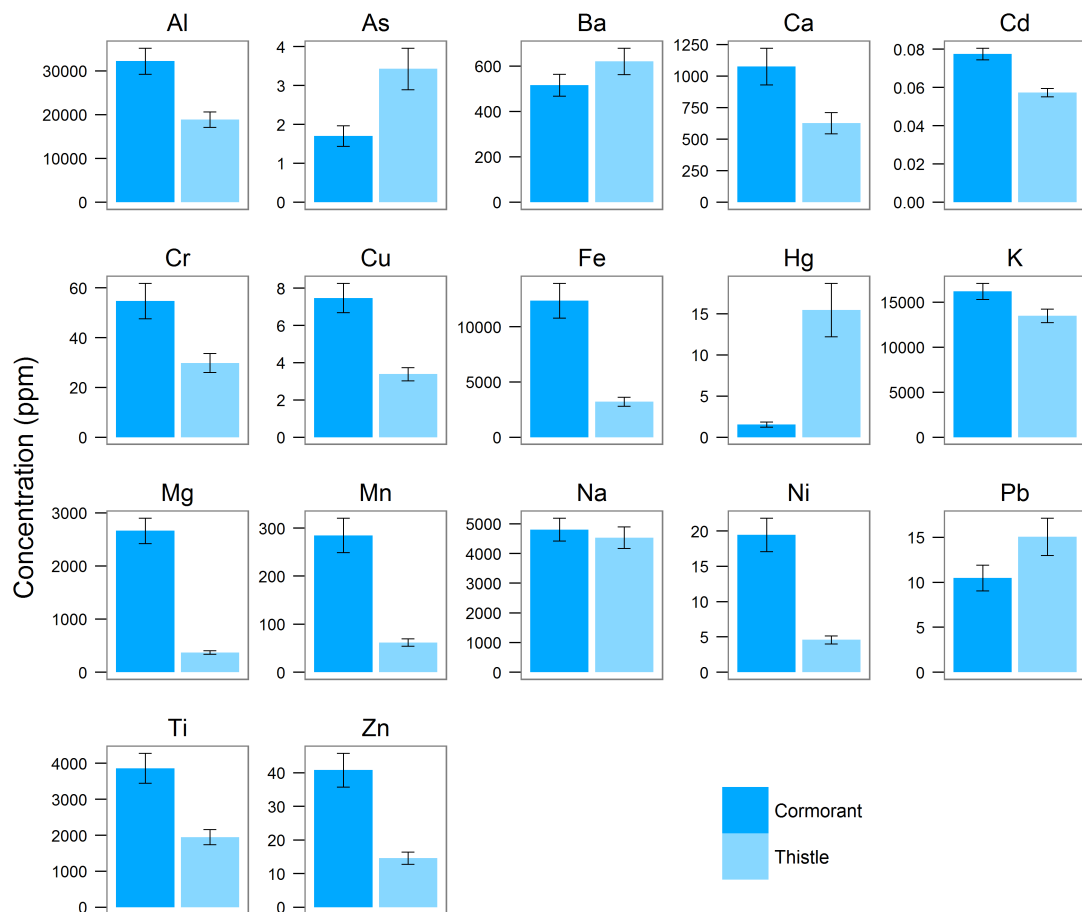
Figure 3.13: *Comparison of whole rock concentration data by microwave digestions with ICP-OES for Cormorant and Thistle samples (ppm). Error bars are 2s of the average values obtained for Montana SRM2710A and SRM2711A (n = 6, Section 2.10).*

Otherwise, with the exception of Ba, concentrations of all other elements analysed are higher in the *Cormorant* sample, Figure 3.13. This is indicative of a lower quartz (SiO_2) abundance in the *Cormorant*

sample, and higher abundances of other minerals, particularly the clay minerals kaolinite ($Al_2Si_2O_5(OH)_4$) and chlorite ($(Mg,Fe)_3(Si,Al)_4O_{10}(OH)_2 \cdot (Mg,Fe)_3(OH)_6$). These two clays account for 9.3 ± 1.0 wt.% in the *Cormorant* sample, and 4.4 ± 0.6 wt.% in *Thistle* and would probably account for the increased Al, Mg and partly Fe concentrations. Significantly increased Fe (~ 4 times) in the *Cormorant* sample is also probably due to the greater abundance of siderite ($FeCO_3$), although this was only detected in trace concentrations by XRD. A higher abundance of orthoclase feldspar ($KAlSi_3O_8$) in the *Cormorant* sample could be responsible for the increased concentrations of K in this sample compared with *Thistle*.

3.6 Cormorant & Thistle Batch Reaction Experiments

3.6.1 pH

pH was measured throughout the experiment, on days 1 - 7, 9, 10 & 15, Figure 3.14. The CO_2 bottle was replaced on day 3 due to the gas running out, indicated by the vertical dotted line in Figure 3.14.
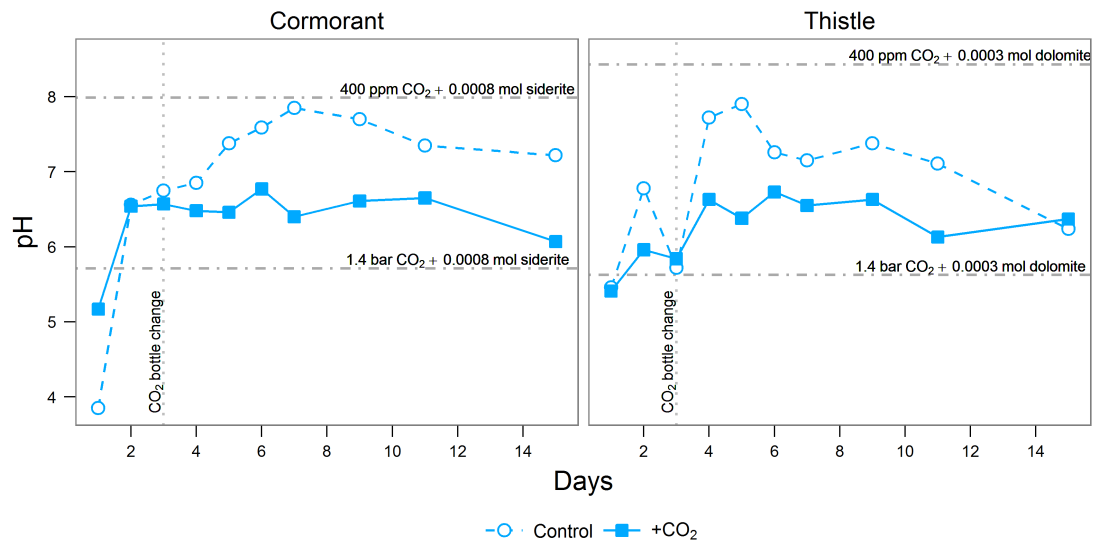
Figure 3.14: *pH values for the batch reaction experiment using samples of the Cormorant and Thistle fields. Vertical dotted line at day 3 indicates replacement of CO_2 bottle. Horizontal dashed lines show PHREEQC modelled equilibrium pH values for atmospheric (400 ppm) CO_2 and bubbled (1.4 bar) CO_2 for the concentrations of siderite and dolomite in the samples (Table 3.6).*

As would generally be expected, the addition of CO_2 to the flasks has the effect of decreasing pH with respect to the no-CO_2 added controls. pH values in the *Cormorant* and *Thistle* flasks which did not have CO_2 added are higher than those flasks with CO_2 added. pH values are similar to those measured for the *Captain* samples *SA7* and *SA10*.

There is an increase in pH values over only a few days in all flasks from ~ 5.5 to between ~ 6.5 (both +CO_2 flasks) and ~ 7.5 in the *Cormorant* control, again likely due to pH buffering by mineral dissolution, Equations 1.4 & 1.5. pH values are similar for both *Cormorant* and *Thistle* samples. Again, modelled pH values using PHREEQC v3.3.3.10424 bracket the experimental data, and show that the experimental pH values are higher than the modelled equilibrium pH's, assuming that siderite and dolomite are the dominant reactive minerals in the *Cormorant* and *Thistle* samples, respectively. The conclusion from this, as with the Captain samples, could be that there are other processes (silicate dissolution, desorption), contributing to buffering of the system.

The effect of running out of CO_2 on day 3 is not noticeable in the +CO_2 flasks. A sharp dip and rise of nearly 2 pH units at this time in the *Thistle* control flask could be due to a measurement error.

3.6.2 Alkalinity

Concentrations of bicarbonate (HCO_3^-) were measured on days 1 - 7, 9, 10 & 15 (Section 2.4.3), except no measurements were taken on day 15 for the *Cormorant* control and day 10 for *Thistle* +CO_2. Bicarbonate values are shown in Figure 3.15 for *Cormorant* and *Thistle* samples with and without added CO_2.

Carbonate alkalinity in the *Cormorant* and *Thistle* control flasks increased from 45 mg/L to 130 mg/L,

and 55 mg/L to 135 mg/L, respectively. The *Cormorant* flask with added CO_2 increased from 60 mg/L to 472 mg/L, while the *Thistle* flask increased from 95 mg/L to 548 mg/L.
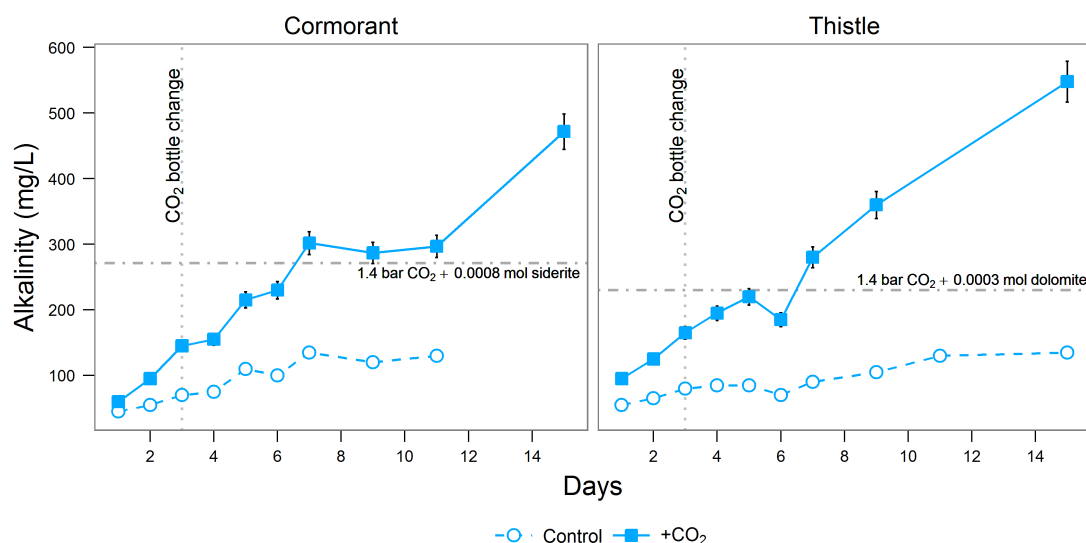
Figure 3.15: *Alkalinity values, as HCO_3^- (mg/L) for the batch reaction experiment using samples from Cormorant and Thistle fields. Vertical dotted line at day 3 indicates replacement of CO_2 bottle. Error bars $2s$. Data not collected for final Cormorant control sample. Horizontal dashed lines show PHREEQC modelled equilibrium alkalinity values (as HCO_3^-) for bubbled (1.4 bar) CO_2 for the concentrations of siderite and dolomite in the samples (Table 3.6).*

Both samples exhibit very similar trends for the control and $+CO_2$ flasks. From the XRD data, Figure 3.11, the general mineral assemblage is quite similar, although as discussed in that section, there is a greater abundance of clays and feldspars in the *Cormorant* sample. There is slightly more carbonate present in the *Cormorant* sample, however carbonate alkalinity values are lower for this sample and generally lower than for *Thistle* by around 20%.

Modelled alkalinity values with PHREEQC appear to show that the main carbonate minerals in the Cormorant and Thistle samples aren't the only contributors of alkalinity. The addition of CO_2 enhances total alkalinity through the dissolution of minerals, even if it is not clear which of the minerals are contributing to the fluid chemistry at this stage.

3.6.3 Trace metals of interest

Concentrations of the 8 trace metals of interest (As, Cd, Cr, Cu, Hg, Ni, Pb, Zn) were obtained for the *Cormorant* and *Thistle* flasks $+CO_2$ and control flasks, by ICP-MS and ICP-OES (Sections 2.5.2 & 2.6.1).

Unlike the *Captain* batch experiment, blank flasks without rock samples were not used throughout the *Cormorant* and *Thistle* experiment. Instead, to correct for concentrations in blank samples, 3 aliquots each of the 2 synthetic NaCl solutions used in the experiments were analysed and their average concentrations (where greater than analytical detection limits) were subtracted from the experimental concentration values to give the 'blank corrected' data used in this thesis, Appendix C.

Concentrations of the 8 metals are generally low for both *Cormorant* and *Thistle* samples, and with the exceptions of Ni and Zn show no apparent trends with respect to the addition of CO_2 to the flasks, Figure 3.16. Arsenic concentrations were not detected above the analytical LODs for either *Cormorant* or *Thistle* (LODs of 9.2 µg/L and 6.6 µg/L, respectively). Cadmium concentrations show a slightly increasing trend for *Thistle* $+CO_2$ flask, and are elevated above the control flask, however the difference between the two flasks is in the order of only 1 µg/L. The maximum Cd concentration was 2.64 ± 0.21 µg/L on

day 1 of the *Thistle* control.

Ephemeral spikes in concentrations, possibly due to sample contamination, are evident in the *Cormorant* control flask on day 2 for Cu and Pb (33.9 ± 3.1 µg/L and 16.2 ± 4.4 µg/L, respectively), and on day 3 for Cr (62.0 ± 5.4 µg/L). *Thistle* control Cr concentrations range between ~ 1.5 and 5 µg/L for the duration of the experiment, with *Thistle* +CO_2 concentrations tracking closely, and both *Cormorant* flasks are generally < LOD. Copper concentrations are largely < LOD for both *Cormorant* and *Thistle*, although concentrations of < 10 µg/L were recorded on a number of days in the *Cormorant* control flask, Figure 3.16. Pb concentrations are < LOD with the exception of the aforementioned *Cormorant* control, day 1 *Thistle* +CO_2 (13.4 ± 6.3 µg/L) and day 7 *Cormorant* +CO_2 (20.2 ± 5.5 µg/L).

The apparent downward trend in Hg for the *Cormorant* control flask, Figure 3.16 is unfortunately an analytical artefact caused by Hg carry-over from high Hg calibration standards run through the instrument immediately preceding this set of samples. Since Hg is prone to accumulating in the peristaltic tubing of the ICP-OES, the downward trend is Hg washing out of the instrument with subsequent samples (see Methodology chapter, Figure 2.7). This is therefore not a real trend and could mask any underlying sample concentrations. Otherwise, Hg concentrations are < LOD for the experiment for both *Cormorant* and *Thistle*.

Nickel and Zn appear to show a strong positive correlation between the addition of CO_2 and their mobilisation. Nickel shows the strongest trend, with control flasks for both *Cormorant* and *Thistle* recording concentrations < LOD from day 3 to the end of the experiment, while +CO_2 flasks are elevated above the LOD and the *Cormorant* flask shows increasing concentrations with time. *Cormorant* +CO_2 concentrations increase from 37.7 ± 3.7 µg/L to 164 ± 16 µg/L, while *Thistle* +CO_2 concentrations remain fairly constant between 27.0 ± 3.5 µg/L and 53.8 ± 7.0 µg/L for the duration of the experiment.

3.6.4 Major elements

Concentration data for ten other elements analysed by ICP-OES (Al, Ba, Ca, Fe, K, Li, Mg, Mn, Si and Sr) are plotted in Figure 3.17.

Aluminium concentrations are generally low compared with the other major elements analysed, with the control flasks for *Cormorant* and *Thistle* containing higher concentrations than the +CO_2 flasks. The maximum concentration recorded was on day 3 in the *Cormorant* control flask (320 ± 37 µg/L). Fe concentrations in the control flasks for both *Cormorant* and *Thistle* are < LOD for the duration of the experiment, with the exception of *Thistle*, day 1 (49 ± 10 µg/L), however significant concentrations of Fe are mobilised by CO_2 with a maximum value of 8 ± 2 mg/L in the *Thistle* +CO_2 flask, and concentrations increasing to 43 ± 4 mg/L by the end of the *Cormorant* +CO_2 experiment.

The highest major element concentrations recorded were of Si, with the control flasks significantly elevated for both *Cormorant* and *Thistle*, compared with the +CO_2 flasks. +CO_2 concentrations rise from 0.87 ± 0.08 mg/L to 22 ± 2 mg/L (*Cormorant*), and 0.74 ± 0.09 mg/L to 12 ± 1 mg/L (*Thistle*) through the duration of the experiment, compared with a rise in the control flasks from 1.2 ± 0.1 mg/L to 65 ± 6 mg/L (*Cormorant*), and 1.6 ± 0.2 to 98 ± 12 mg/L (*Thistle*).

Barium, Ca and Mg display very similar concentrations trends through the duration of the experiment, including a characteristic dip in *Thistle* +CO_2 and spike in *Cormorant* +CO_2 concentrations on day 3. Concentrations are higher for *Thistle* than for *Cormorant*, increasing through time, and the addition of CO_2 has enhanced the concentrations of these elements compared with the Controls. Barium concentrations for the *Thistle* +CO_2 flask decrease from day 5 and are overtaken by the control flask concentrations on day 10. Calcium concentrations are the highest of these three elements, reaching maximum concentrations on day 15 of 29 ± 1 mg/L (*Cormorant*) and 46 ± 1 mg/L (*Thistle*). The maximum Ba and Mg concentrations recorded were 2.07 ± 0.03 mg/L (*Thistle*, control, day 15) and 21.1 ± 0.5 mg/L (*Thistle*, +CO_2, day 10), respectively. While Ca concentrations appear to be increasing at the end of the experiment, Ba and Mg concentrations have levelled off or have decreased, Figure 3.17.
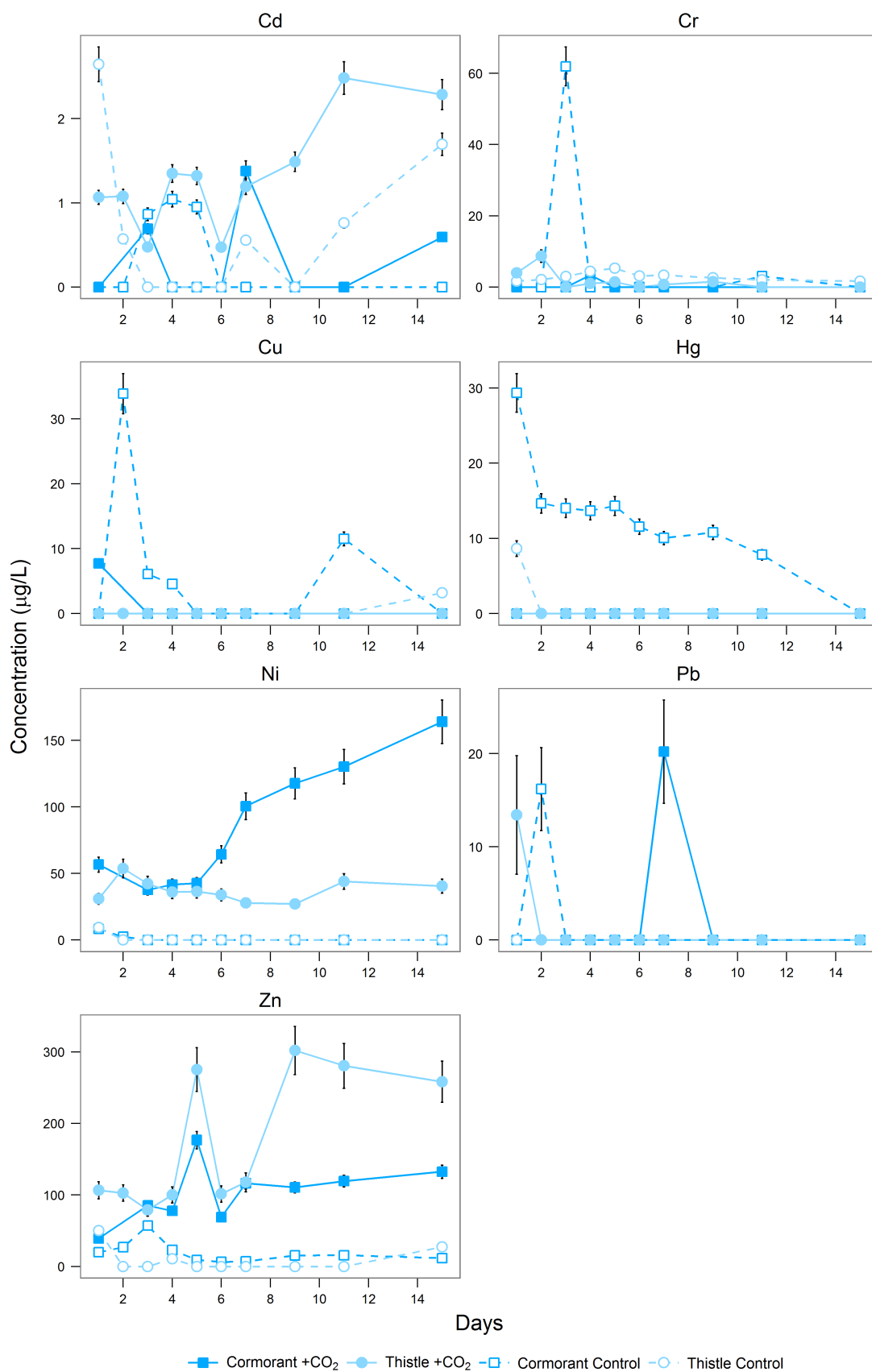
Figure 3.16: *Concentrations of trace metals obtained by ICP-OES (mg/L) for the Cormorant and Thistle samples. Error bars are 2s of the mean of standard reference material values, Section 2.10.*
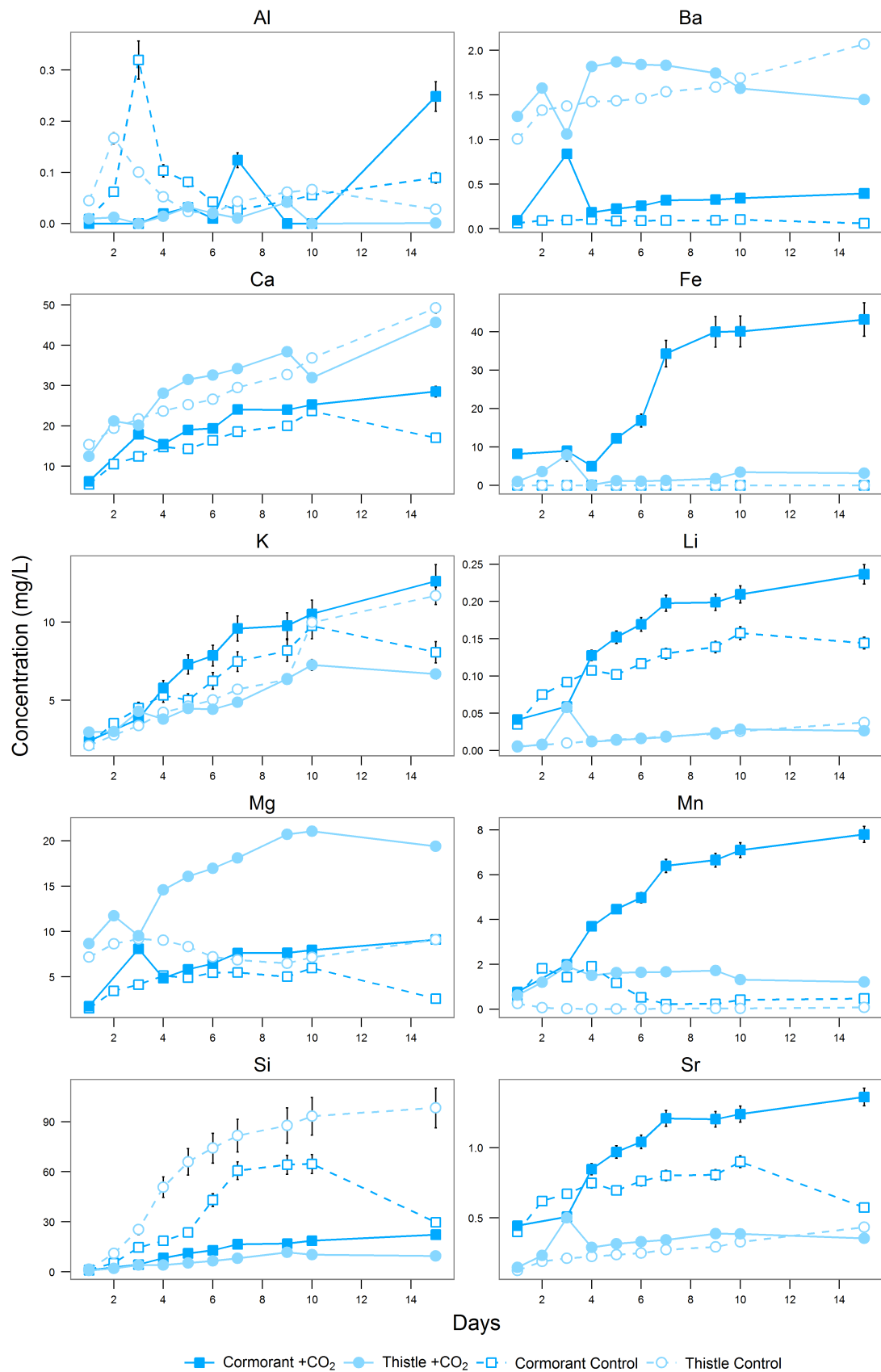
Figure 3.17: *Concentrations of major elements obtained by ICP-OES (mg/L) for the Cormorant and Thistle samples. Error bars are 2s of the mean of standard reference material values, Section 2.10.*

Lithium, Mn and Sr concentrations exhibit an increasing concentration trend with the duration of the experiment, with a plateauing of concentrations from around day 7, however for these elements the *Cormorant* +CO_2 and control flasks are higher than *Thistle*, which is opposite to Ba, Ca and Mg. The addition of CO_2 again increases concentrations with respect to the Controls. Maximum concentrations for Li, Mn and Sr are all on day 15 for the *Cormorant* +CO_2 flask and are 236 ± 13 µg/L, 7.8 ± 0.4 mg/L and 1.36 ± 0.06 mg/L, respectively.

Concentrations of K exhibit a rising trend through time, with *Cormorant* concentrations generally higher than *Thistle*. Similar to *Captain SA7* and *SA10* samples, CO_2 does not seem to significantly alter concentrations, although they are slightly elevated for *Cormorant*. The maximum concentration of K was found to be 13 ± 1 mg/L on day 15, *Cormorant* +CO_2 flask.

3.7 Cormorant & Thistle Sequential Extraction Procedure

As previously described (Section 3.4), in order to better determine the origin of the metals leached during batch reactions, a sequential extraction procedure (SEP) was carried out on sandstone samples from the North Sea. Here the results from the *Cormorant* and *Thistle* fields are described. The experimental rationale and method are outlined in Chapter 2 (Methodology).

Element	Cormorant				Thistle			
	Whole Rock		Sum of SEPs		Whole Rock		Sum of SEPs	
	ppm	±	ppm	±	ppm	±	ppm	±
Al	32,000	3,000	46,000	2,000	18,800	1,700	23,000	2,000
As	1.7	0.3	2.2	0.5	3.4	0.5	2.3	0.7
Ba	520	50	690	15	620	60	1,400	100
Ca	1,100	100	670	100	630	80	600	100
Cd	0.08	0.00	0.035	0.001	0.06	0.00	0.007	0.004
Cr	55	7	61	9	30	4	27	4
Cu	7.5	0.8	14	2	3.4	0.4	14	1
Fe	12,000	1,600	20,500	900	3,200	400	2,800	500
Hg	1.6	0.3	1.7	0.2	15	3	20	2
K	16,200	900	18,800	800	13,500	700	15,000	1,000
Mg	2,700	200	2,800	200	370	30	330	40
Mn	290	36	250	30	62	8	44	2
Na	4,800	390	4,900	200	4,500	400	4,200	300
Ni	19	2	26	2	4.6	0.6	3.7	0.8
Pb	10	1	10.7	0.5	15	2	13	1
Ti	3,900	400	5,500	500	2,000	200	2,300	200
Zn	41	5	42	12	15	2	10	1

Table 3.8: *Concentration data (ppm) for microwave acid digestion and analysis by ICP-OES/ICP-MS for Cormorant and Thistle samples.*

The sum of the concentrations obtained from each of the 6 SEP steps (water soluble, exchangeable, carbonate, oxide, sulphide and silicate (Section 2.3.2)) for each element analysed was compared with the bulk (whole rock) concentrations for *Cormorant* and *Thistle* samples, Table 3.8 and Figure 3.18. Si and Sr were not analysed during the SEP for *Cormorant* and *Thistle*.

For 8 of the 19 elements analysed for *Cormorant* (As, Cr, Hg, Mg, Mn, Na, Pb, Zn), and 9 of the elements for *Thistle* (Ca, Cr, Fe, K, Mg, Na, Ni, Pb, Ti), there is good agreement (within $2s$) between the whole rock and summed SEP concentrations.

There is reasonable agreement between K, Li, Ni, Ti for *Cormorant*, and Al, As, Hg, Li, Mn, Zn for *Thistle*, while the remaining elements Al, Ba, Ca, Cd, Cu, Fe, U, and Ba, Cd, Cu, U, have poor agreement between the SEP sum and the whole rock concentration for *Cormorant* and *Thistle*, respectively, Figure 3.18. Summed concentrations of Cd and U for both samples, and Ca for *Cormorant*, are much lower than the bulk concentrations, possibly due to material losses during the SEP experiment. Barium and Cu for both samples, and Al and Fe for *Cormorant*, are higher in the SEP summed concentrations than the bulk concentration. As previously mentioned (Section 3.4), bulk concentrations would be considered more accurate than the summed SEP values, and so these values are used for further analysis in the chapter.

The results of the 6 SEP steps for the 8 trace metals of interest are given in Figure 3.19, while 8 major elements are shown in Figure 3.20. Similar to *Captain*, concentrations are generally low at $< 15 \, \mu g/g$, again with the exception of Cr which reaches a maximum concentration of $54 \pm 9 \, \mu g/g$ in the *Cormorant* sample. Cadmium concentrations are also very low in both *Cormorant* and *Thistle* samples, at parts per trillion levels, Figure 3.19.

Overall, concentrations of these 8 trace metals are higher in the *Cormorant* sample than in *Thistle*, with total trace metal concentrations ~ 40% higher for *Cormorant*. *Thistle* does, however, have higher
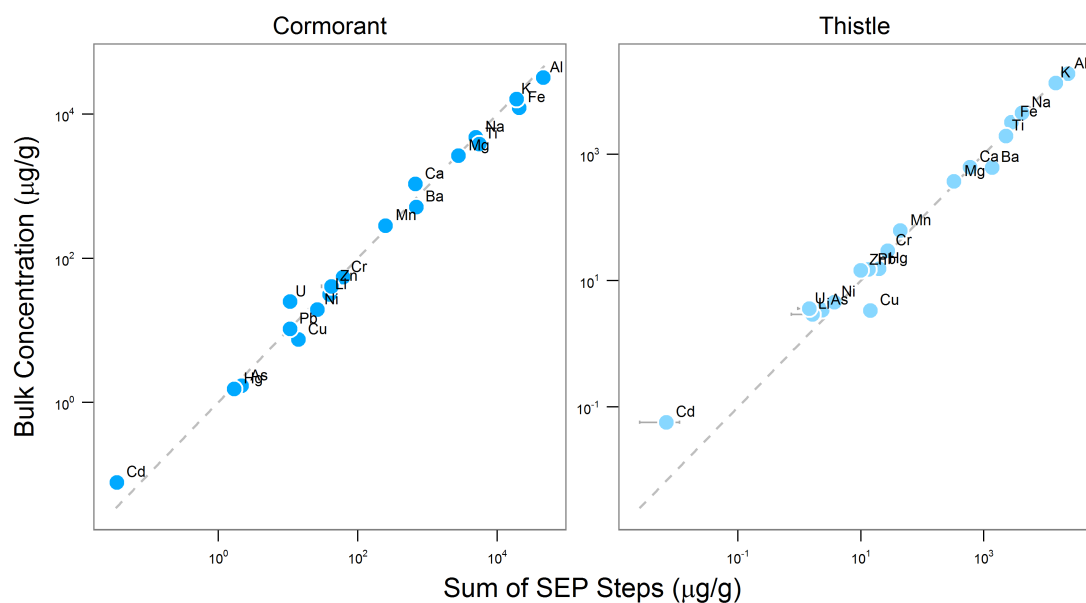
Figure 3.18: *Concentrations of SEP steps summed compared with bulk/whole rock concentrations for 19 elements (μg/g), obtained by ICP-MS and ICP-OES for Cormorant and Thistle samples. Error bars are 2s.*

concentrations of As, Hg and Pb.

Most of the trace metals are present in some quantity across each of the SEP steps for both fields (Figure 3.19), however the only trace metals present in the exchangeable fraction were determined to be Cu and Hg in the *Thistle* sample. Copper and Hg are also the only trace metals in the *Thistle* sample to be present in the sulphide fraction, at concentrations respectively of 0.8 ± 0.1 μg/g and 3.8 ± 0.2 μg/g. Arsenic, Cd, Cr and Hg are not present above their analytical limits of detection (LOD) in the sulphide fraction for *Cormorant*.

The largest concentrations of As, Cd, Cr, Hg, and Pb in both samples are in silicates (quartz, feldspars, clays), Figure 3.19. Nickel concentrations are greatest in silicates for *Cormorant*, although the distribution of Ni in this sample is fairly even across carbonates, oxides, sulphides and silicates. Nickel concentrations in *Thistle* are lower in the silicate fraction compared with carbonates and oxides.

Copper concentrations in *Cormorant* and *Thistle* samples are highest in the carbonate fraction (9 ± 1 μg/g and 10.4 ± 0.8 μg/g, respectively), while Zn is highest in the sulphide fraction for *Cormorant* (15.7 ± 0.2 μg/g) and *Thistle* (6.2 ± 0.7 μg/g).

Cadmium is only present above the analytical LOD in the water soluble and silicate dissolution steps for both *Cormorant* and *Thistle*, with maximum concentrations of 34×10^{-3} μg/g and 6×1010^{-3} μg/g, respectively.

Maximum values of the major elements (Al, Ba, Ca, Fe, K, Li, Mg and Mn) are significantly higher than the 8 trace metals, with 7 of these 8 elements in the range of ∼ 200 - 40,000 μg/g, Figure 3.20. The lowest concentrations determined were for Li, where the maximum concentration recorded is 34 ± 3 μg/g (*Cormorant*), which is lower than the maximum trace metal concentration of 54 ± 9 μg/g (Cr, *Cormorant*).

Cormorant concentrations of these major elements are again higher than for *Thistle* in most cases, Figure 3.20, which is unsurprising given the higher non-quartz content of *Cormorant* compared with *Thistle* (Table 3.6).

Aluminium and K are significantly concentrated in the silicate step for both *Cormorant* and *Thistle*, as would be expected from these elements since both are the primary mineral forming elements in the feldspar minerals albite, microcline and orthoclase, as well as the clay mineral kaolinite, which are
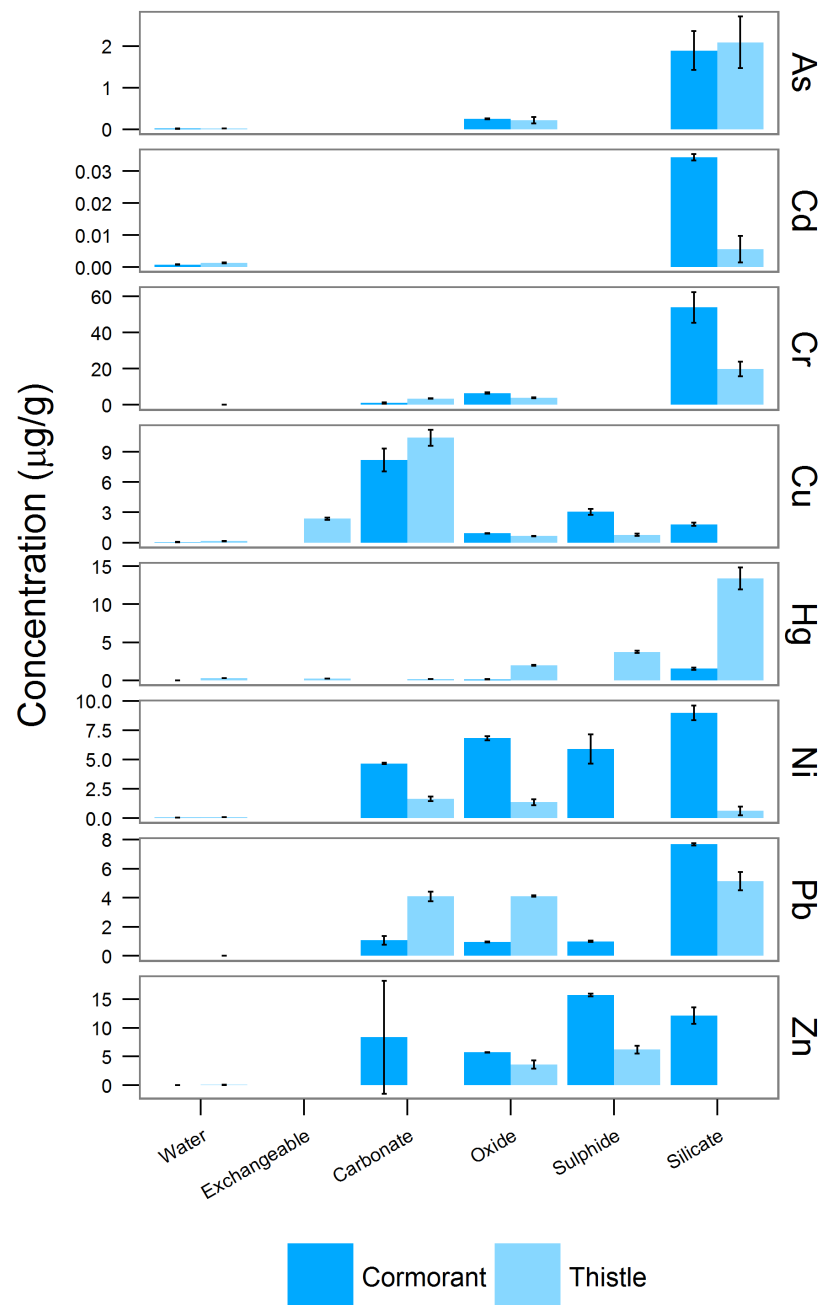
Figure 3.19: *Trace metal results of SEP Steps 1 - 6 on Cormorant and Thistle samples. Concentrations in µg/g, analysed by ICP-OES and ICP-MS.*

present in these samples. The greater concentrations of Al and K in *Cormorant* for the silicate step is validation of the greater abundance of albite, microcline, orthoclase and kaolinite in *Cormorant*, compared with *Thistle* (21 ± 1 wt.% and 17 ± 1 wt.%, respectively, Table 3.6).

Concentrations of Fe and Mg are also much higher in the silicate step for *Cormorant* than for *Thistle*, Figure 3.20, most likely due to the much greater abundance of chlorite (a Mg/Fe rich clay mineral) in *Cormorant* (2.7 ± 0.4 wt.%) compared with *Thistle* (0.9 ± 0.3 wt.%). Iron is also significantly concentrated in the oxide step for *Cormorant* (10,000 ± 200 µg/g) and *Thistle* (910 ± 30 µg/g), although no iron oxides (or indeed any oxides) were detected by XRD, Table 3.6.

Manganese likewise is found in the largest concentrations (190 ± 20 µg/g) in the oxide step for *Cor-*
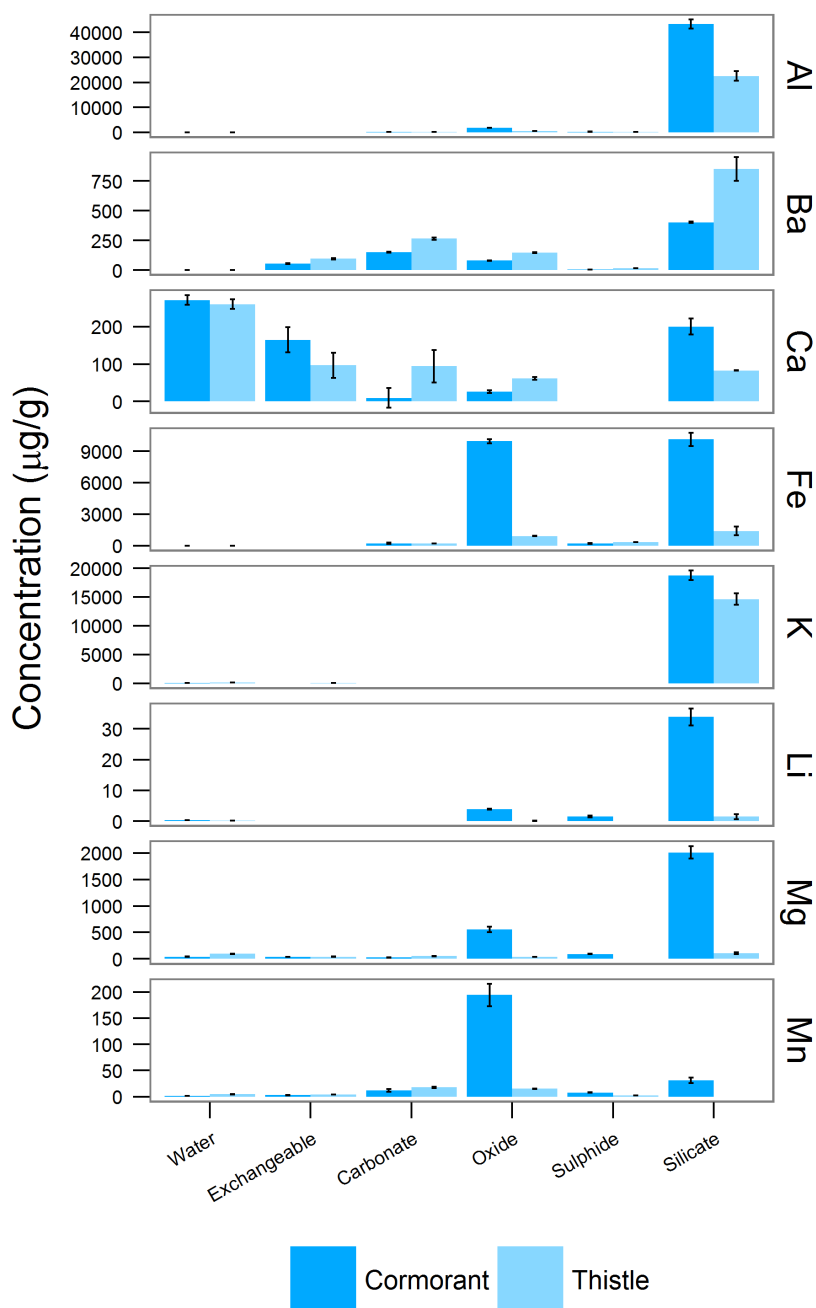
Figure 3.20: *Major element results of SEP Steps 1 - 6 on Cormorant and Thistle samples. Concentrations in µg/g, analysed by ICP-OES and ICP-MS.*

morant, which is to be expected from this extraction step where Fe and Mn oxides are present, although concentrations in *Thistle* are comparable between oxides and carbonates (15.0 ± 0.4 µg/g and 18 ± 1 µg/g, respectively).

Barium concentrations are highest in carbonate and silicate SEP steps, with *Thistle* concentrations being higher than *Cormorant* across all steps. As discussed for *Captain*, Ba is a common carbonate forming element, and is also associated with feldspars.

Unlike *Captain*, however, concentrations of Ca are highest for both *Cormorant* and *Thistle* in the water soluble (270 ± 10 µg/g and 260 ± 10 µg/g) and exchangeable fractions (170 ± 30 µg/g and 100 ± 30 µg/g). Calcium concentrations are low in the carbonate fraction for *Cormorant*, corresponding with an

absence of calcite or dolomite in this sample, whereas Ca concentrations in *Thistle* for the carbonate step are comparable to the exchangeable fraction, at 100 ± 40 μg/g, Figure 3.20. Dolomite ($CaMg(CO_3)_2$) was detected at 0.31 ± 0.07 wt.% in *Thistle*, so it is likely that Ca concentrations in the carbonate step are associated with this mineral, together with *Thistle* Mg carbonate concentrations of 52 ± 6 μg/g. Iron concentrations in *Cormorant* and *Thistle* for the carbonate step are 220 ± 60 μg/g and 192 ± 8 μg/g, respectively. That concentrations are so similar would not be expected from the XRD analysis which shows *Cormorant* containing ~ 30 times more siderite ($FeCO_3$).

Calcium is also significant in the silicate fraction for both *Cormorant* and *Thistle*, Figure 3.20. Like *Captain*, no Ca-feldspars were detected by XRD, however Ca will readily substitute into other feldspars and so these are probably the source of Ca in the silicate fraction, rather than clays.

Lithium is found in greatest concentrations in the silicate (34 ± 3 μg/g) and oxide (3.9 ± 0.1 μg/g) steps for *Cormorant*, although concentrations are low compared with the other major elements. The maximum Li concentration in *Thistle* is in the silicate step, at 1.4 ± 0.9 μg/g.

3.7.1 Comparing with batch experiment data

The element distribution trend is generally for elements to be present in greatest concentrations in oxide, sulphide and silicate associated fractions, and in least concentrations in the water, exchangeable and carbonate fractions, with some exceptions (e.g. Ca, Cu, Ni). As per the *Captain SA7* data (Section 3.4), the results of the *Cormorant* and *Thistle* SEP steps can be classified as "mobile" and "immobile", with elements capable of being leached by water, ion exchange and carbonate dissolution classified as "mobile", while oxide, sulphide and silicate dissolution can be classified as "immobile" (Kirsch *et al.* 2014). While the same caveats as set out in Section 3.4 can apply with respect to the O_2 content of the batch experiment, and the relative kinetics of feldspar dissolution, this classification was considered suitable and applied to the data collected for *Cormorant* and *Thistle* samples.

Element	Cormorant		Thistle	
	Mobile (%)	Immobile (%)	Mobile (%)	Immobile (%)
Al	0.2	99.8	0.6	99.4
As	0.9	99.1	0.9	99.1
Ba	29.8	70.2	26.3	73.7
Ca	66.3	33.7	75.7	24.3
Cd	2.1	97.9	18.3	81.7
Cr	1.7	98.3	12.8	87.2
Cu	58.7	41.3	90.0	10.0
Fe	1.1	98.9	6.8	93.2
Hg	0.3	99.7	3.5	96.5
K	0.4	99.6	1.7	98.3
Li	0.6	99.4	7.1	92.9
Mg	3.8	96.2	56.6	43.4
Mn	6.5	93.5	60.0	40.0
Na	21.9	78.1	33.4	66.6
Ni	17.9	82.1	46.6	53.4
Pb	10.1	89.9	30.6	69.4
Ti	0	100	0	100
U	0	100	0.8	99.2
Zn	20.0	80.0	0.7	99.3

Table 3.9: *Calculated percentages of "mobile" and "immobile" elements for the Cormorant and Thistle samples, as per Kirsch* et al. *(2014), following analysis by sequential extraction procedure. Data plotted in Figure 3.21.*

This classification shows that the bulk of trace metal concentrations are classified as immobile under potential reservoir conditions of enhanced CO_2 and low O_2, Table 3.9 and Figure 3.21. Immobile concentrations account for $> 90\%$ of *Cormorant* for As, Cd, Cr and Hg, and $> 90\%$ of *Thistle* for As, Hg and Zn. Nickel, Pb and Zn in *Cormorant*, and Cd and Cr in *Thistle*, are $> 80\%$ immobile. Nickel and Pb are

53.4% and 69.4% immobile, respectively, for *Thistle*. Copper is the only trace metal where the majority of concentrations in both *Cormorant* and *Thistle* are classified as potentially mobile with enhanced CO_2, with 90% of Cu in *Thistle* classified as mobile, Figure 3.21.

The bulk of major element concentrations are also classified as immobile, Table 3.9 and Figure 3.21, with immobile concentrations accounting for > 90% of *Cormorant* for Al, Fe, K, Li, Mg and Mn, and > 90% of *Thistle* for Al, Fe, K and Li. Barium for both fields are > 70% immobile. Calcium in *Cormorant* and *Thistle* samples is mostly mobile, at 66.3% and 75.7%, respectively. The majority of Mg and Mn are classified as being mobile in *Thistle*, at 56.6% and 60.0%, respectively, which is much different to *Cormorant*, Figure 3.21. This is likely indicating the relative presence of dolomite (carbonate) and absence of chlorite (Fe/Mg rich clay) in the *Thistle* sample, Table 3.6. Mg and Mn would therefore be expected to be more mobile under enhanced +CO_2 from the *Thistle* samples, compared with *Cormorant*. This assumption appears to hold true for Mn, but not for Mg, as Figure 3.17 of batch experiment concentrations shows.

By calculating the masses of the analysed elements released from the batch experiments for *Cormorant* and *Thistle* (μg), and normalising them as concentrations per gram of sample ($\mu g/g$), one can compare these with the whole rock and mobile concentrations to determine the extent of leaching under experimental conditions.

The concentrations of elements released from the batch experiments, Table 3.10, were calculated as per the method give for *Captain* (Section 3.4). Results are plotted for *Cormorant* in Figure 3.22, and for *Thistle* in Figure 3.23.
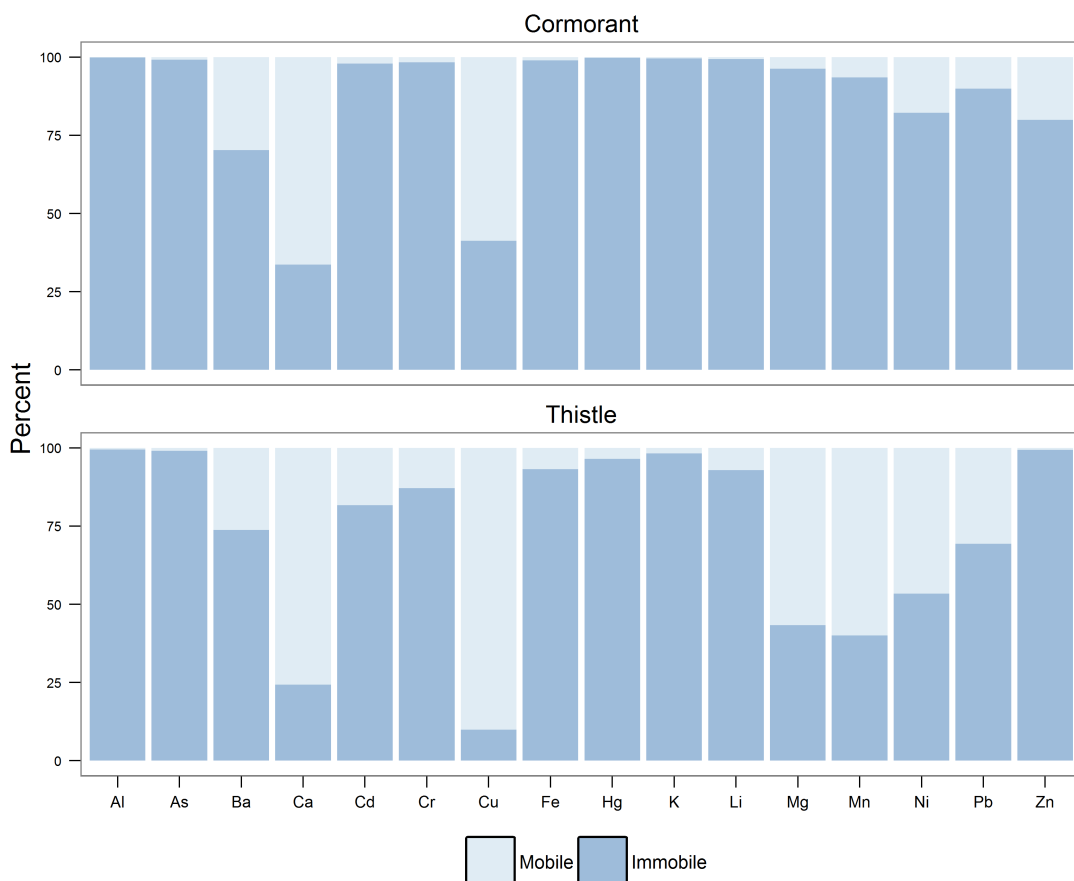
Figure 3.21: *Percentage of 16 elements classified as "mobile" and "immobile" as per Kirsch* et al. *(2014). Data in Table 3.9.*

Element	Cormorant Total µg/g	±	Mobile µg/g	±	Control µg/g	±	+CO$_2$ µg/g	±	Thistle Total µg/g	±	Mobile µg/g	±	Control µg/g	±	+CO$_2$ µg/g	±
Al	32,000	3,000	70	8	0.61	0.07	3.1	0.4	18,800	1,700	133	4	0.19	0.01	0.043	0.003
As	1.7	0.3	0.019	0.005	-	-	-	-	3.4	0.5	0.022	0.003	-	-	-	-
Ba	520	50	206	7	0.57	0.03	6.0	0.3	620	60	360	10	6.9	0.1	14.4	0.2
Ca	1,100	100	450	75	114	5	410	20	630	80	450	90	145	4	400	10
Cd	0.08	0.00	0.0007	0.0001	0.001	0	0.008	0	0.06	0.00	0.001	0.001	0.004	0.001	0.020	0.001
Cr	55	7	1.0	0.3	0.029	0	0.002	0	30	4	3.5	0.2	0.010	0.002	0.005	0.001
Cu	7.5	0.8	8.0	1	0.025	0.002	0.003	0.001	3.4	0.4	12.9	0.9	0.006	0.001	-	-
Fe	12,000	1,600	220	60	-	-	600	60	3,200	400	192	8	0.012	0.003	29	6
Hg	1.6	0.3	0.005	0.001	0.056	0.005	-	-	15	3	0.70	0.03	0.002	0.001	-	-
K	16,2	900	81	4	48	4	180	15	13,482	741	260	20	32	2	60	3
Li	31	4	0.25	0.01	0.87	0.05	3.4	0.2	2.9	0.3	0.12	0.02	0.099	0.008	0.24	0.02
Mg	2,700	200	100	10	26	1	133	6	370	30	190	20	33.6	0.8	177	4
Mn	290	36	16	3	5.2	0.2	111	5	62	8	26	2	0.25	0.01	12.3	0.6
Ni	19	2	4.72	0.06	0.005	0.001	2.3	0.2	4.6	0.6	1.7	0.2	0.002	0.001	0.38	0.05
Pb	10	1	1.1	0.3	0.007	0.002	0.009	0.002	15	2	4.1	0.3	-	-	0.004	0.001
Zn	41	5	8	10	0.12	0.01	2.0	0.1	15	2	0.07	0.01	0.06	0.01	2.3	0.3

Table 3.10: *Table of concentrations comparing masses of elements released during batch experiments with total masses in sample, and masses theoretically mobile with CO$_2$ based on the SEP "Mobile" classification. - Concentration < LOD. Uncertainties are 2s.*

In terms of μg per gram of sample, 7 of the 8 trace metals leached less during the *Cormorant* batch experiments than was determined to be mobile by the SEP. More Cd was mobilised during the batch experiment (both control and +CO_2) by a factor of 10 than is theoretically mobile, although remain much less than total Cd. The addition of CO_2 appears to increase the mass released during the batch experiments for Cd, Ni, and Zn, compared with the controls. CO_2 mobilised half of the mobile Ni in the *Cormorant* sample, Figure 3.22.

For the *Thistle* sample, 6 of the 8 trace metals leached less from the batch experiments than the SEP determined mobile fraction, Figure 3.23. Cadmium and Zn, however, leached more than the mobile fraction, by factors of ~ 20 and 30, respectively, with the addition of +CO_2. The control batch experiment leached ~ 4 times as much Cd as the mobile fraction, although it should be noted that concentrations are still very low, Table 3.10.

Figures 3.22 and 3.23 show that for *Cormorant* and *Thistle*, for the major elements Al, Ba, Fe, K, and Li, mobilised concentrations from the batch experiments are very low compared with total concentrations. Maximum mobilised concentrations of these elements generally do not exceed 5% of bulk concentrations, Table 3.10, with most ~ 1% or less. The exceptions are Fe (~ 5%) and Li (~ 11%) for the +CO_2 *Cormorant* experiment, and Li (~ 8%) for the +CO_2 *Thistle* experiment. In all three of these cases, mobilised concentrations exceed the theoretical mobile fraction of the samples.

Calcium, Mg and Mn, particularly for *Thistle*, are significantly mobilised with CO_2, Figure 3.23. Mobilised Ca and Mg reach ~ 64% and ~ 48%, respectively, of total *Thistle* concentrations, and Mn reaches ~ 39% for *Cormorant*. Magnesium and Mn mobilised by CO_2 in the *Cormorant* experiments are also greater than the mobile fraction determined by the SEP.

Comparing batch experiment mobilised elements with the SEP mobile fraction, one sees that Al and Ba mobility is low, with maximum mobilised concentrations of either element in the batch experiments less than ~ 4.5% of the mobile fraction. Otherwise, mobilised elements from the control experiments are in the range ~12 - 85% (median = 25%) of the mobile fraction, and ~ 23 - 95% (median = 68%) for the +CO_2 experiments, where mobilised concentrations do not exceed the mobile fraction.

Generally speaking, elements associated with carbonates (Ca, Ba, Mg) appear to be mobilised more readily for *Thistle* than for *Cormorant*, with the exception of Fe, which is mobilised more readily from *Cormorant*.
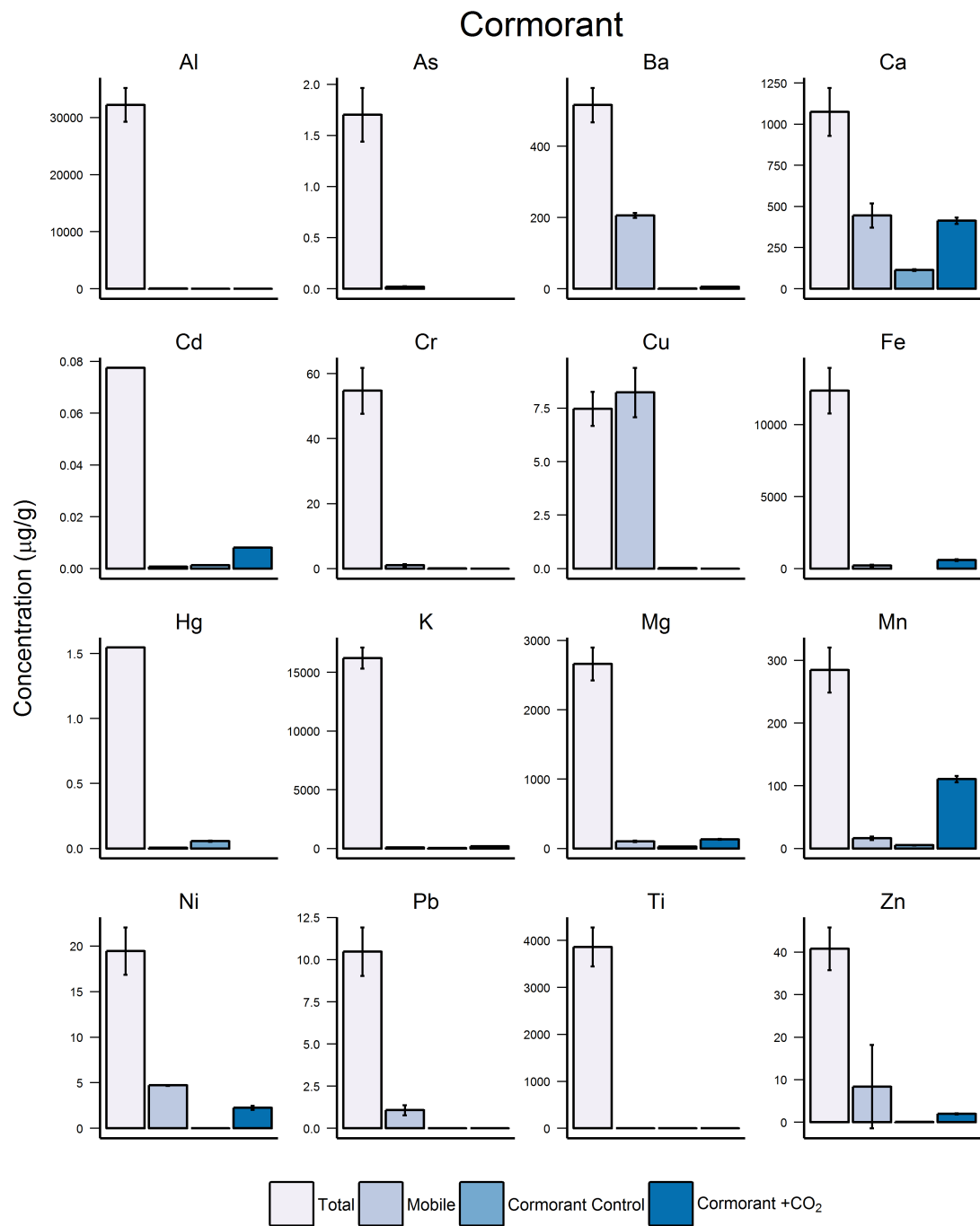
Figure 3.22: *Concentrations of elements leached (μg/g) from the Cormorant sample during batch experiments, compared with the whole rock and mobile fraction determined by the sequential extraction procedure. Error bars are 2s. Data provided in Table 3.10.*
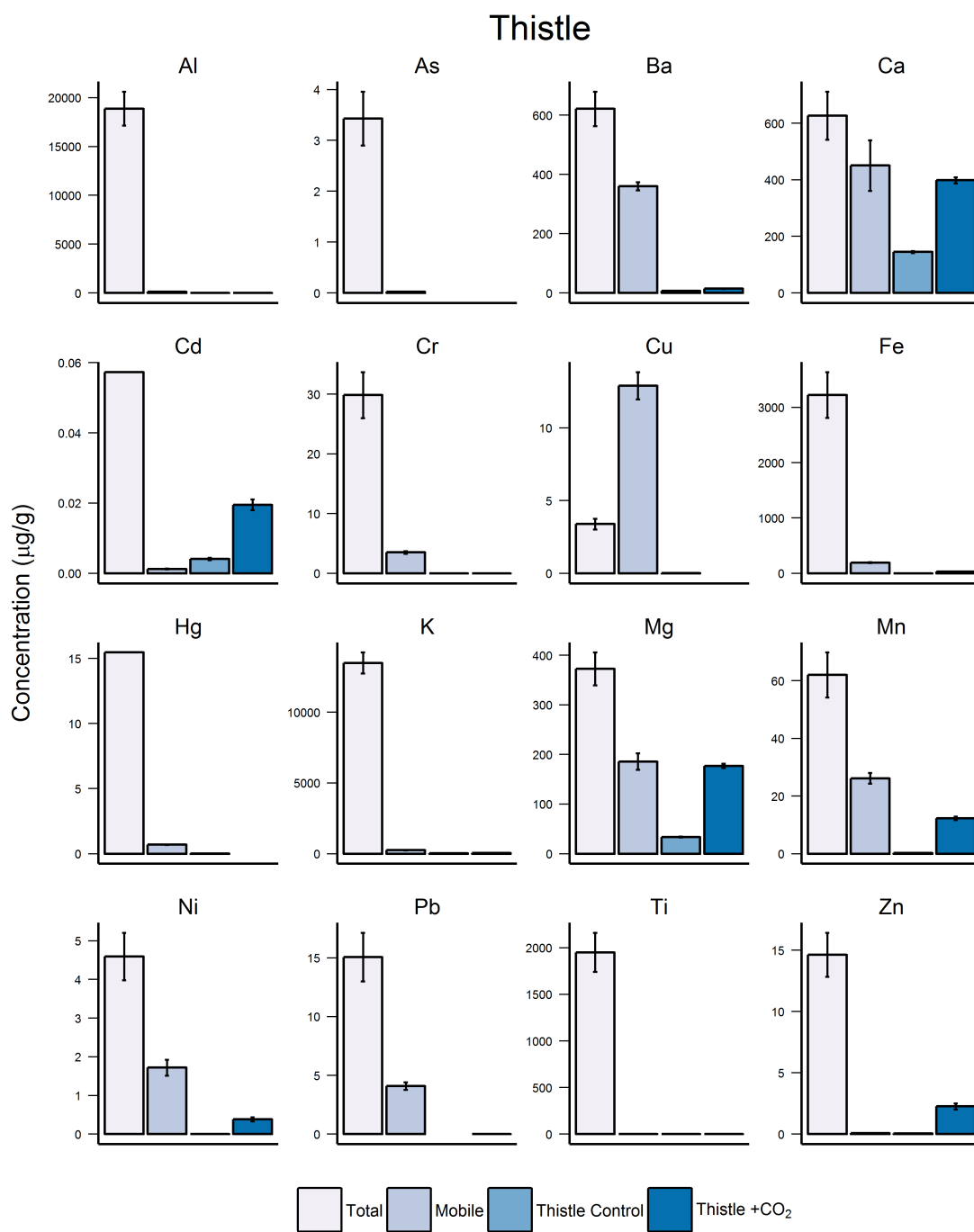
Figure 3.23: *Concentrations of elements leached (μg/g) from the Thistle sample during batch experiments, compared with the whole rock and mobile fraction determined by the sequential extraction procedure. Error bars are 2s. Data provided in Table 3.10.*

3.8 Field X Bulk Analysis

3.8.1 X-ray diffraction

The results of X-ray diffraction (XRD) analysis carried out on *Field X 8518* and *8579* samples (Section 2.8) are given in Table 3.11 as the mineral assemblage by weight % (wt.%). Values < 1 wt.% are trace concentrations and are considered semi-quantitative only, therefore their values should not be taken as accurate but indicative only of their presence in the sample.

Mineral	Type	Field X 8518		Field X 8579	
		wt.%	±	wt.%	±
Gypsum	Water soluble	0.1	0.1	0.2	0.1
Ankerite	Carbonate	0.3	0.3	0.3	0.3
Calcite		0.3	0.1	0.3	0.1
Dolomite	↓	0.2	0.1	0.3	0.1
Siderite		0.15	0.08	0.06	0.07
Corundum	Oxide	-	-	0.1	0.2
Pyrite	Sulphide	0.17	0.06	0.29	0.07
Albite	Silicate	0.2	0.3	-	-
Anorthite		1.1	0.4	1.0	0.4
Chlorite		0.3	0.5	0.3	0.5
Illite		2.0	0.3	2.2	0.3
Kaolinite		0.7	0.3	0.4	0.3
Microcline		2.1	0.7	3.1	0.4
Muscovite		0.8	0.8	1.0	0.4
Orthoclase		3.3	0.4	2.9	0.3
Quartz	↓	88	1	88	1

Table 3.11: *Results of XRD of Field X samples 8518 and 8579 as wt.% of mineral. SEP Type refers to the mineral types targeted by the sequential extraction procedure (Section 2.3.2).*

The minerals identified in *Field X* samples *8518* and *8579* have been broadly grouped in Table 3.11 by mineral type, as per the SEP method outlined in Section 2.3.2. As outlined for the previous North Sea samples, this classification is based on dissolution only of the mineral and not any other mechanism of element release. Summing the values of the grouped minerals and plotting them as a bar plot produces Figure 3.24.
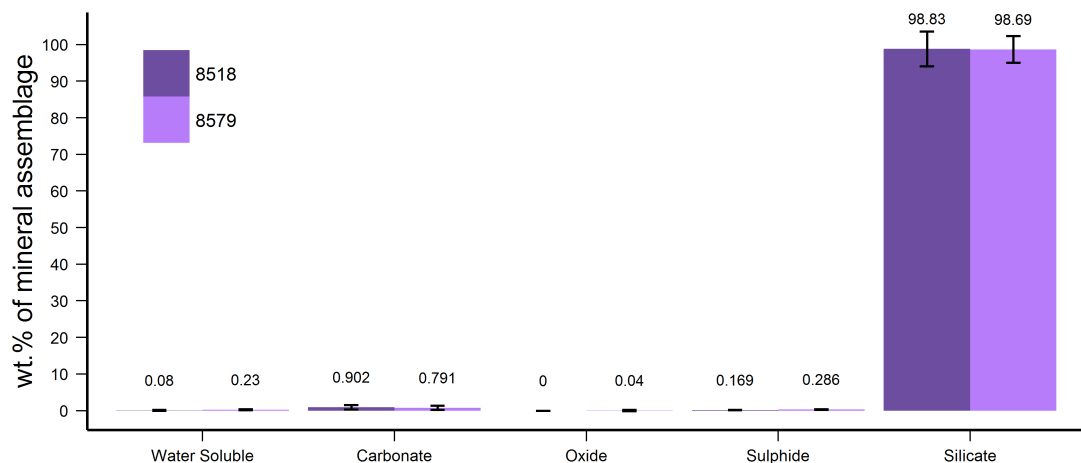
Figure 3.24: *Results of XRD analysis of Field X samples 8518 and 8579 grouped by mineral type, as wt.% of mineral. Summed values are given above each bar.*

As expected of these sandstone samples, silicate minerals dominate the mineral assemblage, with

essentially equal silicate content in both samples *8518* and *8579*, Figure 3.24. Clays and feldspars make up 11 ± 4 wt.% of silicates in *8518*, and 11 ± 3 wt.% in *8579*. Trace amounts of gypsum ($CaSO_4 \cdot 2\,H_2O$) were detected in both samples, and corundum (Al_2O_3) detected in trace concentrations in sample *8579*. Both samples contain the sulphide mineral pyrite (FeS_2) and < 1 wt.% carbonates, Figure 3.24.

Field X samples have a more diverse mineral assemblage than *Captain*, *Cormorant* or *Thistle* samples, with 16 minerals detected across two *Field X* samples compared with 12, 8 and 9, respectively, for the other fields.

3.8.2 X-ray fluorescence

Bulk chemical analysis of powdered *Field X* samples *8518* and *8579* was carried out by X-ray fluorescence (XRF) (Section 2.9). Results of the analysis are given in Table 3.12. Concentrations of the two samples are quite similar for most elements. Only one sample each of *8518* and *8579* was prepared, however, therefore any heterogeneity of the samples will not be captured by repeat analysis.

As previously mentioned, the XRF method employed at the University of Edinburgh does not allow for analysis of As, Cd and Hg, however the other five trace metals of interest were analysed for. Chromium and Cu concentrations are low compared with other elements, and Ni, Pb and Zn are all < 10 ppm. Aluminium and K are the dominant elements in both samples, probably due to the presence of the feldspars microcline and orthoclase (both $KAlSi_3O_8$).

Iron is also at significant concentrations in *8579*. The obvious associations are siderite ($FeCO_3$), ankerite ($Ca(Fe,Mg,Mn)(CO_3)_2$) and pyrite (FeS_2), however combined wt.% values of these minerals are 0.6 ± 0.4 (*8518*) and 0.5 ± 0.4 (*8579*), Table 3.12, which are similar enough that an explanation of a 10-fold difference in Fe concentrations between the samples is not evident.

Element	Field X 8518 XRF		Field X 8579 XRF	
	ppm	±	ppm	±
Al	6,000	300	7,800	400
Ba	2,500	0	1,300	0
Ca	2,900	500	1,800	300
Cr	16	0	13	0
Cu	40	0	33	0
Fe	560	5	6,330	60
K	5,100	100	7,000	200
Mg	1,000	200	900	100
Mn	-	-	7.8	0.6
Na	-	-	-	-
Ni	0.8	0	1.8	0
Pb	4.8	0	7.4	0
Ti	432	9	540	10
Zn	-	-	-	-

Table 3.12: *Results of bulk element analysis by XRF of Field X samples 8518 and 8579 (ppm). - Not detected in sample.*

Calcium and Mg concentrations are likely associated with the carbonate minerals ankerite, calcite ($CaCO_3$) and dolomite ($CaMg(CO_3)_2$). High Ba concentrations in these samples are most likely associated with the barium drilling mud used during extraction of the original rock core from *Field X*.

3.9 Field X Batch Reaction Experiments

3.9.1 pH

pH was measured throughout the experiment, on days 1 - 10, 13, 15 & 22. The CO_2 bottle was replaced on days 5 and 15 due to the gas running out, indicated by the dotted lines in Figure 3.25.

The addition of CO_2 to the *8579* flask appears to have little or no effect on pH values compared with the control flask, Figure 3.25, with pH values rising in both flasks from ∼ 5.4 to ∼ 7.0, with a dip at the end of the experiment in both flasks. Adding CO_2 to the *8518* flask does, however, appear to lower pH values compared with the control flask, however the difference in values is only around 0.2 pH units.

Compared with PHREEQC v3.3.3.10424 modelled pH values, using the carbonate concentrations in Table 3.11, the +CO_2 data for both *8518* and *8579* are in reasonably good agreement with the model, however pH values rise above this during the experiment, indicating that there is addition buffering occurring. pH values do, however, drop back down to close to the equilibrium pH value by the end of the experiment for sample *8518*; the batch experiment system may therefore have reached, or be approaching, equilibrium at that point.
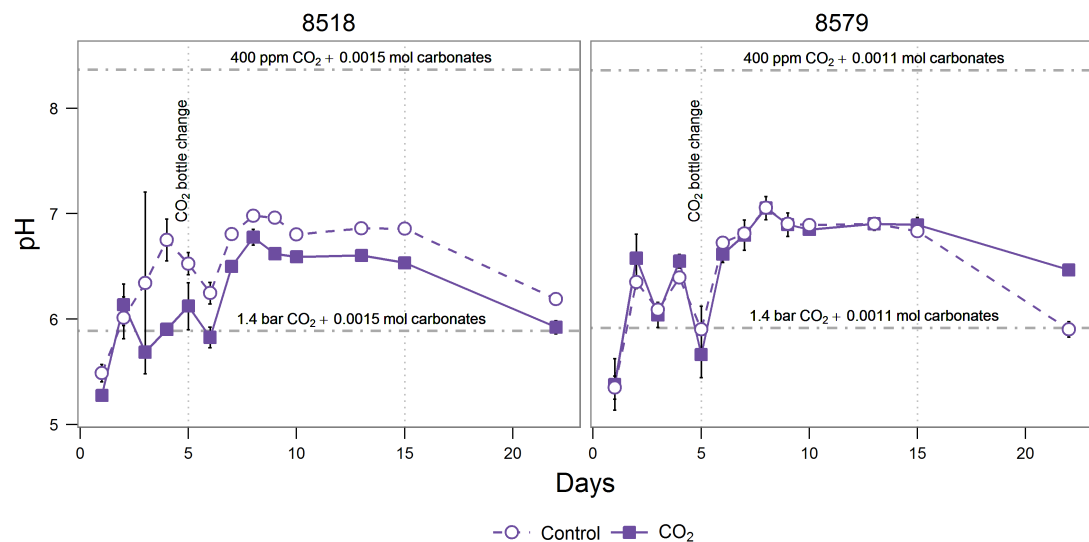
Figure 3.25: *pH values for the batch reaction experiment using samples of Field X. Dotted lines at days 5 and 15 indicate replacement of CO_2 bottle. Data points are the mean of three samples, error bars are 1s of measurements of 3 fluid samples. Horizontal dashed lines show PHREEQC modelled equilibrium pH values for atmospheric (400 ppm) CO_2 and bubbled (1.4 bar) CO_2 for the concentrations of carbonates (calcite, dolomite, siderite and ankerite) in the samples (Table 3.11).*

pH values are broadly very similar for all four flasks, with only the *8518* +CO_2 flask showing any deviation. One also can see that pH values fall within a much narrower band of values (5.4 - 7.0), compared with the *Captain*, *Cormorant* or *Thistle* samples.

Mineral buffering of pH does not appear to be strongly influencing pH values in sample *8579*, based on the similarity between no-CO_2 and +CO_2 values, however there is a slightly stronger effect for sample *8518*.

3.9.2 Alkalinity

Concentrations of bicarbonate (HCO_3^-) were measured on days 1 - 10, 13, 15 & 22 (Section 2.4.3). Bicarbonate values are shown in Figure 3.26 for *Field X* samples *8518* and *8579*, with and without added

CO$_2$.
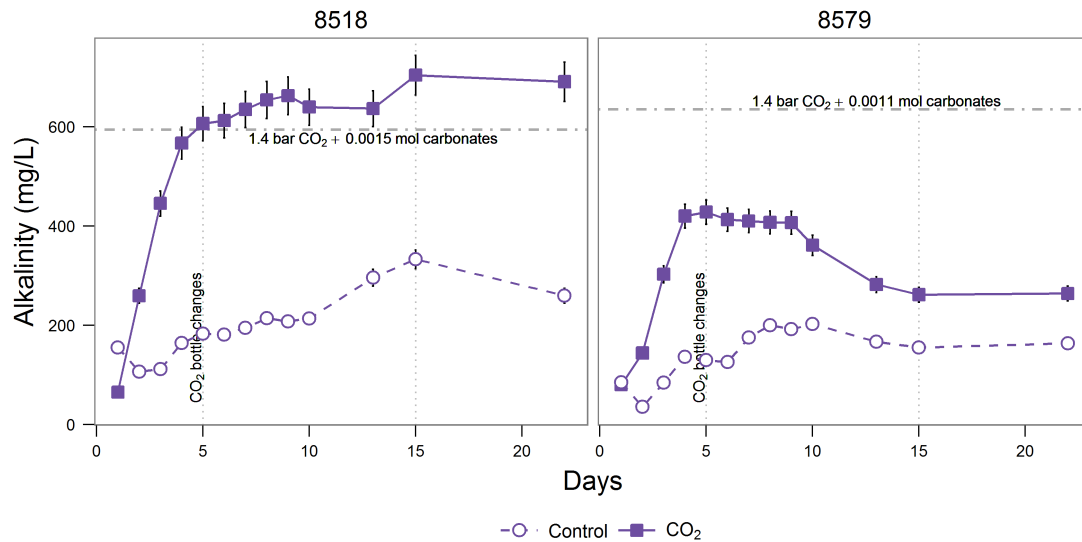
Figure 3.26: *Alkalinity values for the batch reaction experiment using samples of Field X. Dotted lines at days 5 and 15 indicate replacement of CO$_2$ bottle. Error bars are 2s. Horizontal dashed lines show PHREEQC modelled equilibrium alkalinity values (as HCO$_3^-$) for bubbled (1.4 bar) CO$_2$ for the concentrations of carbonates (calcite, dolomite, siderite and ankerite) in the samples (Table 3.11).*

Carbonate alkalinity in the *8518* and *8579* control flasks ranged from 106 mg/L to 333 mg/L, and 35 mg/L to 163 mg/L, respectively. Both control flasks reach a maximum concentration before decreasing slightly, Figure 3.26. The *8518* flask with added CO$_2$ increased rapidly from 65 mg/L to $\sim$ 600 mg/L over days 1-5, and then steadily increased to $\sim$ 700 mg/L. The *8579* flask increased from 80 mg/L to 428 mg/L by day 5 before levelling off to day 9 and then decreasing to $\sim$ 265 mg/L by the end of the experiment.

Carbonate alkalinity values are again higher for the +CO$_2$ flasks, indicating that mineral dissolution is affecting the fluid chemistry. Both *8518* flasks have consistently higher alkalinity concentrations than the *8579* flasks, which could be explained by the greater abundance of carbonate minerals in sample *8518*, albeit only slightly higher abundance (Table 3.11). Experimentally derived alkalinity values for sample *8518* are close to the PHREEQC modelled concentrations, Figure 3.26, however *8579* experiment values are $\sim$ 3 times lower than the model output. As with pH, this appears to show that sample *8518* is near, or reached, equilibrium in this batch CO$_2$-water-rock system. Sample *8579* also appears to have reached an equilibrium, albeit at a lower value than the model. Given the uncertainty on the presence of individual carbonate minerals, the model output could be an overestimate.

The alkalinity concentration trend of sample *8518* +CO$_2$ would indicate initial rapid dissolution mineral, which then becomes limited by the mass of mineral available for dissolution. In sample *8579* +CO$_2$ the decrease in alkalinity after an early peak would suggest that the mineral(s) contributing to alkalinity have been completely dissolved and that alkalinity is being consumed to buffer pH.

3.9.3 Trace metals of interest

Concentrations of As, Cr, Hg and Pb are all below detection limits (Table 2.11), after removing high outlier values for Hg (7.41 µg/L, *8518* control day 15) and Pb (344 µg/L), Cu (9,164 µg/L), and Zn (5,414 µg/L) for *8518* +CO$_2$ day 22. Cadmium, Cu Ni and Zn are plotted in Figure 3.27.

Leached concentrations of Cd are mostly < LOD for the duration of the experiment for both *Field X* samples, with a maximum concentration of 3.24 ± 0.12 µg/L on day 1 in the *8518* control flask.

Copper concentrations increase in both *8518* +CO_2 and control flasks to maximums on day 3, with the control flask higher at 2,757 ± 200 μg/L compared with 2,063 ± 150 μg/L in the +CO_2 flask. Concentrations decline from these points in both cases, with the +CO_2 concentrations declining more rapidly. Sample *8579* concentrations increased slightly in both flasks, again to maximums on both days not exceeding 127 ± 9 μg/L before dropping below the analytical LOD. Concentrations spike again at 2,781 ± 202 μg/L on day 15 in the *8579* control flask, before dropping again, Figure 3.27.
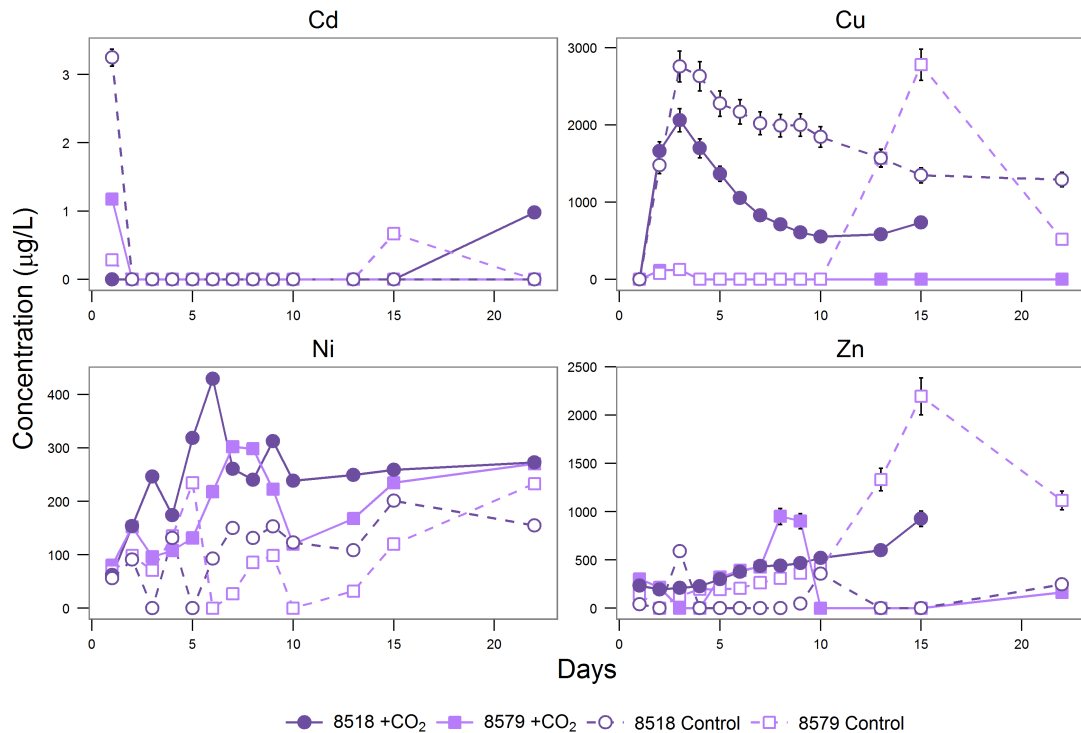
Figure 3.27: *Concentrations of Cd, Cu, Ni and Zn obtained by ICP-MS for Field X samples 8518 and 8579. Error bars are 2s of the mean of standard reference material values, Section 2.10.*

Zinc exhibits a similar trend to Cu for the *8579* control flask, peaking on day 15 at 2,194 ± 191 μg/L. Concentrations in the *8518* control flask are mostly < LOD, with a maximum reached on day 3 of 589 ± 51 μg/L, however the *8518* +CO_2 flask had steadily increasing concentrations, elevated above the control flask, reaching a maximum of 927 ± 81 μg/L on day 15.

Similarly, Ni shows gradual increases in concentration in all flasks over the duration of the experiment, with the +CO_2 flasks consistently higher than the Controls, indicating that for Ni - and Zn for *8518* - concentrations are enhanced with the addition of CO_2 to the flasks.

For Cu, the addition of CO_2 appears to retard metal release, and decreasing concentrations might be indicative of mineral formation, incorporating Cu.

3.9.4 Major elements

Six of the seven major element concentrations obtained by ICP-MS are plotted in Figure 3.28. Lithium was also analysed for but all values obtained were less than the instrumental LOD.

Calcium, Mg and Mn show similar trends for both samples *8518* and *8579*. *8518* +CO_2 concentrations peak at day 10, before decreasing slightly and then levelling off for the remainder of the experiment. The control flask for *8518* shows a more steady increase, with concentrations significantly lower than the +CO_2 flask. The *8579* +CO_2 flask increases concentrations at essentially the same rate as the *8518* +CO_2

flask, but peaks at days 4-5, before declining to approximately half the concentration values of the peaks, while the control flask for *8579* has an initial rapid increase at a similar rate to the $+CO_2$ flask until days 3-5, but then concentrations flatten out (Mg, Mn) or decrease (Ca). The decrease in $+CO_2$ flask concentrations in *8579* reduce values to below the control flask by day 13, Figure 3.28.

The Ca, Mg and Mn trends would be indicative of the dissolution of the carbonates present in the samples. Sample *8518* has slightly more carbonate content than *8579* (Figure 3.24), which can be seen by the increased concentrations of these elements in solution for this sample. The decrease in concentrations of *8579* is suggestive of the near-complete dissolution of the mineral(s). The control flasks don't decrease with time as their dissolution rate is slower than with the addition of CO_2.
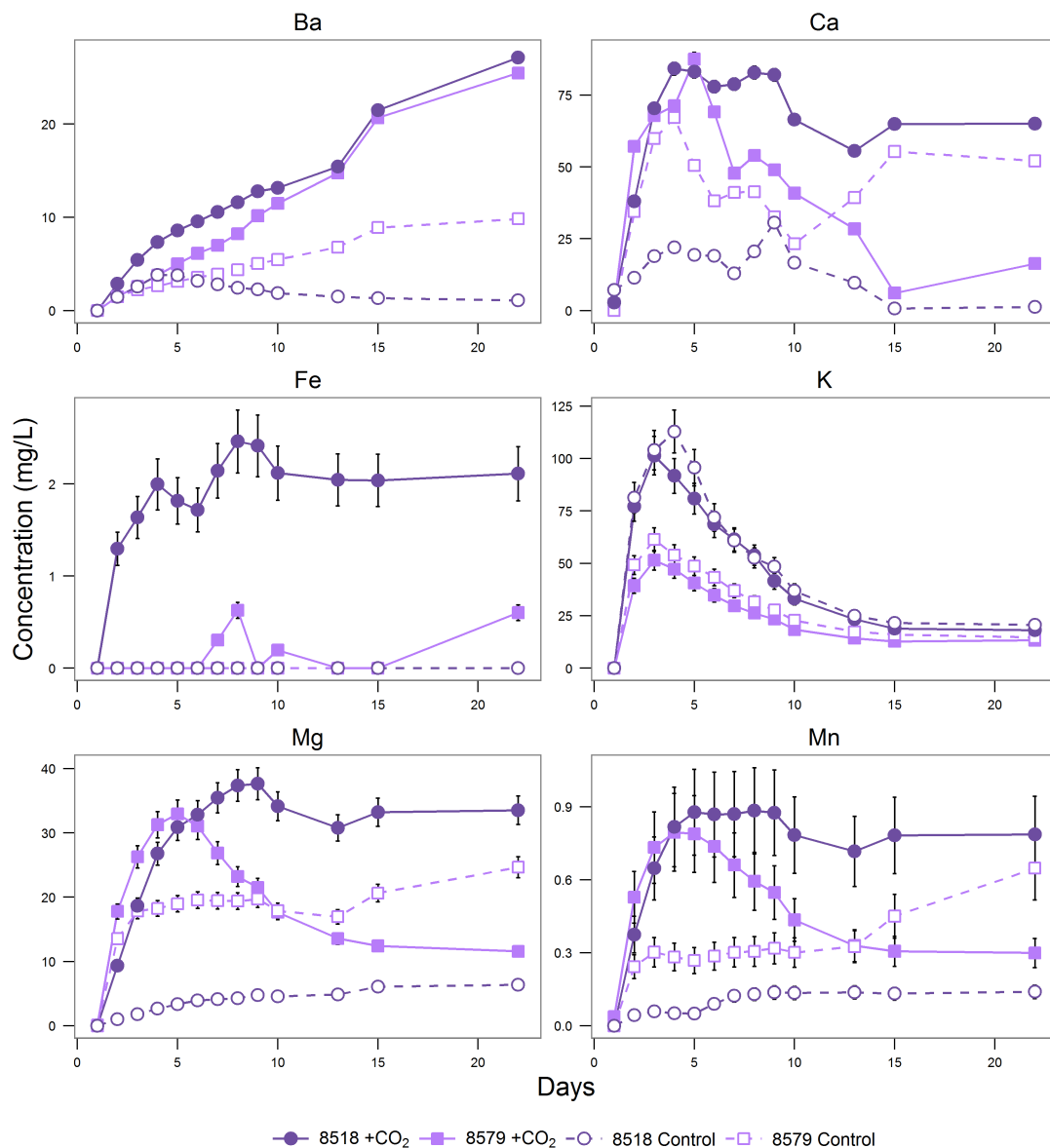
Figure 3.28: *Concentrations of major elements obtained by ICP-MS (mg/L) for Field X samples 8518 and 8579. Error bars are 2s of the mean of standard reference material values, Section 2.10.*

Iron is another element associated with carbonate in the samples (siderite & ankerite) which are both higher in abundance in *8518* than in *8579*. Fe increases to a peak of 2.5 ± 0.3 mg/L at day 8, with a slight decrease and subsequent levelling off. A maximum concentration of 0.6 ± 0.1 mg/L is reached by day 8

for *8579*, but otherwise displays no trend, and concentrations of the control flasks for both samples are < LOD. The Fe concentration trends for *8518* +CO_2 is also indicative of carbonate dissolution, with only low amounts of siderite (the most likely suspect) available for dissolution. Otherwise, the apparent high concentrations of Fe in *8579* (Table 3.12) are not available for ready leaching with +CO_2.

Barium concentrations for both +CO_2 flasks show a largely linear rise through the duration of the experiment, and are consistently higher than the control flasks. Concentrations of Ba in both +CO_2 flasks are similar, with final concentrations of 27.1 $\pm$ 0.6 and 25.5 $\pm$ 0.5 for *8518* and *8579*, respectively. Given the mineral assemblage of both samples containing $\sim$ 1 wt.% carbonates, one might conclude that Ba is being released from these minerals, given Ba can be a common carbonate forming element, however the trend in concentrations is different to the aforementioned Ca, Mg, Mn and Fe. As noted previously (Section 3.8.2), Ba is most likely associated with barium drilling muds which have penetrated the core, and this could explain the similarities between concentrations with the addition of CO_2.

Potassium concentrations are the largest of the 6 major elements reported here, with the *8518* control peaking at 113 $\pm$ 10 mg/L on day 4. All flasks exhibit the same trends of rapid increases in concentrations, peaking at days 3 or 4, before declining to $\sim$ 13-20 mg/L. Unlike the previous metals discussed, concentrations in the control flasks exceed the +CO_2 flasks, suggesting that the addition of +CO_2 has no significant influence over the release of K from these samples. Mineral dissolution appears to be occurring, however, with concentrations limited by the mass of the mineral(s). Potassium would be most strongly associated with the feldspars present in the samples, however they are much more abundant than carbonates yet leached K concentrations don't reflect this difference. Partial dissolution of already weathered feldspars may be occurring, or the source of K may be another type of mineral entirely.

3.9.5 Mobilised concentrations comparison

The sequential extraction procedure was not carried out on *Field X* samples, therefore the mobile and immobile fractions of the elements analysed for the batch experiments have not been determined.

A comparison can be made, however, between the mobilised concentrations from the batch experiments (as μg/g of sample) and the bulk concentrations determined by XRF (Section 2.9). One can then see the relative mobility of these elements, since the more an element is proportionally mobilised, the more mobile that element is assumed to be. The comparison was only carried out where data was available for both XRF and ICP-MS derived concentration values, Figures 3.29 and 3.30, and Table 3.13.

| Element | Field X 8518 | | | | | | Field X 8579 | | | | | |
| | Total | | Control | | +CO_2 | | Total | | Control | | +CO_2 | |
	μg/g	$\pm$	μg/g	$\pm$	μg/g	$\pm$	μg/g	$\pm$	μg/g	$\pm$	μg/g	$\pm$
Ba	2,500	0	30.2	0.6	437	9	1,300	0	156	3	424	9
Ca	2,900	500	223	6	1,760	50	1,800	300	1,210	30	920	30
Cr	16	0	-	-	-	-	13	0	-	-	-	-
Cu	40	0	42	3	140	10	33	0	11.7	0.9	0.28	0.02
Fe	560	5	-	-	53	7	6,330	60	30	4	10	1
K	5,100	100	1,050	100	970	90	7,000	200	630	60	590	50
Mg	1,000	200	132	9	820	50	900	100	540	40	470	30
Mn	-	-	3.1	0.6	20	4	7.8	0.6	12	3	12	2
Ni	0.8	0	3.45	0.01	6.99	0.03	1.8	0	4.13	0.02	6.44	0.03
Pb	4.8	0	-	-	4.7	1.0	7.4	0	-	-	-	-
Zn	-	-	4.5	0.4	80	7	-	-	21	2	6.5	0.6

Table 3.13: *Table of concentrations comparing masses of elements released during batch experiments with total masses in sample, and masses theoretically mobile with CO_2 based on the SEP "Mobile" classification. Uncertainties are 2s.*

Figures 3.29 and 3.30 show that most major elements, with the exceptions of Fe and K, are quite strongly mobilised with respect to the bulk concentrations; maximum mobilised concentrations are in the range of $\sim$ 12 - 98% (median 38.5%) of the bulk concentrations, with Ca and Mg most strongly mobilised.
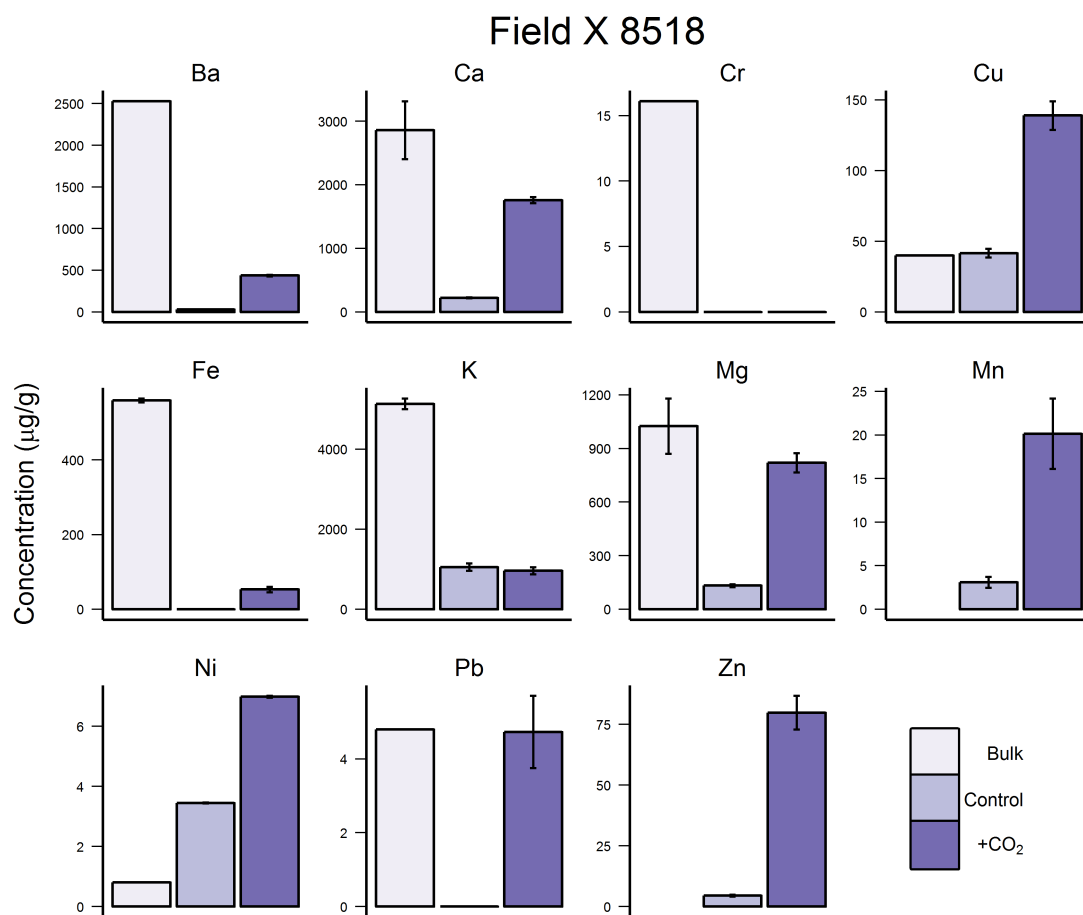
Figure 3.29: *Concentrations of elements leached (µg/g) from Field X sample 8518 during batch experiments, compared with the whole rock fraction determined by XRF. Error bars are 2s. Data provided in Table 3.13.*

Maximum mobilised Mn concentrations are ~ 1.5 times the bulk concentrations (*Field X 8579*), and Mn is mobilised in concentrations which exceed the XRF LOD value for sample *8518* (0.5 µg/g).

The addition of CO_2 elevates mobilised concentrations above the control in sample *8518* for all of the major elements except K, although does not appear to enhance mobilisation in sample *8579*, except for Ba. If one considers the concentration trends, Figure 3.28, it is apparent that CO_2 does enhance concentrations, but in some cases CO_2 enhanced concentrations decrease and by the end of the experiment are lower than the Controls. Since the calculation for mass of element released is sensitive to the final volume of batch fluid, and since the final *Field X* volume was large (250 mL, compared with the 20 mL sample aliquots), then the final concentration makes a large difference to the overall calculation. The exception is K, where concentrations for both samples rise and fall in tandem, with the Controls having slightly higher concentrations throughout the experiment, Figure 3.28.

Mobilised concentrations of Cu (*8518*), Ni, and Zn exceed the bulk sample concentrations for these elements, Figure 3.29. In the case of Zn, mobile concentrations were higher than the Zn analytical LOD for the XRF technique (0.5 µg/g). Cu concentrations are ~ 3 times higher, and Ni concentrations are ~ 3 - 8 times higher than bulk concentrations. These, and the major element concentrations which are also higher than the bulk composition, could be the result of sample heterogeneity, since the batch reacted samples were not the same as samples prepared for XRF. Large volumes of *Field X* material were not available for homogenising to reduce the effect of single random mineral grains significantly influencing the results.
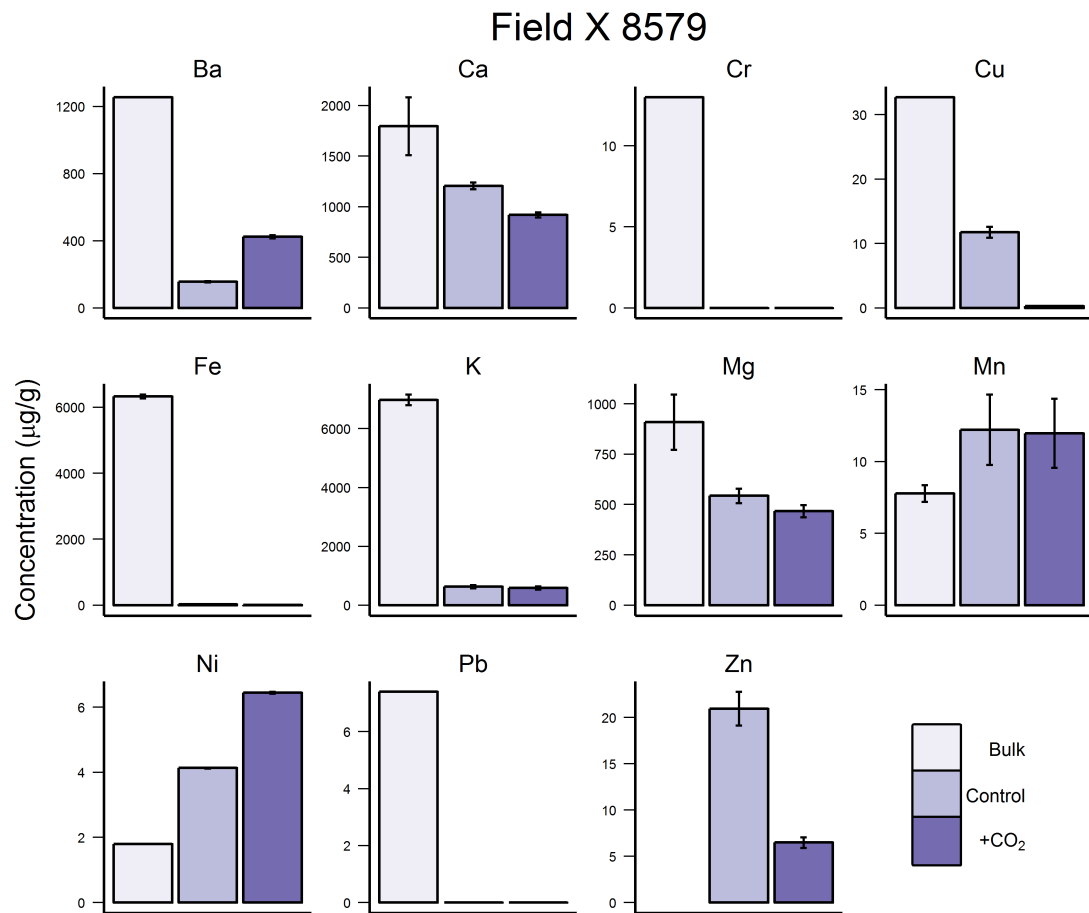
Figure 3.30: *Concentrations of elements leached (μg/g) from Field X sample 8579 during batch experiments, compared with the whole rock fraction determined by XRF. Error bars are 2s. Data provided in Table 3.13.*

Otherwise, trace metal mobility is very low for Cr, Cu (*8579*) and Pb, since these elements are largely < LOD. The exception is Pb for sample *8518* where mobilised concentrations are similar to bulk composition, Figure 3.29.

3.10   Discussion

3.10.1   pH and alkalinity

The results of the batch experiments on samples of North Sea reservoir rocks indicate that the addition of CO_2 to a system of synthetic NaCl brine and arkosic sandstone reduces pH by up to 1 pH unit, Figures 3.2, 3.14 and 3.25.

Modelled pH values using PHREEQC v3.3.3.10424 for the batch experiments conducted with just NaCl solutions and 1.4 bar bubbled CO_2, give pH values of $\sim$ 4.0. These compare very well with values of $\sim$ pH 4 for the blank $+CO_2$ experiment conducted for the 2011 MSc project (Figure 3.2), and with pH values of $\sim$ 5.5 - 6.5 for the batch experiments with rock samples.

This $\sim$ 1 pH unit reduction in the batch experiments would therefore be larger were it not for the buffering capacity of the rock samples, whereby protons generated by CO_2 dissolution and subsequent H_2CO_3 dissociation in the brine are consumed in the process of mineral dissolution, as per Equations 3.1 and 3.2.

$$CaMg(CO_3)_2 + 2\,H_2CO_3 \longleftrightarrow Ca^{2+} + Mg^{2+} + 4\,HCO_3^{-} \tag{3.1}$$

$$2\,KAlSi_3O_8 + 2\,H_2CO_3 + 9\,H_2O \longrightarrow Al_2Si_2O_5(OH)_4 + 2\,K^{+} + 4\,H_4SiO_4 + 2\,HCO_3^{-} \tag{3.2}$$
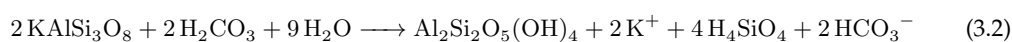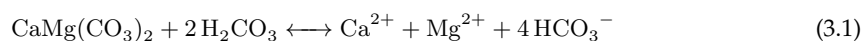
A further indication of mineral buffering of pH, as per Equations 3.1 and 3.2, is the significant increase in alkalinity (as HCO_3^{-}) in $+CO_2$ experiments, compared with the Controls. Again, the blank experiments undertaken for the 2011 MSc show that the addition of CO_2 alone does not affect HCO_3^{-} concentrations (Figure 3.3), with recorded values in the range 25 - 65 mg/L, regardless of whether CO_2 was added. These compare with PHREEQC modelled value of 9 mg/L for a 13,500 ppm NaCl solution at 58°C (Figure 3.3), which is lower than experimental values. Measured alkalinities in the experiments are of similar values to those found in the literature from similar experiments (e.g. Lu *et al.* 2014).

3.10.2   Batch experiment metals

Tables 3.14 and 3.15 summarise the results of the batch experiments on *Captain*, *Cormorant*, *Thistle* and *Field X* samples. In the first table, Table 3.14, an assessment has been made on whether the addition of CO_2 to the batch flasks has increased concentrations of the listed elements with respect to the control flasks. Table cells marked with a cross mark (✗) indicate that CO_2 has not enhanced concentrations, cells with a checkmark (✓) indicate that it has, cells with a tilde (~) indicate some uncertainty, and blank cells are where concentrations fell below analytical detection limits (LODs), or were not analysed for.

In the majority of cases, concentrations of the 8 trace metals of interest (As, Cd, Cr, Cu, Hg, Ni, Pb, Zn) were found be either below analytical detection limits, or at 10's µg/L level, Figures 3.4, 3.16, and 3.27. Trace metals also, on the whole, do not appear to be mobilised to a greater extent with the addition of CO_2, Table 3.14. The main exceptions to this are Ni and Zn, where in the majority of batch experiments, their concentrations were enhanced with $+CO_2$. Copper also was considered to be additionally mobile with CO_2 addition for *Field X 8518*, and possibly for *Captain SA7*. Cadmium is also considered enhanced with CO_2 for *Thistle*, and Pb enhanced for *Captain SA7*, Table 3.14.

Nickel and Zn are metals commonly cited as mobile with enhanced CO_2 conditions (e.g. Humez *et al.* 2013; Little and Jackson 2010; Lu *et al.* 2010; Varadharajan *et al.* 2013), with Cu generally considered to have low mobility. In this respect, the results of the batch experiments are similar to those in published studies, although Terzi *et al.* (2014) found that the addition of CO_2 significantly mobilised Cu, as well as Ni and Zn, from deionised water saturated sands with artificially modified grain coatings of various metals. Moderate Cr and Cd mobilisation was also determined from the Terzi *et al.* (2014) study.

Element	Captain SA7	Captain SA10	Cormorant	Thistle	Field X 8518	Field X 8579
Al	✗	✗	✗	✗	< LOD	< LOD
As	✗	✗	< LOD	< LOD	< LOD	< LOD
Ba	✓	✓	✓	✓	✓	✓
Ca	✓	✓	✓	✓	✓	✓
Cd	✗	✗	✗	✓	✗	✗
Cr	✗	~	✗	✗	< LOD	< LOD
Cu	~	✗	✗	✗	✓	✗
Fe	✗	~	✓	✓	✓	~
Hg	✗	✗	✗	✗	< LOD	< LOD
K	✗	~	✓	✗	✗	✗
Li	-	-	✓	✗	-	-
Mg	✓	✓	✓	✓	✓	✓
Mn	✓	✓	✓	✓	✓	✓
Ni	✓	✓	✓	✓	✓	✓
Pb	✓	✗	✗	✗	< LOD	< LOD
Si	-	-	✗	✗	-	-
Sr	-	-	✓	✓	-	-
Ti	✗	✗	-	-	-	-
Zn	✓	✓	✓	✓	✓	✗

Table 3.14: *Summary of whether CO_2 has enhanced element concentrations in batch experiments. ✓ = enhanced concentrations with CO_2, ✗ = not enhanced with CO_2, ~ = possible enhancement, - = data not available, < LOD = data less than analytical detection limit.*

Major elements Ba, Ca, Fe, Mg, Mn, and Sr exhibit, in virtually all cases, enhanced concentrations with the addition of CO_2, Table 3.14. This strong response in these elements is also noted in other published studies, with the large and rapid increases in concentration with CO_2 addition largely attributed to dissolution of carbonates (e.g. Kjöller *et al.* 2011; Rosenbauer *et al.* 2005; Shiraki and Dunn 2000; Varadharajan *et al.* 2013), or desorption mechanisms (e.g. Cahill *et al.* 2013; Mickler *et al.* 2013; Varadharajan *et al.* 2013). Slower releases of elements, e.g. Fe, K and Al are then attributable to silicate or oxide dissolution by these authors.

Table 3.15 classifies the elements analysed in each of the $+CO_2$ batch experiments based upon their general behaviours with respect to time-dependent mobility. **Type I** elements increased concentrations through time; **Type II** elements increased in concentration before levelling off for the remainder of the experiment; **Type III** elements increased in concentrations, either slowly or rapidly, before decreasing again before the end of the experiment; and **Type IV** elements were either not detected above the analytical LOD's, *or* did not display any time-dependent trend *and/or* varied randomly in concentration. This classification does not indicate anything with regard to whether concentrations are enhanced with respect to the Controls: see Table 3.14 for this information.

	Type I	Type II	Type III	Type IV
Captain SA7	Ca, K, Mg, Mn, **Ni**, **Zn**		Ba	Al, **As**, **Cd**, **Cr**, **Cu**, Fe, **Hg**, **Pb**, Ti
Captain SA10	Ba, Ca, K, Mg, Mn, **Ni**, **Zn**		Fe	Al, **As**, **Cd**, **Cr**, **Cu**, **Hg**, **Pb**, Ti
Cormorant	Ba, Ca, Fe, K, Li, Mn, **Ni**, Si, Sr	Mg, **Zn**		Al, **As**, **Cd**, **Cr**, **Cu**, **Hg**, **Pb**
Thistle	Ca, **Ni**	K, Li, **Zn**	Ba, Mg, Mn, Si, Sr	Al, **As**, **Cd**, **Cr**, **Cu**, Fe, **Hg**, **Pb**
Field X 8518	Ba, **Zn**	Fe, **Ni**	Ca, **Cu**, K, Mg, Mn	**As**, **Cd**, **Cr**, **Hg**, **Pb**
Field X 8579	Ba	**Ni**	Ca, K, Mg, Mn	**As**, **Cd**, **Cr**, **Cu**, Fe, **Hg**, **Pb**, **Zn**

Table 3.15: *Classification of element mobility from batch experiments with bubbled CO_2. Type I: Concentrations rise through time; Type II: concentrations rise and then level off; Type III: concentrations rise initially then decrease through time; Type IV: concentrations vary randomly and/or independently of time, or are < LOD. Bold lettering highlights 8 trace metals of interest.*

One can see that most elements analysed fall into either Type I or Type IV time-dependent categories, particularly for *Captain* and *Cormorant* samples. *Thistle* and *Field X* samples tend to have more elements in the Type III category of decreasing concentrations after an initial peak. It is also apparent that the 8 trace metals of interest are also mostly categorised as Type IV elements, therefore they are of low concentrations, or are not being systematically mobilised with time with the addition of CO_2. The exceptions again here are, for the most part, Ni and Zn, which are categorised in Types I and II in 6 out of 6, and 5 out of 6 of the batch experiments, respectively. The only other trace metal to show increasing concentrations is Cu during the *Field X 8518* experiment (Figure 3.27), which peaks rapidly before tailing off again.

The major elements identified in Table 3.14 as being enhanced by CO_2 (Ba, Ca, Mg, Mn) largely occupy Type I and III categories, Table 3.15. Potassium and Si are unusual here, since they are not additionally mobilised by CO_2, but nonetheless display distinct concentration trends.

Comparing concentrations of mobilised elements with other work, four previous studies' results are cited in Table 3.16, for which data was easily available. Minimum and maximum concentrations from all experiments reported in each study are summarised for both $+CO_2$ and control experiments, and compared with the results of this study. Mercury is an element which is not routinely analysed for in other studies, possibly due to the difficulty in sample preservation and analysis, and therefore the results of this project cannot be compared with the published literature, due to a lack of data.

One can see that, in fact, the range of values of the 8 trace metals of interest mobilised from the North Sea sandstones is broadly similar to the range of concentrations seen by other authors, albeit with some variability depending on the sample type used (e.g. organic-rich soils, chalks, arkosic sandstones, etc.). Chromium, for example, is present in high concentrations in the Lu *et al.* (2014) study, compared with this study, while Pb is typically higher in concentration from this study's North Sea sandstones than other samples referred to in Table 3.16. It is interesting to note that, although the Lu *et al.* (2014) study is carried out at reservoir pressures (200 bar), the range of concentrations measured during their experiments are not dissimilar to other studies (including this one) carried out at atmospheric pressures. Bulk metal composition data is not available for the Lu *et al.* (2014) study, and so it may be that their samples were low in total metals and that CO_2 was more effective at leaching than the experiments described for this thesis. Whether the concentration ranges from the Lu *et al.* (2014) would have been different if their experiments were carried out at atmospheric pressure is unknown, however it appears that greater pressures (and hence greater CO_2 dissolution) do not necessarily equate to greater element mobilisation, especially with respect to the trace metals of interest, Table 3.16.

Barium, K and Li concentrations are generally higher in this study's batch experiments than those reported by other authors, Table 3.16, however elements such as Ca, Ba and Sr are significantly lower than maximum concentrations reported by others, which would be expected since these studies often use calcareous sandstones (Lu *et al.*, 2010) or carbonate-rich soils (Cahill *et al.*, 2013). Only minor carbonate is present in the rocks considered for this study.

Increasing or increasing/levelling concentrations with time (Type I and II) would suggest steady mineral dissolution and supply of cations to solution, rather than rapid desorption from mineral surfaces with pH changes. Since most of the 8 trace metals do not fit this categorisation (i.e. Type IV), then their concentrations are perhaps not dependent on mineral dissolution, but rather on pH-dependent desorption. To determine this, firstly one can compare the mobilised concentrations from the batch experiments with the first two SEP steps (water soluble and exchangeable). These steps represent the most mobile elements, which do not require mineral dissolution with anything more than just water.

Element (µg/L)	Little and Jackson (2010) Soils 1 bar 20°C +CO$_2$	Control	Lu *et al.* (2010) Sandstones 1 bar 25°C +CO$_2$	Control	Cahill *et al.* (2013) Sediments[†] 1 bar 25°C +CO$_2$	Lu *et al.* (2014) Sandstones 200 bar 70-100°C +CO$_2$	Control	This study Sandstones 1 bar 57-98°C +CO$_2$	Control
Al	0 - 9,658	0 - 13,444	0 - 31,063	0 - 27,704	0 - 601	70 - 17,433	5 - 2,436	0 - 249	0 - 320
As	0 - 10	0.010 - 20	0 - 110	0 - 19		0 - 23	0 - 35	0 - 4	0 - 9
Ba	8 - 1,141	0.482 - 235	3 - 1,161	0.34 - 394	3 - 276	7 - 9,630	0.062 - 12,875	0 - 27,123	0 - 9,847
Ca	4,132 - 963,053	85 - 515,535	1,261 - 470,843	0 - 278,659	391 - 917,399	545 - 237,674	46 - 1,071,189	2,304 - 180,290	0 - 67,180
Cd	0 - 3	0 - 4	0 - 45	0 - 3	0 - 0.63	0 - 6	0 - 4	0 - 2	0 - 3
Cr	0 - 30	0 - 27	0 - 117	0 - 15	0 - 5	5 - 1,852	2 - 3,859	0 - 9	0 - 62
Cu	0.02 - 46	0 - 49	0 - 1,458	0 - 801	1 - 12	660 - 3,171	0.10 - 2,348	0 - 2,063	0 - 2,781
Fe	0 - 11,954	7 - 3,258	0 - 8,402	0 - 38,748	0 - 232	14 - 68,423	11 - 217,282	0 - 43,208	0 - 116
Hg								0 - 4	0 - 29
K			422 - 91,371	154 - 67,702	285 - 20,394	3,107 - 30,801	2 - 31,914	0 - 101,375	0 - 112,906
Li	2 - 333	0 - 85	0 - 24	0 - 24	0 - 84			0 - 236	0 - 158
Mg	1,725 - 342,575	77 - 232,054	182 - 630,230	26 - 312,243	183 - 81,398	331 - 28,821	1 - 34,676	0 - 37,675	0 - 24,671
Mn	25 - 2,722	0 - 1,664	0.87 - 3,773	0 - 2,299	2 - 10,958	0.88 - 4,623	0.28 - 5,655	0 - 7,800	0 - 1,909
Ni	1 - 2,207	0 - 2,314	0 - 161	0 - 140	0 - 74	50 - 22,931	0.27 - 20,583	0 - 429	0 - 480
Pb	0 - 4	0.001 - 0.25	0 - 51	0 - 8	0 - 1	0 - 53	0 - 269	0 - 434	0 - 40
Si			937 - 73,259	0 - 15,495		2,832 - 50,571	28 - 29,259	741 - 22,270	1,228 - 98,269
Sr	22 - 6,332	0.53 - 4,363	9 - 6,164	0.24 - 5,216	3 - 78,313	9 - 6,411	0.081 - 5,780	147 - 1,361	126 - 900
Ti						0 - 3.49	0 - 4.59	0 - 37	0 - 28
Zn	0 - 3,311	0.15 - 2,529	0 - 192	0 - 362	1 - 46	9 - 24,906	1 - 37,308	0 - 951	0 - 2,194

Table 3.16: *Minimum & maximum concentration data from recent batch experiment studies.* [†]*Includes two chalks.*

On the assumption that elements are mobilised by water solubility and ion exchange preferentially to mineral dissolution in the batch experiments, a comparison can be made between the mobilised elements and the sum of SEP Steps 1 and 2. This is represented in Table 3.17 as the mobilised concentrations as a percentage of the sum of SEP Steps 1 and 2. Where values are > 100%, it is assumed that element concentrations are supplemented or dominated by mineral dissolution.

Element	Captain		Cormorant		Thistle	
	Control	+CO_2	Control	+CO_2	Control	+CO_2
Al	17%	7%	> 100%	> 100%	> 100%	28%
As	15%	6%	-	-	-	-
Ba	6%	79%	1%	11%	7%	15%
Ca	87%	> 100%	26%	95%	41%	> 100%
Cd	67%	52%	> 100%	> 100%	> 100%	> 100%
Cr	> 100%	> 100%	-	-	> 100%	93%
Cu	16%	44%	52%	7%	0.2%	-
Fe	2%	70%	-	> 100%	69%	> 100%
Hg	2%	-	> 100%	-	0.4%	-
K	4%	3%	60%	> 100%	12%	23%
Li	-	-	> 100%	> 100%	85%	> 100%
Mg	33%	52%	33%	> 100%	25%	> 100%
Mn	> 100%	> 100%	> 100%	> 100%	3%	> 100%
Na	3%	4%	-	-	-	-
Ni	23%	> 100%	9%	> 100%	3%	> 100%
Pb	> 100%	> 100%	-	-	-	> 100%
Ti	18%	23%	> 100%	> 100%	> 100%	> 100%
Zn	> 100%	> 100%	> 100%	> 100%	97%	> 100%

Table 3.17: *Mobilised elements from batch experiments as a percentage of summed SEP steps 1 (water soluble) and 2 (exchangeable). Values greater than 100% are assumed to be the result of mineral dissolution.*

Considering just the trace metals, where detected above the analytical LOD, As, Hg and Cu are generally mobilised less than the total available in these steps. The value of Hg > 100% is an artefact of the wash-out problem identified in the Methodology chapter. Ni displays the effect already noted with respect to increased mobilisation with CO_2, with control concentrations low (< 25% of SEP steps 1 and 2), while the addition of CO_2 in all cases likely results in mobilisation with mineral dissolution. Chromium, Pb and Zn are, in all cases, > 100% regardless of control or +CO_2 experiments, and again perhaps symptomatic of mineral dissolution. Cadmium mobilises less than the SEP steps for *Captain SA7*, but > 100% for both *Cormorant* and *Thistle*.

These results would then indicate that Cd, Cr, Ni, Pb and Zn are mobilised by CO_2, enhancing desorption due to pH changes, or by mineral dissolution, or more likely a combination of both. That leached concentrations are, mostly, a significant portion of the concentrations available due to desorption, and that desorption increases with decreasing pH then one would expect a relationship between element concentrations and pH. Plotting all elements analysed with pH values for the batch experiments, Figure 3.31, shows no strong relationships with the exception of Si which was only analysed for *Cormorant* and *Thistle* samples. There is an indication of a positive correlation between increasing pH and As concentrations for the *Captain* samples, however the R^2 value of 0.32 for a linear regression through these data indicates a weak correlation only.

Si concentrations show an increase with experiment duration, Figure 3.17, with the control experiments in both cases exhibiting higher concentrations than the +CO_2 experiments. Quartz (SiO_2) solubility increases with both temperature and pH, with solubility calculated to be 15 mg/L at 50°C and 53 mg/L at 100°C below pH 7.8 (Langmuir, 1997), Figure 3.32. The temperatures for the *Cormorant* and *Thistle* batch experiments were set at 95°C and concentrations averaged ~ 28 mg/L, so the experiments are approaching the theoretical solubility of quartz, Figure 3.32. Theoretical quartz solubility increases between pH 9 - 10 (Langmuir, 1997) and rises with increasing pH.

Quartz solubility was modelled for the *Cormorant* and *Thistle* batch experiments with PHREEQC
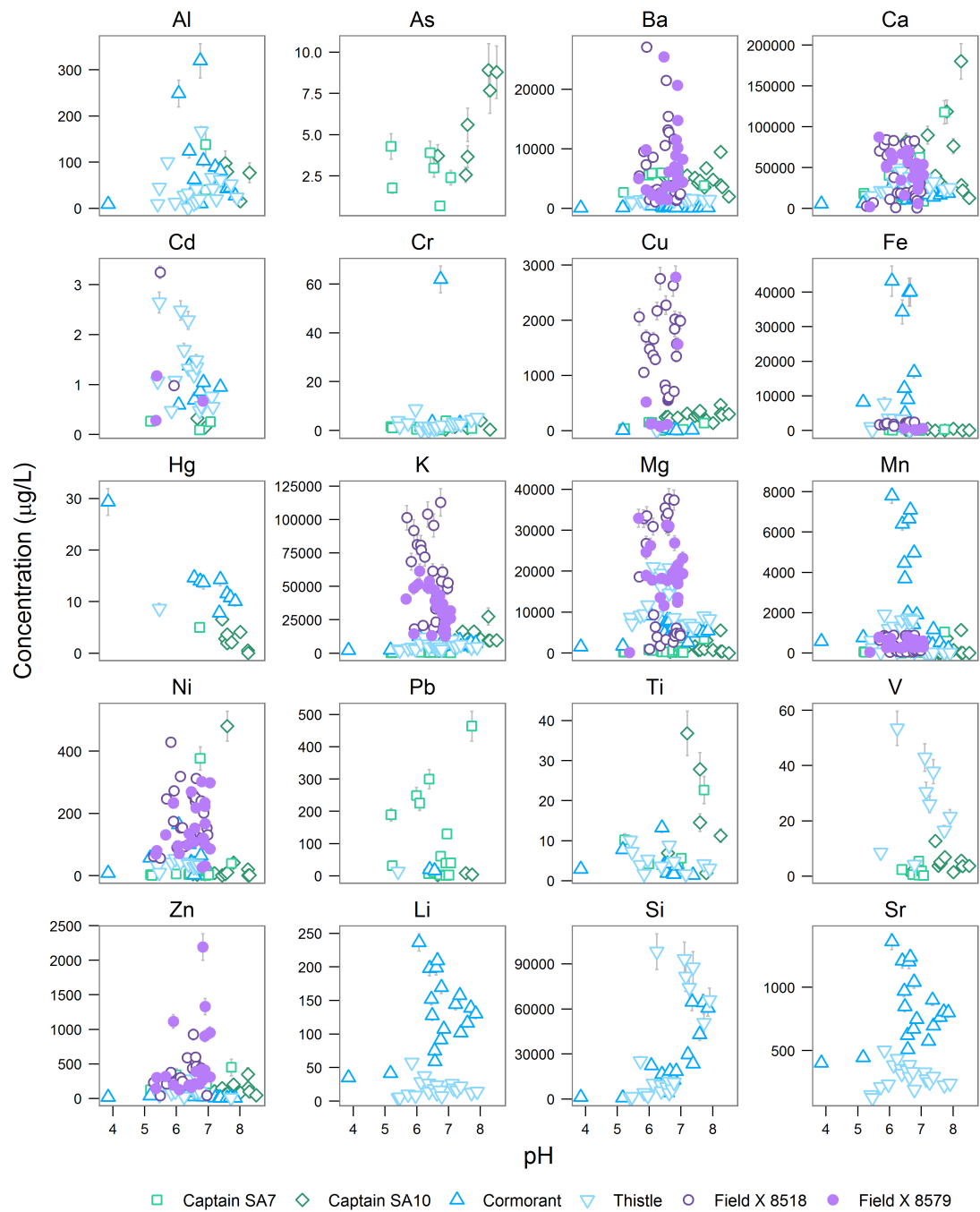
Figure 3.31: *pH values plotted against all elements analysed for the 6 North Sea batch experiment fluid samples. Error bars are 2s of the mean of standard reference materials.*

v3.3.3.10424, using the parameters in Table 3.18. The resulting dissolved Si values, Table 3.18, are essentially the same for both experiments, with the Cormorant values plotted in Figure 3.32. A similar trend is observed with the *Cormorant* and *Thistle* batch experiment data, with the control (higher pH) experiment data associated with higher dissolved Si and the $+CO_2$ experiments, Figure 3.32. However, experimental quartz solubility appears to change at pH 7, rather than pH 7.8 as documented in the literature (Langmuir, 1997) and replicated with the PHREEQC model. Below pH 7 Si concentration values are lower than the modelled concentrations, while they are higher above pH 7, Figure 3.32. This elevation at pH >
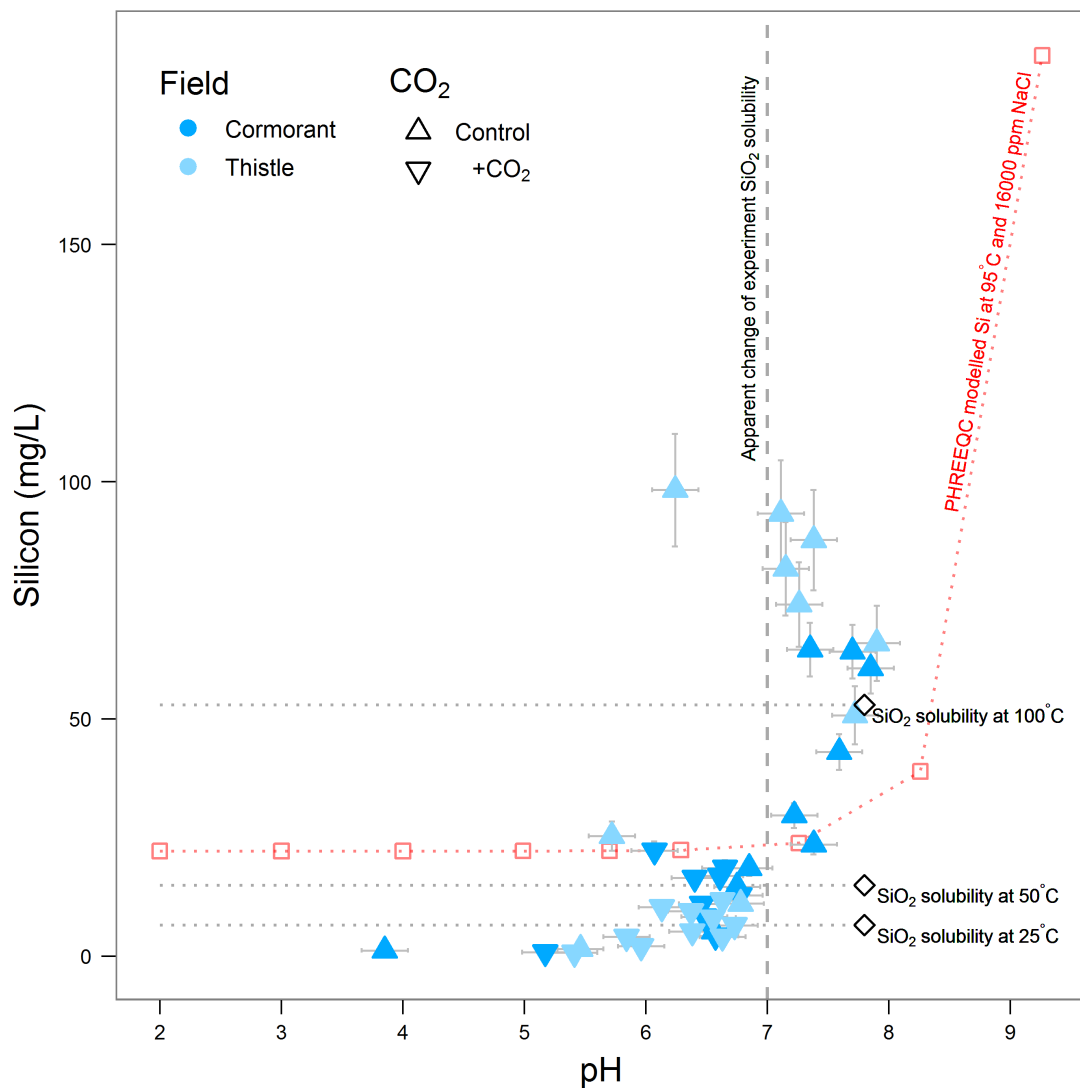
Figure 3.32: *Si concentration values (mg/L) for Cormorant and Thistle plotted against measured pH values. Dashed line at pH 7 represents apparent value at which quartz solubility increases. PHREEQC modelled values, Table 3.18, denoted with squares. Literature values (Langmuir, 1997) for quartz solubility below pH 7.8 denoted with diamonds.*

7 in the experiments may indicate another source of Si, for example feldspar dissolution, or the presence of amorphous silica which is more soluble than quartz (Langmuir, 1997).

Si concentrations do not correlate well with other elements, particularly trace metals, since Si is a Type I or III element (Table 3.14), increasing concentrations without the addition of CO_2, while most trace metals are Type IV. Even if there was a correlation with trace metals, since CO_2 injection and storage would reduce pH, quartz is unlikely to see much dissolution and, hence, poor mobility of any elements associated with it.

3.10.3 Carbonate dissolution

The dissolution of carbonate minerals is often cited as the primary source of elements mobilised into solution during batch and field experiments (e.g. Kirste *et al.* 2014; Kjöller *et al.* 2011), with mobilisation largely enhanced by the addition of CO_2 since calcite solubility in water increases with increasing pCO_2. Pure carbonate minerals are commonly formed from Ca, Mg, Mn, Fe, Sr, and Ba, and less commonly

Start pH[†]	16,000 ppm NaCl		23,500ppm NaCl	
	End pH	Si (mg/L)	End pH	Si (mg/L)
2	2	22.19	2	22.19
3	3	22.19	3	22.19
4	4	22.19	4	22.19
5	5.0	22.20	5.0	22.20
6	5.7	22.23	5.7	22.24
7	6.3	22.37	6.2	22.38
8	7.3	23.86	7.2	24.01
9	8.3	38.95	8.2	40.40
10	9.3	190	9.2	204
11	10.3	1,700	10.2	1,800

[†]95°C, 250 mL NaCl, 0.1 mol Quartz

Table 3.18: *Experiment conditions modelled with PHREEQC v3.0.0.7430 for quartz dissolution, and resulting outputs of pH and dissolved Si values, for Cormorant (16,000 ppm) and Thistle (23,500 ppm) batch NaCl solutions. Data plotted in Figure 3.32.*

from Pb, Cu and Zn. These elements, plus others such as Co and Ni, can substitute into the mineral structure of carbonates, Table 3.19, such that calcite, dolomite, siderite, etc. can contain varying amounts of these elements (Deer *et al.*, 1992).

Mineral	Chem. Formula	Common substitutes	SA7	SA10	Cormorant	Thistle	8518	8579
Ankerite	$Ca(Fe,Mg,Mn)(CO_3)_2$	Sr	-	-	-	-	0.3	0.2
Calcite	$CaCO_3$	Fe^{2+}, Mg, Mn, Sr	1.6	0.4	-	-	0.3	0.3
Dolomite	$CaMg(CO_3)_2$	Fe^{2+}, Mn, Ni, Pb, Zn	-	-	-	0.31	0.2	0.3
Siderite	$FeCO_3$	Mg, Mn	-	-	0.9	0.03	0.2	0.1
		Totals	1.6	0.4	0.9	0.34	1.0	0.9

Table 3.19: *Common carbonate substituting elements and carbonate content of North Sea samples, wt.% from XRD analysis*

Four different carbonate minerals were detected by XRD in the six samples used in the batch experiments: ankerite, calcite, dolomite and siderite. Only the *Field X* samples contain all four minerals, with the *Captain* samples only containing detectable calcite, and *Cormorant* only siderite, Table 3.19. *Thistle* contains dolomite and siderite. Only the *Captain* sample *SA7* has a carbonate content of > 1 wt.%. Below this, XRD becomes semi-quantitative only, therefore while there are values available for carbonate minerals in the North Sea samples, they should be treated only as indicating their presence, rather than a well-defined amount.

Nonetheless, given the presence of carbonates in the samples, albeit in low amounts, one would expect the reaction of these minerals with CO_2 in the batch experiments to be discernible in the data. With the addition of CO_2, elevated concentrations of common carbonate forming elements Ca, Mg, Mn, and Ba were found in all the batch experiments undertaken, as well as elevated Fe where siderite was determined (e.g. *Cormorant* and *Field X 8518*). Sr was only analysed for *Cormorant* and *Thistle* samples, but this was also found to be elevated with the bubbling of CO_2. Trace metals which have an association with carbonates (Cu, Ni, Pb and Zn) were also found in some cases to be more readily mobilised with $+CO_2$ (Table 3.14), perhaps indicating that carbonate dissolution is the mechanism by which these elements are released into solution.

Based on the assumption that all Ca released during the batch experiments is from carbonate dissolution, concentrations of these associated elements were plotted against Ca concentrations, to determine any correlations. If concentrations of these elements have a linear correlation with Ca, then as a first order approximation it would therefore be assumed that carbonate dissolution is the primary source. This is true for Ba, Cu, Fe, Mg, Mn, Ni, Pb, Sr and Zn. Where correlations are weak, or non-existent, then another mode of element release must be invoked; either dissolution of another mineral type, or

desorption from mineral surfaces.

Copper and Pb were not found to have any correlation with Ca concentrations for any of the North Sea samples. Nickel concentrations only correlate with Ca concentrations for *Captain SA7* (R^2 = 0.96) and *Cormorant* (R^2 = 0.94) +CO_2 experiments, if outliers on day 11 and day 1, respectively, are removed, Figure 3.33c. Zinc correlates with Ca only for the *Captain SA10* (R^2 = 0.89) and *Cormorant* (R^2 = 0.92) +CO_2 experiment after removing an outlier at day 5 for *Cormorant*, Figure 3.33d.

Barium concentrations correlate very well for *Captain SA10* and *Cormorant* +CO_2 experiments, with R^2 values of 0.98 for both, Figure 3.33a although again an outlier was removed for *Cormorant* at day 3.
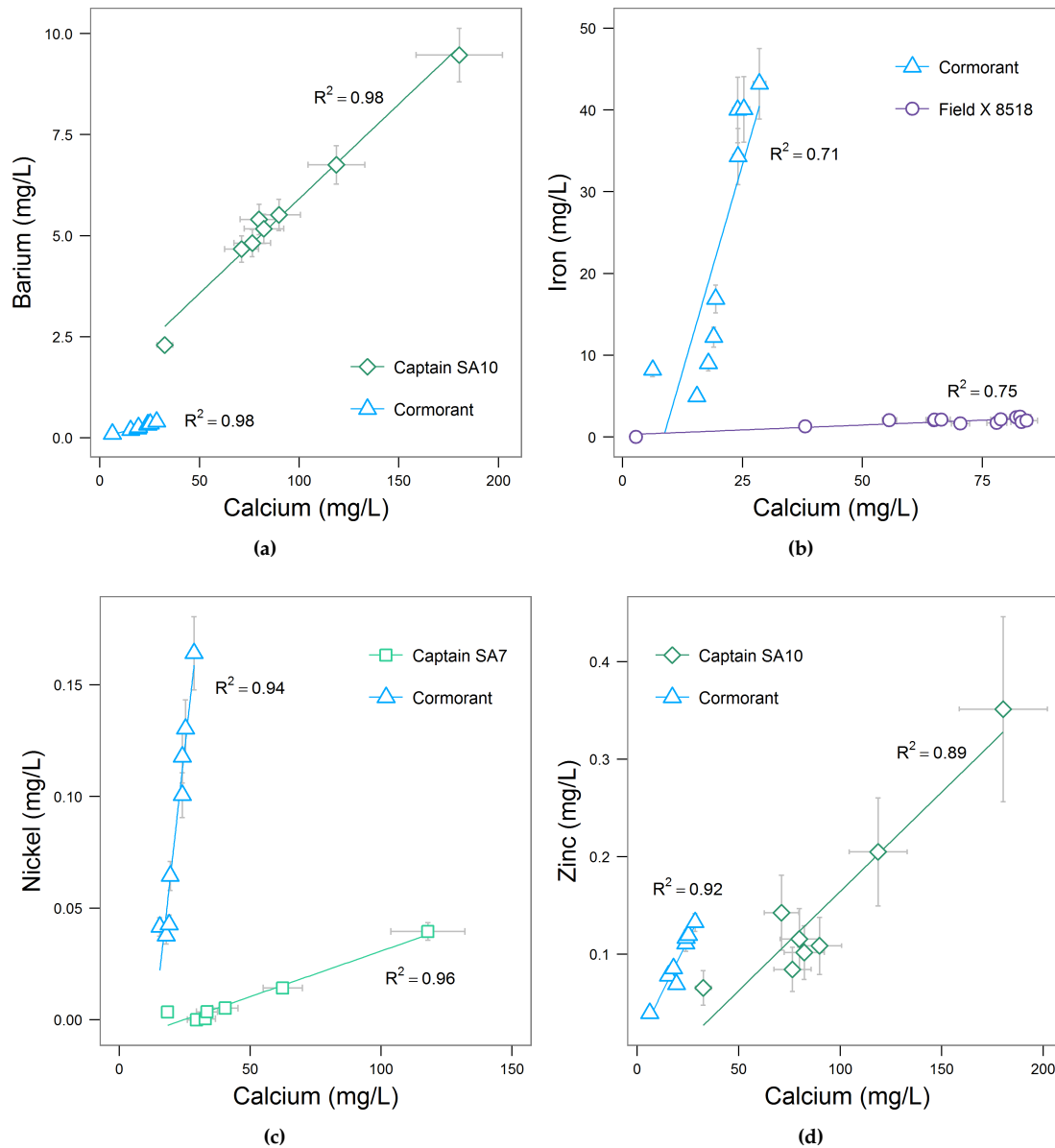
Figure 3.33: *Plots of Ca vs (a) Ba, (b) Fe, (c) Ni and (d) Zn batch concentrations (mg/L) for +CO_2 experiments where strong correlations (R^2 > 0.7) were found.*

Unsurprisingly, given the presence of siderite, Fe concentrations in *Cormorant* correlate well with Ca concentrations, Figure 3.33b, (R^2 = 0.71) and have a Ca:Fe ratio range of 0.60 - 3.12 (median = 0.76, n = 9). The Ca:Fe ratio determined from the carbonate SEP step for *Cormorant* is 0.04, indicating that siderite is the dominant carbonate phase in this sample, however the higher Ca:Fe ratio determined from the

results of the batch experiments and the results of the carbonate SEP step, Figure 3.20, would lead to the conclusion that while Ca is associated with siderite dissolution, it is also largely mobilised from a source other than the carbonate phase.

The SEP suggests a water soluble Ca mineral (e.g. calcium sulphate, $CaSO_4$), or Ca which is adsorbed to mineral surfaces. Iron also correlates well with Ca for *Field X 8518* +CO_2 experiment (R^2 = 0.75), Figure 3.33b. *Field X 8518* contains a small amount of siderite (0.15 wt.%) and this is reflected in the much higher Ca:Fe ratios than *Cormorant*, in the range 27 - 46 (mean = 34, n = 12). The SEP wasn't performed on either *Field X* sample, so the Ca:Fe ratio is unknown for the carbonates in these samples, however if siderite dissolution was dominating release of cations from the carbonate phase we would expect a range of ratios closer to the *Cormorant* values. In the case of *Field X 8518*, calcite and ankerite make up the bulk of the carbonate phase (62%) and so Ca concentrations will dominate. It is therefore more difficult to determine whether there are any other sources of Ca from this correlation alone.

Given that siderite dissolution dominates over Ca-carbonates in the *Cormorant* sample, correlations of other elements found to be associated with Ca in the batch experiments (Figure 3.33) were checked against Fe as well. R^2 values for Ba, Ni and Zn are, respectively, 0.84, 0.92 and 0.67, confirming their strong association with siderite dissolution in this sample.

Concentrations of Sr were only measured for the *Cormorant* and *Thistle* experiments, and here they are plotted for the +CO_2 experiments against Ca concentrations, Figure 3.34. Strontium and Ca values were considered outliers for day 3 (Figure 3.17), so excluding this data gives R^2 values of 1 and 0.79 for *Cormorant* and *Thistle*, respectively. Correlation of Sr with Fe for *Cormorant* gives an R^2 of 0.73, suggesting correlation with carbonate dissolution, although more strongly with Ca-carbonate than siderite.
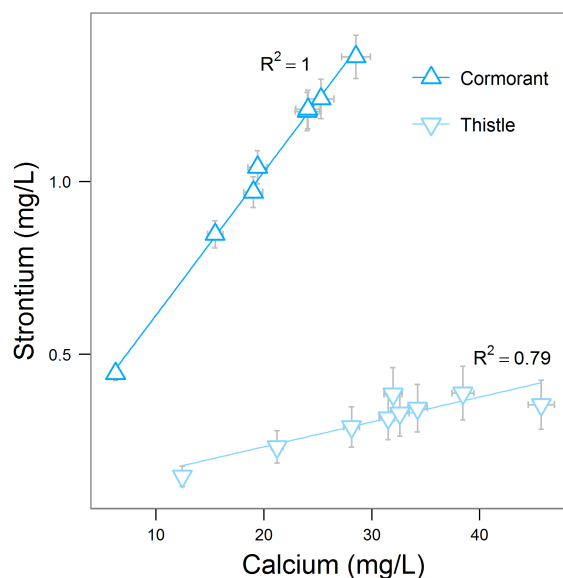
Figure 3.34: *Plot of Ca vs Sr batch experiment concentrations for Cormorant and Thistle +CO_2 batch experiments.*

While the elements considered so far (Ba, Cu, Fe, Ni, Pb, Zn) have strong correlations with Ca in only a limited number of samples, Mg and Mn show strong correlations with virtually all samples analysed. Figure 3.35 shows Mn concentrations plotted against Ca concentrations, for all 6 samples. Both *Captain* samples and both *Field X* samples have similar trends, with R^2 values of 0.99 (*Captain SA7*), 0.92 (*Captain SA10*), 0.93 (*Field X 8518*) and 0.89 (*Field X 8579*).

The *Cormorant* trend is similar to those of Fe, Ni and Zn (Figure 3.33), due to lower concentrations of Ca than the other samples, but higher concentrations of Mn. The R^2 value for *Cormorant* is 0.88. Ca:Mn ratios for *Cormorant* range from 3.56 to 8.98 (median = 3.90, n = 9), compared with ratios of ~ 100 - 200 for *Captain* and *Field X* samples. *Thistle* shows no significant correlation, with an R^2 of 0.14.
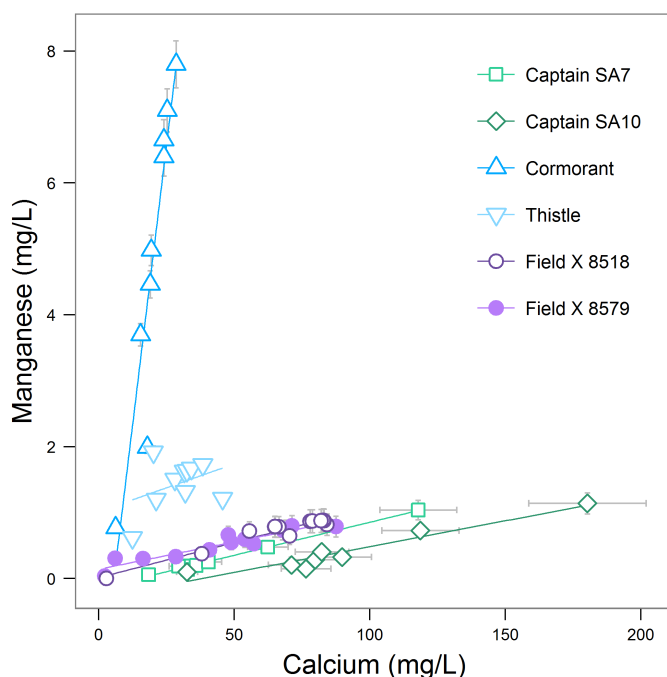
Figure 3.35: *Plot of Ca vs Mn batch experiment concentrations for all 6 North Sea +CO$_2$ batch experiments.*

Magnesium concentrations show a strong correlation with Ca for all 6 samples, with R^2 values ranging from 0.72 (*Field X 8518*) to 0.99 (*Captain SA7*) for the +CO$_2$ experiments. The linear regression lines are not plotted on Figure 3.36; instead three lines have been plotted indicating the Ca:Mg ratio as calculated from the SEP carbonate step for *Captain SA7*, *Cormorant* and *Thistle*. This shows again the strong corre-
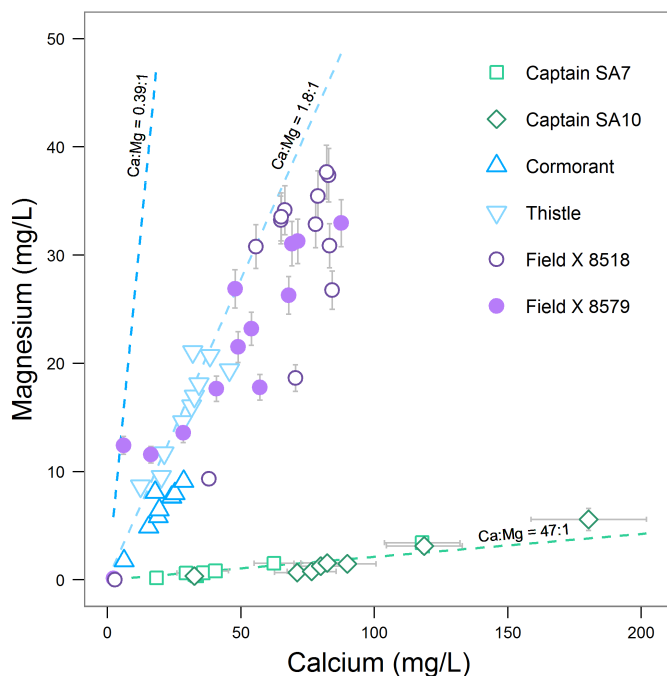
Figure 3.36: *Plot of Ca vs Mg batch experiment concentrations for all 6 North Sea +CO$_2$ batch experiments. Dashed lines are the calculated ratios of Ca:Mg from the carbonate SEP step for Captain SA7 (47:1), Cormorant (0.39:1) and Thistle (1.8:1). The SEP was not carried out on Field X samples.*

lation for *Captain* and *Thistle* samples, where Ca:Mg ratios from the batch experiments closely match the Ca:Mg ratios in the carbonates that are present, suggesting that dissolution of carbonates is the primary mobiliser of Mg for these samples. *Cormorant*, on the other hand, shows Ca:Mg ratios which are higher than the carbonate Ca:Mg ratio, suggesting some other source of Ca for this sample, as already discussed with regard to the other elements since *Cormorant* is dominated by siderite.

So far, the assumption has been that Ca concentrations are primarily the function of carbonate dissolution, and that any other common carbonate forming elements which strongly correlate with Ca are also mobilised by carbonate dissolution. To test whether carbonate dissolution is indeed the primary mechanism for release of these elements, and given that Ca and Mg are the main indicators of carbonate dissolution, the *equivalents* (as milliequivalents per liter, meq/L) of Ca and Mg can be calculated and plotted against equivalent alkalinity (as HCO_3^-) (Stallard and Edmond, 1983). Carbonate dissolution will give a 1:1 stoichiometric equivalent relationship of $(Ca^{2+} + Mg^{2+})/HCO_3^-$, based on Equation 3.1 where the charge balance on the right hand side of the equation between cations and anions is 1:1, after reaction of a Ca-Mg carbonate with carbonic acid.

Equivalents were calculated for Ca^{2+}, Mg^{2+} and HCO_3^- as per equation 3.3, for all batch data, and subdivided by control and $+CO_2$ experiments. The results are plotted as Figure 3.37, with the dashed line in each plot representing the 1:1 relationship $(Ca^{2+} + Mg^{2+})/HCO_3^-$.

$$\text{milliequivalent (meq/L)} = (\text{Concentration (mg/L)} \div \text{molar mass (g)}) \times \text{ionic charge} \qquad (3.3)$$
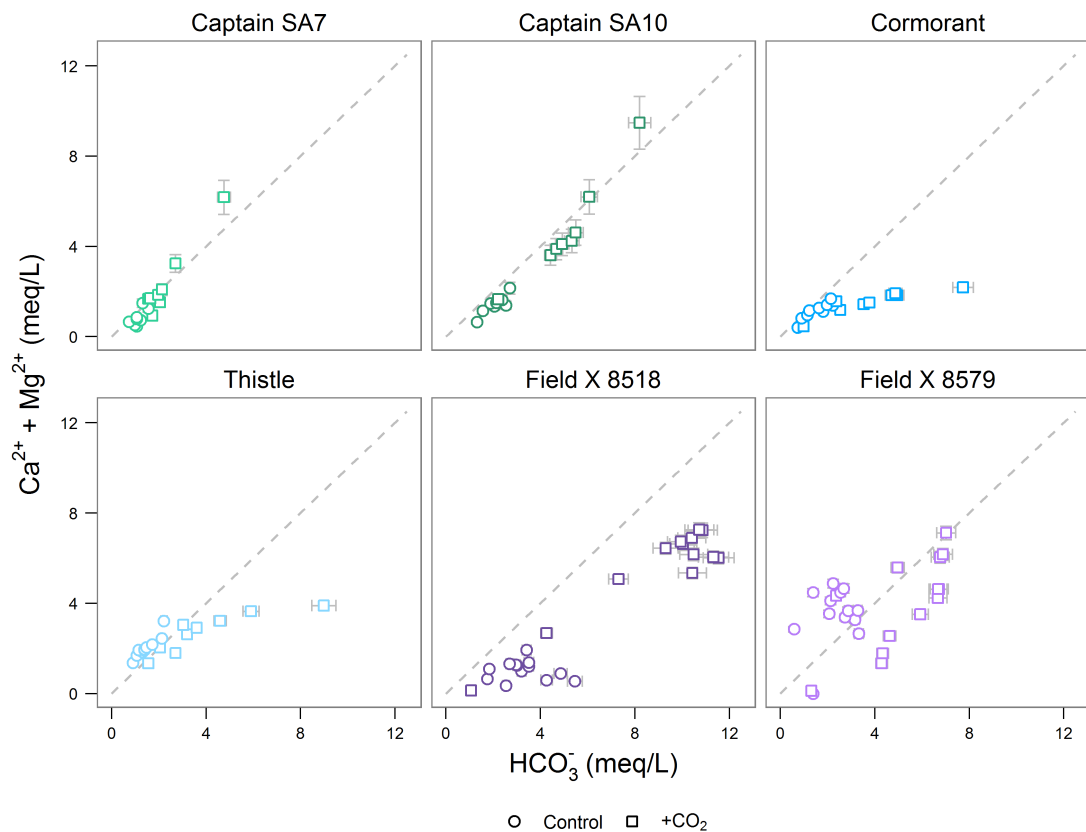
Figure 3.37: *Plot of batch experiment ($Ca^{2+} + Mg^{2+}$) milliequivalent concentrations (meq/L) against HCO_3^- meq/L for all North Sea batch samples. Circles represent the control experiments, squares represent $+CO_2$ experiments. Dashed line represents 1:1 stoichiometric relationship. All plots to same scale.*

Captain results plot either on, or slightly below the 1:1 line for lower equivalents, with the highest

equivalents for both *SA7* and *SA10* (+CO$_2$ results) plotting slightly greater than 1:1. There is a close relationship, therefore, between (Ca + Mg) and alkalinity for the *Captain* samples, suggesting that calcite dissolution is the dominant mechanism of element mobility for these samples.

Cormorant and *Thistle* samples also show an increase in alkalinity equivalent with an increase in (Ca + Mg). For these samples, the trend is close to 1:1 for the control samples, however with the addition of +CO$_2$, the trend is around 1:4 for *Cormorant* from the start of the experiment, and becomes 1:2 for *Thistle* as concentrations increase with added CO$_2$. For *Cormorant*, this may be because siderite is dissolving. Figure 3.38 shows the effect of adding Fe to the calculation of equivalents for *Cormorant* only. This brings the data closer to the 1:1 relationship, but is still lower. Fe concentrations for the other samples are so low that adding them to their equivalent plots does not significantly alter the trends. So it can be seen that, as alkalinity increases, (Ca + Mg) increase more slowly than a 1:1 relationship for carbonate dissolution; this would imply another significant source of alkalinity.
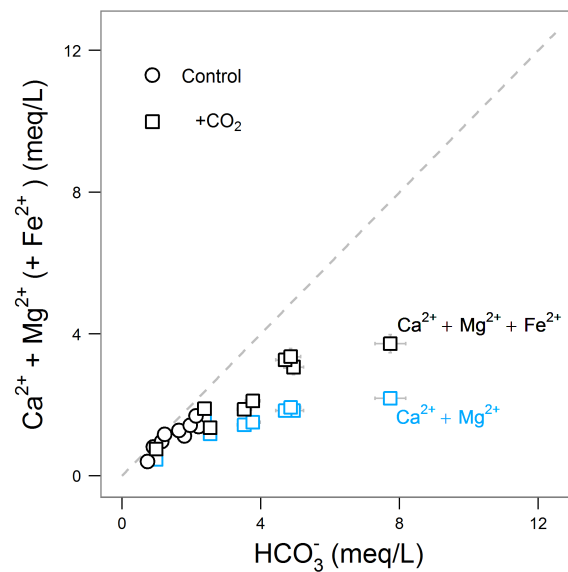
Figure 3.38: *Plot of batch experiment (Ca^{2+} + Mg^{2+} + Fe^{2+}) milliequivalent concentrations (meq/L) against HCO$_3^-$ meq/L for Cormorant, and compared with Cormorant data for (Ca^{2+} + Mg^{2+}), plotted in Figure 3.37. Circles represent the control experiments, squares represent +CO$_2$ experiments. Dashed line represents 1:1 stoichiometric relationship.*

Field X 8518 shows clustering of control and +CO$_2$ data, which fall under the 1:1 relationship line, suggesting that the addition of +CO$_2$ leads to both increased (Ca + Mg) and increased alkalinity. *Field X 8579* shows a clustering of control results which are mostly about the 1:1 line, but without any trend, while the +CO$_2$ data shows an initially slower increase in (Ca + Mg) with alkalinity below 1:1, but with a later and more rapid increase from an alkalinity of $\sim$ 7 meq/L. Again, one could conclude that calcite dissolution is a major source of cations for both *Field X* samples, particularly with the addition of CO$_2$, but that there is another source of alkalinity, similar to *Cormorant* and *Thistle*.

As noted in the Methodology chapter (Section 2.4.1), HCO$_3^-$ values measured during the experiments may be some 30% higher or lower than actual values. The alkalinity data were not corrected for this $\pm$ 30% error in accuracy, and is therefore not represented in the data displayed in Figures 3.37 and 3.38. If one were to include these potential inaccuracies as error bars, for example, on the HCO$_3^-$ data, then some data (e.g. *Captain* and *Field X 8518*) could fall closer to the 1:1 relationship. Equally, however, the trends could be further away. Either way this does not drastically affect the conclusions here. However, more accurate analysis is preferable, and if these experiments were to be repeated then a better method of measuring alkalinity would be used such as titration to a fixed end-value pH, as used for measurement of the Utah field samples, Chapter 4.

Trace metals, as already established, are not mobilised in significant concentrations or with any discernible trends. The exceptions, Ni and Zn, do correlate well with concentrations of Ca and Mg, indicative of calcite dissolution for *Captain*, and with Ca, Mg and Fe for *Cormorant*, indicating siderite dissolution. The relationship is not clear for *Thistle* and *Field X* samples, however, perhaps suggesting some other mechanism for their mobilisation.

Given that the SEP data for *Captain*, *Cormorant* and *Thistle* indicate that Ni and Zn are largely "immobile" (which does not include mobilisation from carbonates), this would also suggest dissolution of other mineral types.

3.10.4   Feldspar dissolution

Carbonate dissolution appears to be the dominant mechanism for mobilisation of major elements into solution for *Captain* and *Field X* samples, whose mineralogy is dominated by quartz, with minor feldspars and clays, and carbonates. *Cormorant* and *Thistle* samples have lower quartz and higher feldspar content than *Captain* and *Field X*, and this could reflect the trends shown in Figure 3.37, with a significant other source of alkalinity instead of carbonate dissolution.

Since carbonate dissolution does not appear to provide all of the increase in alkalinity for the North Sea batch experiments, other mineral dissolution could be considered to be occurring to increase alkalinity. The addition of CO_2 alone, without interaction with the samples, does not increase alkalinity as can be seen from the *Captain* control experiment, Figure 3.3. One possible source could be the dissolution of feldspars, which are more common in these North Sea samples than are carbonates (Tables 3.1, 3.6, 3.11). Feldspar dissolution, e.g. microcline/K-feldspar, provides HCO_3^-, Equation 3.2.

Comparing feldspar dissolution (Equation 3.2) with carbonate dissolution (Equation 3.1), one sees that twice as much HCO_3^- is generated per mole of carbonic acid during carbonate dissolution than during feldspar dissolution, therefore the signal from feldspar dissolution will likely be weaker when carbonates are also dissolving.

Feldspar dissolution could be fingerprinted with the concentrations of Ca, Na, K and Al, the most common feldspar forming elements. Calcium concentrations have already been assumed to be due to carbonate dissolution, the most significant source of this element. Sodium concentrations were not determined for the batch experiments due to the difficulty of measuring changes in concentrations against a background experimental fluid matrix of NaCl. Aluminium is relatively insoluble in water, preferring to form oxides and precipitate out of solution. The Type IV classification of Al (Table 3.14), and generally low concentrations in all batch experiments it was measured in would confirm this.

This leaves K as the strongest proxy for feldspar dissolution, and is classified as either Type I (*Captain* and *Cormorant*), Type II (*Thistle*) or Type III (*Field X*) and so concentrations are increased during the batch experiments, likely due to feldspar dissolution. Any correlation of trace metal concentrations with K could therefore be determined as potential mobilisation from feldspars.

From Equation 3.2, there is also a 1:1 stoichiometric relationship between K^+ and HCO_3^- for feldspar dissolution, as with carbonate dissolution. Concentrations of K (as milliequivalents) were therefore plotted against HCO_3^- to determine how close values fell to the 1:1 relationship. For all fields, since K concentrations are low compared with alkalinity, values fell well below 1:1. Correlation was also poor (R^2 = 0.12 - 0.66) between K^+ and HCO_3^- for *Captain* and *Field X* samples, however for the *Cormorant* and *Thistle* samples, which are both from deeper reservoirs and contain more feldspars than *Captain* and *Field X* (and hence larger weathered surface areas), there were good linear relationships between values, Figure 3.39. R^2 values are 0.82 - 0.93 for *Cormorant* and *Thistle*, indicating that there is indeed a strong relationship between feldspar dissolution and alkalinity, albeit fairly insignificant compared with carbonate dissolution.

If K concentrations are strongly associated with feldspar dissolution, then the assumption can be made that correlation between K and trace metals would indicate dissolution of these minerals is a mech-
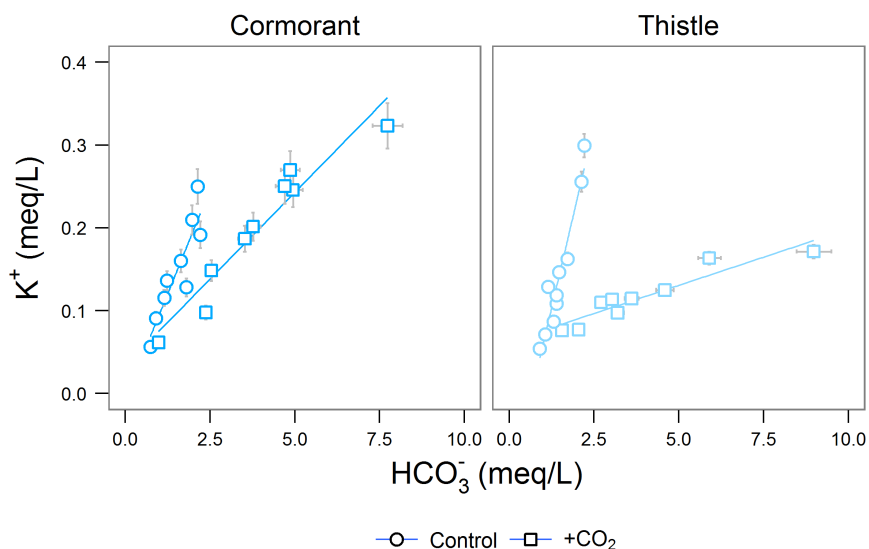
Figure 3.39: *Plot of K^+ vs HCO_3^- batch experiment concentrations (meq/L) for Cormorant and Thistle experiments. Linear regression lines plotted through each set of control and +CO_2 data. R^2 values for Cormorant are 0.82 (control) 0.93 (+CO_2), and for Thistle are 0.92 (control) and 0.87 (+CO_2).*

anism for trace metal mobilisation. Concentrations of the 8 trace metals of interest were plotted against K concentrations for all batch experiment results. The only significant linear correlations were for Cu (*Field X 8518*) and Zn (*Captain SA10*) for +CO_2 experiments, Figure 3.40. The correlation between K and Cu is not surprising, given the concentration trends apparent in the batch experiment data (Figures 3.27 and 3.28) where both elements peak in concentration before tailing off again. A linear regression through the data give an R^2 value of 0.87, Figure 3.40a.
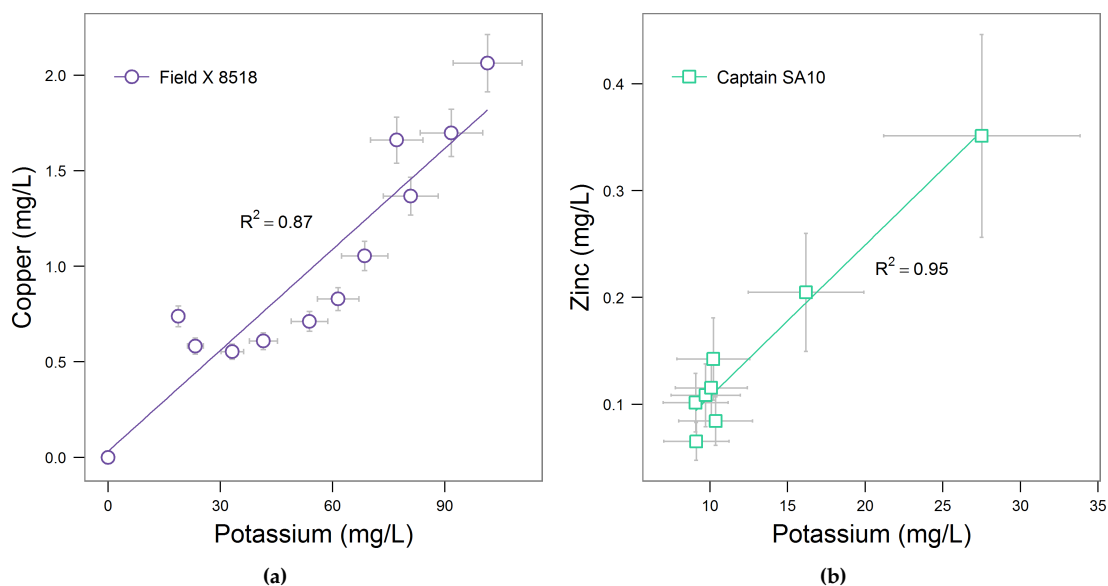
Figure 3.40: *Plots of K vs (a) Cu and (b) Zn batch concentrations (mg/L) for +CO_2 experiments where strong correlations ($R^2 > 0.8$) were found.*

The linear correlation between K and Zn gives an R^2 of 0.95, Figure 3.40b, which is a better correlation than for Ca and Zn for *Captain SA10* ($R^2 = 0.89$, Figure 3.33d).

No other trace metals correlated well with K. Low concentrations of K, compared with Ca and Mg, would suggest that while feldspars are probably dissolving, their significance to trace metal mobility is minor compared with carbonate. While feldspar concentrations are much greater than carbonates, the reaction of carbonates to carbonic acid is much stronger and dominates the resulting batch fluid chemistry.

3.11 Conclusions

- The addition of CO_2 to batch experiment flasks containing NaCl brines and North Sea sandstones lowers pH by ~ 1 pH unit, with acidity buffered by mineral dissolution, evident in increasing alkalinity.

- 6 of the 8 trace metals of interest (As, Cd, Cr, Cu, Hg, Pb) are not readily mobilised either in the control or $+CO_2$ experiments, for samples investigated. Nickel and Zn are the exceptions, being readily mobilised, particularly with the addition of CO_2.

- Trace metals tend to be concentrated in mineral phases which are classified as immobile under enhanced CO_2 conditions, which would generally tie in with their lack of mobility under the batch experiment conditions.

- The most common major elements to be mobilised were Ba, Ca, Fe, K, Mg and Mn, with the addition of CO_2 a strong control on enhanced concentrations.

- Calcite dissolution is the primary mechanism of major element release in the *Captain* $+CO_2$ batch experiments, and the major mechanism for *Field X* samples. *Cormorant* and *Thistle* major element release is mostly calcite, but with feldspar dissolution also evident, which aligns with the larger amounts of feldspars in these samples.

- Little correlation exists between major element and trace metal concentrations, with the exception of Ni and Zn - and occasionally Cu - suggesting mineral dissolution (rather than desorption) is the primary mechanism for the mobility of Ni and Zn, and therefore carbonate dissolution is the primary source of these two metals.

- Where feldspars are more abundant, their dissolution may also contribute to Cu and Zn mobility.

- pH changes, a control on the desorption mechanism of trace metal release, do not correlate with trace metal concentrations for the batch experiments. However, concentrations of released metals often exceed those available through water soluble and exchangeable (desorption) phases determined by the sequential extraction procedure (SEP). This suggests that desorption does indeed occur, if the assumption is made that metals will desorb before - or more quickly than - mineral dissolution. This can be significant for some elements e.g. Cd, Cr and Pb, however this may not be the case and these elements could be be entirely mobilised by mineral dissolution.

- X-ray diffraction (XRD) does not appear to capture the complete picture of the mineralogy of the samples used and so cannot be relied upon here as a prediction of trace metal leaching under enhanced CO_2 conditions.

- Ultimately, where carbonates are present, CO_2 is likely to partly dissolve these minerals and mobilise Ni and Zn, with some contribution from feldspar dissolution. Other trace metals may desorb from mineral surfaces, but in low concentrations. Prediction of concentrations based on the SEP is, however, difficult with no particular relationship between apparent mobility and actual leached concentrations.

Utah Results & Discussion

4.1 Introduction

The following chapter describes the data collected from sampling natural waters and sandstones at 10 CO_2-driven springs and 5 outcrop locations in the San Rafael desert, Utah, using the field and experimental methods described in the Methods chapter (Chapter 2). Following data presentation, the data is analysed and conclusions drawn here within the chapter. CO_2-water-rock batch experiments were used to determine concentrations of a suite of major elements and trace trace metals which could be leached from these sandstones. A sequential extraction procedure (SEP) was conducted on *Entrada*, *Wingate* and *Navajo* formation aquifer sandstone samples to determine the distributions within these sandstones of trace metals which could be leached from various mineral phases. Trace metal concentration data was also collected in the field to compare with the experimental results.

Data obtained for the experiments and field work include: mineralogy by X-ray diffraction (XRD), fluid pH, alkalinity, cation concentrations by Inductively Coupled Plasma Mass Spectroscopy (ICP-MS) and Inductively Coupled Plasma Optical Emission Spectroscopy (ICP-OES), and whole rock composition by acid digestions and ICP-OES/ICP-MS.

The focus of the data analysis is the mobilisation of the suite of 8 trace metals of interest (As, Cd, Cr, Cu, Hg, Ni, Pb, Zn), with major cations such as Ca and Mg used as potential fingerprints for mobilisation mechanisms. These data are combined with the SEP to assess how predictable trace metal concentrations are, based on information on their distribution in 'mobile' phases of the rocks. Simple geochemical modelling was also carried out using PHREEQC to aid with data interpretation. The chapter conclusions are summarised on pg. 177, with overall thesis conclusions found in Chapter 6, pg. 199.

4.2 Green River Springs

4.2.1 pH & alkalinity

The pH and alkalinities of CO_2-driven spring waters were measured at 10 locations in the Green River area of the San Rafael desert, Utah. pH was measured in-situ using a portable pH meter and probe (Chapter 2, Section 2.4.2) while alkalinity was measured on bottled samples, Section 2.4.4. The temperatures of the spring waters were measured at the same time as pH. These data are presented in Table 4.1.

Spring	pH	HCO_3^- (mg/L)	T (°C)
Green River Airport Well	6.31	2,334	26.6
Crystal Geyser	6.71	4,419	17.3
Big Bubbling Spring	6.65	4,148	15.6
Little Bubbling Spring	6.49	4,539	15.3
Side Seep	6.61	-	22.3
Tenmile geyser	6.34	3,589	16.5
Pseudo-Tenmile Geyser	6.56	3,820	17.4
Torrey's Spring	6.67	4,837	16.2
Tumbleweed Geyser	6.63	4,166	18.5
Champagne Geyser	6.80	3,616	13.8

Table 4.1: *Field measurements of pH and alkalinity (as HCO_3^-) of samples collected from 10 springs near Green River, Utah. Sample locations are provided in Fig 2.1, Chapter 2). Temperatures of the spring waters are also noted for reference. No sample collected at Side Seep for alkalinity measurement.*

pH values for all spring locations lie in the pH range 6.3 - 6.8, Table 4.1. The lowest pH values were measured at *Green River Airport Well* (pH 6.31) and *Tenmile Geyser* (pH 6.34). Alkalinity, measured as the concentration of bicarbonate in solution, HCO_3^-, is also relatively constant across all the spring locations, with the obvious exception of *Green River Airport Well* again, which has an alkalinity value of 2,335 mg/L. This is 35% lower than the next lowest value of 3,589 mg/L at *Tenmile Geyser*. A sample was not collected at *Side Seep* for alkalinity measurement.

Temperatures were also consistent, ranging from 13.8 - 18.5°C, with the exceptions of *Green River Airport Well* (26.6°C) and *Side Seep* (22.3°C). Temperatures were measured as close to the bubbling point of the spring, where possible, therefore temperatures should reflect the upwelling water temperature, rather than stagnant water which could be affected by time-of-day and/or climatic temperature variations. *Green River Airport Spring* was noticeably warmer during sampling, and had a slight 'eggy' or sulphurous odour. The *Side Seep* location was stagnant water in a dried up creek, and measurements were taken mid-afternoon, therefore the elevated value of this location is probably not a reflection of the upwelling water temperature.

Figure 4.1 shows the locations of the springs for which alkalinity was measured, with each location colour-shaded depending on it's alkalinity. It is clear from the map that *Green River Airport Well* is an anomalous value, compared with the other springs.

4.2.2 Cation & anion data

Major cation (Ca^{2+}, K^+, Li^+, Mg^{2+}, Na^+, NH_4^+) and anion (Br^-, Cl^-, F^-, NO_2^-, NO_3^-, PO_4^{3-}, SO_4^{2-}) data for the 10 spring water samples was obtained by Ion Chromatography (IC) at the University of Texas (UT), Section 2.7. Total dissolved solids (TDS) were calculated from the sum of these data. Major and trace cation data was obtained by Inductively Coupled Plasma Mass Spectroscopy (ICP-MS) for the 35 elements Ag, Al, As, B, Ba, Bi, Ca, Cd, Co, Cr, Cs, Cu, Fe, K, Li, Mg, Mn, Mo, Na, Ni, P, Pb, Rb, Sb, Se, Si, Sn, Sr, Th, Ti, Tl, U, V, Zn & Zr, Section 2.5.1.
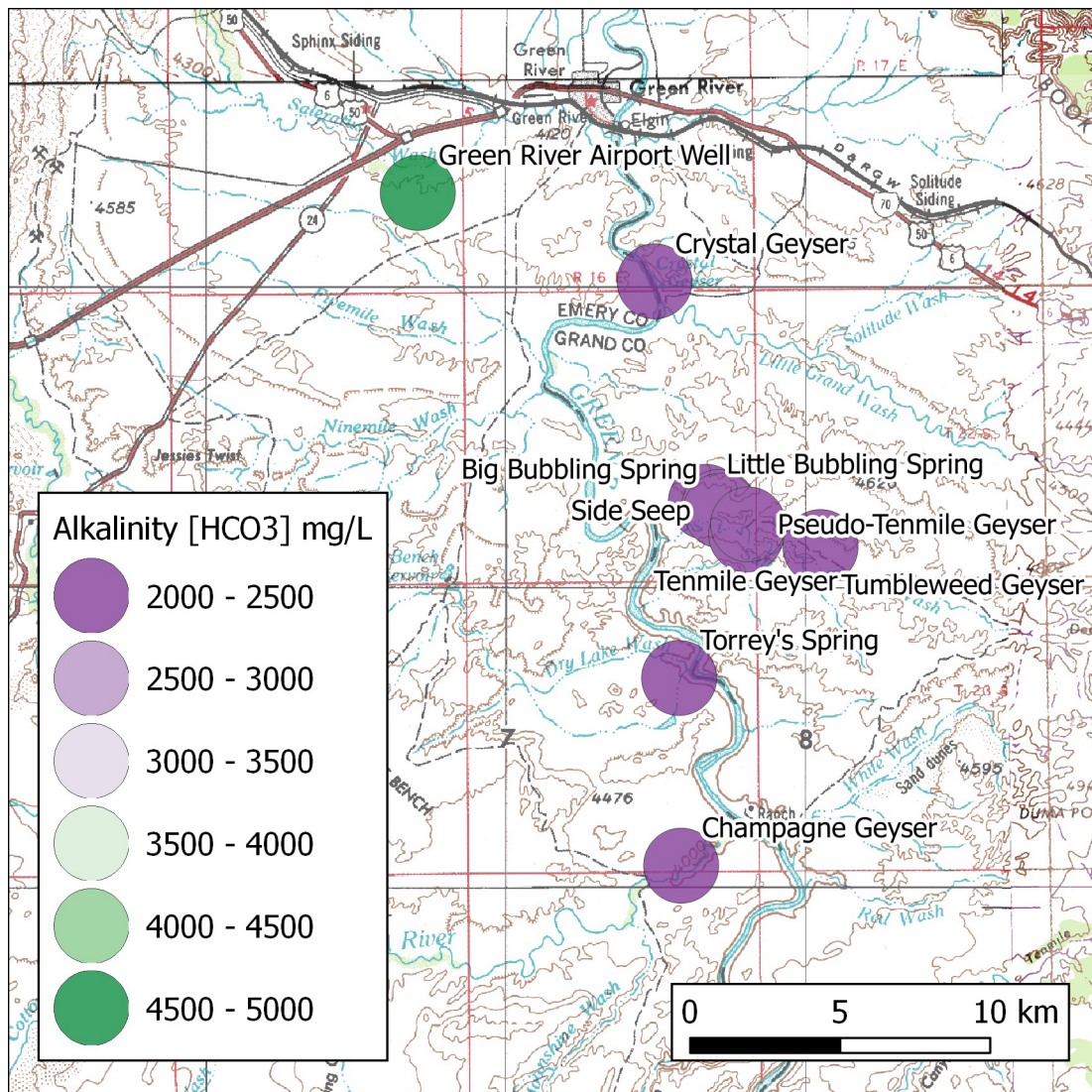
Figure 4.1: *Alkalinity, as HCO_3^-, mapped to Utah spring locations. Data presented in Table 4.1.*

Many of the elements analysed for by UT were not considered during analysis of the North Sea data (e.g. Ag, B, Co, Rb) however are part of a standard suite of analysis by UT. Only the element data of interest for this thesis is presented here, namely concentration data for the 18 elements Al, As, Ba, Ca, Cd, Cr, Cu, Fe, K, Li, Mg, Mn, Na, Ni, Pb, Si, Sr & Zn are included in the main text of this thesis for consideration. These selected elements from the ICP-MS analysis, and all of the IC analysis, are given in Table 4.2. This table also includes Hg, which was analysed by ICP-MS at the University of Edinburgh.

TDS values, Table 4.2, show that the spring waters are saline (Kharaka and Hanor, 2007) with concentrations generally ranging from $11,250 \pm 44$ mg/L (*Crystal Geyser*) to $17,798 \pm 65$ mg/L (*Torrey's Spring*), with a median of 14,889 mg/L. The exception, Figure 4.2, is *Green River Airport Spring* which has a TDS value of $3,749 \pm 21$ mg/L.

Chloride (Cl^-) concentrations are likewise lowest at *Green River Airport Well*, Figure 4.2, with a value of 115 ± 0.4 mg/L. This compares with the median value of the springs of 5,898 mg/L. The highest Cl^- concentration was found at *Tenmile Geyser*, with a value of $7,085 \pm 27$ mg/L, Table 4.2.

	LOD*	Airport	±	Crystal	±	Little Bubbling	±	Big Bubbling	±	Side Seep	±	Tenmile	±	Pseudo-Tenmile	±	Torrey's	±	Tumbleweed	±	Champagne	±
	Inductively Coupled Plasma Mass Spectroscopy (ICP-MS)																				
	µg/L	µg/L	±	µg/L	±	µg/L	±	µg/L	±	µg/L	±	µg/L	±	µg/L	±	µg/L	±	µg/L	±	µg/L	±
Al	0.183	-	-	-	-	-	-	-	-	-	-	-	-	-	-	-	-	-	-	-	-
As	0.021	8.63	0.62	38.9	7.1	38.3	5.5	55.4	7.4	-	-	13.3	2.4	59.8	7.0	56.2	11.2	17.5	2.6	6.59	2.13
Ba	0.034	16.2	0.5	14.3	0.9	13.9	0.5	8.96	0.51	34.4	0.8	13.9	0.9	8.79	0.84	9.57	0.58	9.65	0.77	6.21	0.48
Ca†	0.011	781	4	1,019	5	1,035	13	870	6	541	0	900	9	790	2	939	6	856	2	1,060	6
Cd	0.030	-	-	-	-	-	-	-	-	-	-	-	-	-	-	-	-	-	-	-	-
Cr	0.279	-	-	-	-	-	-	-	-	-	-	-	-	-	-	-	-	-	-	-	-
Cu	-0.07	-	-	13.5	2.8	36.5	0.7	24.5	1.6	21.2	1.2	31.3	0.9	26.2	0.9	40.0	3.1	24.4	1.4	25.6	2.0
Fe	0.111	4,856	51	11,638	176	14,817	202	6,707	113	1,190	14	3,763	58	4,817	99	7,382	100	3,753	39	3,351	49
Hg§	0.018	-	-	-	-	-	-	-	-	-	-	-	-	-	-	-	-	-	-	-	-
K†	0.006	92	2	308	4	312	6	390	3	411	9	259	5	393	5	453	10	336	5	303	6
Li	0.245	119	1	2,916	29	3,635	12	4,904	37	4,986	6	3,545	45	5,127	33	5,469	51	4,191	52	4,260	52
Mg†	0.004	186	2	226	1	230	1	214	1	222	1	233	1	200	1	192	0	212	1	237	1
Mn	0.145	1,216	2	1,634	9	1,135	3	416	4	355	2	1,052	9	120	1	1,069	6	943	8	935	2
Na†	0.042	495	2	3,570	14	3,831	33	5,484	31	5,690	23	5,598	15	5,811	28	6,234	181	4,807	21	4,916	44
Ni	0.041	7.41	0.28	8.13	0.62	11.6	1.5	7.43	0.97	4.36	0.55	8.96	1.27	6.36	0.72	8.24	0.74	8.61	0.85	11.7	0.9
Pb	0.035	-	-	-	-	-	-	-	-	-	-	-	-	-	-	-	-	-	-	-	-
Si	4.52	31,556	2,648	6,877	676	5,127	357	4,551	367	4,253	415	4,558	508	4,215	238	4,076	415	4,381	395	3,910	319
Sr	0.313	9,748	9	14,756	100	15,715	143	14,004	38	8,364	12	20,429	116	14,532	129	12,929	125	13,552	53	14,341	110
Zn	0.192	6.66	0.26	-	-	30.2	1.4	-	-	-	-	15.4	9.9	-	-	-	-	37.0	7.1	-	-
	Ion Chromatography (IC)																				
	mg/L	mg/L	±	mg/L	±	mg/L	±	mg/L	±	mg/L	±	mg/L	±	mg/L	±	mg/L	±	mg/L	±	mg/L	±
Ca²⁺		820	1	1,034	1	1,050	1	912	1	596	1	939	1	821	1	998	1	907	1	558	1
K⁺		91	0.1	303	0.2	317	0.2	385	0.3	383	0.3	261	0.2	389	0.3	450	0.3	336	0.3	298	0.2
Li⁺		-	-	3	0	4	0	5	0	5	0	3	0	5	0	6	0	4	0	4	0
Mg²⁺	*Not Supplied*	197	2	236	2	233	2	217	2	230	2	236	2	204	2	202	2	221	2	244	2
Na⁺		458	1	3,272	5	3,887	5	5,076	7	5,367	7	5,203	7	5,372	7	5,971	8	4,447	6	4,584	6
NH₄⁺		-	-	-	-	-	-	-	-	-	-	-	-	-	-	-	-	-	-	-	-
Br⁻		-	-	2.15	0.01	2.03	0.01	3.90	0.02	3.22	0.01	5.89	0.02	2.93	0.01	3.88	0.02	2.75	0.01	2.61	0
Cl⁻		115	0.4	3,966	15	4,777	18	6,122	23	6,432	24	7,085	27	6,352	24	6,975	26	5,334	20	5,676	21
F⁻		-	-	-	-	-	-	-	-	-	-	-	-	-	-	-	-	-	-	-	-
NO₂⁻		-	-	-	-	-	-	-	-	-	-	-	-	-	-	-	-	-	-	-	-
NO₃⁻		-	-	-	-	-	-	-	-	-	-	0.52	0.00	-	-	-	-	-	-	-	-
PO₄³⁻		-	-	3.72	0.06	38	0.6	29	0.4	-	-	-	-	26	0.4	-	-	30	0.5	-	-
SO₄²⁻		2,068	17	2,431	20	2,517	21	3,003	25	3,277	28	1,978	17	3,226	27	3,191	27	2,786	23	2,633	22
TDS		3,749	21	11,250	44	12,825	49	15,752	59	16,295	62	15,712	54	16,398	62	17,798	65	14,068	53	14,000	53

Table 4.2: *Concentrations of selected elements at Utah spring locations, obtained by ICP-MS and IC at the University of Texas. Uncertainties are 1s. *Analytical limit of detection. †Concentrations in mg/L. §Hg analysed by ICP-MS at University of Edinburgh. Blank concentration values are < LOD, or not reported.*
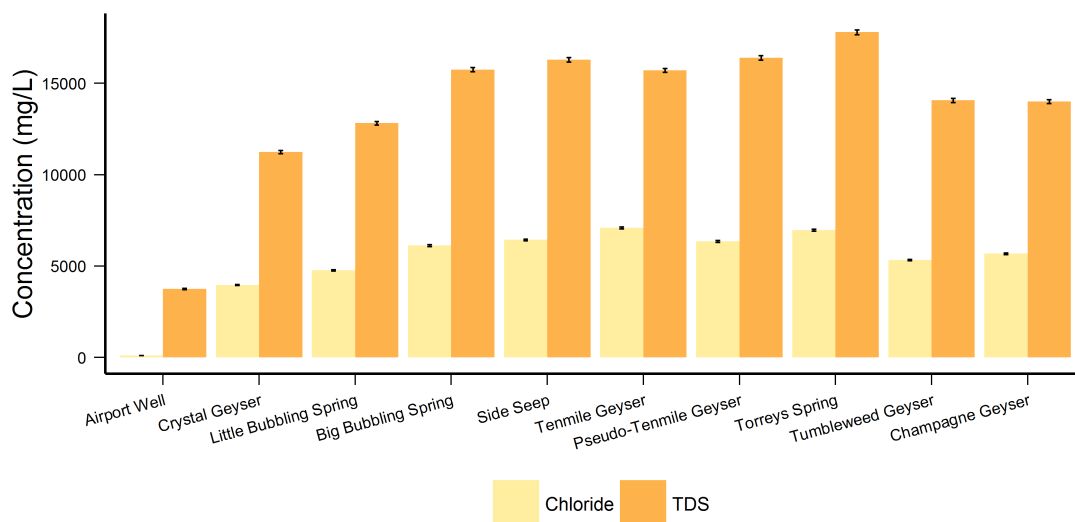
Figure 4.2: *Chloride (Cl⁻, mg/L) and total dissolved solids (TDS, mg/L) values for samples collected at the Utah spring locations. Error bars are 2s. Data given in Table 4.2.*

Concentrations of 4 trace metals of interest, As, Cu, Ni and Zn, are plotted in Figure 4.3. Concentrations of As were below LOD for *Side Seep*, and range between 6.59 ± 2.13 µg/L (*Champagne Geyser*) and 59.8 ± 7.0 µg/L (*Pseudo-Tenmile Geyser*), with a median concentration of 38.85 µg/L. Copper is not detected at *Green River Airport Well*, and has a maximum concentration at *Torrey's Spring* of 40.0 ± 3.1. Zinc concentrations were less then LOD for most of the springs except *Green River Airport Spring* (6.66 ± 0.26 µg/L), *Little Bubbling Spring* (30.2 ± 1.4 µg/L), *Tenmile Geyser* (15.4 ± 9.9 µg/L) and *Tumbleweed Geyser* (37.0 ± 7.1 µg/L). Nickel concentrations were detected in all the springs with values ranging from 4.36 ± 0.55 µg/L (*Side Seep*) to 11.7 ± 0.9 µg/L (*Champagne Geyser*), with a median value of 8.18 µg/L. *Green River Airport Well* concentrations for As, Cu, Ni and Zn are generally lower than other springs, with *Side Seep* also being consistently below other springs. The remaining of the 8 trace metals of interest (Cd, Cr, Hg & Pb) were not detected above analytical detection limits at any of the springs.

Of the other 13 elements analysed, Table 4.2, many follow similar patterns to each other, with respect
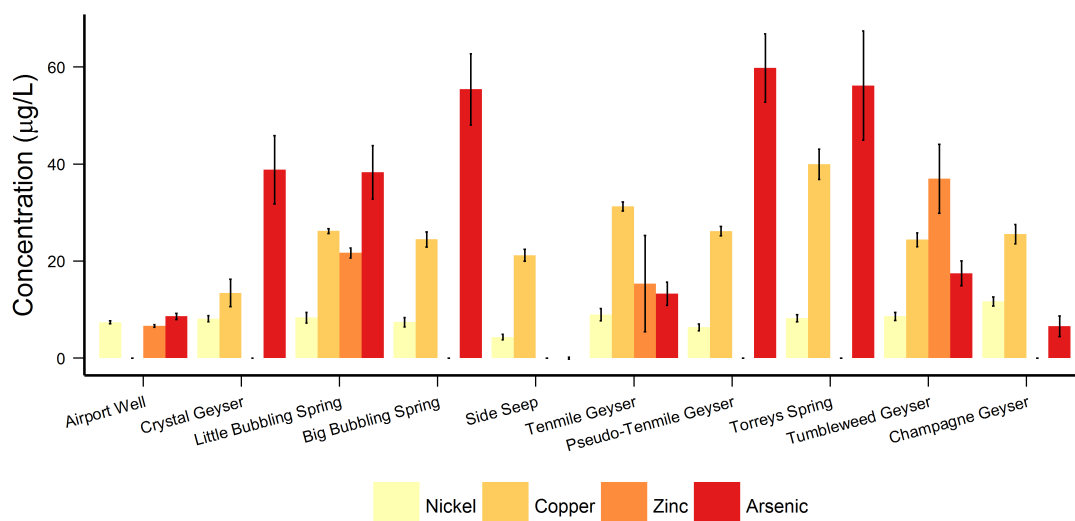
Figure 4.3: *As, Cu, Ni and Zn concentration data (µg/L) for samples collected at the Utah spring locations. Error bars are 2s. Data given in Table 4.2.*

to the concentrations present at each spring. For example, *Little Bubbling Spring* is regularly higher in concentrations in many elements than the other springs, while *Green River Airport Well* and *Side Seep* are generally lower. See Figure 4.4 as an example for calcium concentrations.
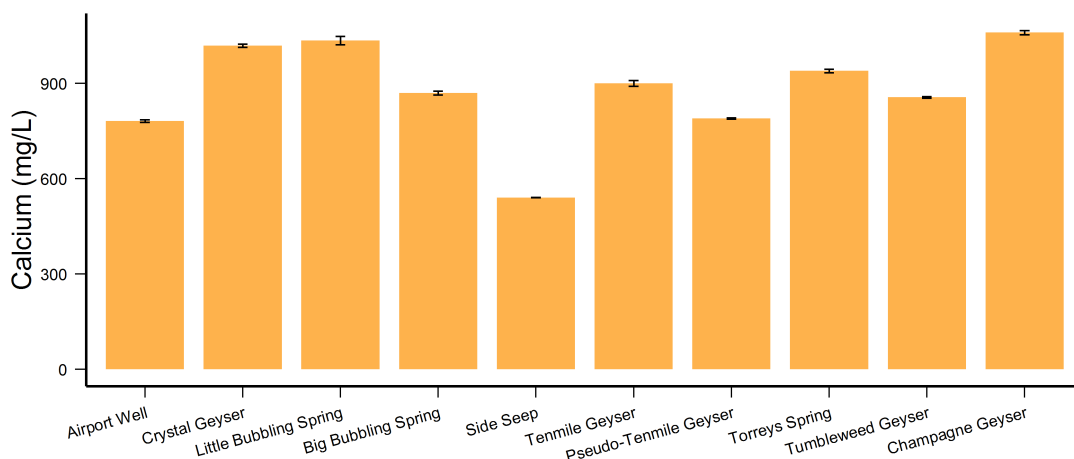
Figure 4.4: *Ca concentrations (mg/L) at each of the 10 Utah springs sampled. Error bars are 2s. Data given in Table 4.2.*

A notable exception to this general observation is Si. Concentrations of this element are higher in *Green River Airport Well* (31.6 ± 2.6 mg/L) than at any of the other spring locations by a factor of ~8, Figure 4.5.
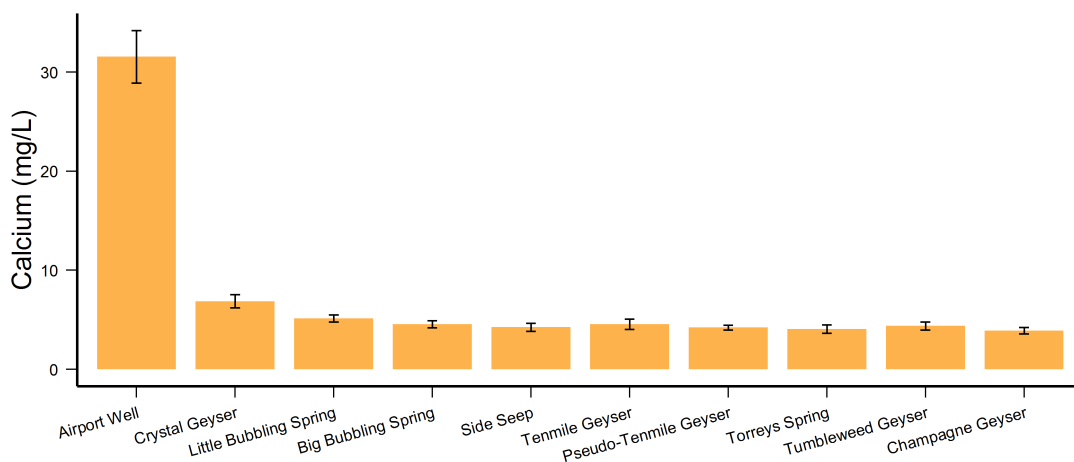
Figure 4.5: *Si concentrations (mg/L) at each of the 10 Utah springs sampled. Error bars are 2s. Data given in Table 4.2.*

4.2.3 X-ray diffraction (XRD)

The results of X-ray diffraction (XRD) analysis carried out on sandstone samples *Entrada S1 - Navajo S5* from the San Rafael Swell, Utah, are given in Table 4.3, as the mineral assemblage by weight % (wt.%). Values < 1 wt.% are trace concentrations and are considered semi-quantitative only (pers. comm. Dr. Nic Odling, University of Edinburgh), therefore their values should not be taken as accurate but indicative only of their presence in the sample.

Mineral	Type	Entrada S1 wt.%	±	Entrada S2 wt.%	±	Wingate S3 wt.%	±	Navajo S4 wt.%	±	Navajo S5 wt.%	±
Gypsum	Water soluble	0.4	0.1	0.4	0.1	0.4	0.2	0.3	0.1	0.3	0.1
Ankerite	Carbonate	2.5	0.3	3.7	0.4	0.3	0.4	0.1	0.2	-	-
Calcite		5.1	0.2	4.7	0.3	0.3	0.1	0.7	0.1	0.07	0.08
Dolomite	↓	5.4	0.3	3.3	0.5	-	-	0.2	0.1	0.1	0.3
Siderite		0.01	0.06	-	-	0.2	0.1	0.01	0.05	-	-
Hematite	Oxide	0.2	0.1	0.3	0.1	0.2	0.1	0.3	0.0	0.3	0.1
Pyrite	Sulphide	0.12	0.05	-	-	0.01	0.06	0.13	0.05	0.08	0.05
Albite	Silicate	6.1	0.4	3.4	0.3	1.2	0.3	0.5	0.2	0.5	0.3
Anorthite		1.8	0.4	1.2	0.4	0.1	0.3	0.4	0.3	0.3	0.3
Chlorite		1.9	0.6	1.1	0.4	1.3	0.4	0.7	0.3	0.8	0.3
Illite		6.6	0.4	2.6	0.6	2.1	0.3	1.6	0.3	1.0	0.3
Kaolinite		0.8	0.2	0.4	0.2	1.9	0.3	0.4	0.2	0.3	0.2
Microcline		4.0	0.3	4.8	0.4	5.9	0.5	5.3	0.4	3.6	0.4
Muscovite		4.1	0.4	1.2	0.4	2.1	0.3	1.4	0.3	1.1	0.3
Orthoclase		4.4	0.3	4.6	0.4	3.4	0.3	3.9	0.3	1.6	0.3
Quartz	↓	56.7	1.0	68.3	0.1	80.7	1.1	84.2	0.9	89.7	0.9

Table 4.3: *Results of XRD analysis for 5 Utah sandstone samples, S1 - S5. Minerals are grouped by type, as per the targeted phases in the sequential extraction procedure (Section 2.3), with the exception of the exchangeable phase. Summed data for each mineral type are plotted in Figure 4.6.*
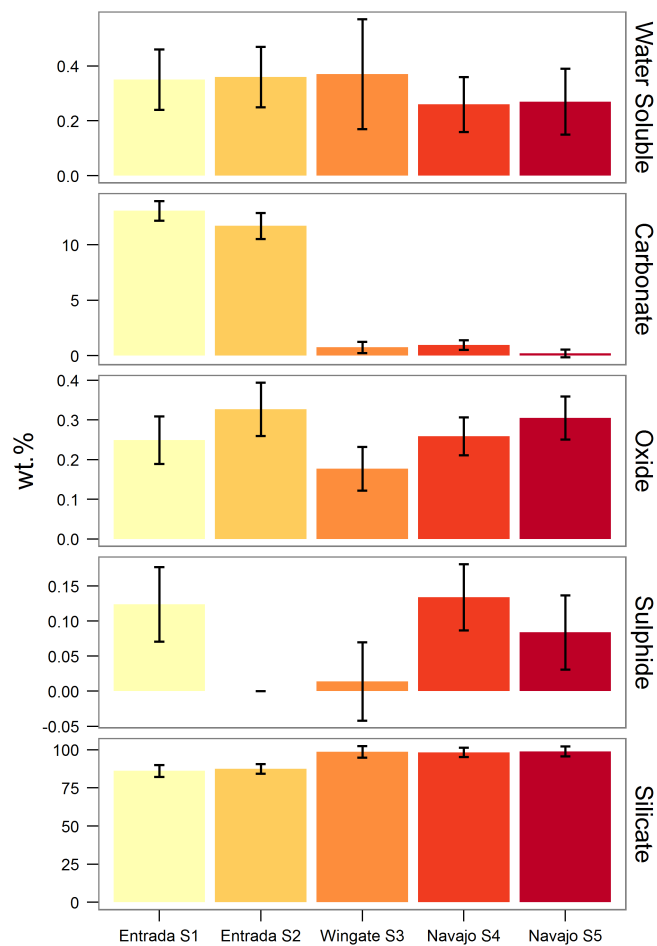
Figure 4.6: *Results of XRD analysis on Utah samples S1 - S5, as weight % of the rock, grouped by mineral type.*

The minerals identified in the Utah samples have been grouped in Table 4.3 by mineral type, as per the phases defined in the sequential extraction procedure (SEP) method outlined in the Methods (Section 2.3). These data are plotted in Figure 4.6.

Similar to the North Sea sandstones, the Utah sandstones are dominated by silicates, Table 4.3. Of these silicates, quartz is the main mineral, ranging from 56.7 ± 1.0 wt.% (*Entrada S1*) to 89.7 ± 0.9 wt.% (*Navajo S5*). Quartz make up a higher proportion of the *Wingate* and *Navajo* samples (average 84.9 wt.%), compared with the the *Entrada* sandstones (average 62.5 wt.%), Table 4.3. Of the other silicate minerals, the clay minerals chlorite, illite and kaolinite constitute between 2.15 ± 0.81 wt.% and 9.2 ± 1.2 wt.% (median 4.1 wt.%) of the samples. Feldspars, which make up the remainder of the silicate minerals identified in the Utah samples, make up between 7.14 ± 1.48 wt.% and 20.4 ± 1.7 wt.% (median 12.63 wt.%). Overall, silicates account for a higher proportion of the *Wingate S3*, *Navajo S4* and *Navajo S5* samples (average 98.7 wt.%) then the *Entrada S1* and *S2* samples (86.9 wt.%)

Gysum, hematite and pyrite, Table 4.3, are below 1 wt.% and therefore these values are considered indicative only of the presence of trace amounts of water soluble, oxide and sulphide minerals. The proportions of each are, however, quite similar across all of the samples.

Finally, carbonate minerals account for 13.1 ± 0.9 wt.% of *Entrada S1* and 11.7 ± 1.2 wt.% of *Entrada S2*, but less than 1 wt.% of the *Wingate* and *Navajo* samples, Table 4.3 and Figure 4.6. Calcite ($CaCO_3$), dolomite ($CaMg(CO_3)_2$) and ankerite ($Ca(Fe,Mg,Mn)(CO_3)_2$) make up the majority of the carbonate content, with only trace siderite present ($FeCO_3$), Table 4.3. *Entrada* formation sandstones are therefore much more carbonate rich, compared with the trace amounts in the *Wingate* and both *Navajo* sandstones, and therefore with fewer silicates, particularly quartz.

4.3 Batch Experiment

A long-term (6 months) set of batch experiments were run at the University of Edinburgh, using sandstone samples collected in the San Rafael desert, Utah. The rock sampling rationale and methodology is detailed in the Methods chapter, Section 2.1.1, and the batch experiment set up is described in Section 2.2.2.

Five samples were collected, *S1 - S5*: two from the *Entrada* formation, one from the *Wingate* formation and two from the *Navajo* formation. These formations are thought to be possible source aquifers for the CO_2-driven spring waters which emanate south of Green River, Utah (e.g. Wilkinson *et al.* 2009). The aim of the experiments was to determine the mobility of metals from these sandstones using spring water collected from nearby *Crystal Geyser* and bubbled CO_2.

The use of collected spring water differed from the North Sea batch experiments (Chapter 3) in that the batch saline solution was not a synthetic NaCl solution (see Section 2.2.2), but a natural water sample which - theoretically - was already in equilibrium with the rocks from which it was sourced, rather than the far-from-equilibrium conditions of the North Sea experiments. Also, the use of aquifer rocks which have already reacted with CO_2-enriched porewaters in this area of Utah, albeit sampled from a weathered outcrop and not a borehole core, differed from the North Sea rocks which had been hydrocarbon reservoirs and not known to be subject to reactions with CO_2-enriched formation waters.

Finally, the experiment also differed from the North Sea batch experiments with respect to the length of time they were run for (24 weeks compared with 2 - 4 weeks), and that the batch solution and rocks were allowed to equilibrate, if necessary, for a long period of time (3 months) before CO_2 bubbling began. Thus, the use of aquifer sandstones and the waters which emanate from them, are potentially a useful test of the simple batch experiments in simulating the effect of CO_2 on metal mobility.

4.3.1 pH

The pH of the experimental batch fluids was measured throughout the duration of the experiment, Figure 4.7. Values were measured more frequently within the first 10 days of the experiment and immediately following the start of CO_2 bubbling at day 82. The increased frequency at these times was to ensure that rapid initial changes in pH were captured in the data. Previous batch experiments on North Sea sandstones did not sample so frequently, possibly missing interesting data, and so the sampling frequency was changed for the Utah experiment.

Experimental pH values begin very close to the field-measured pH for *Crystal Geyser* of 6.71, Table 4.1, although are slightly higher initially, probably due to some CO_2 degassing during transport and storage of the samples collected 6 months prior. pH values then increase for all 4 batch reaction vessels in essentially the same manner to maximum values of between 8.77 (*Entrada S1*) and 9.03 (*Wingate S3*), recorded just after CO_2 bubbling commenced.

There is then a rapid drop in pH values for all samples after CO_2 bubbling begins, as would be expected from the reaction of CO_2 with the *Crystal Geyser* water, to pH values of between 6.09 (*Entrada S2*) and 6.21 (*Wingate S3*). pH values then increase slightly for all the samples, Figure 4.8, and maintain a steady mean pH of ~ 6.35 for the remainder of the experiment. These steady pH values are lower than at the start of the experiment, and therefore lower than the field-measured value at *Crystal Geyser* (although similar to the *Green River Airport Spring* and *Tenmile Geyser* field values, Table 4.1).

4.3.2 Cation data

Aliquots of batch fluids were drawn throughout the experiment and concentrations of a suite of elements were determined by Inductively Coupled Plasma Mass Spectroscopy (ICP-MS) at the University of Edinburgh (Chapter 2, Section 2.5.2). Aliquots were taken in the periods prior to, and following, the
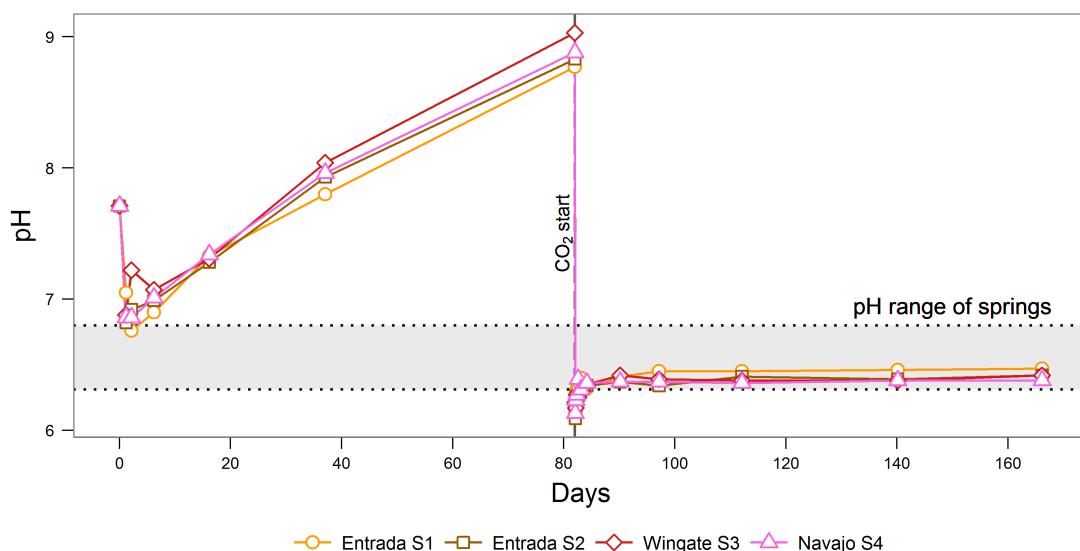
Figure 4.7: *pH values for the batch reaction experiment using water collected from Crystal Geyser, and rock samples collected from the nearby San Rafael Swell, Utah (see Figure 2.1, Chapter 2). CO_2 flow commences at day 82. Shaded area indicates the field-measured pH values of the Green River spring waters, Table 4.1).*
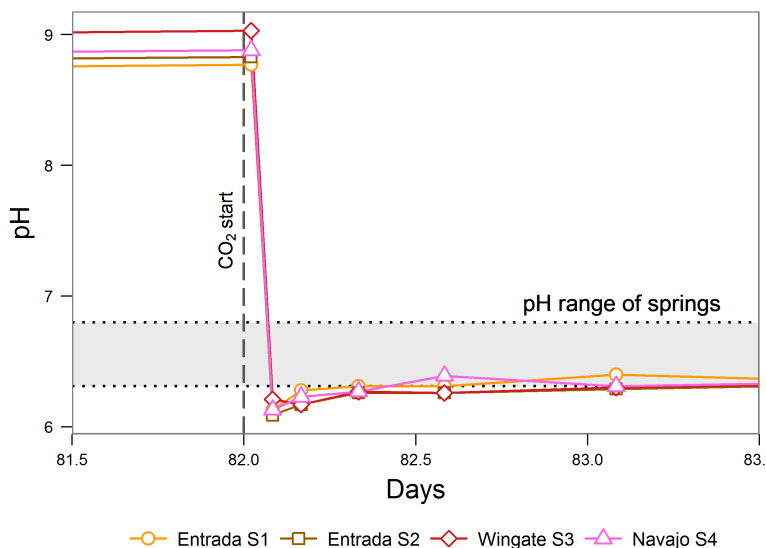
Figure 4.8: *An expanded x-axis scale view of pH values for the Utah batch reaction experiment, to better visualise the changes in pH immediately following the start of CO_2 bubbling at day 82. Shaded area indicates the field-measured pH values of the Green River spring waters.*

commencement of bubbling CO_2, with particular focus on the beginnings of these periods in order that rapid changes (in the order of hours) in geochemistry could be observed. While previous batch experiments on North Sea sandstones sampled once per day as the shortest time interval, sampling intervals were shortened to several hours.

The suite of elements selected for analysis was chosen based on those analysed by the University of Texas (UT) for the field samples (Section 2.5.1), however of the 34 elements analysed for, only 16 have been selected for further analysis and discussion. These elements are generally the same as those presented for the North Sea analysis, Chapter 3, and include the 8 trace metals of particular interest to this thesis: As, Cd, Cr, Cu, Hg, Ni, Pb & Zn.

The concentration data for the 16 elements is presented in a series of graphs over the following pages, divided into the trace metals and other elements including Al, Ba, Ca, Fe, K, Mg, Mn & Sr. As with the pH data, two figures (Figures 4.11 and 4.14) show a section of time covering the first 2 days of sampling following commencement of CO_2 bubbling, for ease of interpretation compared with the graphs showing the entire time series data.

On all of the following plots, shaded areas show the maximum and minimum concentrations of each element as determined by UT from the 10 field samples, which are discussed in more detail in Section 4.2. Where UT data was less than the analytical detection limit, no shaded area has been plotted. In the case of Fe, concentrations were determined to be in the range $1,190 \pm 10$ to $20,600 \pm 300$ µg/L; values which are significantly higher than the batch fluid concentrations (Figure 4.12). When plotted, the field concentrations affected the y-axis scale such that the batch fluid data trends became unreadable. To aid visualisation, these values were not plotted and instead noted on the relevant graph.

4.3.2.1   Trace metals of interest

Concentrations of As and Cd were not detected above the analytical detection limits, with the exception of a single Cd data point for the *Entrada S2* sample, Figure 4.9. Concentrations of Cr, Hg and Pb are also low throughout the 6 month duration of the experiment, Figures 4.9 and 4.10. The addition of CO_2 at day 82 appears to mobilise some Hg (2.1 ± 0.4 µg/L, *Entrada S2*) and Pb (11 ± 2 µg/L, *Entrada S2*), but these increased concentrations only persist for a few days before returning to pre-CO_2 concentrations, Figure 4.11. Chromium concentrations for *Entrada S1* reduce to lower than pre-CO_2 levels. Of these elements (As, Cd, Cr, Hg, Pb), only As was detected in the field spring samples, Figure 4.9.

Copper concentrations before CO_2 bubbling appear to be fairly constant and remain within the spring water range, Figure 4.9. Several days after CO_2 bubbling commences, spikes in concentrations occur for the *Entrada S1* and *Wingate S3* samples, with a maximum value of 49 ± 5 µg/L which is out-with the maximum spring value of 40 ± 3 µg/L (*Torrey's Spring*). However, concentrations then reduce back to lower than pre-CO_2 levels, and therefore within the range of the spring values, Figure 4.9.

Concentrations of Ni are below detection limits for the majority of initial 3 months of the experiment, and therefore below the spring samples range of 4.4 ± 0.6 - 11.7 ± 0.9 µg/L, and remain so until day 97 where concentrations begin to increase for *Navajo S4*. *Entrada S1* follows suit from day 112 and *Entrada S2* and *Wingate S3* from day 140. Final concentration values on day 166 are 5.5 ± 0.7 µg/L, 2.9 ± 0.4 µg/L, 8 ± 1 µg/L and 14 ± 2 µg/L for samples *S1 - S5*, respectively, with values now for *Entrada S1* and *Wingate S3* within the springs' range, Figure 4.10.

Zinc concentrations effectively remain constant throughout the experiment, with values at or exceeding the upper end of the springs' range of 6.7 ± 0.3 - 37 ± 7 µg/L, Figure 4.10. The addition of CO_2 at day 82 results in some spikes in concentrations for several days following, however final concentrations (20 ± 7 - 30 ± 10 µg/L) are slightly lower than starting concentrations (28 ± 9 - 38 ± 13 µg/L).

Where detected, stable concentrations define the majority of the trace metal trends through the 6 months of these batch experiments, with essentially similar trends between the 4 different rock samples used. The addition of bubbled CO_2 to the flasks results in some temporary instability in concentrations for most of these elements, however concentrations stabilise again at similar, or lower, concentrations than pre-CO_2 bubbling. The exception is Ni, where concentrations begin to rise from around 15 days after commencing CO_2 bubbling. Concentrations of As, Cu, Ni and Zn are comparable to those measured in the spring waters, while Cr, Hg and Pb were all mobilised to some extent during the experiments but not detected at all in the spring water samples.
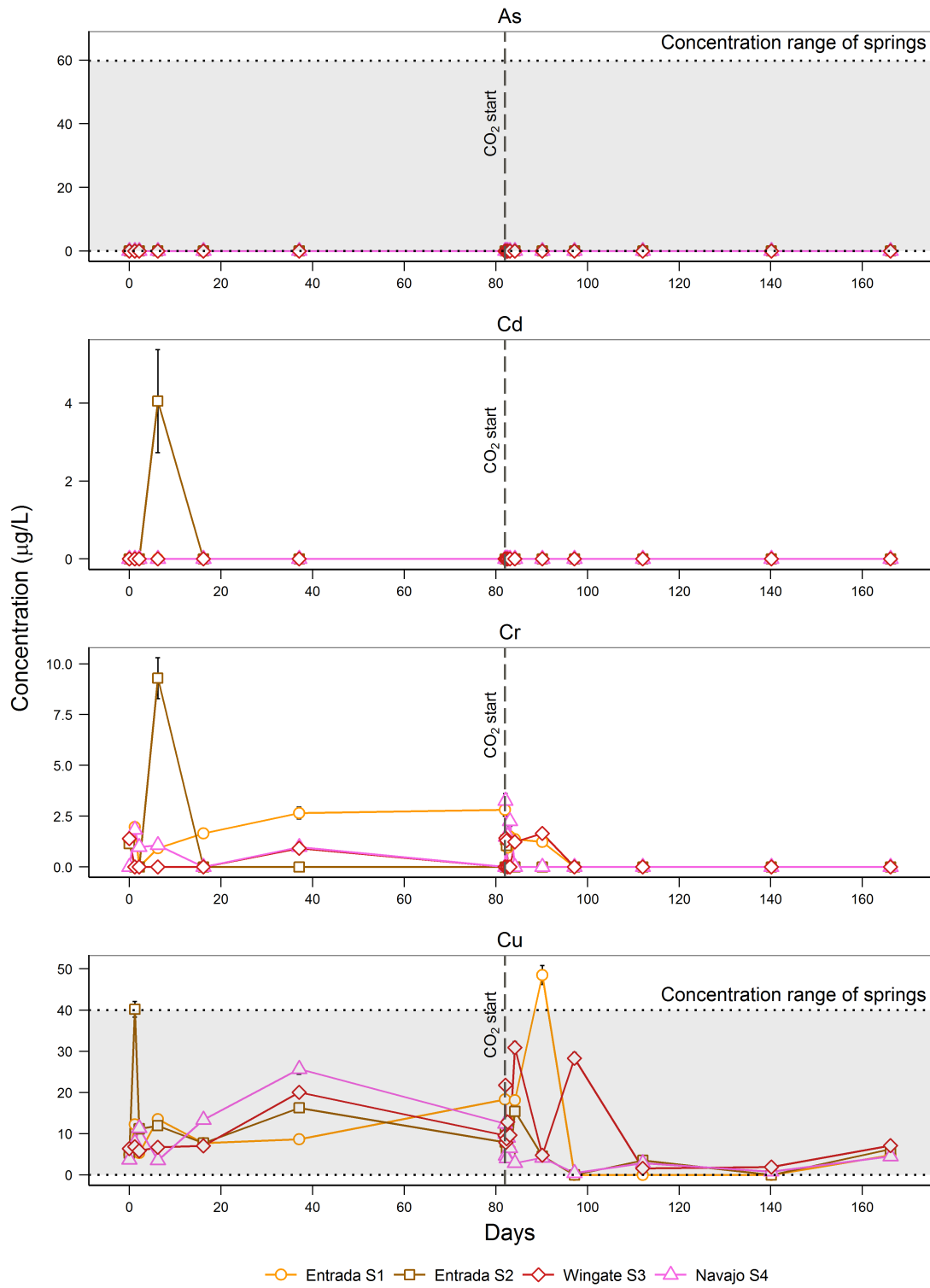
Figure 4.9: *Concentrations of As, Cd, Cr, Cu through the duration of the batch experiments, for 4 Utah sandstone samples. Dashed vertical line at day 82 represents start of CO_2 flow. Shaded areas indicate the range of concentrations detected across 10 Green River spring locations (Figure 2.1). No shading present indicates element concentrations fall below analytical detection limits.*
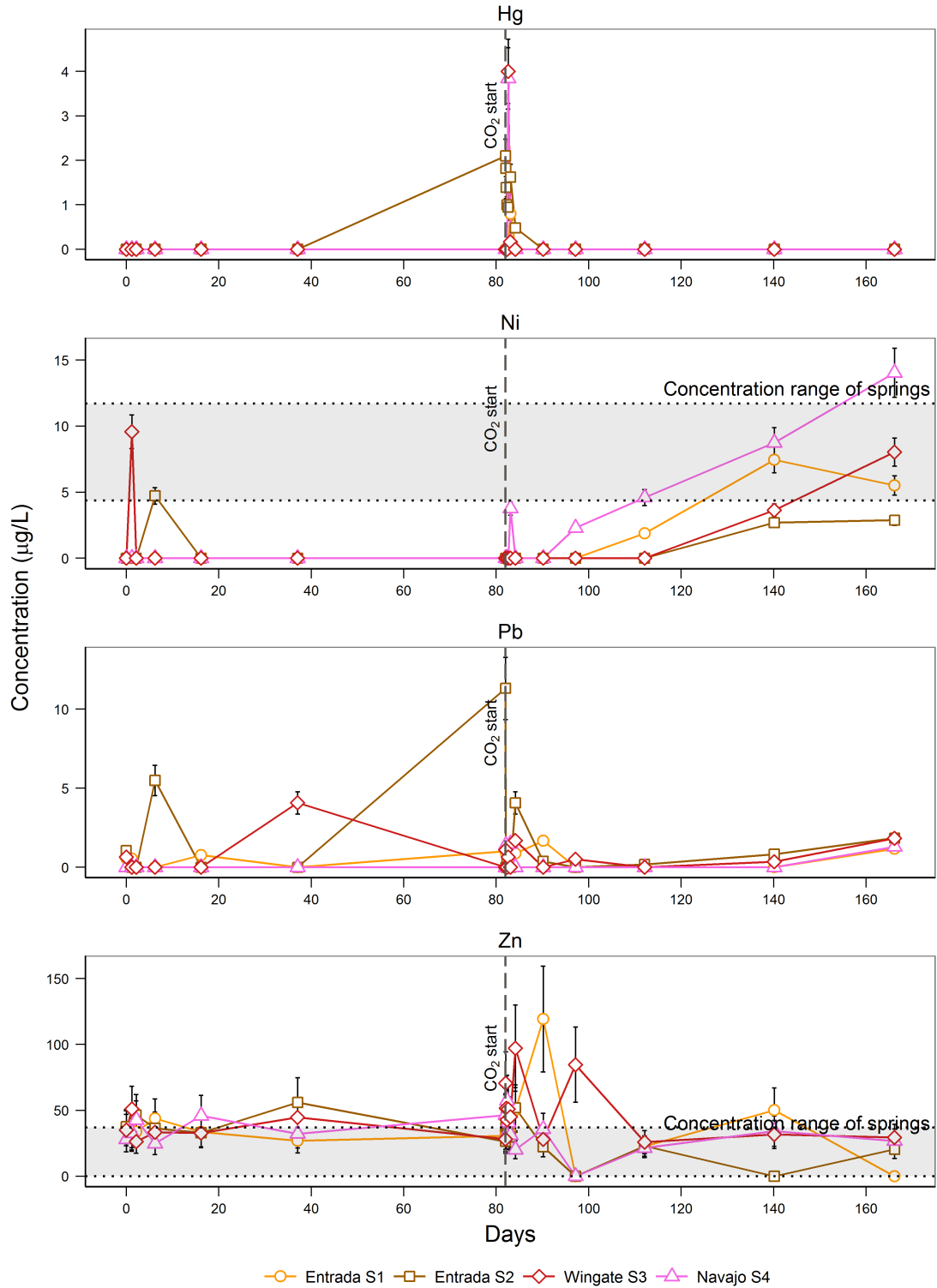
Figure 4.10: *Concentrations of Hg, Ni, Pb, Zn through the duration of the batch experiments, for 4 Utah sandstone samples. Dashed vertical line at day 82 represents start of CO_2 flow. Shaded areas indicate the range of concentrations detected across 10 Green River spring locations (Figure 2.1). No shading present indicates element concentrations fall below analytical detection limits.*
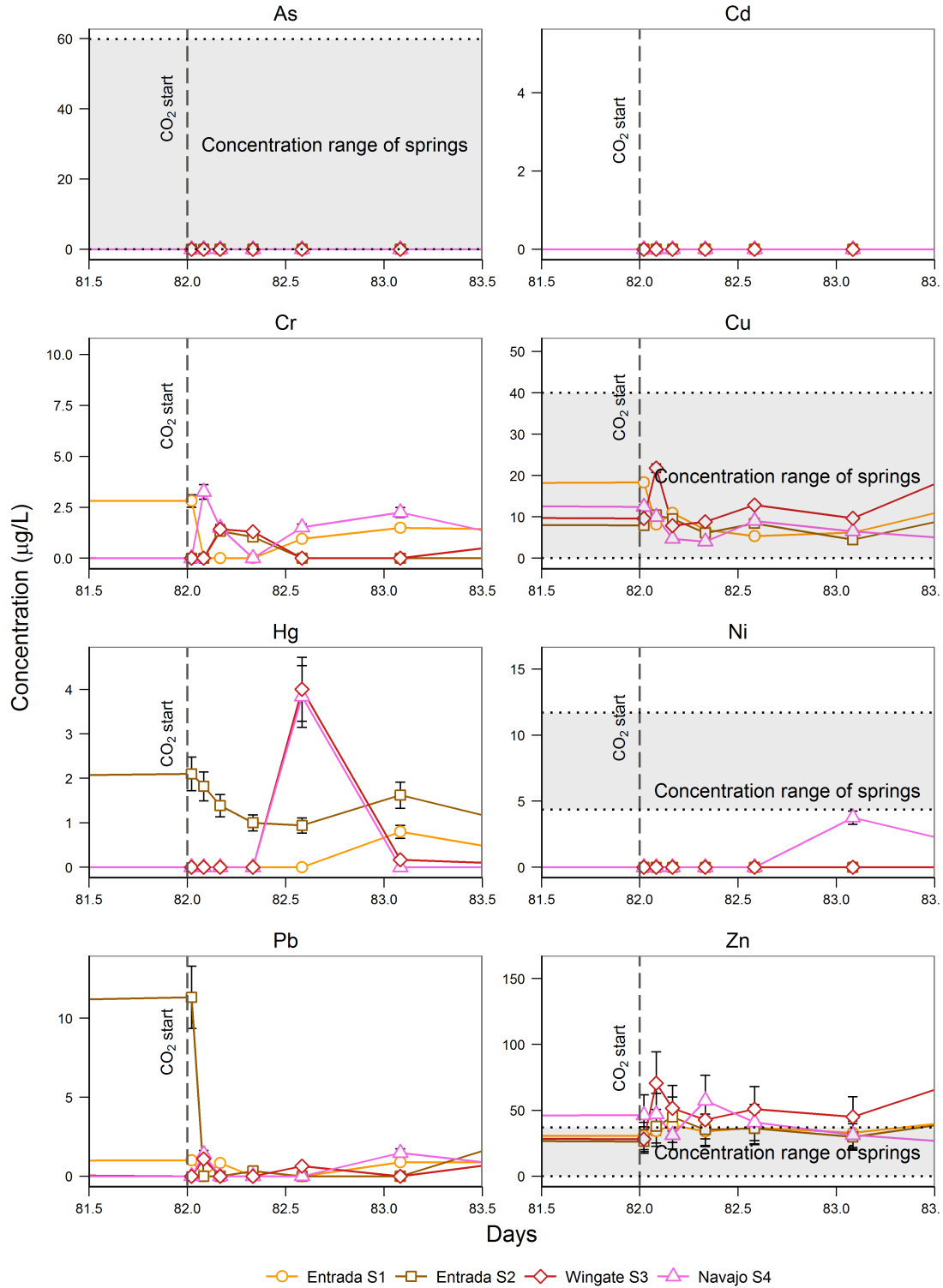
Figure 4.11: *Concentrations of 8 trace metals of interest for the period day 81.5 to 83.5, to better highlight changes immediately following commencement of CO_2 flow to the flasks (dashed vertical line). Shaded areas indicate the range of concentrations detected across 10 Green River spring locations (Figure 2.1). No shading present indicates element concentrations fall below analytical detection limits.*

4.3.2.2 Major elements

Concentrations of 8 major elements are presented here: Al, Ba, Ca, Fe, K, Mg, Mn & Sr. For the most part, concentrations for all these elements are very similar between each of the 4 batch samples (*S1 - S4*), with concentrations of 5 of these 8 elements falling into two distinct trends.

Firstly, after a small initial rise, both K and Mg maintain constant concentrations up to the start of CO_2 bubbling, thereafter having a slight initial decrease (Figure 4.14) but going on to slowly rise for the remainder of the experiment with bubbled CO_2. Concentrations of K remain within the springs' range, although by the end of the experiment they have increased to slightly above. Mg concentrations for the batch experiments are consistently above the narrow range for the springs, Figure 4.13.

Secondly, Ca, Mn and Sr show a decreasing concentrations through the initial 3 months of the experiments for all samples to low concentrations, with minimum values of $4,500 \pm 900$ μg/L, 1.3 ± 0.1 μg/L, and 36.3 ± 0.4 μg/L, respectively, for the *Wingate S3* sample. These minima are outwith the spring concentration range, Figures 4.12 and 4.13. The addition of CO_2 to the flasks result in a rapid increase and then stabilisation of concentrations over a matter of days, Figure 4.14. The stabilised concentrations are within, or just below, the lower bounds of the spring concentrations.

Barium concentrations are initially within the range of spring concentrations for the first 3 months of the experiment, with the exception of *Navajo S4* which initially increases in concentration to 71 ± 6 μg/L before returning to similar concentrations as the other samples by the end of this period. After CO_2 bubbling starts, there is a rapid increase in a matter of hours to maximum concentrations for all of the samples, with *Navajo S4* again having the highest concentration of 140 ± 10 μg/L, Figure 4.12. This is a similar trend to Ca, Mn and Sr after CO_2 bubbling starts, however unlike these elements, concentrations of Ba then decline steadily over the next three months, possibly reaching stable concentrations by the end of the experiment. With the exception of *Navajo S4*, the batch concentrations lie mostly within the range of spring values, Figure 4.12.

Of the remaining 3 elements, Fe does not appear to exhibit any trend, although at the commencement of CO_2 bubbling, there is a slight increase in concentrations for *Entrada S1* and *Navajo S4*, to values of 60 ± 20 μg/L and 110 ± 40 μg/L, respectively. However these are not the highest concentrations achieved, Figure 4.12, and there is no indication that CO_2 has affected Fe concentrations. Maximum batch Fe concentration values (180 ± 70 μg/L) are also significantly lower than the spring range of 1,190 - 20,600 μg/L. This range was not drawn on the plot, Figure 4.12, to better show the batch concentrations.

Finally, Al was detected at concentrations fluctuating between 140 ± 50 μg/L and 600 ± 200 μg/L prior to CO_2 bubbling, which compares with concentrations in the spring samples where are lower than the ICP-MS analytical detection limit of 0.18 μg/L. Concentrations then drop by a factor of ~10 several days after CO_2 bubbling begins, and remain at this level (or below detection limit) for the remainder of the experiment.
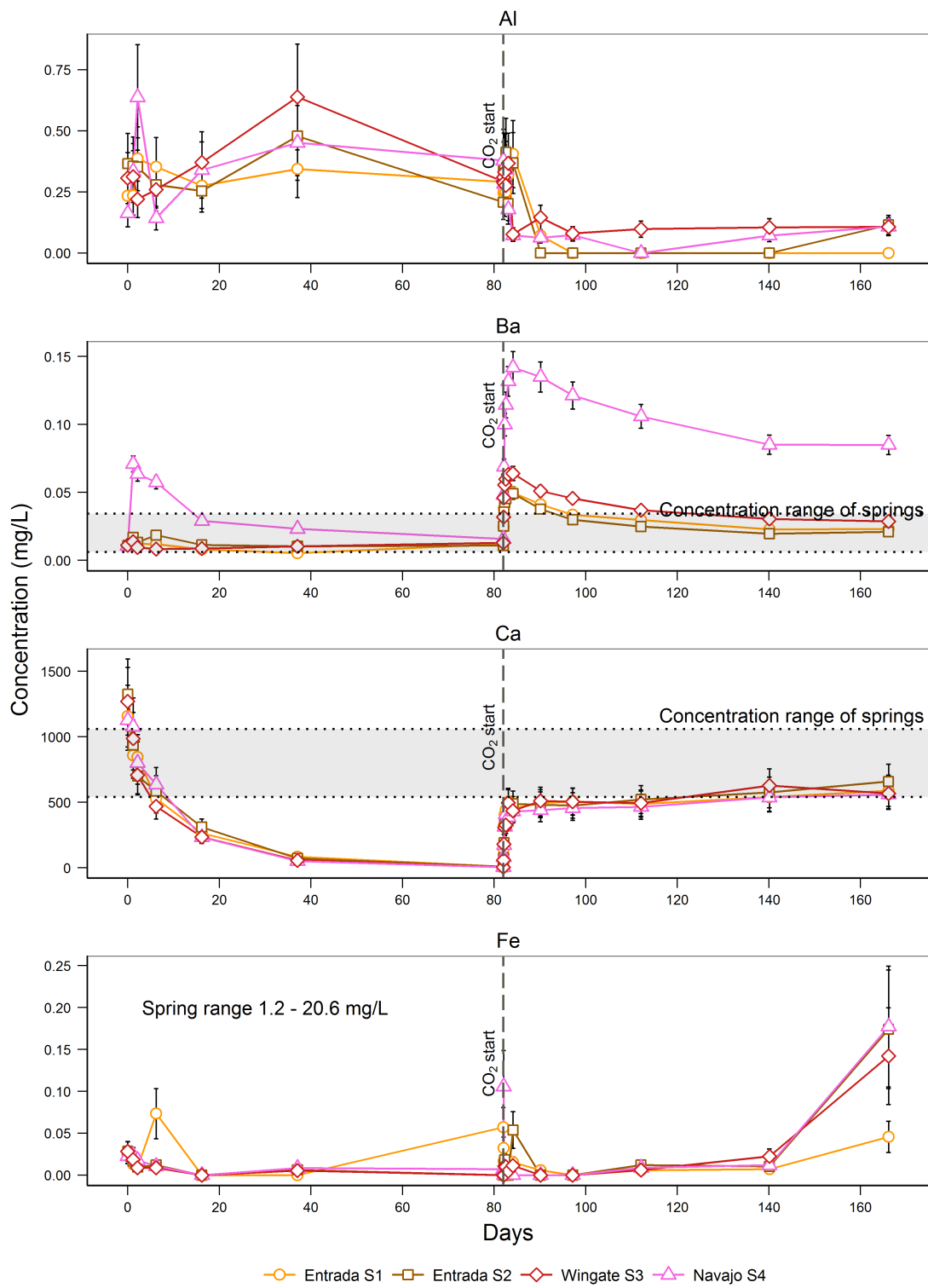
Figure 4.12: *Concentrations of Al, Ba, Ca, Fe through the duration of the batch experiments, for 4 Utah sandstone samples. Dashed vertical line at day 82 represents start of CO_2 flow. Shaded areas indicate the range of concentrations detected across 10 Green River spring locations (Figure 2.1). No shading present indicates element concentrations fall below analytical detection limits, except Fe where the springs' range is significantly greater than the batch concentrations.*
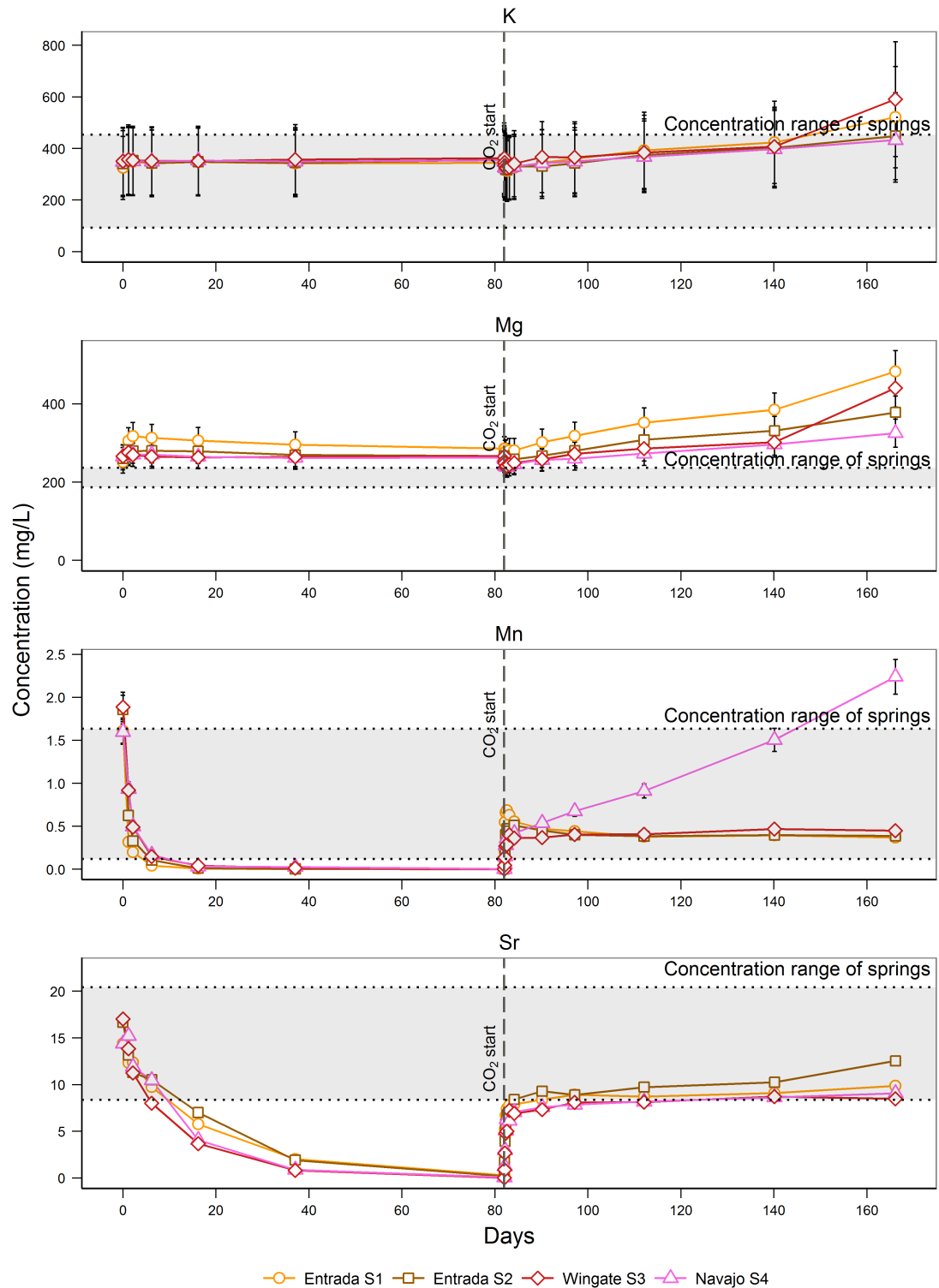
Figure 4.13: *Concentrations of K, Mg, Mn, Sr through the duration of the batch experiments, for 4 Utah sandstone samples. Dashed vertical line at day 82 represents start of CO_2 flow. Shaded areas indicate the range of concentrations detected across 10 Green River spring locations (Figure 2.1). No shading present indicates element concentrations fall below analytical detection limits.*
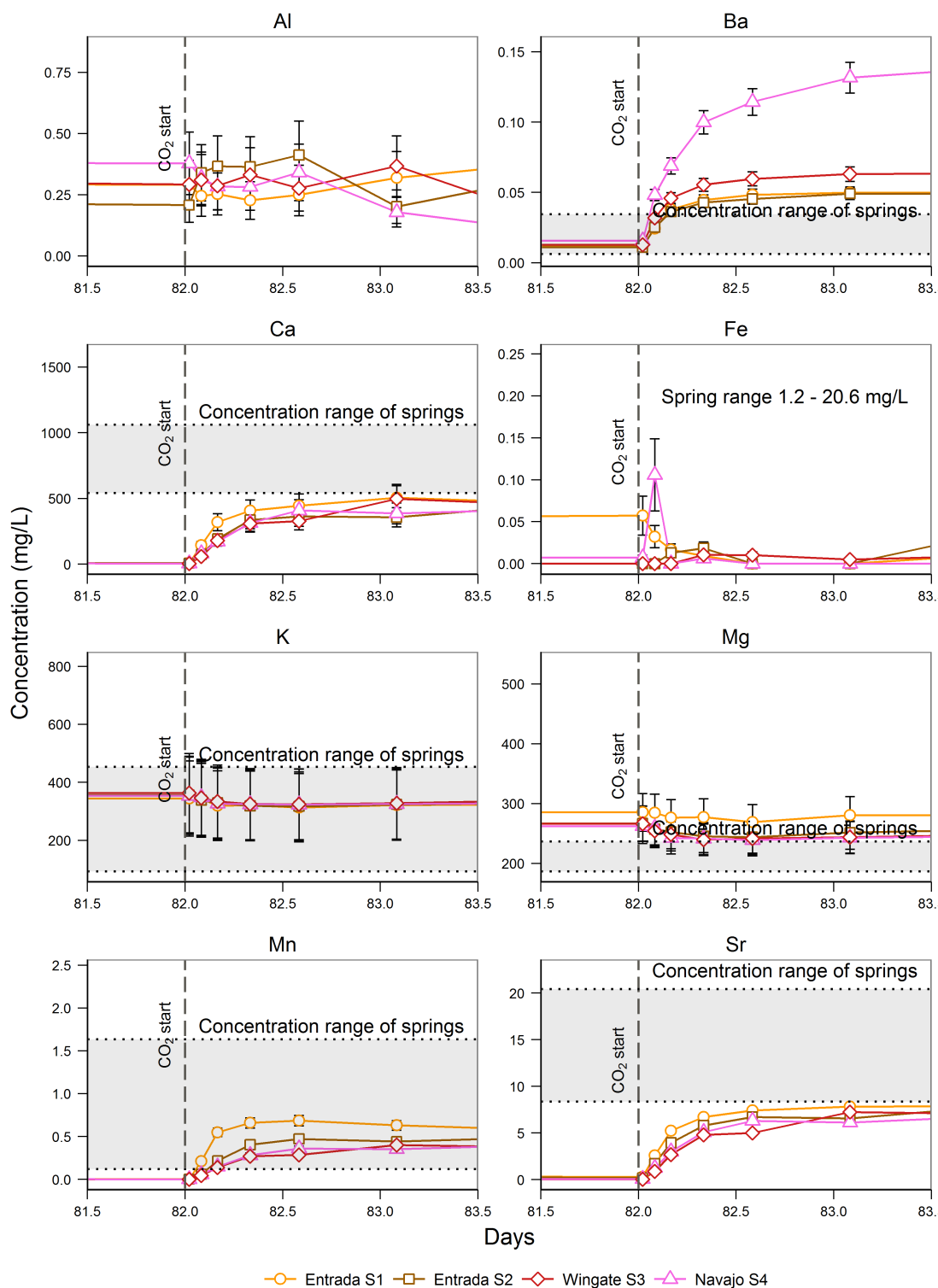
Figure 4.14: *Concentrations of 8 major elements of interest for the period day 81.5 to 83.5, to better highlight changes immediately following commencement of CO_2 flow to the flasks (black vertical line). Shaded areas indicate the range of concentrations detected across 10 Green River spring locations (Figure 2.1). No shading present indicates element concentrations fall below analytical detection limits, except Fe where the springs' range is significantly greater than the batch concentrations.*

4.4 Sequential Extraction Procedure

In order to better determine the origin of the elements leached during batch reactions, a sequential extraction procedure (SEP) was carried out on sandstone samples collected in the San Rafael desert, Utah. The experimental rationale and method are described in the Methods chapter.

The SEP generates data in the form of micrograms of element extractable per gram of sample, for each of the 6 different steps (water soluble, exchangeable, carbonate, oxide, sulphide, silicate). These concentrations (μg/g) are therefore an indication of how much of an element is available to be mobilised in each defined phase in the rock.

The sum of the concentrations obtained from each SEP step for each element analysed can be compared with the bulk (whole rock) concentrations for the 5 Utah sandstone samples (*S1 - S5*), to check for systematic biases in the extraction procedure, such as loss of material when transferring supernatant to the sampling containers. In such cases, the sum of the steps would under report concentrations, compared with the bulk analysis. Concentrations of the summed SEP steps and bulk concentrations were plotted against each other, Figure 4.15 (data: Appendix C), using a $\log_{10}$ scale to show all element concentrations on one plot. This was done for each element, and for each of the 5 samples. If concentrations are comparable, elements will plot on a 1:1 line. Where the bulk and summed concentrations vary, they will plot off the line.
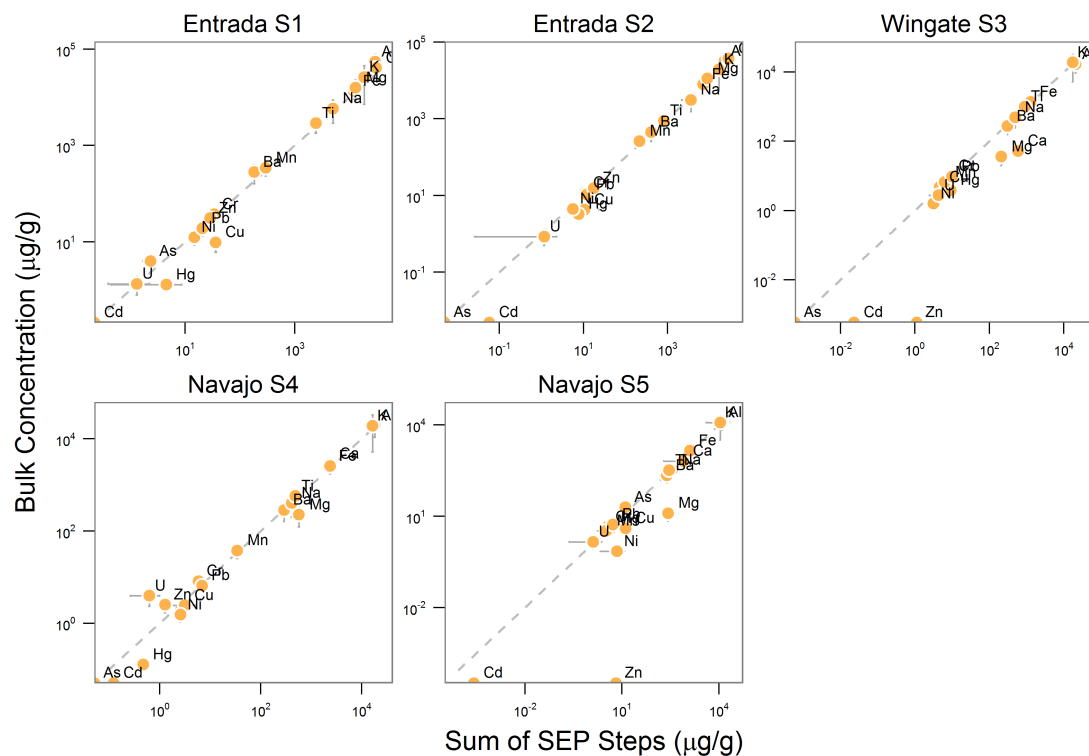
Figure 4.15: *Sum of the concentrations of the 6 SEP steps compared with the bulk analysis, for each of the 5 Utah samples. Note $\log_{10}$ scale. Error bars are 2s.*

For the majority of elements analysed, the bulk and summed concentrations plot together on the 1:1 line, indicating good agreement, although a log-log plot will tend to mask differences unless significantly different.

Common elements with which there is a discrepancy between summed and bulk values are As, Cd, Cu, Hg and Mg. In most of these cases, the summed concentrations tend to be larger than the bulk value,

Figure 4.15. Cadmium, in particular, was not detected in any of the 5 samples during bulk analysis, despite it's detected presence in the SEP steps. Similarly for Zn in the *Wingate S3* and *Navajo S5* samples. As was largely not detected during any of the SEP or bulk analysis.

That the majority of elements appear to have a good 1:1 relationship is encouraging that the total errors involved in the SEP are low, on the whole. It would not be expected that good agreements exist since random error is introduced throughout each SEP step, including loss of material, carry-over of elements from one step to another as well as analytical error. And while obtained from the same powdered sample as the SEP, the bulk analysis was carried out on a different sample and therefore this introduces the uncertainty of sample heterogeneity. This may explain, more than the accumulation of random SEP errors, any mismatches between the summed and bulk concentrations. Given that the bulk sample has gone through only one analytical procedure, these values would be considered more accurate than the sum of the SEP steps, and so will be used throughout the remainder of the thesis, with respect to bulk concentrations.

4.4.1 Cation concentrations of SEP steps

The concentrations of 16 elements (Al, As, Ca, Ca, Cd, Cr, Cu, Fe, Hg, K, Li, Mg, Mn, Ni, Pb & Zn), including the 8 trace metals of interest, are plotted for each of the 5 Utah rock samples (*Entrada S1 - Navajo S5*), and for each of the SEP steps (water soluble, exchangeable, carbonate, oxide, sulphide and silicate) in Figures 4.16 and 4.17. The data is presented in Appendix C.

Of the 8 major elements considered, Figure 4.16, the distributions fall into two main categories: concentrations greatest in silicates (Al, Ba, Fe, K), and concentrations greatest in carbonates (Ca, Mg, Mn). The exception to this is Li, which is distributed fairly evenly between water soluble, exchangeable, carbonates and oxides for two the *Entrada* samples, and was not detected in either sulphide or silicate steps.

Concentrations of Al and K are low in all SEP steps except the silicate phase, with maximum concentrations of 662 ± 7 µg/g (*Entrada S1*, oxide) and 283 ± 4 µg/g (*Entrada S1*, water soluble), respectively. These compare with a maximum Al concentration in the silicate phase of $28,600 \pm 2,800$ µg/g (*Entrada S1*) and a maximum K concentration of $18,000 \pm 1,500$ µg/g (*Entrada S1*). Al was not detected in the exchangeable phase, and K was not detected in any of the carbonate, oxide or sulphide steps for any of the 5 samples.

Barium is present in all phases, with the greatest concentrations found in *Entrada S2* in the exchangeable (70.0 ± 2.1 µg/g) and carbonate (93.7 ± 4.2 µg/g) phases. These are lower than Ba concentrations in the silicate phase, which range from 162 ± 2 µg/g to 258 ± 5 µg/g. Iron was not detected in the exchangeable phase, but is associated moderately with carbonate and oxide phases for the *Entrada* samples, with concentrations of $1,650 \pm 85$ µg/g (*S1*) and $1,300 \pm 14$ µg/g (*S2*), and $1,900 \pm 50$ µg/g (*S1*) 420 ± 20 µg/g (*S2*) in the carbonate and oxide phases, respectively. Iron concentrations in the silicate phase are significantly higher, however, for *Entrada S1* and *S2*, with values of $8,600 \pm 570$ µg/g and $5,300 \pm 215$ µg/g, respectively. *Wingate* and *Navajo* concentrations are comparatively low, ranging from 825 ± 280 µg/g to $1,940 \pm 170$ µg/g, Figure 4.16.

Concentrations are dominated in the carbonate phase for the *Entrada S1* and *S2* samples by Ca, Mg and Mn, Figure 4.16. This is unsurprising given that the results of the X-ray diffraction (XRD) analysis show that these samples are some 11 - 14 wt.% carbonates, compared with < 1 wt.% for the other samples. Ca, Mg and Mn are higher in *Entrada S1* than *S2*, again because of the greater abundance of carbonate minerals in *Entrada S1* (Table 4.3). For the two *Entrada* samples, Ca, Mg and Mn concentrations range $25,600 \pm 1,100$ - $26,600 \pm 1,700$ µg/g, $6,620 \pm 20$ - $7,165 \pm 315$ µg/g, and 179 ± 5 - 205 ± 9 µg/g, respectively. These elements are also present to a lesser extent in the silicate phase, and again predominantly in the *Entrada* samples. Magnesium and Mn are also detected in the oxide phase, with maximum values of $2,235 \pm 80$ µg/g and 30.8 ± 3.1 µg/g, respectively, for *Entrada S1*.

The distribution of the trace metals is apparently more random than the major elements, Figure 4.17.
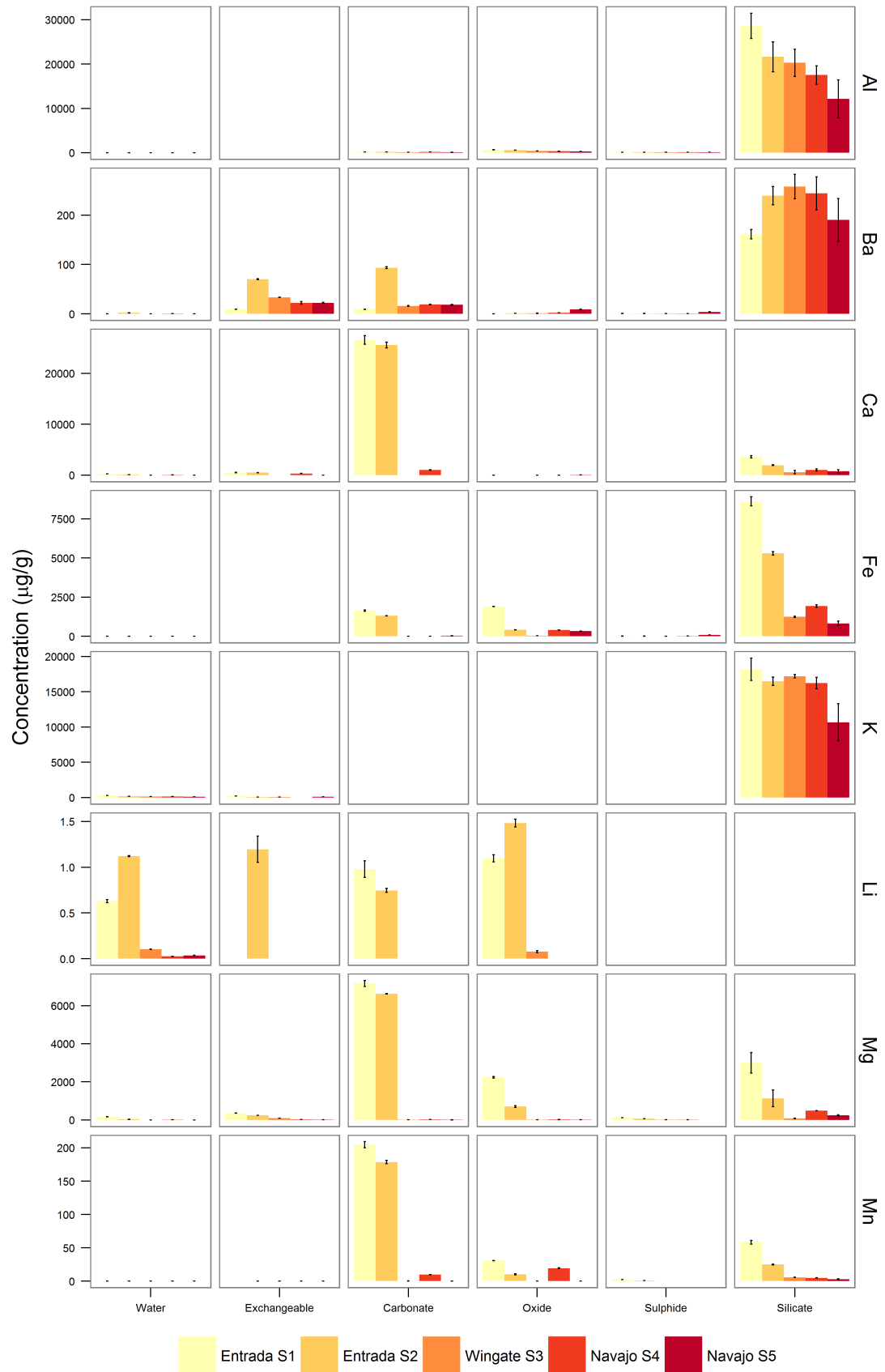
Figure 4.16: *Concentrations of major elements for each of the 6 sequential extraction procedure (SEP) steps. Error bars are 1s.*
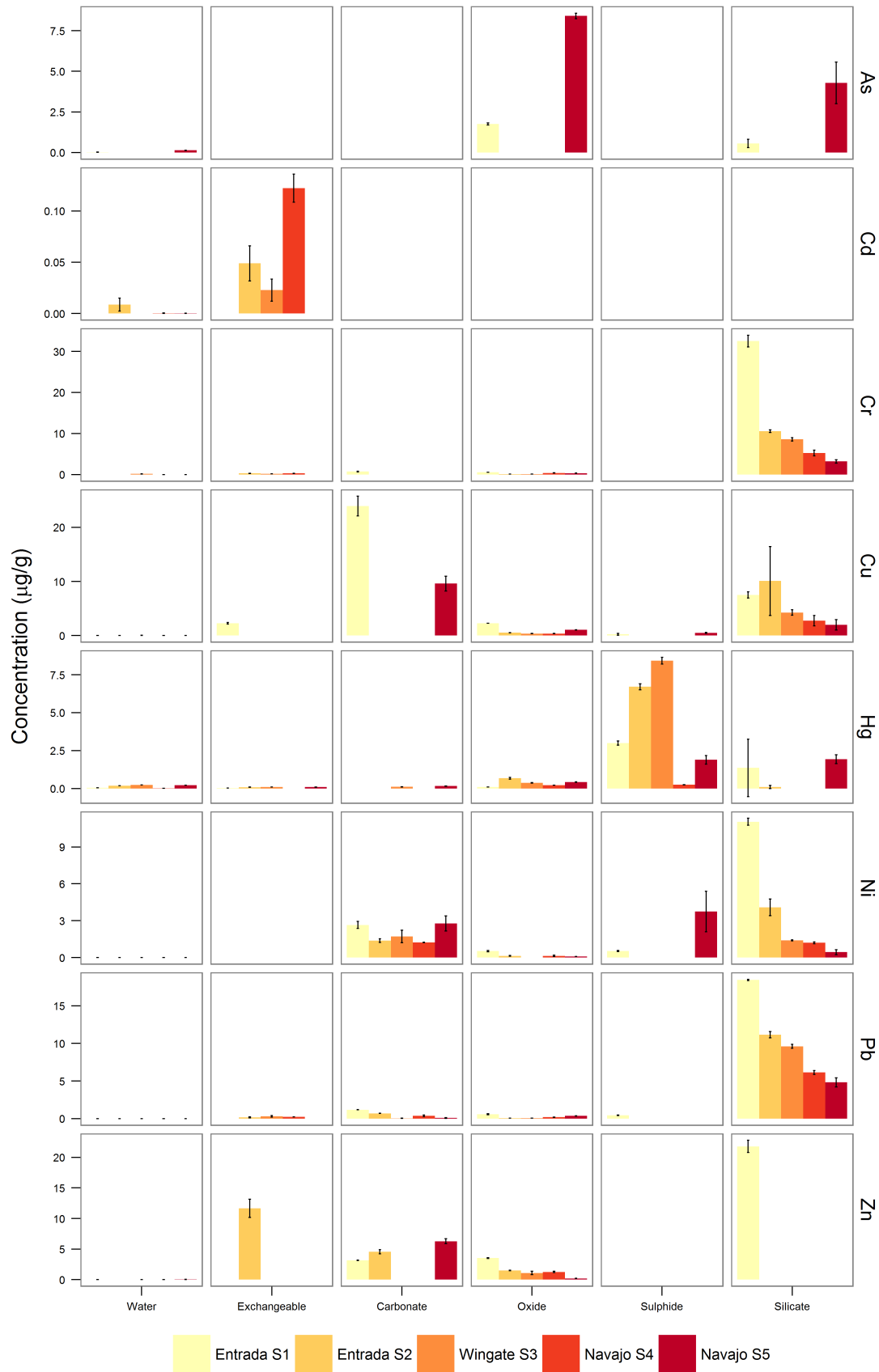
Figure 4.17: *Concentrations of trace metals for each of the 6 sequential extraction procedure (SEP) steps. Error bars are 1s.*

Concentrations overall are low, with the maximum value of any of the 8 trace metals being 32.5 ± 2.9 μg/g for Cr (*Entrada S1*). The mean concentration of these elements is < 5 μg/g and the median is < 1 μg/g.

The trace metals are distributed throughout the phases, although As, Cd, Cr, and Zn were not detected in the sulphide phase for any of the samples, Figure 4.17. Cadmium was only detected in the water soluble and exchangeable phases, with a maximum detected concentration of 0.12 ± 0.03 μg/g in the *Wingate S3* sample. Arsenic, likewise, was detected only for the *Entrada S1* and *Navajo S5* samples, in only 3 of the phases: water soluble, oxide and silicate, Figure 4.17.

The highest concentrations of Hg were detected in the sulphide phase of all 5 samples, with concentrations ranging from 0.25 ± 0.02 μg/g (*Navajo S4*) to 8.4 ± 0.5 μg/g (*Wingate S3*). Maximum concentrations of Cr (32.5 ± 2.9 μg/g), Ni (11.1 ± 0.6 μg/g), Pb (18.4 ± 0.2 μg/g) and Zn (21.8 ± 2.0 μg/g) are found in the *Entrada S1* sample, in the silicate phase. Lead concentrations for the other samples are also highest in this phase.

4.4.2 Mobile & immobile fractions

The general distributions of major elements in the Utah samples *S1 - S5* are very similar to those determined for *Captain*, *Cormorant* and *Thistle* (Chapter 3). The major elements Al, Ba, Fe and K tend to be present in greatest concentrations in oxides, sulphides and silicates, and in least concentrations in the water, exchangeable and carbonate steps, with Ca, Li, Mg and Mn displaying the opposite. The 8 trace metals of interest also tend to be in greatest concentrations in the oxide, sulphide and silicate steps, apart from Cd and Cu.

As discussed in Chapter 3, Kirsch *et al.* (2014) carried out SEP analysis on samples from Colorado, and classified the SEP steps into "mobile" and "immobile", based on susceptibility to leach metals during enhanced CO_2, low O_2 and short duration experimental conditions (similar to batch experiments described above). Metals capable of being leached by water, ion exchange and carbonate dissolution were classified as "mobile", while oxide, sulphide and silicate dissolution steps were classified as "immobile" (Kirsch *et al.*, 2014). This same classification was applied to the data collected for the Utah samples. Mobile and immobile fractions were calculated as a percentage for each element, Table 4.4 and Figure 4.18.

In Chapter 3, it was discussed that while one would expect conditions used by Kirsch *et al.* (2014) (enhanced CO_2, low O_2) to apply to a CO_2 storage reservoir, they are not necessarily representative of experimental conditions. To summarise that discussion, the mobile/immobile classification may not be ideal since: (i) the batch experiments conducted for this thesis were not low or free of oxygen so that, for example, pyrite present in trace quantities in the Utah samples could leach metals under weak CO_2 acid conditions in the experiments, despite being classified as immobile. Pyrite would be expected to remain relatively immobile (or indeed precipitate under reducing conditions) within a CO_2 storage reservoir where anoxic conditions prevail; (ii) silicate minerals such as feldspars can be readily 'weathered' with CO_2, therefore classifying all silicates (and associated elements) as being susceptible only to strong acid digestions is not necessarily accurate.

However, the mobile/immobile classification scheme does give some impression overall of how likely elements are to be leached, although caution needs to be exercised with regard to the calculated values attributed each to mobile and immobile categories.

Element	Entrada S1		Entrada S2		Wingate S3		Navajo S4		Navajo S5	
	Mobile (%)	Immobile (%)	Mobile (%)	Immobile (%)	Mobile (%)	Immobile (%)	Mobile (%)	Immobile (%)	Mobile (%)	Immobile (%)
Al	0.5	99.5	0.7	99.3	0.6	99.4	0.9	99.1	0.7	99.3
As	0.9	99.1	-	-	-	-	-	-	1.0	99.0
Ba	10.3	89.7	40.7	59.3	16.1	83.9	14.5	85.5	16.8	83.2
Ca	88.4	11.6	93.0	7.0	2.2	97.8	57.6	42.4	1.0	99.0
Cd	-	-	100	0	100	0	100	0	100	0
Cr	2.2	97.8	2.5	97.5	3.5	96.5	4.9	95.1	0.3	99.7
Cu	72.3	27.7	0.1	99.9	0.4	99.6	0.2	99.8	73.1	26.9
Fe	13.5	86.5	18.7	81.3	0.5	99.5	0.5	99.5	2.5	97.5
Hg	1.7	98.3	3.4	96.6	4.8	95.2	2.9	97.1	9.9	90.1
K	2.6	97.4	1.5	98.5	1.1	98.9	0.9	99.1	1.8	98.2
Li	59.5	40.5	67.4	32.6	56.9	43.1	100	0	100	0
Mg	58.9	41.1	78.4	21.6	33.0	67.0	14.2	85.8	8.6	91.4
Mn	69.1	30.9	83.2	16.8	6.4	93.6	28.8	71.2	5.9	94.1
Na	1.7	98.3	1.2	98.8	1.8	98.2	1.3	98.7	1.4	98.6
Ni	18.0	82.0	24.7	75.3	37.8	62.2	48.0	52.0	39.3	60.7
Pb	5.7	94.3	7.2	92.8	3.4	96.6	8.8	91.2	1.6	98.4
Ti	0	100	0	100	0	100	0	100	0	100
U	9.3	90.7	0.4	99.6	0	100	0.3	99.7	0	100
V	39.4	60.6	77.2	22.8	15.5	84.5	2.9	97.1	9.9	90.1
Zn	11.1	88.9	91.6	8.4	1.6	98.4	1.1	98.9	97.0	3.0

Table 4.4: *Calculated percentages of "mobile" and "immobile" elements, as per Kirsch et al. (2014), following analysis by a sequential extraction procedure. Data plotted in Figure 4.18.*

Figure 4.18: *Percentages of 16 elements classified as "mobile" and "immobile" as per Kirsch et al. (2014). Data in Table 4.4.*

Using this classification we can see that, for all samples, the majority of the 16 elements considered here were determined to be immobile under potential reservoir conditions of enhanced CO_2 and low O_2, Table 4.4 and Figure 4.18. The exceptions are as follows: Ca is mostly mobile in the two *Entrada* samples (88% and 90% mobile) and the *Navajo S4* sample (58%); Cd was detected as a mobile phase only, for all of the samples except *Entrada S1*; Cu was predominantly mobile in *Entrada S1* (72%) and *Navajo S5* (73%); Li was mostly mobile in all samples; Mg and Mn were found to be highly mobile in both *Entrada* samples, similar to Ca; and Zn was highly mobile in *Entrada S2* (92%) and *Navajo S5* (97%).

4.4.3 Comparing SEP data with batch experiments

The masses released from the batch experiments of the 16 elements considered for the SEP experiments can be calculated and normalised as concentrations per gram of sample ($\mu g/g$), to compare with the

whole rock and mobile concentrations to determine the extent of leaching under experimental conditions. The concentrations of elements released from the batch experiments, Table 4.5, were calculated by:

- Multiplying the concentration of each element (µg/L) by the volume removed for element analysis (L), for each time step sampled except the final

- Multiplying the final concentration of each element (µg/L) by the final volume remaining (L) at the end of the experiment

- Summing the calculated masses (µg) for all time steps, and dividing by the mass of samples used in the experiment (Methods, Table 2.6)

This calculation was carried out for the North Sea batch experiments, Chapter 3, with calculated batch data divided by control and $+CO_2$ conditions. In that case, the data was already present as the control and $+CO_2$ experiment flasks were run separately. In the case of the Utah experiments, the control and $+CO_2$ data was split at the point where CO_2 bubbling commenced. All data before this point was considered the control, and all data after was with $+CO_2$ conditions.

The results of the calculations for Utah samples *Entrada S1*, *Entrada S2*, *Wingate S3* and *Navajo S4* are given in Table 4.5, and visualised in Figures 4.19, 4.20, 4.21 and 4.22, respectively. Table 4.5 confirms the findings of the batch experiment concentrations (see Sections 4.3.2.1 and 4.3.2.2), insofar as recognising that the addition of CO_2 appears to increase the mass of elements released during all four Utah batch experiments for Ba, Ca, K, Li, Mg, Mn and Zn compared with the control period.

Other elements also display this behaviour of increased mass with $+CO_2$, albeit not consistently across all four samples: Cr (*S3*, *S4*), Cu (*S3*), Fe (*S2*, *S3*, *S4*), Hg (*S3*, *S4*), Ni (*S1*, *S3*, *S4*), Pb (*S1*, *S2*, *S4*). The remaining elements were generally either not detected in one or more batch experiments (e.g. As, Cd) or released masses were equal, such as for Ni (*S2*) and Pb (*S3*). The notable exception is Al, which was higher in the control part of all four experiments than with $+CO_2$, Table 4.5.

Comparing the leached concentrations of elements from the batch experiments (as µg per gram of sample, µg/g) with the bulk compositions for the 4 samples, one can see that leached concentrations are, for the most part, significantly less than the bulk concentrations (Figures 4.19, 4.20, 4.21 & 4.22). For the majority of elements, < 1% of bulk composition was mobilised during the 3 month durations of the control and $+CO_2$ batch experiments. In approximately half of these cases, < 0.01% was mobilised.

Leached Mg concentrations exceeded 1% of bulk Mg in the *Entrada S2* experiment with bubbled CO_2, and were between 10% and 50% of bulk Mg for *Wingate S3* and *Navajo S4* control and $+CO_2$ experiments, Table 4.5. Calcium concentrations for both control and $+CO_2$ were between 20% and 25% of bulk Ca for *Wingate S3*, and a little over 5% for *Navajo S4*, although there is high uncertainty on the *Wingate S3* bulk Ca concentration, Figure 4.21.

Leached concentrations of Li are also high, compared with bulk Li, with concentrations between 18% and 48% of bulk composition for the two *Entrada* experiments, Table 4.5. However, Li concentrations leached during both control and $+CO_2$ experiments for the *Wingate S3* and *Navajo S4* samples were calculated to be 450 - 550% and 3,000 - 5,000% higher than the bulk composition of *Wingate S3* and *Navajo S4*, respectively. These extremely large differences could be due to significant sample heterogeneity which affects only Li (since no other element displayed this discrepancy), or an error in sample analysis.

The comparison between the bulk analysis and the sum of the SEP steps for the *Wingate S3* and *Navajo S4* samples, Figure 4.15, shows good agreement for Li and so it is unlikely that the sum of the SEP steps is incorrect and underestimating bulk concentrations.

| | Entrada S1 | | | | | | | | Entrada S2 | | | | | | | |
| | Bulk | | Mobile | | Control | | +CO$_2$ | | Bulk | | Mobile | | Control | | +CO$_2$ | |
Element	µg/g	±	µg/g	±	µg/g	±	µg/g	±	µg/g	±	µg/g	±	µg/g	±	µg/g	±
Al	30,000	6,000	142	9	0.07	0.02	0.06	0.02	22,000	7,000	165	14	0.08	0.03	0.07	0.02
As	2.3	0.6	0.02	0.006	-	-	-	-	-	-	-	-	-	-	-	-
Ba	180	20	18.7	0.9	0.0024	0.0002	0.014	0.001	410	40	166	6	0.0031	0.0003	0.013	0.001
Ca	31,000	2,000	27,000	2,000	126	26	164	33	28,000	1,000	26,000	1,000	130	30	150	30
Cd	-	-	-	-	-	-	-	-	0.06	0.05	0.06	0.05	0.0001	0	-	-
Cr	34	3	0.7	0.2	0.0003	0	0.0002	0	11	0.7	0.28	0.03	0.0004	0	0.0001	0
Cu	36	5	26	4	0.002	0	0.004	0.0001	11	13	0.01	0.01	0.0034	0.0002	0.0023	0.0001
Fe	12,000	700	1,650	80	0.006	0.002	0.005	0.001	7,000	200	1310	14	0.003	0.001	0.01	0.004
Hg	4.5	4	0.08	0.01	-	-	0.00003	0	7.7	0.7	0.26	0.01	0.0001	0	0.0003	0
K	19,000	3,000	490	11	81	30	130	50	17,000	1,000	248	15	80	30	130	50
Li	2.7	0.3	1.6	0.2	0.8	0.6	1.3	1	4.5	0.4	3.1	0.3	0.8	0.6	1.3	1
Mg	13,000	1,500	7,700	300	70	8	118	13	8,800	1,000	6,900	30	65	7	100	10
Mn	300	20	205	9	0.073	0.007	0.18	0.02	215	8	179	5	0.01	0.009	0.14	0.01
Ni	15	1	2.7	0.6	-	-	0.0005	0.0001	5.6	1.7	1.4	0.3	0.0002	0	0.0002	0
Pb	20.6	0.4	1.18	0.05	0.0001	0	0.0002	0	12	1	0.87	0.18	0.0001	0	0.0003	0
Zn	28	2	3.2	0.1	0.008	0.003	0.014	0.005	18	3	16	4	0.009	0.003	0.01	0.003

| | Wingate S3 | | | | | | | | Navajo S4 | | | | | | | |
| | Bulk | | Mobile | | Control | | +CO$_2$ | | Bulk | | Mobile | | Control | | +CO$_2$ | |
Element	µg/g	±	µg/g	±	µg/g	±	µg/g	±	µg/g	±	µg/g	±	µg/g	±	µg/g	±
Al	21,000	6,000	124	14	0.08	0.03	0.07	0.02	18,000	4,000	158	8	0.08	0.03	0.06	0.02
As	-	-	-	-	-	-	-	-	-	-	-	-	-	-	-	-
Ba	310	50	50	2	0.0024	0.0002	0.017	0.001	290	75	42	6	0.009	0.001	0.038	0.003
Ca	600	700	8.9	0.6	120	25	145	30	2,400	550	1,350	100	130	30	140	30
Cd	0.02	0.02	0.02	0.02	-	-	-	-	0.12	0.03	0.12	0.03	-	-	-	-
Cr	9	0.9	0.32	0.02	0.00007	0.00001	0.0002	0	6	2	0.3	0.09	0.0002	0	0.0003	0
Cu	5	1	0.02	0.05	0.002	0	0.0044	0.0002	3	2	0.005	0.003	0.0026	0.0001	0.0017	0.0001
Fe	1,300	75	6.7	0.2	0.002	0.001	0.007	0.002	2,400	200	13	1	0.003	0.001	0.01	0.004
Hg	9.2	0.5	0.44	0.03	-	-	0.0001	0	0.47	0.02	0.014	0.001	-	-	0.0001	0
K	17,400	500	195	16	80	30	130	50	16,000	2,000	154	3	80	30	130	50
Li	0.18	0.03	0.103	0.007	0.8	-0.6	1	-1	0.026	0.003	0.026	0.003	0.8	-0.6	1.3	-0.9
Mg	210	40	108	8	60	7	100	10	570	10	60	6	62	7	100	10
Mn	6.4	0.3	0.4	0.04	0.11	0.01	0.12	0.01	34	2	9.8	0.4	0.11	0.01	0.25	0.02
Ni	3	1	1.7	1	0.0003	0	0.0004	0	2.6	0.3	1.24	0.03	-	-	0.0011	0.0001
Pb	10	1	0.3	0.2	0.0002	0	0.0002	0	6.9	0.8	0.6	0.2	-	-	0.0001	0
Zn	1.1	0.5	0.02	0.01	0.008	0.002	0.018	0.006	1.3	0.2	0.013	0.001	0.008	0.003	0.012	0.004

Table 4.5: *Concentrations of elements analysed by ICP-MS for bulk analysis, calculated mobile fraction, and control and +CO$_2$ portions of batch experiments, for samples S1 - S4. Uncertainties are 2s. Data plotted in Figures 4.19, 4.20, 4.21 & 4.22.*
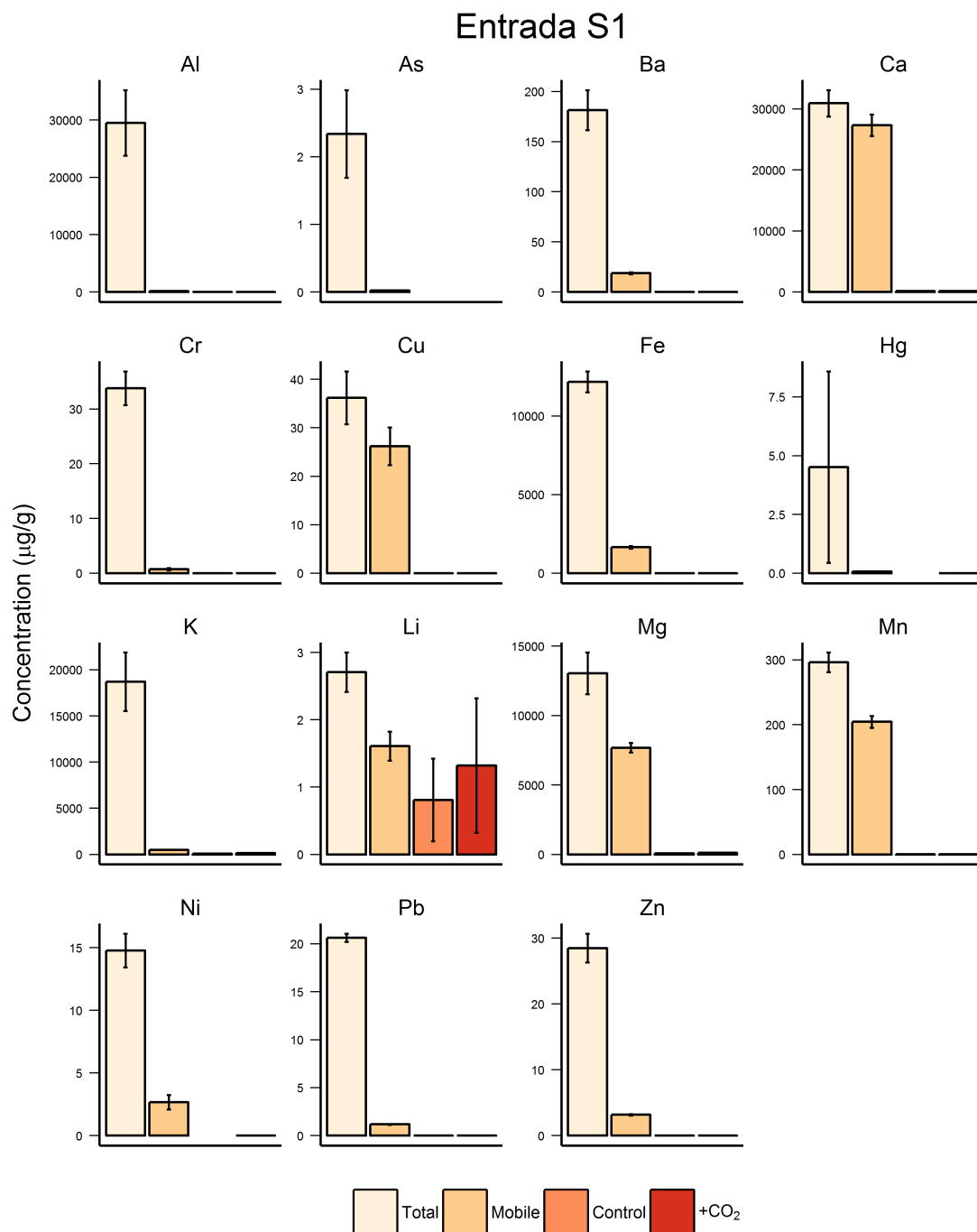
Figure 4.19: *Concentrations of 15 elements leached from Entrada S1 sample during Control (Days 0 - 82) and +CO₂ (Days 82 - 163) batch experiments, compared with the mobile fractions determined by the sequential extraction procedure (SEP), and the sum of the (SEP) steps representing bulk concentrations. Error bars are 2s. Data in Table 4.5.*

There is likewise little to suggest that the batch experiment analysis for Li was flawed just for those samples, since the concentration data is consistent with each other for all four samples, and not, for example, significantly higher for *Wingate S3* and *Navajo S4*. Since concentrations are so similar for each of the four samples, and that only Li appears to be affected, it is unlikely that sample heterogeneity is a main cause. It is, however, more likely that the high background Li concentration in the *Crystal Geyser* spring water used in the experiments (Table 4.2) is the source of the majority Li mass calculated,

particularly in the control stage. The difference in abundance of Li between the four samples used, as determined by the SEP (Figure 4.16), has little measurable effect on dissolved Li, compared with the already significant concentrations in the spring waters.

Next, one can compare element concentrations mobilised during the batch experiments with just the mobile fraction, rather than the bulk composition. Again, the percentages of the mobile fraction which
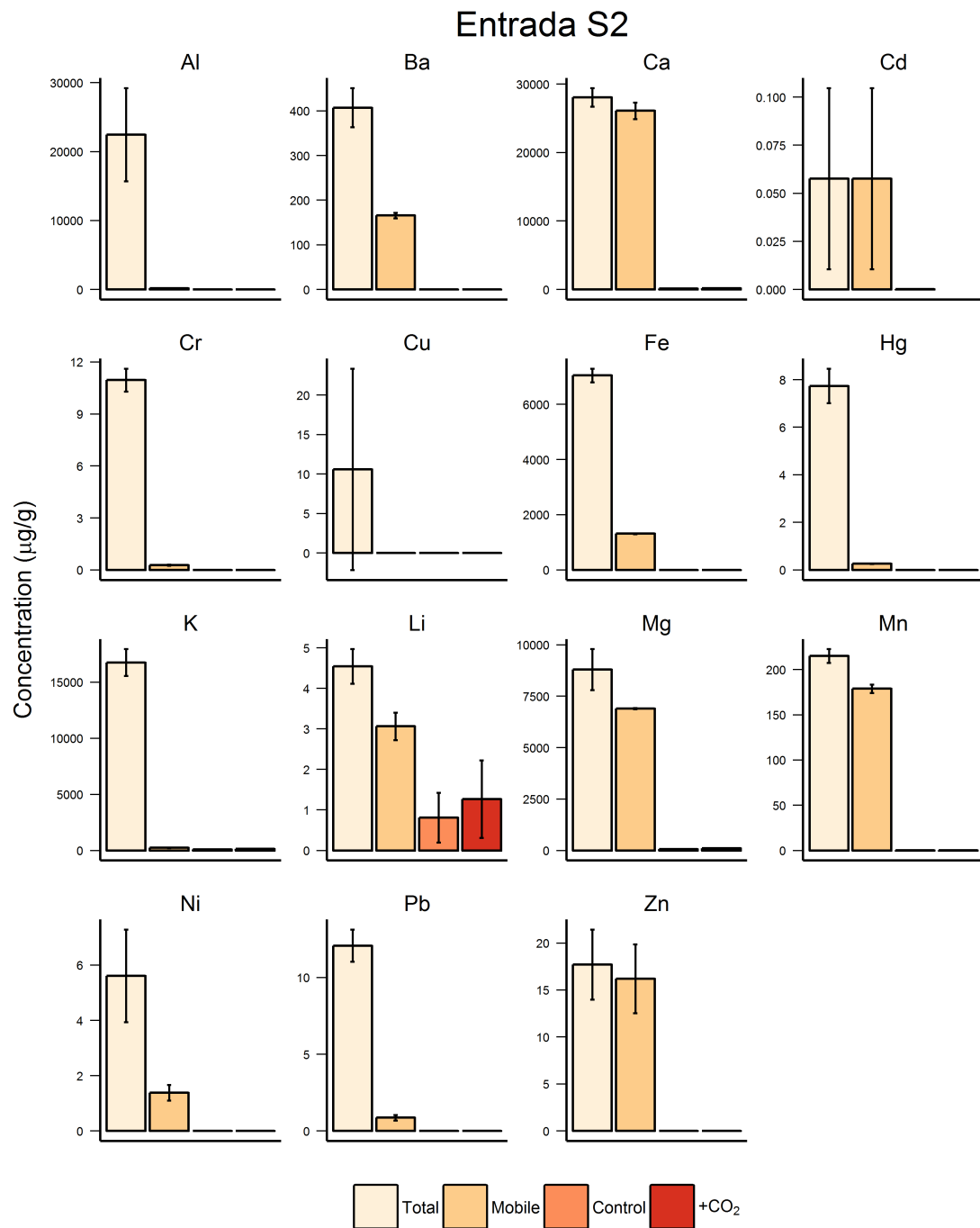
Figure 4.20: *Concentrations of 15 elements leached from Entrada S2 sample during Control (Days 0 - 82) and +CO$_2$ (Days 82 - 163) batch experiments, compared with the mobile fractions determined by the sequential extraction procedure (SEP), and the sum of the (SEP) steps representing bulk concentrations. Error bars are 2s. Data in Table 4.5.*

are apparently mobilised during both control and batch experiments are very low (< 1%) for all four samples, and for the majority of elements, Table 4.5 and Figures 4.19, 4.20, 4.21 and 4.22. Lithium data, again, appears to be skewed by the high spring water concentration relative to the composition in the sample rocks, as previously explained.

Data for Ca indicates that, where Ca is highly mobile and in large concentrations (*Entrada S1* and
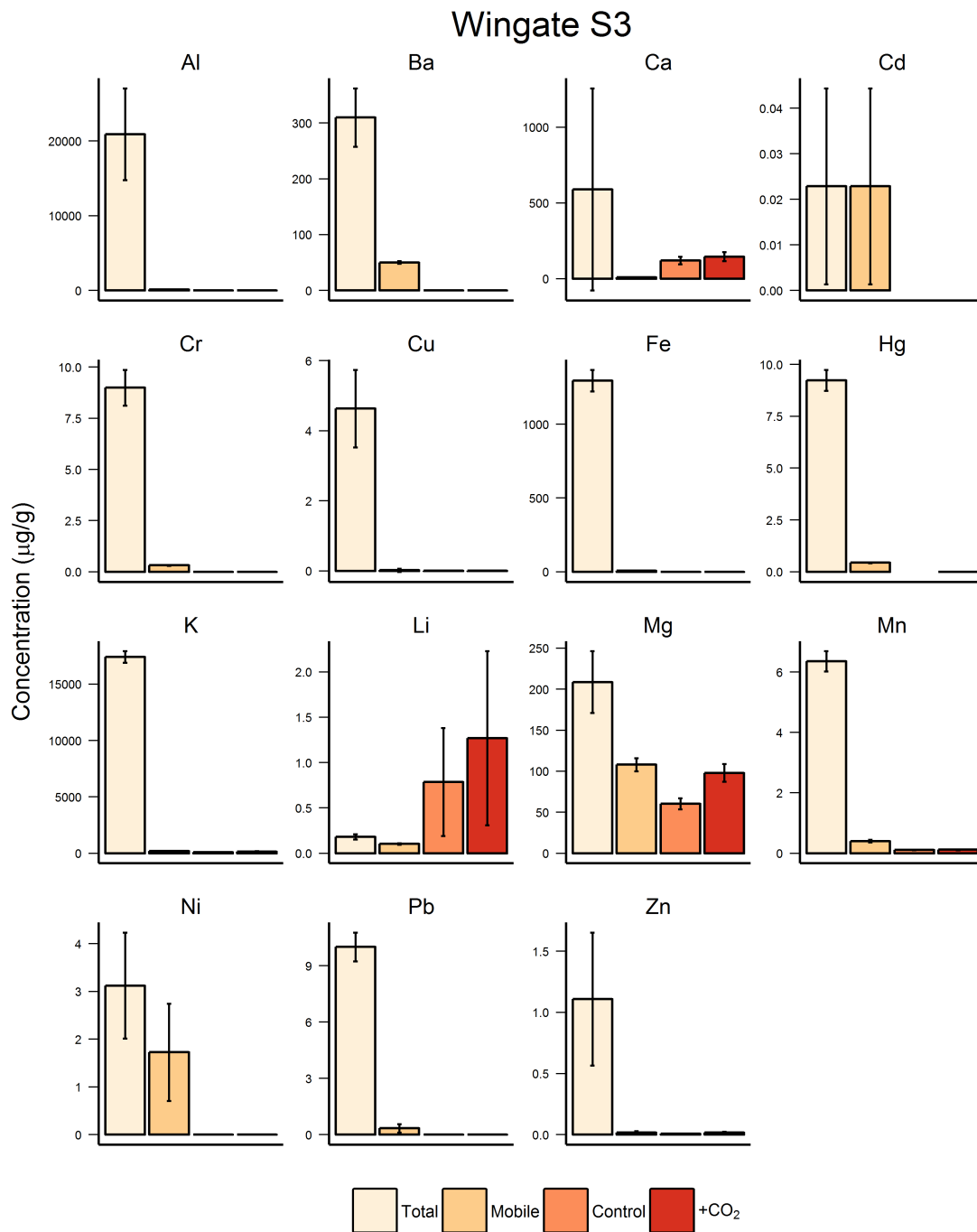
Figure 4.21: *Concentrations of 15 elements leached from Wingate S3 sample during Control (Days 0 - 82) and +CO₂ (Days 82 - 163) batch experiments, compared with the mobile fractions determined by the sequential extraction procedure (SEP), and the sum of the (SEP) steps representing bulk concentrations. Error bars are 2s. Data in Table 4.5.*

S2), that the overall percentage mobilised is low, however where Ca bulk and mobile concentrations are lowest (*Wingate S3* and *Navajo S4*), then the mobilised concentrations are higher as a proportion. In the case of *Wingate S3*, mobilised Ca is > 1,000% of the mobile fraction, while Ca mobilised from *Navajo S4* is ~ 10% for both control and $+CO_2$, Table 4.5.

Mobilised Cu and K constitute a significant percentage of the mobile fractions for the four samples,
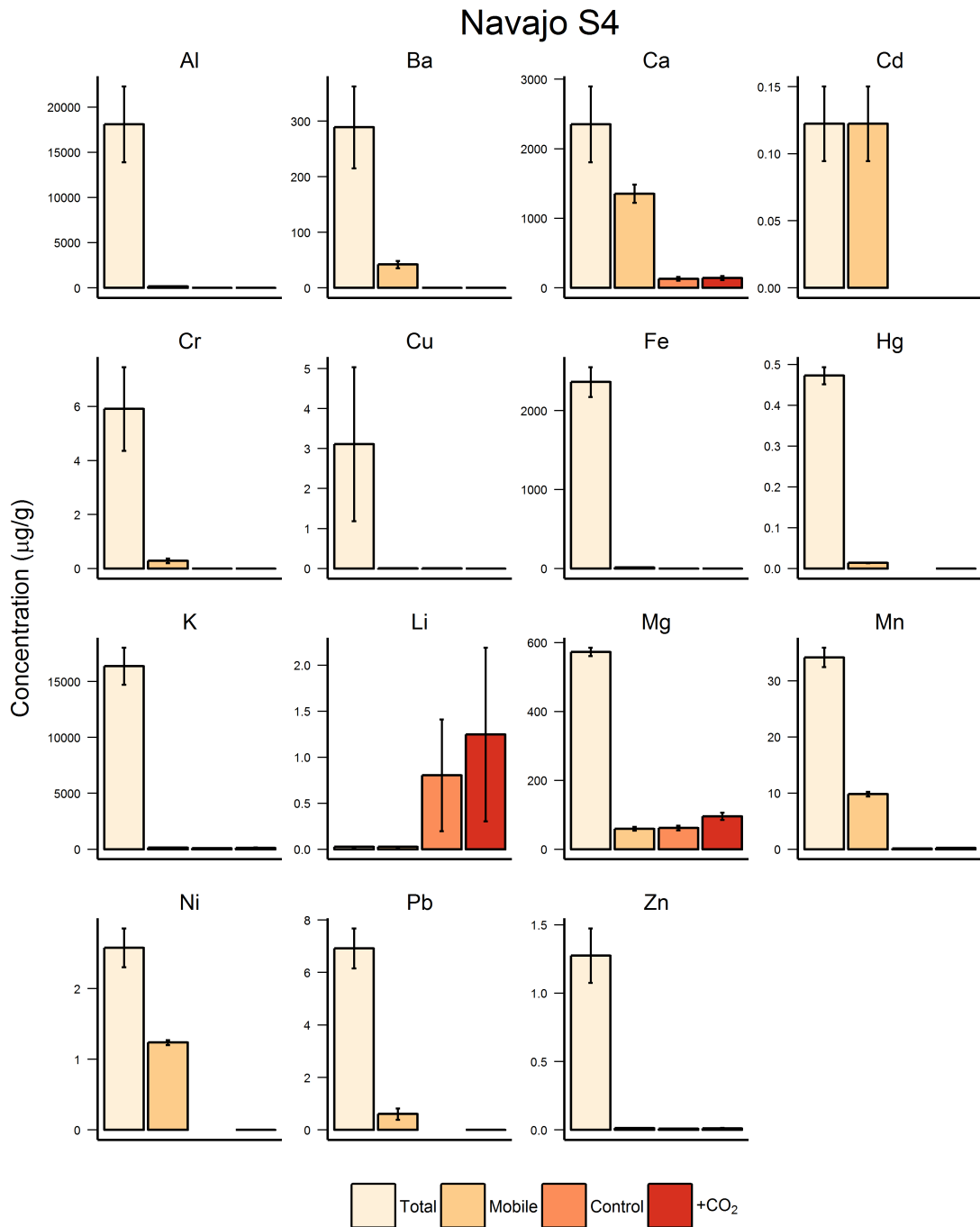
Figure 4.22: *Concentrations of 15 elements leached from Navajo S4 sample during Control (Days 0 - 82) and $+CO_2$ (Days 82 - 163) batch experiments, compared with the mobile fractions determined by the sequential extraction procedure (SEP), and the sum of the (SEP) steps representing bulk concentrations. Error bars are 2s. Data in Table 4.5.*

ranging from 10% (Cu, *Wingate S3* control) to 84% (K, *Navajo S4* +CO$_2$), with medians of 22.5% and 52% for Cu and K, respectively, across control and +CO$_2$ experiments.

Magnesium is mobilised at $\sim$ 1.5% for both *Entrada* +CO$_2$ experiments, but increases to 93% and 170% for *Wingate S3* +CO$_2$ and *Navajo S4* +CO$_2$ experiments, respectively. Similar masses of Mg are being mobilised from the *Wingate* and *Navajo* samples compared with the *Entrada* samples, however the *Entrada* samples contain an order of magnitude more Mg than the *Wingate* and *Navajo* samples. The amount of Mg leached is comparable, but overall comprises a much larger proportion of these samples. Finally, Zn is also leached in similar quantities across all four batch experiments, but again is present in much lower concentrations in *Wingate S3* and *Navajo S4*. As a percentage, therefore, of the mobile fraction Zn is high at 90% and 92%, respectively, for *Wingate S3* and *Navajo S4* +CO$_2$ experiments, Table 4.5. As with Li, it is likely that the concentrations present within the *Crystal Geyser* spring water sample used in the experiments are contributing more to the calculated released masses, than actual dissolution of vulnerable minerals, especially given the similarities in experiment concentration trends (see Figures 4.10 and 4.13).

4.5 Discussion

4.5.1 Field data

A significant amount of literature is now available on the geochemistry of spring waters in the Green River area of Utah, as it has been researched as a natural analogue for CO_2 storage by various authors. Papers reviewed for this thesis included Busch *et al.* (2014); Dockrill and Shipton (2010); Haszeldine *et al.* (2005); Heath *et al.* (2009); Kampman *et al.* (2009, 2014, 2012); Purser *et al.* (2014); Shipton *et al.* (2004); Wigley *et al.* (2013a,b, 2012) and Wilkinson *et al.* (2009). The aim of the field sampling undertaken in Utah for this thesis was not to replicate the work carried out by others, but to analyse collected samples for a specific set of metals relevant to this thesis, and to collect rock samples to be used in batch experiments. The set of metals of interest are the 8 trace metals referred to throughout this thesis: As, Cd, Cr, Cu, Hg, Ni, Pb and Zn. Data were not available in the literature for the majority of these elements in solution from natural waters at Green River. The concentrations of the 8 trace metals were given previously in Table 4.2, but are summarised here for ease of reference in Table 4.6. Major element data were, however, also collected for this study (e.g. Ca, Mg, K, Sr), and are used here mainly as a comparison with those collected by other authors.

Concentration data for Ca^{2+}, K^+, Mg^{2+}, Na^+, Cl^-, SO_4^{2-} and alkalinity (CO_3^{2-} + HCO_3^-) was collected from the literature, where available, for the Green River springs. Data from Heath *et al.* (2009); Kampman *et al.* (2009, 2014) and Shipton *et al.* (2004) were plotted with the ion chromatography (IC) and field data from this study on a Piper diagram for each of the springs, Figure 4.23. Heath *et al.* (2009) did not provide SO_4^{2-} data, therefore it was calculated from the S_{total} value given in their Table 1, assuming SO_4^{2-} is the dominant species. Data from *Side Seep* for this study was not included as alkalinity was not measured for that spring.

Piper diagrams are a useful way of determining differences between groundwater samples. Concentrations of anions and cations are plotted as a percentage of overall concentrations. Figure 4.23 shows that, for most of the springs, concentrations of Ca^{2+}, K^+, Mg^{2+}, Na^+, Cl^-, SO_4^{2-} and alkalinity are essentially the same across the entire literature sampling period (~ 15 years). This would appear to show little evolution of groundwaters during this time, although this is a geologically insignificant period and so this would be expected, without some recent external influence or seasonal variation.

	As µg/L	±	Cd µg/L	±	Cr µg/L	±	Cu µg/L	±	Hg§ µg/L	±	Ni µg/L	±	Pb µg/L	±	Zn µg/L	±
Airport Well	8.63	0.62	<0.03	-	<0.28	-	<0.07	-	<0.02	-	7.41	0.28	<0.04	-	6.66	0.26
Crystal Geyser	38.9	7.1	<0.03	-	<0.28	-	13.5	2.8	<0.02	-	8.13	0.62	<0.04	-	<0.19	-
Little Bubbling Spring	38.3	5.5	<0.03	-	<0.28	-	36.5	0.7	<0.02	-	11.6	1.5	<0.04	-	30.2	1.4
Big Bubbling Spring	55.4	7.4	<0.03	-	<0.28	-	24.5	1.6	<0.02	-	7.43	0.97	<0.04	-	<0.19	-
Side Seep	<0.63	-	<0.03	-	<0.28	-	21.2	1.2	<0.02	-	4.36	0.55	<0.04	-	<0.19	-
Tenmile Geyser	13.3	2.4	<0.03	-	<0.28	-	31.3	0.9	<0.02	-	8.96	1.27	<0.04	-	15.4	9.9
Pseudo-Tenmile Geyser	59.8	7.0	<0.03	-	<0.28	-	26.2	0.9	<0.02	-	6.36	0.72	<0.04	-	<0.19	-
Torrey's Spring	56.2	11.2	<0.03	-	<0.28	-	40.0	3.1	<0.02	-	8.24	0.74	<0.04	-	<0.19	-
Tumbleweed Geyser	17.5	2.6	<0.03	-	<0.28	-	24.4	1.4	<0.02	-	8.61	0.85	<0.04	-	37.0	7.1
Champagne Geyser	6.59	2.13	<0.03	-	<0.28	-	25.6	2.0	<0.02	-	11.7	0.9	<0.04	-	-	-

Table 4.6: *Concentrations of 8 trace metals at Utah spring locations, obtained by ICP-MS and IC at the University of Texas. < concentrations below detection limit value given. Uncertainties are 1s. §Hg analysed by ICP-MS at University of Edinburgh.*

The *Green River Airport Well* plots separately to the other
springs, being proportionally higher in Ca^{2+} and sulphate, and lower in Na^+ and Cl^-. From Figure 4.25a, and conclusions in the literature (Kampman *et al.*, 2009, 2012; Wigley *et al.*, 2013a), the *Green River Airport Well* is less saline than the other local springs, and therefore has had less deep brine input to mix with groundwaters replenished from meteoric recharge through the *Entrada* formation (Wilkinson *et al.*, 2009). Since the *Green River Airport Well* is located closer to the area of recharge - the San Rafael Swell - it would be expected to be fresher and less affected by deep fluids migrating through the Little Grand and Salt Wash faults at Green River (Kampman *et al.*, 2009; Shipton *et al.*, 2004).
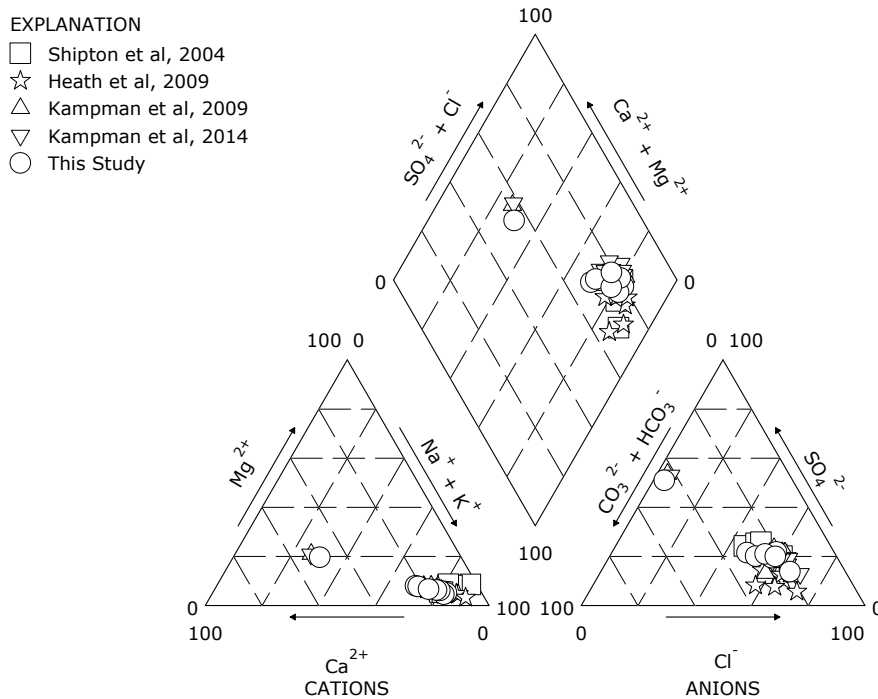
Figure 4.23: *Piper diagram of Utah spring water data using data from the literature (Heath* et al., *2009; Kampman* et al., *2009, 2014; Shipton* et al., *2004) and this study.*

Concentrations of other commonly analysed constituents (Ba, Fe, Mn and Sr) were also compared between the literature (Heath *et al.*, 2009; Kampman *et al.*, 2009, 2014; Shipton *et al.*, 2004) and this study, Figure 4.24. This box-and-whisker plot of Green River spring data for the 5 studies shows that there can indeed be some large difference in absolute fluid compositions with time, despite the relative proportions of major constituents remaining fairly stable, Figure 4.23. The three most recent studies (Kampman *et al.* 2009, 2014; this study) are fairly consistent, based on the box-and-whisker representation of median, 50 [th] percentile and outlier data for Mn and Sr data, with Shipton *et al.* (2004) and Heath *et al.* (2009) data lying within the same broad ranges. Barium values, where detected for the three most recent studies, are likewise quite similar, although were not detected for the earlier studies. Aluminium concentrations were also not detected by Shipton *et al.* (2004), Heath *et al.* (2009), or this study whereas Kampman *et al.* (2009) and Kampman *et al.* (2014) give detected Al values of 87 - 135 µg/L and 116 - 156 µg/L, respectively.

Concentrations of Fe vary greatly, with the same sampling locations having highly variable Fe content between each round of sampling. The highest concentrations were detected for Kampman *et al.* (2014) at *Champagne Geyser* (14.9 mg/L) and at *Little Bubbling Spring* (14.8 mg/L) for this study. These naturally occurring concentrations are similar to experimentally-leached Fe^{2+} concentrations by Purser *et al.* (2014)
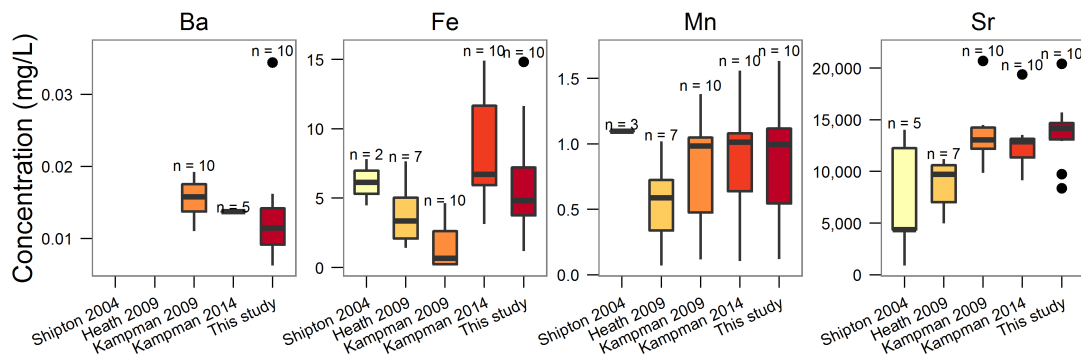
Figure 4.24: *Box-and-whisker plot comparison of Ba, Fe, Mn and Sr concentrations for published Green River spring data from Heath* et al. *(2009); Kampman* et al. *(2009, 2014) and Shipton* et al. *(2004) with this study. Box shows median, lower and upper quartiles (interquartile range, IQR). Whiskers are 1.5×IQR. Circles are outlier values > 1.5×IQR. Number of samples (n) given above each plot.*

of up to 15 mg/L, using an H_2S-equivalent reductant (thioacetamide) with CO_2. Using CO_2 with CH_4, a maximum of 3 mg/L Fe^{2+} was achieved, and < 1 mg/L for using only CO_2 (Purser *et al.* 2014, their Figure 3), which is consistent with low concentrations obtained with the experiments for this study. Significant differences in Fe concentrations between sampling regimes may therefore indicate changes in reducing conditions in the Entrada formation with time.

Evidence for deep brine migration, and the increasing influence thereof towards the fault zone at Green River, is the relationship between Cl^-, a conservative tracer, and Na^+ where concentrations are dominated by the input of very saline fluids (184,000 mg/L total dissolved solids, Spangler 1992). Sodium and Cl data from the Green River springs collected for this study fit well with the published literature, Figure 4.25a, and follow the same linear relationship on a mixing line between surface waters (Mayo *et al.*, 2003) and Ismay Brine (Spangler, 1992) concentrations, Figure 4.25b. *Green River Airport Well* con-
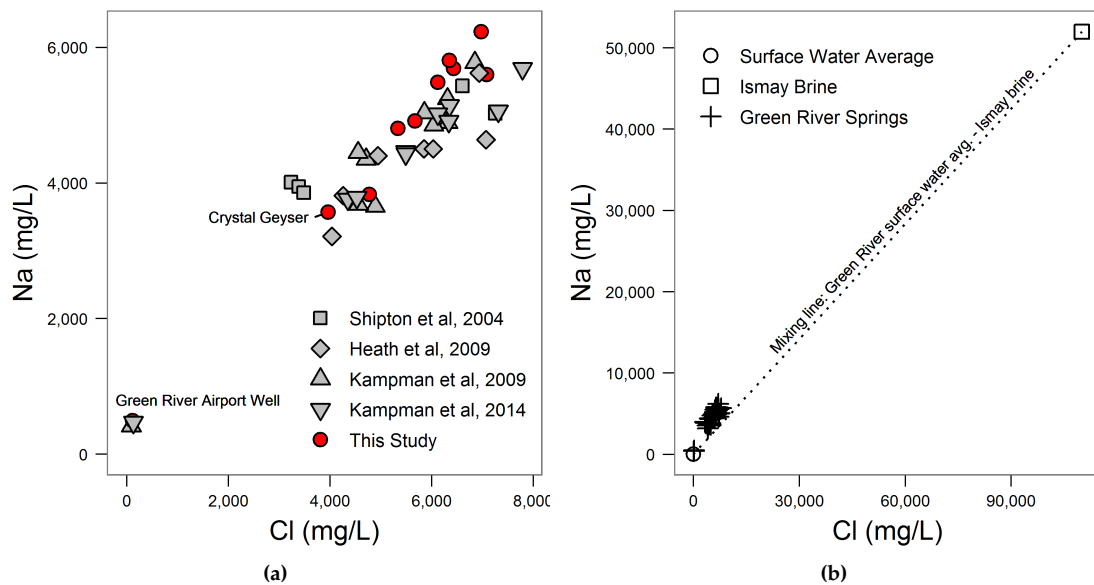
Figure 4.25: *Na and Cl concentration data: (a) Green River spring data from Heath* et al. *(2009); Kampman* et al. *(2009, 2014) and Shipton* et al. *(2004), and this study. The Green River Airport Well data for the Kampman studies and this study are labelled, as well as the Crystal Geyser data for this study (b) Green River spring data plotted with average surface water NaCl data from Mayo* et al. *(2003) and Ismay Brine data from Spangler (1992).*

157

centrations are closest to surface water values and NaCl concentrations increasing with distance away from this point, showing also that this spring is closest to the area of meteoric recharge, as noted above.

While not possible for the experimental data, here a test can be made for whether carbonate dissolution is contributing to concentrations of Ca, Mg and alkalinity in the Green River springs. In Chapter 3 (North Sea), one of the tests for carbonate dissolution was to plot Ca^{2+} and Mg^{2+} equivalent concentrations (meq/L) against HCO_3^- (meq/L), with a 1:1 relationship representative of a stoichiometric relationship between the cations and anion indicative of carbonate dissolution (Stallard and Edmond, 1983). This was repeated for the Green River springs data, with equivalent concentrations calculated for this study, and plotted with those obtained and calculated from the literature (Heath *et al.* 2009; Kampman *et al.* 2009, 2014 and Shipton *et al.* 2004), Figure 4.26. The 1:1 stoichiometric relationship line is plotted for comparison.
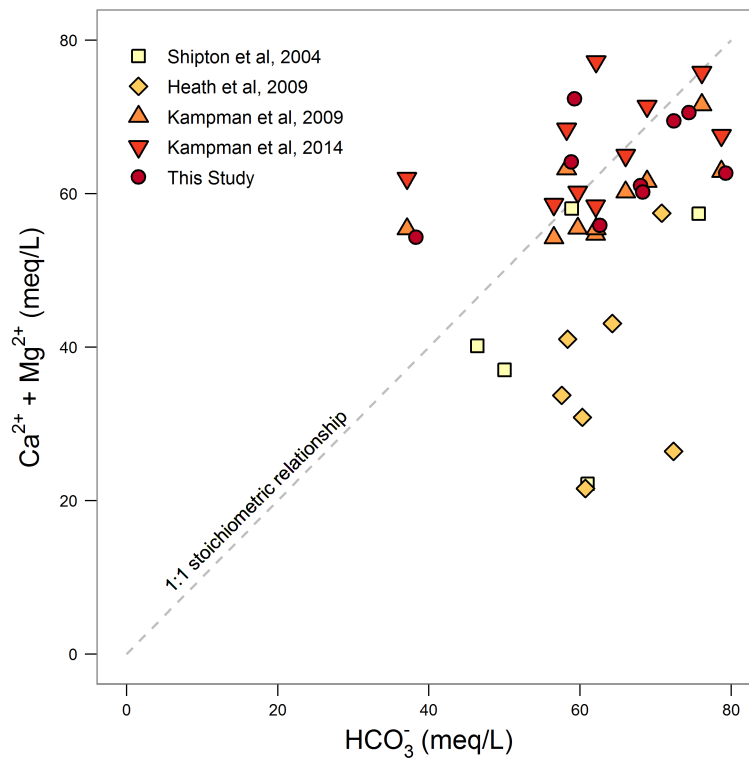
Figure 4.26: *Crossplot of (Ca^{2+} +[Mg^{2+}) milliequivalent concentrations (meq/L) against HCO_3^- meq/L for Green River spring data from this study, and Heath* et al. *(2009); Kampman* et al. *(2009, 2014); Shipton* et al. *(2004).*

The data from Heath *et al.* (2009) and Shipton *et al.* (2004) clearly do not fit the 1:1 trend. The Kampman studies and this study's data cluster around the 1:1 relationship, Figure 4.26, and display a quasi-linear relationship. However, this relationship is unlike those seen with some of the North Sea batch experiments (e.g. *Captain*, Figure 3.37). The clustering is similar to that for the *Field X* North Sea data; the conclusion therefore is that carbonate dissolution is occurring, however this is not the sole supply of Ca^{2+}, Mg^{2+} and HCO_3^- to the groundwaters. This fits with the conclusions drawn separately by others (e.g. Kampman *et al.* 2009) that there is some dissolution of carbonate minerals together with minerals such as K-feldspars.

Trace metal concentrations, where detected in the Green River springs, correlate poorly with the major elements in most cases (Figure D.7, Appendix D). While Pearson's correlation coefficients for a number of element pairs are indicative of strong relationships, further examination shows that these are often skewed by high and low values. Only Ca and Ni show a strong positive linear correlation, Figure 4.27. Nickel concentrations may therefore be related to carbonate dissolution, however this is not clear.

The presence of trace metals in Green River spring waters cannot be conclusively linked to K-feldspar and carbonate dissolution, unlike the major elements.
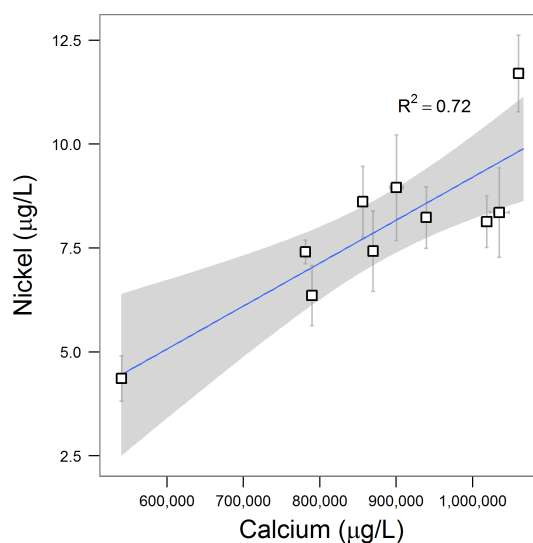
Figure 4.27: *Plot of Ca vs Ni concentrations in Green River spring waters. Error bars are 2s.*

Trace metal concentrations could be the result of other mineral dissolutions. Using bulk chemistry of cored transects across white 'bleached' *Entrada* sandstones to 'unbleached' red Entrada sandstones, Wigley *et al.* (2012) speculated that trace metals (such as Cu, Ni, Zn) are in fact mobilised from Fe-oxide grain coatings and re-deposited at the reaction front, limiting their overall mobility in the migrating fluids. Iron oxide grain coating dissolution in the *Entrada* formation is most plausibly the result of a reducing mobile fluid, and not simply a CO_2 plume, with minor H_2S or CH_4 incorporation (Busch *et al.*, 2014; Haszeldine *et al.*, 2005; Kampman *et al.*, 2014; Purser *et al.*, 2014; Wigley *et al.*, 2012). Iron concentrations, however, do not correlate with any of the trace elements detected in the spring waters collected for the this study ($R^2 < 0.25$ in all cases), with no fluid trace element data available from the literature for comparison.

Trace metals may have therefore been mobilised and re-deposited within the aquifer, as demonstrated by Wigley *et al.* (2012), or bulk trace metal concentrations are low in the *Entrada* formation to begin with, Table 4.7. Overall, trace metal concentrations are low in water samples from 10 CO_2-driven springs in the Green River area of Utah, and where present, their source or sources are uncertain.

Element	Entrada S1	Entrada S2	Wingate S3	Navajo S4	Navajo S5
			μg/g		
As	3.94	< 0.40	< 0.40	< 0.40	19.7
Cd	< 0.007	< 0.007	< 0.007	< 0.007	< 0.007
Cr	37.3	11.7	9.98	8.20	4.45
Cu	9.73	4.25	4.71	2.44	4.02
Hg	1.28	3.26	3.85	0.13	4.07
Ni	12.4	4.47	1.57	1.53	0.70
Pb	19.0	10.5	9.51	6.53	5.38
Zn	30.9	15.7	< 1.9	2.51	< 1.9

Table 4.7: *Bulk Utah sandstone trace element concentrations*

4.5.2 Batch experiments (pH)

Clear trends are apparent in the batch experiment data, using rock and spring water samples collected in Utah. Recorded batch experiment pH values rose from ~ pH 6.8 to ~ pH 8.9 prior to bubbling CO_2, before stabilising at ~ pH 6.35 soon after commencement of CO_2 bubbling, Figure 4.7. The range of recorded pH values for the San Rafael desert springs is 6.3 - 6.8, Table 4.1.

The results show that without the addition of CO_2 to the experiments, pH values rise in a linear fashion over a 3 month reaction period by ~ 2 pH units from the field-measured spring waters' values. Upon commencement of CO_2 bubbling, pH drops immediately by around 3 pH units before recovering within 12 hours to steady values at the lower end of the spring waters' pH range, Figure 4.8.

The pH trend prior to the addition of CO_2 is most likely indicative of minor mineral dissolution. The rise in pH shows that H^+ (proton) activity is decreasing, and therefore protons are being consumed during dissolution, as previously discussed in Section 3.10.1 of Chapter 3 (North Sea chapter). Without a supply of protons to offset the consumption during mineral dissolution, pH continues to rise over the course of the initial 3 month batch reaction period. However, once CO_2 bubbling begins, the dissociation of H_2CO_3 as per equations 1.1, 1.2 and 1.3 in Chapter 1 (Introduction) provides a supply of H^+ to the system, which is sufficient initially to counteract the depletion by dissolution and to reduce pH. It then takes only a matter of hours for the system to equilibrate between mineral dissolution and proton supply, resulting in a level pH trend for the second 3 month reaction period.

Inputting the geochemical data for *Crystal Geyser* spring waters (Table 4.2) into PHREEQC v3.3.3.10424, theoretical equilibrium pH values can be calculated for before and after the addition of CO_2 to the batch experiment, assuming only the most reactive minerals species - carbonates, Table 4.3 - are interacting with the *Crystal Geyser* waters in the experiment. Using CO_2 partial pressures of 1 bar (400 ppm CO_2) and 1.4 bar for pre-CO_2 and +CO_2 conditions, respectively, the model calculates equilibrium pH values of 8.43 - 8.73 and 6.22 - 6.29, Table 4.8.

	Initial flask pH	Final flask pH	Modelled pH
Pre-CO_2 bubbling	6.82 - 7.05	8.77 - 9.03	8.43 - 8.73
CO_2 bubbling	6.09 - 6.21	6.38 - 6.47	6.22 - 6.29
Field pH		6.31 - 6.80	

Table 4.8: *Comparing batch experiment pH values with field pH values, and PHREEQC v3.3.3.10424 modelled pH using the fluid geochemistry for Crystal Geyser in Table 4.2, and mineralogy by XRD, Table 4.3.*

Modelled pH values are close to measured experimental values, Table 4.8. The final measured pH values for both the pre-CO_2 bubbling control and the +CO_2 periods are slightly higher than the model would suggest, however results are close to the equilibrium model values. This would appear to show that the carbonate minerals in the Utah rock samples are reacting to buffer pH and, at least for the +CO_2 period, reached some state close to equilibrium.

However, applying the same model but without reactive minerals gives a pH value with bubbled CO_2 of 6.27, which is essentially the same as with carbonate minerals included. Therefore, while some mineral interaction is occurring, it is the buffering capacity of the *Crystal Geyser* solution that is dictating the pH value, based on the model. Given that the spring water chemistry has been set by fluid-mineral interactions anyway, then here the distinction between fluid-buffered and mineral-buffered pH cannot be made and is most likely a combination of the two processes, which are dependent on each other.

4.5.3 Batch experiments (metals)

In Chapter 3, Section 3.10.2 (North Sea), the results of the cation analysis for the North Sea batch experiments were tabulated and assessed on a) whether CO_2 enhanced mobilisation of elements with respect to the controls (North Sea, Table 3.14); and b) the apparent trends in concentrations (North Sea, Table

3.15). The same exercise has been carried out here for the Utah batch experiments, however since all 4 samples exhibited essentially identical trends and behaviours (with some exceptions, discussed later), then the 4 samples (*S1 - S4*) will be treated simply as a single Utah sample to avoid duplication.

The Utah results are also different from the North Sea samples in that the experiments were neither control and $+CO_2$ flasks running parallel, nor did they use a synthetic NaCl solution. Instead, the Utah experiments ran for a control period where field-collected spring water was allowed to equilibrate with the rock samples, before the addition of bubbling CO_2. The results in Table 4.9 are therefore taken as whether concentrations increase from the end of the equilibration control period, and not whether the concentrations have increased with respect to the initial control period values. Large fluctuations in concentrations occurred for several elements in the first hours and days after commencing CO_2 bubbling (e.g. Cu, Fe, Zn, Figures 4.11 & 4.14), however the long term overall trend was taken, ignoring short initial variations. The North Sea data assessment has been included in Table 4.9 in order to compare that assessment with the Utah samples, with the text greyed out to highlight the Utah samples. Table cells marked with a cross mark (✗) indicate that CO_2 has not enhanced concentrations, cells with a checkmark (✓) indicate that it has, cells with a tilde ($\sim$) indicate some uncertainty, blank cells are where elements were not analysed for, and '< LOD' denotes concentrations below analytical detection limits.

Element	Utah	Captain SA7	Captain SA10	Cormorant	Thistle	Field X 8518	Field X 8579
Al	✗	✗	✗	✗	✗	< LOD	< LOD
As	< LOD	✗	✗	< LOD	< LOD	< LOD	< LOD
Ba	✓	✓	✓	✓	✓	✓	✓
Ca	✓	✓	✓	✓	✓	✓	✓
Cd	< LOD	✗	✗	✗	✓	✗	✗
Cr	< LOD	✗	$\sim$	✗	✗	< LOD	< LOD
Cu	$\sim$	$\sim$	✗	✗	✗	✓	✗
Fe	$\sim$	✗	$\sim$	✓	✓	✓	$\sim$
Hg	< LOD	✗	✗	✗	✗	< LOD	< LOD
K	✓	✗	$\sim$	✓	✗	✗	✗
Li	✓	-	-	✓	✗	-	-
Mg	✓	✓	✓	✓	✓	✓	✓
Mn	✓	✓	✓	✓	✓	✓	✓
Ni	✓	✓	✓	✓	✓	✓	✓
Pb	$\sim$	✓	✗	✗	✗	< LOD	< LOD
Si	-	-	-	✗	✗	-	-
Sr	✓	-	-	✓	✓	-	-
Ti	-	✗	✗	-	-	-	-
Zn	$\sim$	✓	✓	✓	✓	✓	✗

Table 4.9: *Summary of whether CO_2 has enhanced element concentrations in batch experiments. ✓ = enhanced concentrations with CO_2, ✗ = not enhanced with CO_2, $\sim$ = possible enhancement, - = data not available, < LOD = data less than analytical detection limit.*

This assessment shows that 8 elements in the Utah batch experiments have concentrations enhanced with the addition of CO_2 to the batch flasks. Of these elements, only Ni is a trace metal of interest, with the remainder considered major elements. Four of the remaining trace elements (As, Cd, Cr, Hg) were below, or eventually fell below, their respective analytical LOD's, while it was unclear whether CO_2 significantly affected the concentrations of Cu, Pb and Zn. For example, Cu shows a large amount of variability initially after CO_2 bubbling starts, before reducing to levels below the pre-CO_2 equilibrium period and then apparently increasing at the end of the experiment. Lead shows a similar behaviour, and Fe likewise remains similar to pre-CO_2 concentrations until the final sample where concentrations dramatically increase. Meanwhile Zn concentrations show greater variability and variation of values between the samples during CO_2 bubbling than pre-CO_2.

Batch experiment trace metal concentrations with bubbled CO_2 were determined to be, for the majority of cases, within the range of the spring water concentrations (where detected above LOD), Figures 4.9 and 4.10. Nickel concentrations were below the spring water values prior to the addition of CO_2, but increased to within the range after bubbling started. Concentrations of Zn were at the higher end of

the range pre-CO_2 but overall reduced to within the spring water range after the initial highly variable period, and Cu has a large spring water range therefore only one batch experiment value fell outwith this range (48 ± 2 µg/L, *Entrada S1*, day 90). Arsenic was not detected above LOD in any of the batch fluid samples, matching only *Side Seep* in this respect, with the other spring water values being significantly higher (mean = 33 µg/L).

As previously discussed in Chapter 3 (North Sea), Ni is commonly cited in the literature as being enhanced with the addition of CO_2 to batch experiments, as demonstrated in this study, with examples of this in the literature occurring in calcareous sandstones/sands - such as the Utah samples - given in Little and Jackson (2010), Lu *et al.* (2010) and Cahill *et al.* (2013). Whereas Cd and Cr were found to be somewhat mobile with CO_2 in previous studies (Terzi *et al.*, 2014), their mobility in this batch experiment was low.

Cadmium, Cr, Hg and Pb were not detected in the spring waters, and were mostly less than the LOD for the batch experiments. Mercury responded initially to the CO_2 bubbling with increased concentrations, particularly for *Entrada S2*, but within days had returned back to < LOD. The effect of CO_2 for Hg appeared therefore to be a temporary mobilisation, but which was not sustained beyond a few days, possibly due to volatilisation. Lead was the only element to record concentrations during CO_2 bubbling which were consistently above the LOD, albeit at low concentrations (< 1.5. µg/L), compared with the spring waters where Pb was not recorded at all, Figure 4.10.

The major elements where the addition of CO_2 increased their concentrations were found to be Ba, Ca, K, Li, Mg, Mn and Sr. These are elements cited in the literature as having the same response to CO_2 as these experiments, with authors citing the mechanisms of carbonate mineral dissolution (e.g. Kjöller *et al.* 2011; Rosenbauer *et al.* 2005; Shiraki and Dunn 2000; Varadharajan *et al.* 2013) or desorbtion (e.g. Cahill *et al.* 2013; Mickler *et al.* 2013; Varadharajan *et al.* 2013). Again, concentrations from the batch experiments fall within the range of the spring waters, Figures 4.12 and 4.13. Magnesium is interesting since the range of values for the springs is quite narrow (186 - 237 mg/L, Table 4.2) and lower than the ranges for the batch experiments both pre-CO_2 (251 - 317 mg/L) and during-CO_2 (239 - 483 mg/L) phases. Magnesium concentrations increase slowly with time away from the spring waters' values after CO_2 bubbling begins, after an initial small drop, Figures 4.13 and 4.14. Sample *Navajo S4* is also curious since for Ba and Mn concentrations increase much more than for the other samples, which is unusual given how consistent other concentrations are between all 4 samples, Figures 4.12 and 4.13.

Concentrations of Fe are low (0.005 - 0.177 mg/L) compared with concentrations found in the spring waters (1.2 - 14.8 mg/L). Iron mobility is low where it is being oxidised in the presence of water and oxygen from soluble Fe^{2+} to insoluble Fe^{3+}. Concentrations of Fe are higher in the spring waters most likely due to reducing conditions caused by dissolved methane (Wigley *et al.*, 2013b) or hydrogen sulphide (e.g. Purser *et al.* 2014). Purser *et al.* (2014) demonstrated that significant Fe^{2+} (3 - 15 mg/L) could be leached from Utah sandstone collected in the same area as this thesis, using these reducing agents.

With the exception of Fe, the addition of CO_2 to the batch flasks containing rock samples and a CO_2-driven spring sample from Utah, appears to replicate well the concentrations of metals found in the 10 springs sampled in the same area.

And comparing the Utah data with the North Sea samples, common elements which are mobilised by CO_2 (where analysed for) across all the experiments are Ba, Ca, Mg, Mn, Ni and Sr. Al and As, likewise, exhibit consistent behaviours across Utah and North Sea experiments. Zinc was not obviously mobilised by CO_2 for the Utah experiments, in contrast to the majority of North Sea samples, however K was more mobile than the majority of the North Sea experiments. Otherwise, trace metal concentrations are consistently immobile with CO_2 across the majority of North Sea and Utah experiments, Table 4.9.

4.5.4 Concentration trends

The general trends in concentrations with respect to time dependent mobility, instead of whether they are influenced by CO_2, can be summarised for the batch experiments, Table 4.10. Again the Utah samples were grouped together, and the trends categorised in the same way as for the North Sea experiments, based on concentrations during CO_2 bubbling: **Type I** elements increased concentrations through time; **Type II** elements increase in concentration before levelling off for the remainder of the experiment; **Type III** elements increased in concentrations, either slowly or rapidly, before decreasing again before the end of the experiment; and **Type IV** elements were either not detected above the analytical LOD's, *or* did not display any time-dependent trend *and/or* varied randomly in concentration. This classification does not indicate anything with regard to whether concentrations are enhanced with respect to the controls: see Table 4.9 for this information. The assessment for the North Sea experiments has been included for comparison with the Utah experiments, and greyed out to highlight the Utah assessment.

	Type I	Type II	Type III	Type IV
Utah	Ca, Fe, K, Mg, **Ni**	Li, Mn, Sr	Ba	Al, **As**, **Cd**, **Cr**, **Cu**, **Hg**, **Pb**, **Zn**
Captain SA7	Ca, K, Mg, Mn, **Ni**, **Zn**		Ba	Al, **As**, **Cd**, **Cr**, **Cu**, Fe, **Hg**, **Pb**, Ti
Captain SA10	Ba, Ca, K, Mg, Mn, **Ni**, **Zn**		Fe	Al, **As**, **Cd**, **Cr**, **Cu**, **Hg**, **Pb**, Ti
Cormorant	Ba, Ca, Fe, K, Li, Mn, **Ni**, Si, Sr	Mg, **Zn**		Al, **As**, **Cd**, **Cr**, **Cu**, **Hg**, **Pb**
Thistle	Ca, **Ni**	K, Li, **Zn**	Ba, Mg, Mn, Si, Sr	Al, **As**, **Cd**, **Cr**, **Cu**, Fe, **Hg**, **Pb**
Field X 8518	Ba, **Zn**	Fe, **Ni**	Ca, **Cu**, K, Mg, Mn	**As**, **Cd**, **Cr**, **Hg**, **Pb**
Field X 8579	Ba	**Ni**	Ca, K, Mg, Mn	**As**, **Cd**, **Cr**, **Cu**, Fe, **Hg**, **Pb**, **Zn**

Table 4.10: *Classification of element mobility from batch experiments with bubbled CO_2. Type I: Concentrations rise through time; Type II: concentrations rise and then level off; Type III: concentrations rise initially then decrease through time; Type IV: concentrations vary randomly and/or independently of time, or are < LOD. Bold lettering highlights 8 trace metals of interest.*

This classification shows that the majority of the major elements fall into the Type I and II categories, while the majority of the trace elements fall into Type IV. The major elements identified in Table 4.9 to be mobile with CO_2 are therefore categorised here as Types I, II or III. Aluminium was not identified to be mobile with CO_2 and is classified here as a Type IV element. Type IV elements, which constitute the majority of the trace elements, indicate that concentrations are low, or apparently random and with no discernible influence of bubbled CO_2. Nickel is the exception here, with concentrations increasing with time once CO_2 bubbling commences, and therefore classified as Type I.

While the Utah samples have been grouped together since the batch experiment results indicated essentially identical trends (where evident) in concentrations, a notable deviation of behaviour is found for Mn concentrations in the *Navajo S4* sample. It can be classified as Type I, rather than Type II, since concentrations continue to rise through the duration of the experiment.

Comparing the Utah assessment with the North Sea experiments, Table 4.10, it is clear again that similar behaviours are exhibited for the elements across all the batch experiments undertaken, with respect to concentration trends. That is, for the most part highly mobile elements consistently include Ba, Ca, K, Li, Mg and Ni, with the Utah samples differing insofar as Zn does not appear to be as mobile as from the North Sea samples. This assessment is not sophisticated enough to determine, however, the rate at which concentration trends occur. For example, the North Sea batch experiments were typically short in duration (< 1 month) whereas the Utah experiments with bubbled CO_2 lasted significantly longer. Any trends in increasing concentrations determined for the North Sea samples may in fact level off in the same time

period as the Utah experiments, had they been allowed to run that long. Furthermore, Ca concentrations for the Utah experiments were categorised as Type I (increasing concentrations), but if one looks at the trend, it is only slightly increasing above a flat trend, compared with the rapid concentration increases occurring early on in the CO_2 bubbling period (Figure 4.12.

Nonetheless, the trends in concentrations are broadly similar across all the batch experiments undertaken, with most major elements showing distinct increases in concentrations, while the 8 trace elements of interest appear relatively immobile.

4.5.5 Comparison with other batch experiments

Comparing concentrations of mobilised elements with other work, four previous studies' results are cited in Table 4.11, for which data was easily available online. The same comparison was made for the North Sea data in Table 3.16. Minimum and maximum concentrations from all experiments reported in each study are summarised for both $+CO_2$ and control experiments, and compared with the results of the Utah batch experiments in this instance. Again, Hg is an element which is not analysed for in the cited studies, and therefore the Hg results of the Utah batch experiments is project cannot be compared with the published literature. Blank spaces in Table 4.11 denote no data available.

It can be seen that, as with the North Sea data comparison (North Sea, Table 3.16), the range of values of the 8 trace metals of interest mobilised during batch experiments from Utah sandstones for this study is broadly similar to the range of concentrations recorded in the literature, Table 4.11. The values recorded for the Utah batch experiments are mostly at the lower end of concentrations, compared with the literature, particularly for Ni where maximum concentrations are nearly an order of magnitude lower than maximum values recorded by Lu *et al.* (2010), and up to 3 orders of magnitude lower than Lu *et al.* (2014). Arsenic was not recorded above detection limits in the Utah experiments, and therefore lower by default than other studies, including the North Sea batch experiment data presented in Chapter 3.

Chromium, Cu and Zn all tend to be significantly higher in Little and Jackson (2010) and Lu *et al.* (2014) studies compared with the batch experiments presented here, however there are closer values between the batch experiments and Cahill *et al.* (2013). In the same data analysis in Chapter 3 (North Sea) it was noted that while Lu *et al.* (2014) carried out their experiments at reservoir pressures (200 bar), the range of concentrations measured during their experiments were not dissimilar to the North Sea experiments, which were carried out at atmospheric pressures. Similarly, concentrations for some elements are comparable between the Lu *et al.* (2014) study and the Utah batch experiments (e.g. Ca, Mn) carried out at atmospheric pressure, however for elements such as K and Mg, the Utah batch experiments yielded concentrations far in excess of that study. It is unknown whether the concentration ranges from the Lu *et al.* (2014) study would have been different if their experiments were carried out at atmospheric pressure, however the conclusion again is that it appears that greater pressures (and hence greater CO_2 dissolution) do not necessarily equate to greater element mobilisation, especially with respect to the trace metals of interest, Table 4.11. Mobility of elements could be more likely sample/reservoir dependent as a predictor, than pressure dependent.

Comparing with other data collected for this study, Figure 4.28 summarises all concentration data for the batch experiments undertaken for Utah (*Entrada S1*, *Entrada S2*, *Wingate S3*, *Navajo S4*) and North Sea (*Captain SA7*, *Captain SA10*, *Cormorant*, *Thistle*, *Field X 8518*, *Field X 8579*) sandstone samples using box-and-whisker plots for all elements considered in this work. The data has been subdivided further based on control and $+CO_2$ experiments and plotted on $\log_{10}$ y axes to better display the large ranges in concentrations. The boxes shows median, lower and upper quartiles (interquartile range, *IQR*). Whiskers are $1.5 \times IQR$. Circles are outlier values $> 1.5 \times IQR$. The median values ($\tilde{x}$) for each element and subdivision are given in Table 4.12, together with the number of samples (n) used to calculate $\tilde{x}$; concentrations less than the analytical detection limits (LODs) were omitted from the calculations.

Element (µg/L)	Little and Jackson (2010) Soils 1 bar 20°C +CO₂	Control	Lu *et al.* (2010) Sandstones 1 bar 25°C +CO₂	Control	Cahill *et al.* (2013) Sediments* 1 bar 25°C +CO₂	Lu *et al.* (2014) Sandstones 200 bar 70 - 100°C +CO₂	Control	This study (Utah) Sandstones 1 bar 21°C +CO₂	Control
Al	0 - 9,658	0 - 13,444	0 - 31,063	0 - 27,704	0 - 601	70 - 17,433	5 - 2,436	0 - 412	143 - 639
As	0 - 10	0.010 - 20	0 - 110	0 - 19	-	0 - 23	0 - 35	0	0
Ba	8 - 1,141	0.482 - 235	3 - 1,161	0.34 - 394	3 - 276	7 - 9,630	0.062 - 12,875	11 - 142	5 - 70
Ca	4,132 - 963,053	85 - 515,535	1,261 - 470,843	0 - 278,659	391 - 917,399	545 - 237,674	46 - 1,071,189	4,544 - 658,684	51,174 - 1,326,184
Cd	0 - 3	0 - 4	0 - 45	0 - 3	0 - 0.63	0 - 6	0 - 4	0	0 - 4
Cr	0 - 30	0 - 27	0 - 117	0 - 15	0 - 5	5 - 1,852	2 - 3,859	0 - 3	0 - 9
Cu	0.02 - 46	0 - 49	0 - 1,458	0 - 801	1 - 12	660 - 3,171	0.10 - 2,348	0 - 49	4 - 40
Fe	0 - 11,954	7 - 3,258	0 - 8,402	0 - 38,748	0 - 232	14 - 68,423	11 - 217,282	0 - 177	0 - 73
Hg	-	-	-	-	-	-	-	0 - 4	0
K	-	-	422 - 91,371	154 - 67,702	285 - 20,394	3,107 - 30,801	2 - 31,914	312,777 - 591,477	325,077 - 357,877
Li	2 - 333	0 - 85	0 - 24	0 - 24	0 - 84	-	-	3,092 - 5,577	3,173 - 3,550
Mg	1,725 - 342,575	77 - 232,054	182 - 630,230	26 - 312,243	183 - 81,398	331 - 28,821	1 - 34,676	239,020 - 483,120	251,220 - 317,420
Mn	25 - 2,722	0 - 1,664	0.87 - 3,773	0 - 2,299	2 - 10,958	0.88 - 4,623	0.28 - 5,655	1 - 2,241	3 - 1,889
Ni	1 - 2,207	0 - 2,314	0 - 161	0 - 140	0 - 74	50 - 22,931	0.27 - 20,583	0 - 14	0 - 10
Pb	0 - 4	0.001 - 0.25	0 - 51	0 - 8	0 - 1	0 - 53	0 - 269	0 - 11	0 - 6
Sr	22 - 6,332	0.53 - 4,363	9 - 6,164	0.24 - 5,216	3 - 78,313	9 - 6,411	0.081 - 5,780	36 - 12,548	830 - 17,028
Zn	0 - 3,311	0.15 - 2,529	0 - 192	0 - 362	1 - 46	9 - 24,906	1 - 37,308	0 - 119	25 - 56

Table 4.11: *Minimum and maximum concentration data from recent published batch experiment studies, compared with the results of the Utah batch experiments.* *Includes two chalks.*
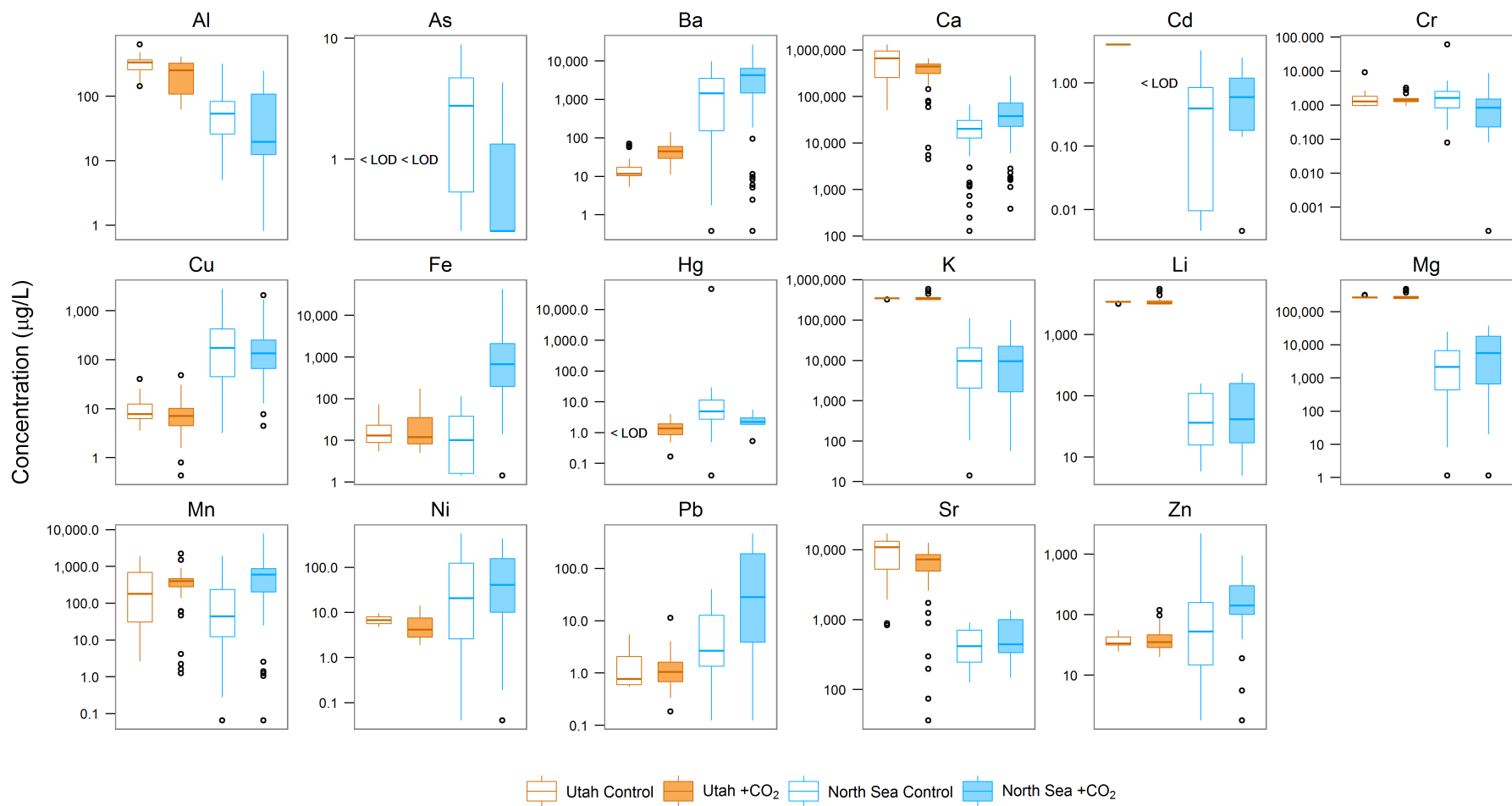
Figure 4.28: *Box and whisker plot comparison of Utah and North Sea batch experiment data, grouped by control and +CO₂ data. Box shows median, lower and upper quartiles (interquartile range, IQR). Whiskers are 1.5×IQR. Circles are outlier values > 1.5×IQR. < LOD denotes where concentrations were not detected above analytical limits of detection. Note y-axes are log_{10} scale. Median and n values in Table 4.12.*

Element	Utah Control		Utah +CO$_2$		North Sea Control		North Sea +CO$_2$	
	$\tilde{x}$	n	$\tilde{x}$	n	$\tilde{x}$	n	$\tilde{x}$	n
Al	340	24	250	39	54	40	20	26
As	< LOD	-	< LOD	-	2.8	24	0.26	12
Ba	12	24	45	48	1,400	84	4,300	83
Ca	670,000	24	440,000	48	20,000	85	38,000	84
Cd	4	1	< LOD	-	0.42	22	0.59	31
Cr	1.3	13	1.4	15	1.6	33	0.86	38
Cu	7.8	24	7.1	43	180	59	140	53
Fe	13	19	12	28	10	20	680	66
Hg	< LOD	-	1.4	11	5	29	2.2	11
K	350,000	24	340,000	48	9,700	81	9,700	82
Li	3,500	24	3,300	48	36	20	42	19
Mg	270,000	24	270,000	48	2,200	82	5,600	84
Mn	180	24	400	48	44	84	610	84
Ni	7.2	2	4.2	12	21	53	41	80
Pb	0.77	7	1.1	22	2.7	28	30	32
Sr	11,000	24	7,300	48	420	20	440	19
Zn	34	24	35	43	53	56	140	79

Table 4.12: *Median ($\tilde{x}$) values and number of samples (n) data from Figure 4.28, for Utah and North Sea controls and +CO$_2$ flasks.*

Common features that are evident between both sets of data (Utah and North Sea) are, firstly, that where distinct concentration trends were noted in this and Chapter 3 (North Sea) - particularly those qualified as Type I and Type II (Tables 3.15 & 4.10) - a large number of outlier values tend to occur. These outliers are usually at the lower concentration values for, for example, Ba, Ca, Mn and Sr, Figure 4.28. These outliers represent where concentration values are increasing through time from low initial values in the batch experiments, and are particularly evident in the North Sea samples since the batch fluids used were always simple NaCl brines, far from equilibrium with the rock samples.

Secondly, concentrations of the 8 trace metals of interest are generally much lower than the other elements considered, with medians ranging between 0.26 and 180 µg/L, where detected above LODs. On this point, it can be seen that on average 40% fewer samples analysed for trace metals were determined to have concentrations > LOD, compared with other other elements. However, the major elements can also show low concentrations in similar ranges to the trace elements although, tellingly, the medians are usually significantly higher. That said, elements such as Al, Fe and Mn display comparable median concentrations to the trace metals in some cases, with lowest $\tilde{x}$ for these elements at 20 µg/L, 10 µg/L and 44 µg/L, respectively.

Where the two datasets begin to differ, though, is that for 11 of the 17 elements, the +CO$_2$ median concentrations are higher than the control for the North Sea data, but for Utah this is only 4 of the 17 elements, Figure 4.28 and Table 4.12. The differences in median values between Utah control and +CO$_2$ data is usually small, however, Table 4.12. Despite the conclusions made earlier that bubbled CO$_2$ increases concentrations of a number of elements, it is not seen in this summary of the Utah data since the concentrations of many of the elements expected to have higher median ($\tilde{x}$) in the +CO$_2$ data (e.g. Ba, Ca, Mg, Mn) started at already elevated values in the control period, and often higher than the +CO$_2$ period concentration equilibria reached by these elements (Figures 4.12 & 4.13). Compare this with the North Sea experiments where concentrations in both control and +CO$_2$ always began at - or close to - zero, but tended to increase significantly more with the addition of CO$_2$ for these elements.

In most cases, concentrations exhibit larger variations in the North Sea data than in the Utah data, as shown by the larger *IQR* and 1.5×*IQR* ranges. The most obvious explanation for the larger variations is that the batch data for the North Sea samples were obtained from 6 different samples, representing 4 geographically distinct hydrocarbon fields (Methods, Figures 2.3 & 2.4), and a variety of reservoir depths (and hence burial and diagenetic history). Therefore one would expect a variety of results, if one assumes that the mineralogy of the samples controls the mobility of elements. However, the mineralogy of all the North Sea samples analysed by X-ray diffraction (XRD) shows little significant differences between sam-

ples (North Sea, Tables 3.1, 3.6 and 3.11), yet concentrations vary much more than they do for the Utah samples, which have larger differences in mineralogy between samples. For example, the total carbonate contents of the *Entrada S1* and *S2* samples are 13 ± 1 wt.% and 12 ± 1 wt.%, respectively, compared with *Wingate S3* and *Navajo S4* at 0.9 ± 0.6 wt.% and 1.0 ± 0.5 wt.%, respectively, yet concentration ranges for elements expected to be mobilised from these minerals (e.g. Ba, Ca, Mg, Sr) are very similar across all 4 samples. Not only that, but there is significant variation in concentrations between the Utah and North Sea sandstones. Median concentrations of Ca, K, Li, Mg and Sr are 1 - 2 orders of magnitude higher than the North Sea, Figure 4.28 and Table 4.12, despite the Utah samples *Wingate S3* and *Navajo S4* having similar carbonate contents as the North Sea sandstones. Assuming that carbonate dissolution is dominating the fluid chemistry for the Utah batch experiments, then perhaps this is a suggestion that more reactive surfaces are available for the Utah samples, compared with the North Sea samples, and are therefore more reactive.

4.5.6   pH-dependent mobilisation

The concentration trends of the Utah batch experiments for the major elements (Type I and II elements, Table 4.10) would suggest mineral dissolution and steady supply of cations to solution from reaction with dissolved CO_2, albeit more rapidly than the North Sea batch experiments. Concentrations for several elements - Ca, Mn, Sr - decrease before the bubbling of CO_2 and then rapidly increase again with CO_2, suggesting the precipitation of minerals containing these elements and then their immediate dissolution. On the other hand, most of the 8 trace metals do not fit this categorisation (i.e. Type IV, Table 4.10) and it is therefore unlikely that they are not controlled by steady dissolution of minerals, and perhaps rapid pH-dependent desorbtion from mineral surfaces would account for their concentrations.

As with the North Sea experiments, in order to make some assessment of pH dependent concentrations, the mobilised concentrations of all the elements from the Utah batch experiments were compared with just the first two sequential extraction procedure (SEP) steps. These were the water soluble and exchangeable steps, which represent the most theoretically mobile elements, which require only mobility with water and pH-dependent ion exchange, rather than dissolution of minerals.

On this assumption, the SEP concentrations for SEP steps 1 and 2 were summed, and compared with the mobilised concentrations from the batch experiments, in terms of μg of element mobilised per gram of sample. The way that they were compared was to calculate the mobilised concentrations for control and $+CO_2$ periods as percentages of the summed SEP steps, Table 4.13. Where calculated percentages are > 100% then it is assumed that element concentrations are supplemented or dominated by mineral dissolution.

Considering just the trace metals, since the assumption is that the major elements are mobilised through mineral dissolution, it can be seen that mobilisation is generally very low with batch concentrations mostly < 0.1% of SEP steps 1 and 2 for As, Cd, Cr, Hg and Pb, Table 4.13. Lead concentrations represent a more significant proportion of SEP steps 1 and 2 for the *Entrada S1* sample and shows enhanced mobility with CO_2 at 34% and 64% for control and $+CO_2$ periods, respectively. Mobilised Ni concentrations are low, at less than < 15%, with the exception of *Navajo S4* $+CO_2$. Copper and Zn are more consistently mobilised in concentrations which are more than 10% of the SEP steps, with Zn indicating that greater concentrations were mobilised with CO_2, in contrast to previous assessments (e.g. Table 4.10), with close to 100% of water soluble and exchangeable Zn being apparently mobilised with CO_2, Table 4.13. With the *Entrada S1* sample, Cr is the only trace element which is mobilised at greater than 100% of the sum of the two SEP steps.

Overall, trace metals are less mobile for the Utah batch experiments than they are for the North Sea samples, which were commonly mobilised in concentrations > 100% of SEP steps 1 and 2 (Table 3.17). However, some elements are mobilised as a significant portion of the water soluble and exchangeble steps, with Ni, Pb and Zn showing increases with bubbled CO_2.

| Element | Entrada S1 | | Entrada S2 | | Wingate S3 | | Navajo S4 | |
	Control	+CO$_2$	Control	+CO$_2$	Control	+CO$_2$	Control	+CO$_2$
Al	37%	31%	12%	11%	1%	1%	1%	0.4
As	< 0.1%	< 0.1%	-	-	-	-	-	-
Ba	< 0.1%	< 0.1%	< 0.1%	< 0.1%	< 0.1%	< 0.1%	< 0.1%	0.2%
Ca	17%	22%	24%	28%	> 100%	> 100%	37%	40%
Cd	-	-	0.2%	< 0.1%	< 0.1%	< 0.1%	< 0.1%	< 0.1%
Cr	> 100%	> 100%	< 0.1%	< 0.1%	< 0.1%	< 0.1%	< 0.1%	< 0.1%
Cu	< 0.1%	0.2%	39%	27%	11%	23%	49%	32%
Fe	64%	50%	2%	6%	< 0.1%	0.4%	< 0.1%	0.4%
Hg	< 0.1%	< 0.1%	< 0.1%	< 0.1%	< 0.1%	< 0.1%	< 0.1%	1%
K	16%	27%	33%	53%	41%	68%	53%	84%
Li	> 100%	> 100%	35%	55%	> 100%	> 100%	> 100%	> 100%
Mg	13%	23%	23%	37%	62%	> 100%	> 100%	> 100%
Mn	> 100%	> 100%	65%	92%	> 100%	> 100%	71%	> 100%
Ni	< 0.1%	14%	4%	4%	4%	5%	< 0.1%	30%
Pb	34%	64%	0.3%	< 0.1%	< 0.1%	< 0.1%	< 0.1%	< 0.1%
Zn	49%	88%	< 0.1%	< 0.1%	44%	98%	62%	85%

Table 4.13: *Mobilised elements from batch experiments as % of summed SEP Steps 1 (water soluble) and 2 (exchangeable). - denotes concentrations less than detection limits.*
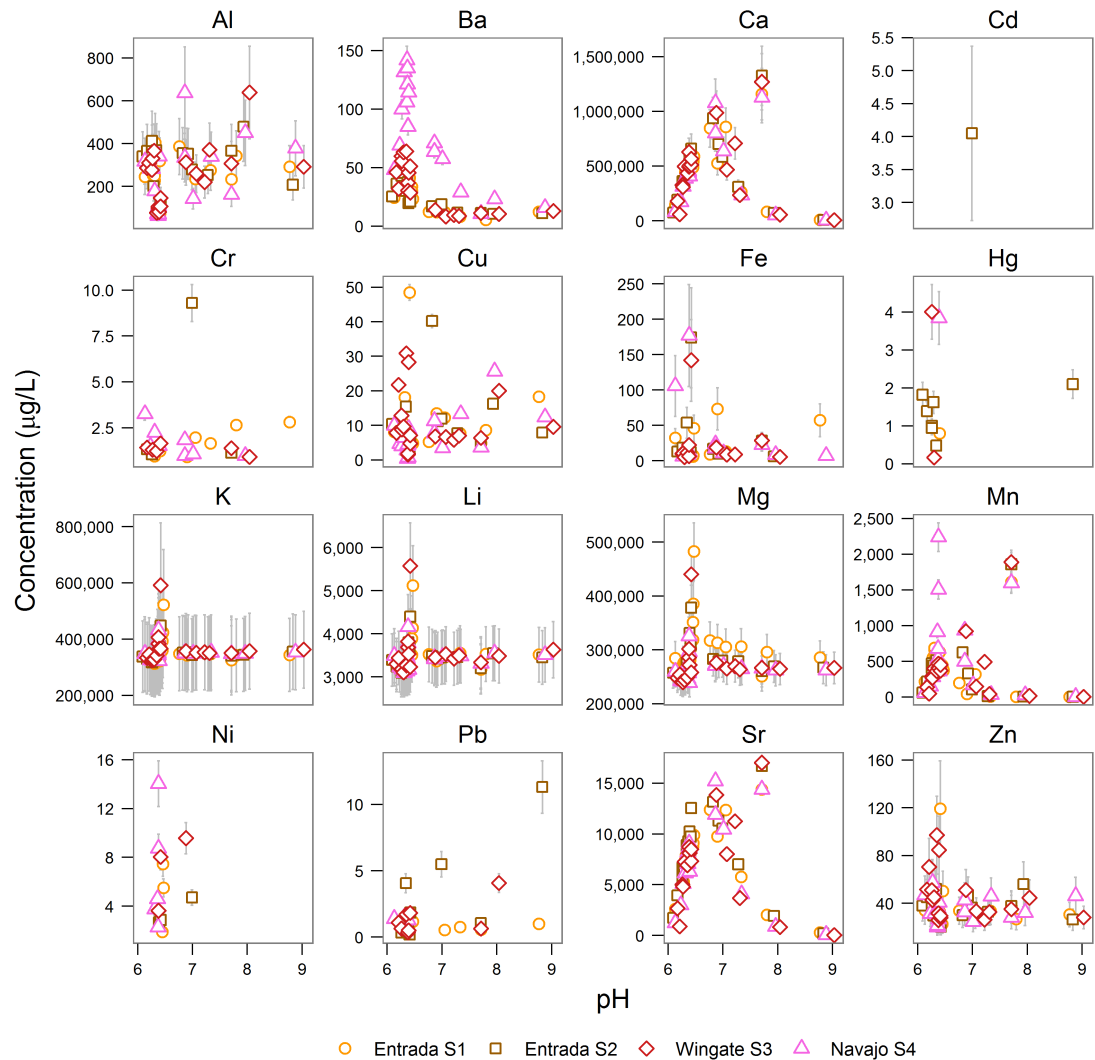
Figure 4.29: *Scatter plot of pH and Utah batch concentration data. Arsenic not shown as concentrations all < LOD. Error bars are 2s of the mean of standard reference materials, Section 2.10.*

If these elements are indeed mobilised by pH-dependent desorbtion (as per SEP Step 2), with an expected increase in mobilisation with decreasing pH, then the concentration data from the batch experiments can be plotted against pH values to determine whether this relationship is apparent. Plotting pH values for the batch experiments against concentration data for 16 elements (As not plotted as no concentrations recorded > LOD) shows no strong or consistent relationships for the majority of the elements, Figure 4.29. There are, however, trends which are visible for Ba, Ca, Mg, Mn and Sr. For these elements, concentrations increase rapidly with increasing pH from pH 6 to a peak of around pH 6.5, before rapidly decreasing again as pH continues to increase, before levelling out so that concentrations do not change with increasing pH, Figure 4.29.

From the separate concentration and pH plots (Figures 4.7, 4.12 & 4.13), one can see that pH increases through the experiments prior to bubbled CO_2 while concentrations decrease. It is likely that the changes in concentrations at this stage are not pH dependent and driven instead by the disequilibrium of these elements between the spring water batch fluids and the rock samples. When CO_2 is bubbled through, the initial drop in pH corresponds to low concentrations, but both pH and concentrations then rise for Ba, Ca, Mg, etc. to reach a steady state for the duration. Reduced pH does not therefore correlate to increased concentrations for these elements.

There is some indication that lower pH values correspond to increased mobility for Hg and Ni, Figure 4.29, but there is no consistent variation with pH value. However, the only solutions with detectable metals tend to be of low pH.

4.5.7 Carbonate dissolution

In Chapter 3 (Section 3.10.3) it was established that carbonate mineral dissolution is commonly cited in the literature as the source of many mobilised elements (e.g. Kirste *et al.* 2014; Kjöller *et al.* 2011) and that carbonates contain a variety of elements which substitute Ca and Mg into the mineral structure. These include Mn, Fe, Sr, Ba, Pb, Cu and Zn (Deer *et al.*, 1992). Four carbonate minerals were identified by XRD in the 5 samples collected in Utah: ankerite, calcite, dolomite and siderite. Calcite was detected in all samples, Table 4.14, albeit in trace quantities only for samples *S3 - S5*. Ankerite was detected in trace quantities only for *Wingate S3* and *Navajo S4*, and not at all for *Navajo S5*. Dolomite was also only detected in trace concentrations, or not at all, for samples S3 - S5. Siderite was barely detectable in *S1*, *S3* and *S4* samples.

The two *Entrada* sandstones contain 13 wt.% (*S1*) and 11.7 wt.% (*S2*) total carbonate, relatively evenly spread between ankerite, calcite and dolomite. This is in contrast both to the other 3 Utah samples, and to the North Sea samples where the highest carbonate content was 1.6 wt% (*Captain SA7*, Table 3.19).

Mineral	Chemical Formula	Common substitutes	S1	S2	S3	S4	S5
				(wt.% by XRD)			
Ankerite	$Ca(Fe,Mg,Mn)(CO_3)_2$	Sr	2.5	3.7	0.3	0.1	-
Calcite	$CaCO_3$	Fe^{2+}, Mg, Mn, Sr	5.1	4.7	0.3	0.7	0.07
Dolomite	$CaMg(CO_3)_2$	Fe^{2+}, Mn, Ni, Pb, Zn	5.4	3.3	-	0.2	0.1
Siderite	$FeCO_3$	Mg, Mn	0.01	-	0.2	0.01	-
		Totals	13.0	11.7	0.8	1.0	0.17

Table 4.14: *Common carbonate substituting elements and carbonate content of Utah samples, wt.% from XRD analysis*

Given the presence of carbonates, particularly in the *Entrada* samples, one would expect the reaction products of these minerals with CO_2 to be apparent in the data. With the addition of CO_2, elevated concentrations of common carbonate forming elements Ca, Mg, Mn, and Sr were found in the Utah batch experiments.

Trace metals which have an association with carbonates (Cu, Ni, Pb and Zn) were also found in some

cases to be more readily mobilised with $+CO_2$ (Tables 4.10 & 4.13), perhaps indicating that carbonate dissolution is the mechanism by which these elements are released into solution. If the assumption is made that Ca, Mg, Mn and Sr concentrations are entirely the product of carbonate dissolution, then the relationships between the trace metals of interest and these four elements might indicate whether or not these elements are sourced from carbonate dissolution. If concentrations of these elements have a positive linear correlation with Ca, Mg, Mn and Sr, then as a first order approximation it would therefore be assumed that carbonate dissolution is their primary source. Where correlations are weak, or non-existent, then another mode of element release must be invoked; either dissolution of another mineral type, or desorption from mineral surfaces.

Correlations between the 8 trace metals of interest and Ca are either weak, or non-existent (see correlation summary plots, Appendix D). There are no apparent relationships between Ca and these elements. The trace metals also do not correlate, or have weak correlations, with the other common carbonate forming elements listed in Table 4.14. Therefore based on our assumption above, carbonates do not appear to be the source of trace metals (where detected) in the batch experiment fluids.

Indeed, there is little correlation between the trace metals, with only Cu and Zn in samples *Entrada S2* and *Wingate S3* showing any strong relationship, with R^2 values for the $+CO_2$ periods being 0.84 and 0.91, respectively, for *S2* and *S3*, Figure 4.30.
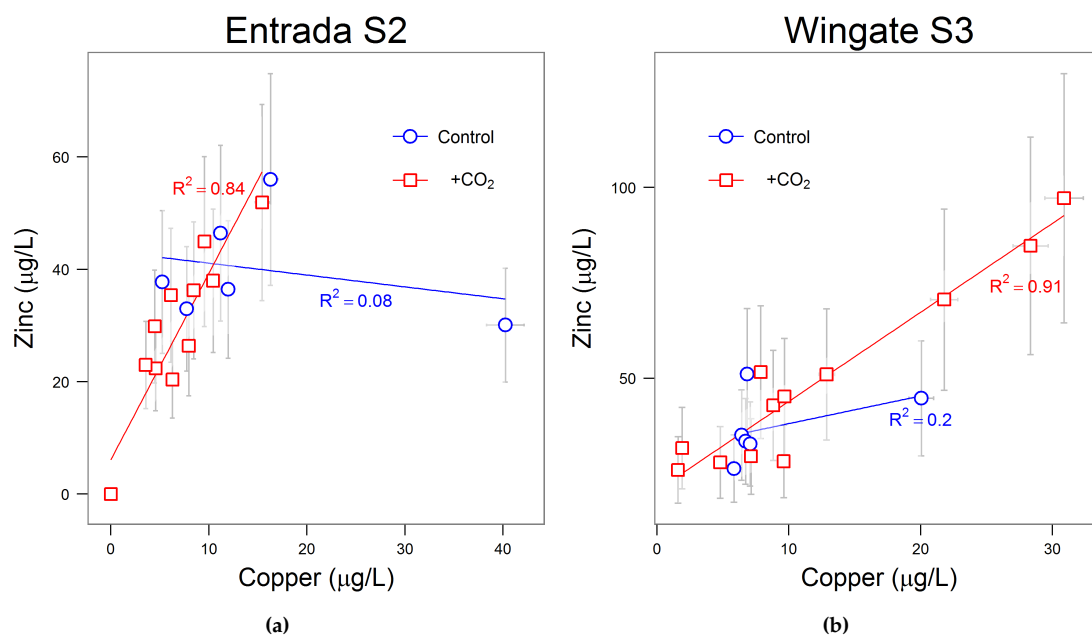
Figure 4.30: *Scatter plots of Cu vs Zn concentrations from control and $+CO_2$ batch experiments, for samples (a) Entrada S2 and (b) Wingate S3. Linear regression lines and R^2 values plotted separately for control and $+CO_2$. Error bars are 2s.*

Data does not appear to correlate well during the control periods for these samples. However these elements don't correlate with any of the major mineral forming cations, and have no apparent relationship between each other in terms of leaching susceptibility; both Cu and Zn are absent from two of the three most mobile fractions (carbonate and the exchangeable) for *Entrada S2* and *Wingate S3*, as determined by the sequential extraction procedure (Figure 4.17), and concentration ratios of Cu:Zn for the water soluble (most mobile) fraction are 1:0 (no Zn) and 1:1 for *Entrada S2* and *Wingate S3*, respectively, compared with 0.2:1 for the batch experiments. Looking at more resistant fractions, only the oxide fraction has both Cu and Zn concentrations recorded for either of these samples, giving Cu:Zn ratios of 0.3:1 for both samples. This is a comparable ratio to the batch experiments, however only trace amounts of

oxide were detected by XRD (hematite, Fe_2O_3), Table 4.3, that it is impossible to discern which mineral(s) these elements are associated with.

The relationship between Ca and the other carbonate forming major elements is also largely weak, with the strongest apparent relationship between Ca and Sr, Figure 4.31. Here we see that for both the control and $+CO_2$ periods, for all Utah batch experiment data, Ca and Sr concentrations have a positive linear relationship with R^2 values of 0.96 for both periods, albeit with a steeper slope for the $+CO_2$ period.
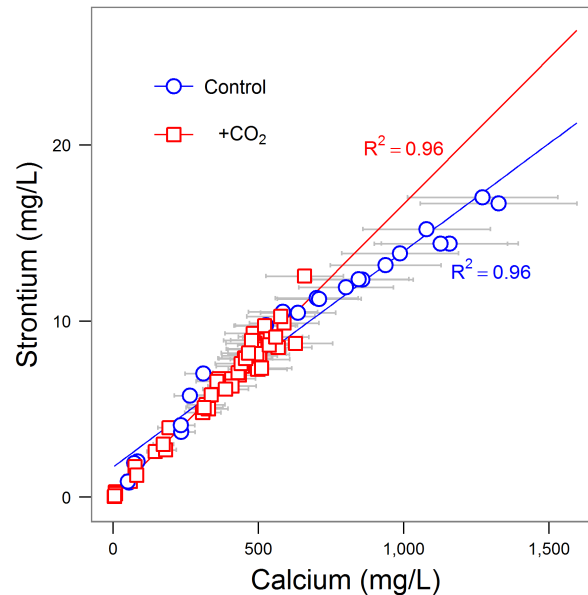
Figure 4.31: *Plot of Ca vs Sr batch experiment concentrations for combined data of all Utah samples, comparing control with $+CO_2$ periods. Error bars are 2s.*

The closeness of the relationship between Ca and Sr during both the control and $+CO_2$ experimental phases, would indicate co-precipitation and dissolution of these elements. Strontium is closely associated with Ca with respect to carbonate minerals, notably aragonite, a polymorph of calcite ($CaCO_3$). Sr can readily substitute into the crystal lattice of aragonite particularly in warm waters (Deer *et al.*, 1992; Langmuir, 1997), and the ratio of Sr to Ca is used to reconstruct palaeo water temperatures in which, for example, calcifying marine organisms have formed their structures (Beck *et al.*, 1992). The greater the amount of aragonite in a marine organism (e.g. corals), the higher the Sr concentration and the Sr/Ca ratio (Siegel, 1960). Strontium, however, will also substitute into other carbonate minerals such as calcite (Deer *et al.*, 1992), and even forms its own carbonate mineral, strontianite ($SrCO_3$).

Of direct relevance to this study, Sr and Ca concentrations were obtained by ICP-MS from non-biogenic aragonite veins sampled close to Crystal Geyser, Utah (Y. Shu 2015, pers. commm., 30 September). Calcium and Sr concentrations for the veins show a close linear relationship ($R^2 = 0.97$) and were formed from CO_2-charged fluids in this area at approximately 5 ka (Shu, in prep.). Concentrations in the aragonite veins are low overall, however, compared with the batch experiment fluids, with aragonite Ca concentrations in the range of $\sim$ 50 - 100 mg/L ($\tilde{x}$ = 58 mg/L) and batch Ca concentrations in the range $\sim$ 5 - 1,300 mg/L ($\tilde{x}$ = 470 mg/L).

Typically the molar Sr/Ca ratio is used to determine the relative abundance of aragonite, with the ratio decreasing as calcite recrystalises from aragonite. In this case, the pure aragonite of the Crystal Geyser veins (Shu, in prep.) have a mean calculated molar Sr/Ca ratio of 11 ± 1 mmol/mol ($n = 15$), which we can therefore interpret to have formed from migrating fluids with the same (or similar) Sr/Ca ratio (Morse W. and Mackenzie T., 1990). The mean calculated Sr/Ca ratios for the control and $+CO_2$ batch experiment fluids are 7.6 ± 1.7 mmol/mol ($n = 24$) and 7.9 ± 3.5 mmol/mol ($n = 48$), respectively. The Sr/Ca ratio is therefore lower than the Sr/Ca ratio in the aragonite veins which formed in this area,

with all three ratios within ranges published by Siegel (1960) for aragonite, and elsewhere for calcite (e.g. Beck *et al.* 1992; Wanamaker Jr *et al.* 2008).

It is not inconceivable that aragonite is forming in the batch flasks, based on the ratios for the experimental fluids. However, the ratios are also similar to calcite (Beck *et al.*, 1992; Wanamaker Jr *et al.*, 2008) and without an analysis of the solid samples in the batch flasks immediately prior to CO_2 bubbling to confirm the precipitation of aragonite, then it is unknown whether it is purely aragonite precipitation, or (more likely) a mixture of carbonate minerals such as calcite, with Sr substitution, or formation of Sr minerals with Ca substitution.
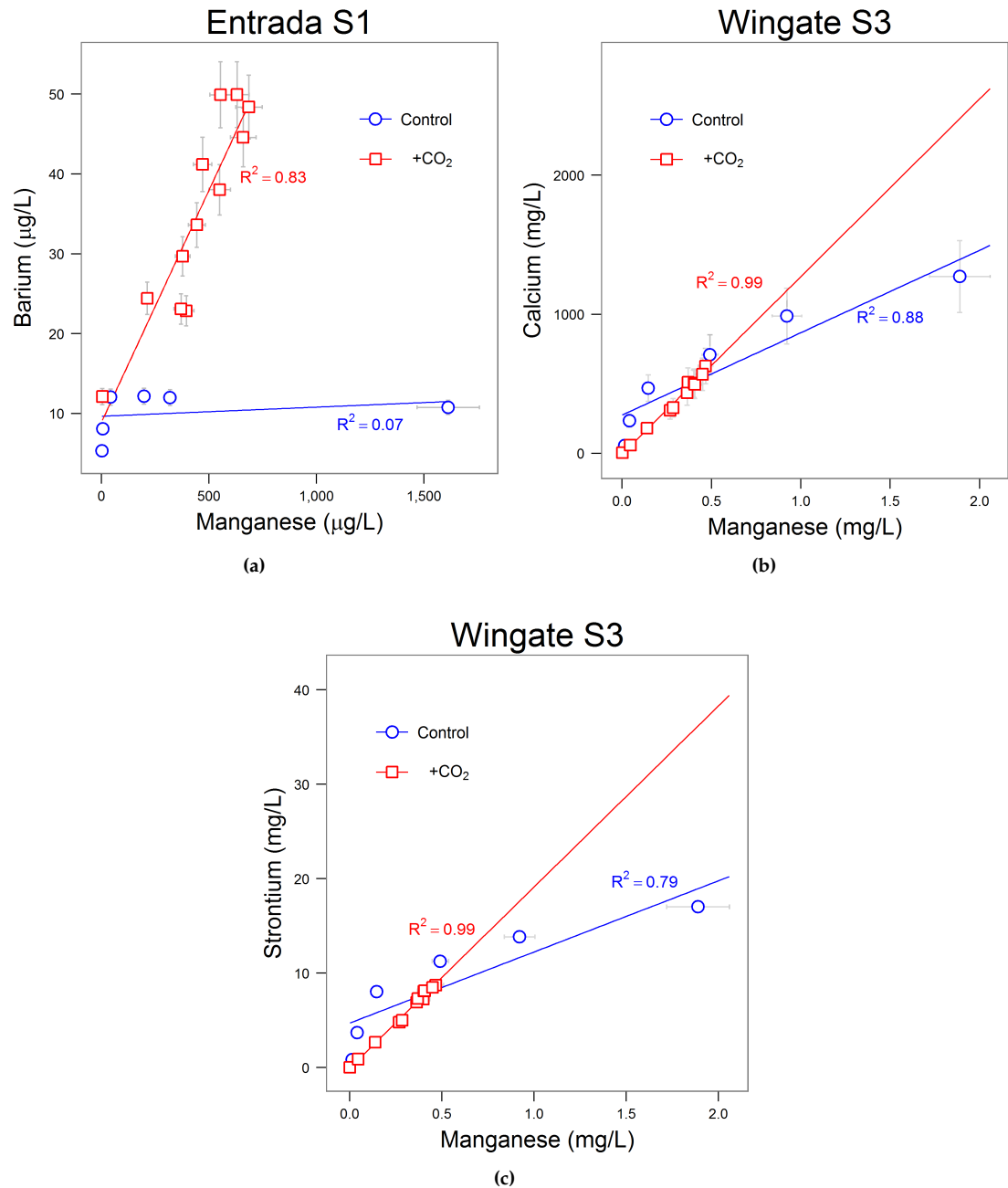
Figure 4.32: *Scatter plots of (a) Mn vs Ba (Entrada S1), (b) Mn vs Ca (Wingate S3) and (c) Mn vs Sr (Wingate S3) concentrations from control and +CO_2 batch experiments. Linear regression lines and R^2 values plotted separately for control and +CO_2. Error bars are 2s.*

There is perhaps some evidence for the precipitation and dissolution of other carbonates, however, with the common carbonate forming and substituting element Mn positively correlated with Ca and Sr concentrations for the *Wingate S3* sample, along with Ba (*Entrada S1*) which is another common carbonate forming element (Deer *et al.*, 1992), Figure 4.32.

Calcium and Sr correlate very strongly with Mn concentrations, with R^2 values of 0.99 for both elements during the $+CO_2$ experimental phase, with less strong correlations for the control periods, Figures 4.32b and 4.32c. Mobilisation of Mn into solution during the $+CO_2$ period may therefore be supplemented by dissolution of calcite or dolomite in addition to, or instead of, dissolution of any mineral precipitated during the control period. Barium concentrations correlate well for the $+CO_2$ period for *Entrada S1*, with an R^2 of 0.83, however there is no correlation between Mn and Ba for the control period (R^2 = 0.07), Figure 4.32a. This would suggest some co-mobilisation of Ba and Mn from this sample during the addition of CO_2, but with no co-precipitation of these elements during the control period. That Ba only correlates with Mn, and not any other carbonate forming elements such as Ca or Sr could be indicative of non-carbonate dissolution, or a chance correlation of these elements which have no clear relationship in this particular sample.

In Chapter 3, the carbonate dissolution hypothesis was tested, firstly, by comparing ratios of batch experiment mobilised elements with the ratio of elements in the SEP experiments. And secondly, by comparing the Ca and Mg equivalents with equivalent alkalinity (see Figure 3.37). Unfortunately this second test cannot be carried out for the batch experiments as alkalinity was not measured as a compromise to save experimental fluids and run a longer duration experiment. The ratio test also can't be carried out for Ca and Sr, since Sr was not measured for the SEP. Besides, Ca was also not detected in the carbonate SEP step for *Wingate S3*, so the ratio would always have Ca as zero, which is clearly not the case for the batch experiment. The ratios of Mn to Ba can be calculated, however, for the *Entrada S1* carbonate SEP step; here we get an SEP *Entrada S1* Mn:Ba ratio by concentration of 22:1, which compares to a mean ratio of around half this in the $+CO_2$ batch experiments at 12:1. This means that almost twice as much Ba is being released (on a concentration basis) in the batch experiments than would be predicted from the SEP, if carbonate dissolution alone was the source of Ba and Mn in the batch fluids. Again, this would strengthen the argument that Ba and Mn are only coincidentally correlated.

Dissolution of carbonates in the 4 Utah samples used in the batch experiments does not appear to be the mechanism for release of trace metals - where mobilised - and is unlikely to be a significant contributor to the release of other elements. Where clear concentration trends are found which would indicate carbonate dissolution, they are most likely the result of dissolution of recently precipitated carbonates following CO_2 degassing from the *Crystal Geyser* spring water with concurrent pH increase in the control period before CO_2 is bubbled. This can be explained for all 4 batch flasks as concentration values and trends are virtually identical across all 4, with the constant being the batch fluid, sampled from *Crystal Geyser*. It is therefore concluded that despite sometimes significant quantities of carbonate minerals in the *Entrada* samples, they are either unreactive under experimental conditions, perhaps because any reactive surfaces have already been attacked by weathering of the rock at surface or during burial, or contribute only very minor amounts to the batch fluids and any signature is swamped by the re-mobilisation of precipitated elements from the control period. Some elements, such as Ba and Mn, which may be associated with carbonates appear to correlate in some instances, but there is no definitive evidence that their mobilisation is related to carbonate dissolution.

4.5.8 Feldspar dissolution

Carbonate precipitation and subsequent dissolution would appear to explain trends in Ca and Sr, with perhaps some relationship with Mn for the *Wingate S3* sample. The 8 trace metals of interest have no significant relationships with the major mineral forming elements. Concentrations of Al are low in the $+CO_2$ experimental period, indicating low solubility, while concentrations of Ba have no strong relation-

ship with any other element except Mn, which may be coincidental only.

Other strong correlations do exist, however. Potassium, Mg and Li all display very similar concentration trends during the batch experiments. The concentration trend for these 3 elements is to remain at constant concentrations during the control period, indicating no (or no detectable) dissolution or precipitation of these elements. When CO_2 begins bubbling, there is a small relative drop in concentrations during the first 24hrs, which then recover and increase beyond the control values. Magnesium values remain above the range of the springs at all times, but K and Li values are within the springs' ranges until the final recorded value for *Wingate S3*.

The correlation analysis, Appendix D, shows high positive correlation coefficients during the +CO_2 period across all 4 batch experiments. Figure 4.33 shows K concentrations plotted with Mg and Li, for all control and +CO_2 data. Magnesium and Li are not plotted against each other as it should be self evident that they will correlate well, based on these plots. R^2 values for K vs Li, K vs Mg and Mg vs Li are 0.97, 0.81 and 0.85, respectively, based on a linear regression, for the combined data of all 4 batch flasks for the +CO_2 period. Note, however, that the uncertainty on the K values is quite large ($\pm$ 38%). Despite similar looking concentration trends, K, Li and Mg don't correlate well during the control periods ($R^2 <$ 0.30 in all cases), which would indicate concentrations varying independently of each other prior to the addition of CO_2.
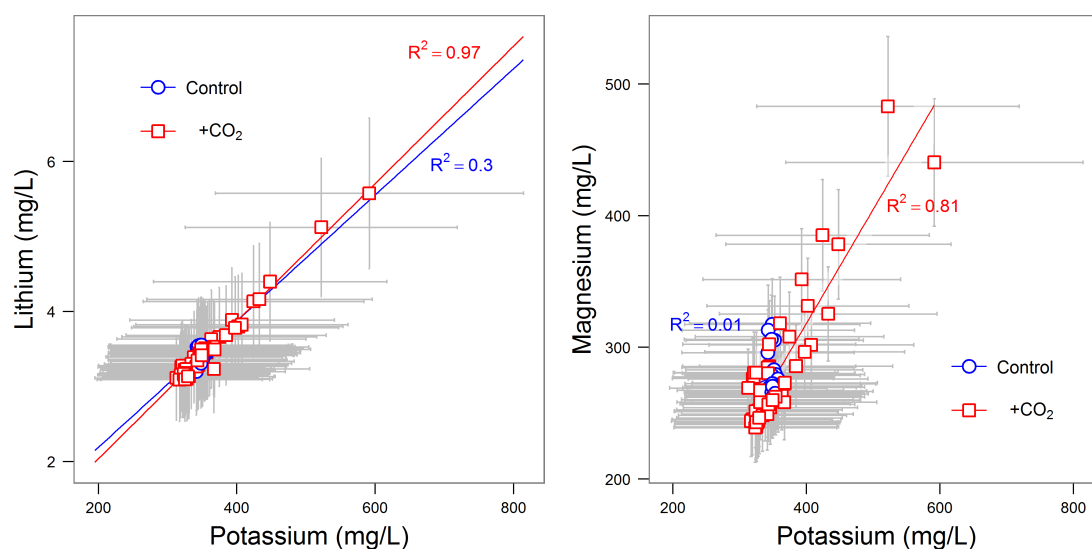
Figure 4.33: *Scatter plots of Ca vs Li (left), and Ca vs Mg (right) concentrations from control and +CO_2 batch experiments, aggregating data from all Utah experimental samples. Linear regression lines and R^2 values plotted separately for control and +CO_2. Error bars are 2s.*

Common elements associated with feldspars are Ca, Na, K and Al, therefore if feldspar dissolution was occurring significantly, then concentrations of these elements would be expected to increase. Calcium concentrations have already been assumed to be entirely due to carbonate dissolution, while Al concentrations actually decrease after the addition of CO_2. Sodium was not analysed for in any of the batch samples due to the difficulty in measuring Na against a strong matrix of NaCl (such as the *Crystal Geyser* spring water) with the ICP-MS method used for analysis. This leaves K as an indicator of feldspar dissolution, and there is certainly an increase in concentrations following the bubbling of CO_2, with a Type I classification (Table 4.10). The XRD analysis of the samples certainly confirm that there are feldspars present, with between 11.5 and 20.4 wt.% of samples *S1 - S4* comprising these minerals: variously albite, anorthite, microcline, muscovite and orthoclase. That Mg and Li also increase in a strongly correlated relationship would also indicate that, if feldspar(s) was dissolving then this also releases these elements; the collated data in Smith and Brown (1988) certainly shows that these fluid concentrations are

within the concentrations ranges of feldspar minerals.

Unfortunately, since bicarbonate (HCO_3^-) concentrations weren't measured, the stoichimetric test used in Chapter 3 (Section 3.10.3) can't be used to determine any relationship between K^+ and HCO_3^- which might demonstrate a release of bicarbonate ions with CO_2 'weathering' of feldspars, as per equation 1.5. It is therefore conjecture that feldspars are dissolving, and contributing K, Li and Mg to solution. In any case, if only the 8 trace elements of interest are considered, there are no apparent correlations between elements which may be associated with feldspar dissolution and these elements, just as with potential carbonate dissolution.

Mobilisation of the 8 trace metals is low, as already determined. Based on the apparent lack of any positive correlations between trace element concentrations and dissolution of minerals in the samples (as opposed to dissolution of newly precipitated minerals), combined with the assessment of mobility of metals from the batch experiments in Table 4.13, the conclusion therefore is that if trace metals are mobilised, they are likely sourced from mineral surfaces through ion exchange/desorbtion processes instead of any significant mineral dissolution. This is in contrast to the results of the North Sea experiments, where carbonates and feldspars were significant contributors to the batch experiment concentrations, but again only where trace metals were actually mobilised. Overall, the 8 trace metals considered are largely immobile during these experiments.

4.6   Conclusions

- Concentrations of 4 of the trace metals of interest (Cd, Cr, Hg, Pb) were not detected in CO_2-driven spring waters collected from the Green River area of Utah. Low concentrations (< 60 µg/l) overall were detected for As, Cu, Ni and Zn.

- All 8 trace metals have low abundance in 5 sandstone samples collected from outcrops of the Entrada, Wingate and Navajo sandstones in Utah and are, essentially, immobile with respect to CO_2-saturated fluids. There is, however, evidence from other studies that under reducing conditions (e.g. CO_2 + H_2S), trace metals may be more mobile, but which are re-deposited within the aquifer.

- The addition of CO_2 to batch experiments with spring water from *Crystal Geyser* and rock samples from the same area reduces experimental pH values to within the range of values for the springs in the Green River area, indicating capacity of the rock to buffer pH.

- Concentrations of major elements Ba, Ca, Mn and Sr reduced during the control period of the batch experiments, before increasing after the addition of CO_2 to within the range of the Green River springs. This is likely due to the precipitation of carbonate minerals from the *Crystal Geyser* spring water, and subsequent dissolution with CO_2. The effect of any dissolution of carbonates within the rocks is potentially masked by this process, which is apparent in the striking similarity in results between 4 different rock samples with varying mineralogy.

- Potassium, Mg and Li strongly correlate with each other in the batch experiments, and have concentration trends which show little change during the control period, but then slowly increase after CO_2 bubbling commences. In the absence of further evidence, it is speculated that this may be due to feldspar dissolution.

- Trace metal concentrations are very low in the batch experiments and do not correlate well with any of the major elements. Therefore, where present, trace metal concentrations in the batch experiments are unlikely due to mineral dissolution, and more likely the result of ion exchange/desorption processes. This is in contrast to the North Sea experiments which showed mineral dissolution as a major contributor to the concentrations of some metals.

- Ultimately, trace metals are low in abundance and mobility in the Utah Entrada, Wingate and Navajo aquifer sandstones, with batch experiments at atmospheric pressure failing to mobilise the trace metals of interest in significant quantities.

Environmental and Emissions Monitoring System (EEMS)

5.1 Overview

The Environmental and Emissions Monitoring System (EEMS) is a database of UK North Sea produced water constituents, with data submitted bi-annually to the system by oil and gas operators as required by their operating permits issued under The Offshore Petroleum Activities (Oil Pollution Prevention and Control) Regulations 2005 (2005) and The Offshore Petroleum Activities (Oil Pollution Prevention and Control) (Amendment) Regulations 2011 (2011).

Data includes measured and calculated emissions from 2006 onwards, and although primarily a joint industry and government resource, the data is publically available via the Department of Energy and Climate Change (DECC). Contact details are provided on the DECC EEMS portal at https://www.gov.uk/oil-and-gas-eems-database.

The most up-to-date data available for EEMS (supplied by DECC January 2015) reports data for offshore operating facilities, for the following grouped emissions of:

- Polyaromatic hydrocarbons (PAH)

- Benzene, toluene, ethylbenzene and xylenes (BTEX)

- Trace metals (As, Cd, Cr, Cu, Hg, Ni, Pb, Zn)

- Alkylphenols

- Organic acids

- Oil-in-water (OIW)

- Naphthalene, phenanthrene and dibenzothiophene (NPD)

- Inorganics (total phosphorous, chlorides, fluorides, total nitrogen, cyanides)[1]

- Total Organic Carbon (TOC)[1]

The full DECC guidance for monitoring methods, locations and reporting is given in the Department of Energy & Climate Change (2014) document Methodology for the Sampling and Analysis of Produced Water and Other Hydrocarbon Discharges.

Unsurprisingly, the majority of the data collected relates to hydrocarbon (oil and gas) compounds, since these are regulated to a maximum of 30 mg/L of OIW in produced water emissions, as per the 1992 Oslo-Paris (OSPAR) Convention and the subsequent follow up recommendations, specifically the Overview assessment of the implementation of OSPAR Recommendation 2001/1 for the management of produced water from offshore installations (OSPAR Commission, 2010). Trace metals are not currently regulated (see Introduction chapter), however DECC collects data on trace metals in emissions through EEMS, referred to as 'heavy metals' in their data.

Of interest to this study are the concentrations of trace metals in produced water emissions. The suite of trace metals reported to EEMS was used as the basis for the selection of the 8 trace metals focussed on for this thesis, and are: As, Cd, Cr, Cu, Hg, Ni, Pb and Zn.

5.1.1 Reporting periods

Data reporting to EEMS is carried out bi-annually, with reports submitted during 6 month periods. Reporting period H1 is January to June, submitted by 1st September, and period H2 is July to December, submitted 1st March. Data is usually from a single sampling of produced water i.e. not averaged data from several samples in a 6 month period. The number of facilities reporting to EEMS by reporting periods from 2006-H1 to 2014-H2 (January 2006 to December 2014) is shown in Figure 5.1. Since the cut-off for reporting H2 is March then at the time of writing not all data may have been received for 2014-H2.

---

[1]Recorded from 2010 onwards
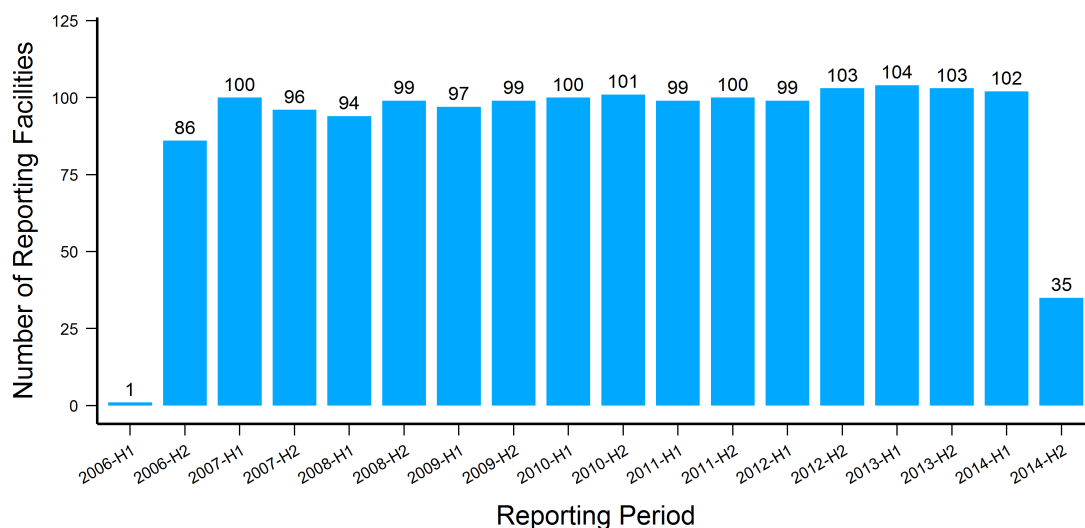
Figure 5.1: *Number of facilities (n) reporting to EEMS by Reporting Period. Bars annotated with n value.*

Figure 5.1 shows that on the scheme's introduction in 2006, only 1 facility reported to EEMS (*Fife FPSO - Uisge Gorm*). From 2007-H1 to 2013-H2 the mean number of reporting facilities has been ~ 99, although the total number of reporting facilities since 2006 is 116, indicating that facilities have begun reporting during the 2006 - 2014 period while some facilities have stopped, either temporarily or permanently. As noted above, data are not complete for 2014-H2, hence the drop in reporting facilities for this period.

A single facility may also report from more than one sampling point in the facility for each reporting period, for example the *Fife FPSO - Uisge Gorm* facility reported from three different sampling points for each period from 2006-H1 to when it stopped reporting to EEMS in 2008-H2. Examples of sampling points listed in the dataset include, but are not limited to, "sump tank", "slops tank discharge", "degasser outlet" and "overboard". These are pre-agreed sampling points as part of the permitting conditions and are located after produced water volumes have been calculated and any or all remedial treatment carried out.

5.1.2 Geographical locations

The locations of the facilities reporting to EEMS are given in Figure 5.2. Exact location data (X-Y coordinates) are not provided in EEMS, however facility names largely correspond to hydrocarbon fields since they are usually the producing facilities for that particular field. Therefore facilities have been plotted in the field locations, and all data associated with the facility is simply assumed to be relevant to that field.

One limitation to this approach is that some facilities deal with production fluids from several fields e.g. the *Amerada Hess AH-001* facility processes oil from the *Renee* and *Rubie* fields, produced from Northern North Sea (NNS) Upper Jurassic and Palaeocene reservoirs, respectively. Reported emissions data from *AH-001* are therefore an aggregate of mixed fluids and not necessarily representative of emissions which could be produced from the individual fields.

Also, since fields may be produced from a number of different stratigraphic horizons, EEMS data may represent bulk field fluid composition rather than for individual horizons. However, since the large majority of reporting facilities are named by field, the assumption is made that these facilities produce from only a single field, and that even with multiple horizons sampled, this is still indicative of field conditions.

One final potential issue with the data could be that sampling points are prone to contamination, given the working environment offshore. Factors such as corroding storage tanks could influence the

data, particularly with respect to the trace metal and inorganic concentrations. Emissions data should therefore be treated cautiously with respect to any conclusions drawn about individual fields' reservoir chemistry.
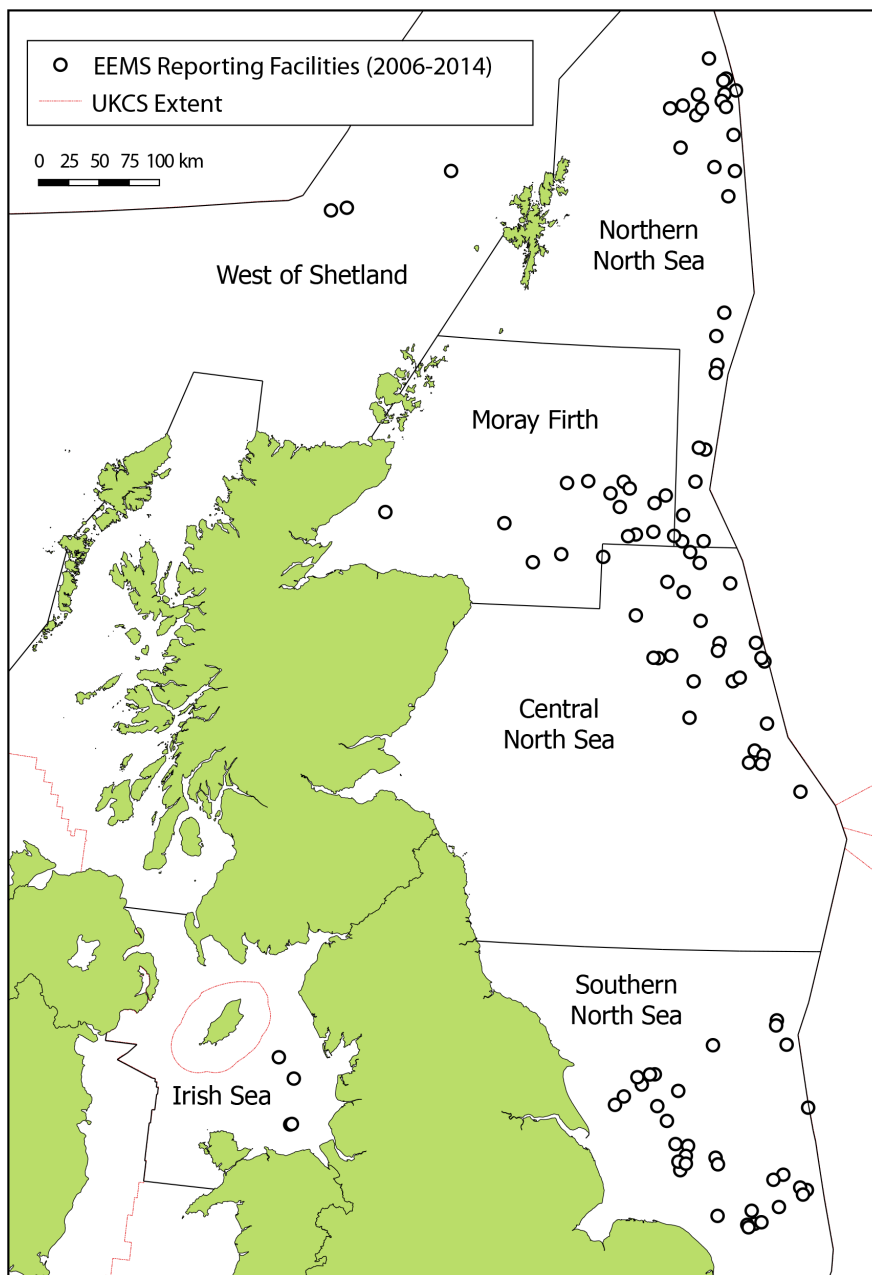

Figure 5.2: *Map of EEMS reporting facilities.*

5.2 Data appended to EEMS

In order to interrogate the EEMS data more extensively, data from other sources was appended to the EEMS dataset. The aim of this was to determine whether there were any significant influencing factors for the collected EEMS data, with particular focus on the 8 trace metals. Reporting facilities were linked to fields by matching names. Where there was more than one entry in EEMS for a field, the average values were calculated and linked to the field. Where a field had multiple areas designated in the map shapefiles provided by DECC, the EEMS data from a single facility was applied to all areas, and where multiple facilities exist with multiple field areas of the same name, then fields and facilities were matched in alphabetical order. The *AH001* facility data was linked to both *Renee* and *Rubie* fields. The data in the following subsections were added to EEMS.

5.2.1 Designated North Sea areas

The UK Continental Shelf (UKCS) is divided up into several areas for the purposes of delineating offshore exploration and production areas, Figure 5.2, including the Moray Firth, Central North Sea, the Irish Sea, etc, see list below. The area designations used in this study were taken from the North Sea Formation Waters Atlas (Geological Society Memoir No. 15, Warren and Smalley 1994) and the United Kingdom Oil and Gas Fields Commemorative Millennium Volume (Geological Society Memoir No. 20 2003), with more recent fields determined by reference to the areal extents mapped out in the British Geological Survey's series of offshore regional geology reports (e.g. The geology of the Moray Firth, British Geological Survey 1990). The extent of offshore activities reported to EEMS therefore covers the following areas:

- The Northern North Sea (NNS)
- The Southern North Sea (SNS)
- The Central North Sea (CNS)
- The Moray Firth (MF)
- The Irish Sea (IS)
- West of Shetland (WOS)

Two of the three facilities designated as WOS for the purposes of interrogating EEMS (*Clair Phase 1 Platform* and *Foinaven - FPSO Petrojarl*) were originally designated in the Geological Society memoirs as "Northern North Sea", however the BGS offshore reports designate them as "North and north-west of Scotland". Here "West of Shetland" is used for ease of reference.

5.2.2 Carbon dioxide

Concentration data for CO_2 gas found in UK North Sea fields is provided in the NW European Gas Atlas (Lokhorst, 1997) and the publications compiled in the United Kingdom Oil and Gas Fields 25 Years Commemorative Volume (Geological Society Memoir No. 20 2003). CO_2 concentrations as vol% are provided in Table 2-1 in the NW European Gas Atlas for 26 fields. Where data was available for matching facilities in EEMS, this was added to the EEMS dataset ($n = 15$). Where multiple values were given for CO_2 concentration, the average value was used (e.g. the *Hewett* field).

5.2.3 Salinity & other constituents

Salinity values, as mg/L total dissolved solids (TDS) were used, where available, with NaCl equivalent used in the absence of TDS. Values are from Geological Society Memoirs No. 14, No. 15 and No. 20

(Geological Society 1993; Geological Society 2003; Warren and Smalley 1994). Concentrations of Ba, Ca, Fe, K, Li, Mg, Sr, HCO_3^-, SO_4^{2-} and SiO_2 were also taken from these literature, together with pH, temperature ($^\circ$C) and initial reservoir pressure (psi). Where multiple horizons are recorded for a field, or maximum/minimum values are provided, then the average is taken and linked to the facility in the EEMS dataset.

5.2.4 Geological age & formation

Geological ages and formation names were taken from Geological Society (1993), Geological Society (2003) and Warren and Smalley (1994) for the main reservoir units, and matched to the EEMS reporting facilities by field name. Where fields comprise multiple reservoir units, then "Multiple" was recorded. Eleven geological ages were recorded from the literature: Devonian, Carboniferous, Permian, Triassic, Jurassic, Mid-Jurassic, Upper Jurassic, Lower Cretaceous, Upper Cretaceous, Palaeocene and Eocene.

5.3   EEMS Trace Metal Data

The 8 trace metals of interest (As, Cd, Cr, Cu, Hg, Ni, Pb & Zn) were selected from the EEMS dataset, and their concentrations analysed against a number of factors, to determine whether any trends could be identified in the data.

Firstly, concentration data for all years 2006 - 2014 was summarised using box-and-whisker plots for the 8 trace metals, Figure 5.3. The data have been subdivided further based on UKCS area and plotted on $\log_{10}$ y-axes to better display the large ranges in concentrations. The boxes shows median value, lower and upper quartiles (interquartile range, *IQR*). Whiskers are 1.5×*IQR*. Open circles are outlier values > 1.5×*IQR* and white diamonds indicate the mean value. Since the data is plotted on a $\log_{10}$ scale, all zero values are discarded for the plot, and hence the calculations of mean, median, *IQR*, and outliers is based on all values > 0. The median values ($\tilde{x}$) for each element calculated for values > 0 are given in Table 5.1, together with the number of concentration values (n) used to calculate $\tilde{x}$.

| Element	All Areas max.	WOS $\tilde{x}$	n	NNS $\tilde{x}$	n	MF $\tilde{x}$	n	CNS $\tilde{x}$	n	SNS $\tilde{x}$	n	IS $\tilde{x}$	n
As	784	0.6	28	1.5	617	1.9	281	5.9	423	20	198	31	53
Cd	543	0.14	24	0.24	564	0.22	243	0.9	399	32	151	1.2	38
Cr	131,900	0.68	27	2.6	627	2	284	3.7	443	11	200	57	50
Cu	4,845	0.3	27	2.3	625	1.5	275	5.6	436	20	202	31	52
Hg	119	0.22	23	0.15	527	0.45	252	0.65	336	2.6	93	3.6	40
Ni	24,931	3	30	3	626	3.4	285	6.8	445	20	217	29	51
Pb	33,790	0.48	27	1	596	0.5	274	9	420	170	197	4.5	51
Zn	162,500	8.8	33	14	655	21	287	79	452	2300	260	62	54

Table 5.1: *Maximum reported trace metal concentrations of all UKCS areas (µg/L), 2006 - 2014, with median ($\tilde{x}$) concentrations (µg/L) per UKCS area, and number of reported concentration values > 0 (n). WOS: West of Shetland. NNS: North North Sea. MF: Moray Firth. CNS: Central North Sea. SNS: Southern North Sea. IS: Irish Sea.*

The UKCS areas are ordered generally north to south as the graphs are read left to right, with the West of Shetland (WOS) considered the most northerly area, with the Southern North Sea (SNS) and Irish Sea (IS) areas given as the most southerly. Given this order, there is an overall increase in median concentrations for each of the elements from north to south, with median concentrations an order of magnitude higher in the SNS and IS than in WOS or Northern North Sea (NNS) for most metals, and up to two orders of magnitude higher for Cd, Pb and Zn. Average concentrations follow the same trend, and on a $\log_{10}$ scale are overall very similar to the median values in most cases.

While median and average values are different for each UKCS area and show a north to south increase, the range of data for each area - as defined by the whiskers and outliers - are effectively the same. The concentration data for Cd, Pb and Zn do, however, show a distribution toward higher concentrations in the SNS than other areas, with maximum concentrations for these elements in the SNS exceeding those in other areas. Broadly, however, taking into account the full range of for all metals then the ranges are very similar across all UKCS areas, Figure 5.3.

With the data subdivided by the geological age of the reservoir, the same plotting technique can be applied, Figure 5.4. Concentrations of the 8 trace metals exhibit wide ranges, spanning up to 5 orders of magnitude within a single reservoir age. Carboniferous, Permian and Triassic reservoirs have median concentrations consistently higher than later ages for most of the trace metals, Figure 5.3. The Southern North Sea reservoirs comprise these horizons and so this ties with the elevated concentrations exhibited by the SNS reservoirs.

Clearly the reservoirs contributing to production water in each area and by each age are extremely heterogeneous, although some ages appear more homogeneous with regard to particular elements, for example the Cretaceous age reservoirs, Figure 5.4.
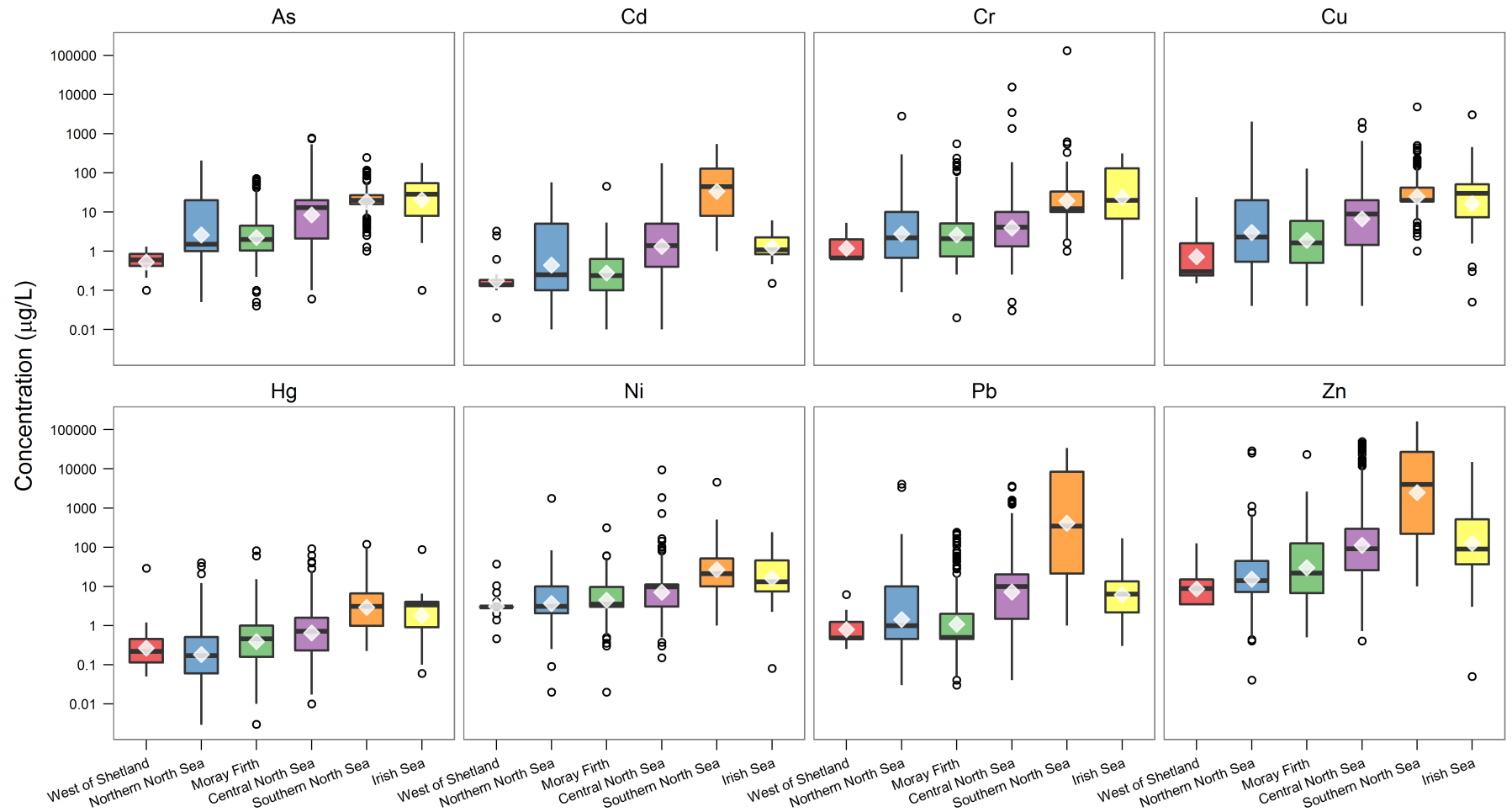
Figure 5.3: *Box-and-whisker plot of trace metal concentrations 2006 - 2014, grouped by UKCS area. Box shows median value, lower and upper quartiles (interquartile range, IQR). Whiskers are 1.5×IQR. Open circles are outlier values > 1.5×IQR. White diamond gives mean value. Note y-axes are $\log_{10}$ scale. UKCS areas are ordered generally north to south as graphs are read left to right. Median and n values given in Table 5.1.*
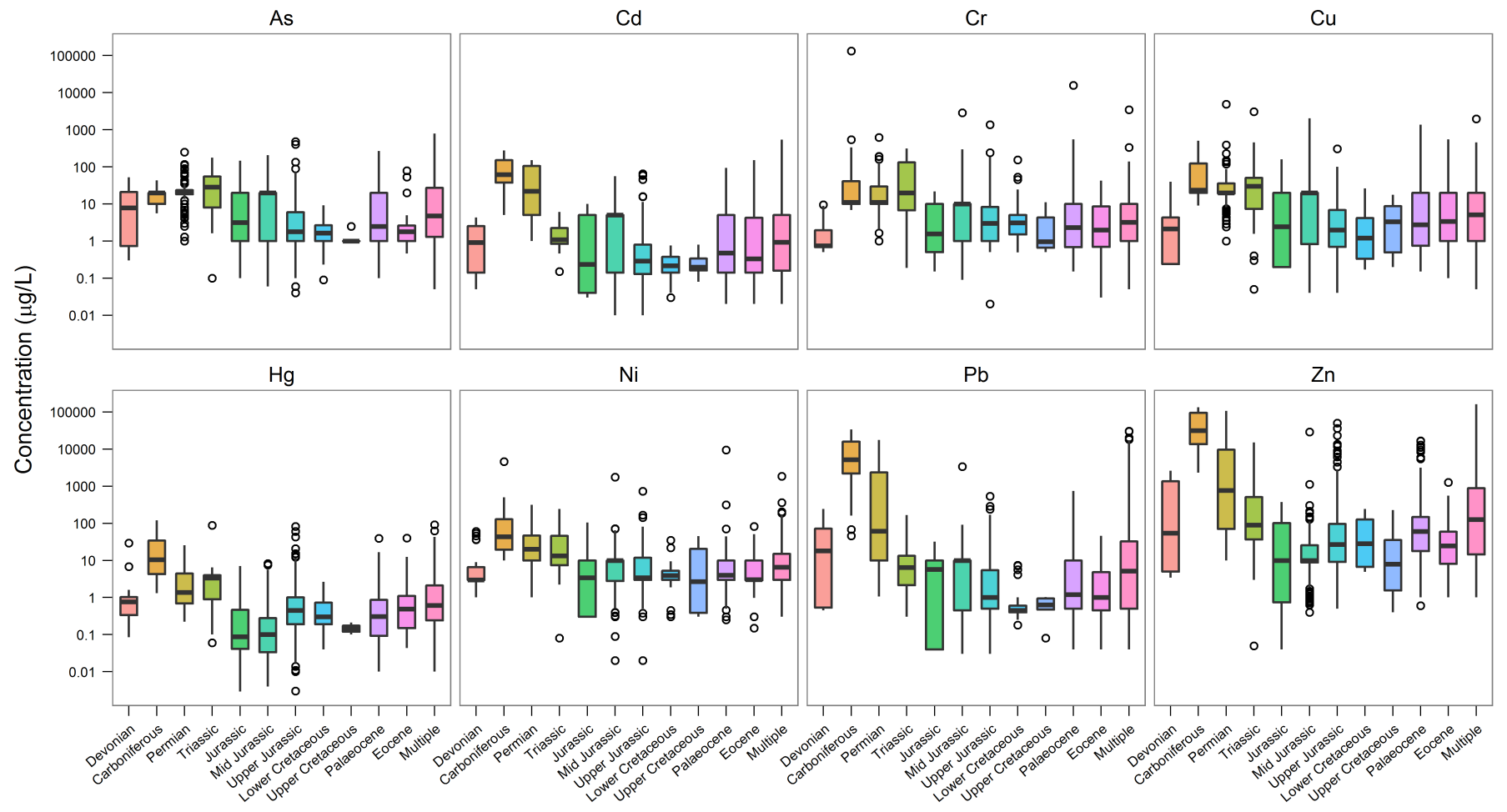
Figure 5.4: *Box-and-whisker plot of trace metal concentrations 2006 - 2014, grouped by geological age of main reservoir. Box shows median value, lower and upper quartiles (interquartile range, IQR). Whiskers are 1.5×IQR. Open circles are outlier values > 1.5×IQR.*

While Figure 5.3 gives a visual indication that Southern North Sea concentrations are generally higher than other areas of the UKCS, a Student's t-test was applied to the EEMS trace metal data to determine whether the means of the SNS data are statistically the same as the other areas. This is the null hypothesis, and Student's two-sample t-test was applied to each pairing of SNS with other UKCS areas, for each of the 8 trace metals. The calculated t and p values are given in Table 5.2 and compared with the 95% confidence limit t-value calculated from the degrees of freedom (n - 2). Where t exceeds the t-value, then the null hypothesis is rejected and the mean of the metal value in that UKCS area is statistically different to the SNS data, within the 95% confidence level. p values are the level of confidence that the means are statistically different, with lower numbers giving higher confidence.

	WOS		NNS		MF		CNS		IS	
	t	p	t	p	t	p	t	p	t	p
As	1.529	0.127	**5.100**	< 0.001	**3.868**	< 0.001	1.841	0.066	0.262	0.794
Cd	**2.722**	0.007	**11.101**	< 0.001	**7.697**	< 0.001	**8.938**	< 0.001	**3.471**	< 0.001
Cr	0.339	0.735	1.439	0.150	0.951	0.3417	1.138	0.255	0.364	0.716
Cu	0.942	0.347	0.965	0.335	**2.463**	0.01397	0.834	0.404	1.555	0.120
Hg	0.605	0.546	**3.041**	0.002	1.544	0.1231	1.94	0.053	0.239	0.812
Ni	0.51	0.610	**2.123**	0.034	1.407	0.1597	1.326	0.185	0.463	0.644
Pb	**2.477**	0.014	**10.656**	< 0.001	**7.104**	< 0.001	**8.059**	< 0.001	**3.441**	< 0.001
Zn	**2.916**	0.004	**12.516**	< 0.001	**8.260**	< 0.001	**9.365**	< 0.001	**3.903**	< 0.001
Degrees of freedom	498		1297		825		1105		541	
t-value[†]	1.965		1.962		1.963		1.962		1.964	

Table 5.2: *t and p values of Student's two-sample t-test, to test the null hypothesis against EEMS Southern North Sea (SNS) trace metal data.* [†] *Calculated t-value at 95% confidence level for a two-tailed test [a]. Bold values reject the null hypothesis with trace metal data means significantly different to SNS at the 95% confidence level.*

---

[a]http://www.danielsoper.com/statcalc3/calc.aspx?id=10

The null hypothesis is rejected at least once for 7 of the 8 trace metals, showing that SNS data are significantly different to other UKCS areas. The NNS data are significantly different at the 95% confidence level for As, Cd, Hg, Ni, Pb and Zn, the most of all the UKCS areas. The Moray Firth is statistically different to SNS for As, Cd, Hg, Ni, Pb and Zn while Cd, Pb and Zn concentrations are also all significantly different to SNS in WOS, CNS and IS, Table 5.2. Produced waters from fields outside of SNS are therefore highly likely to produce formation waters which have lower concentrations of these metals than the SNS, based on the data visualised in Figure 5.3.

5.3.1 Time-dependent trends

Aggregating the concentration data for all reporting facilities and the entire timespan of the EEMS dataset shows that these trace metals are clearly highly variable within each area, as shown by the spread of data of up to 6 orders of magnitude for individual elements within a geographical area (e.g. Cr, Central North Sea), Figure 5.3. Concentration data were then assessed to understand whether there are any notable temporal changes in the data. Data were aggregated by area again for all reporting facilities, and the bulk median concentrations calculated for each year. Unlike the box-and-whisker assessment, the calculations of median values included zero values. In this case, zero values were used only for facilities which reported > 0 m^3 of produced water. It was assumed that where both concentration and produced water values were reported as 0 then no fluids had been tested, and therefore the facility was simply submitting a value to EEMS as required by their permit. Calculated $\tilde{x}$ are plotted in Figure 5.5.
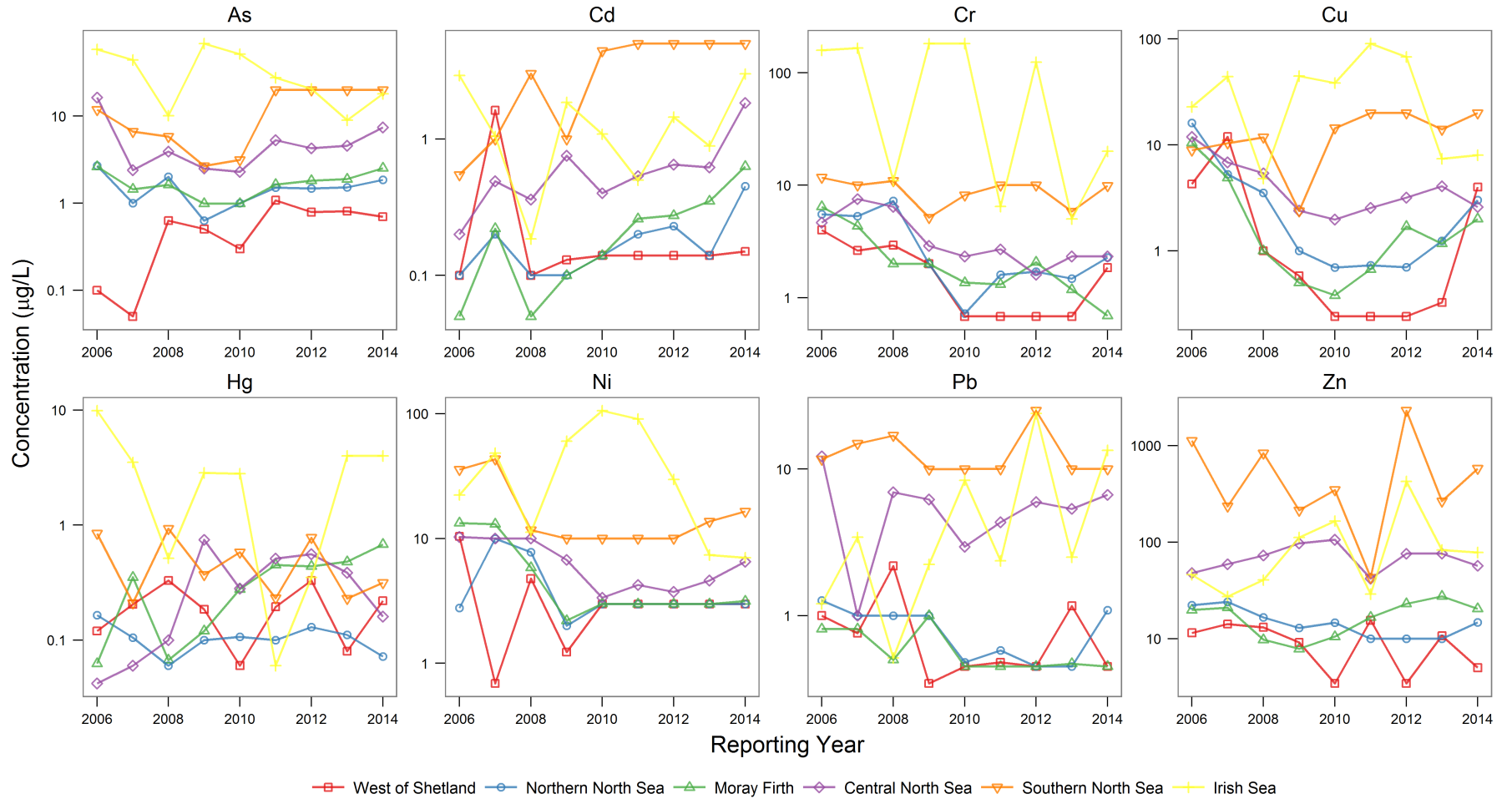
Figure 5.5: *Time series median trace metal concentrations per UKCS area, aggregating all reporting facilities for the period 2006 - 2014. Note log₁₀ y-axes.*

Figure 5.5 also uses a $\log_{10}$ y-axis to show the data trends more clearly. For the majority of the elements and UKCS areas, bulk median concentrations do not appear to change systematically with time. Median values are highest for the Irish Sea and Southern North Sea areas, being up to 10 times higher in most cases than the other areas. The West of Shetland generally has the lowest calculated median concentrations. These are the same conclusions drawn from the box-and-whisker plot, Figure 5.3.

Median Cd concentrations appear to be increasing between 2006 and 2014 for the Northern North Sea, Moray Firth, Central North Sea and Southern North Sea by up to an order of magnitude, whereas Cr concentrations are declining for West of Shetland, Northern North Sea, Moray Firth and Central North Sea, Figure 5.5.

With the exceptions of Cd and Cr, aggregated trace metal concentrations from all reporting facilities appear to have remained relatively stable over the 8 years of data reported to DECC so far, although individual facilities may exhibit their own trends which do not follow those of the wider geographical areas. This was not assessed for all reporting facilities, however the data was investigated for the facilities relevant to this thesis. The reporting facilities closest to the North Sea sandstone samples used for the batch experiments reported in Chapter 3 (*Captain*, *Cormorant*, *Thistle*) were selected, and their concentrations are shown in Figure 5.6.
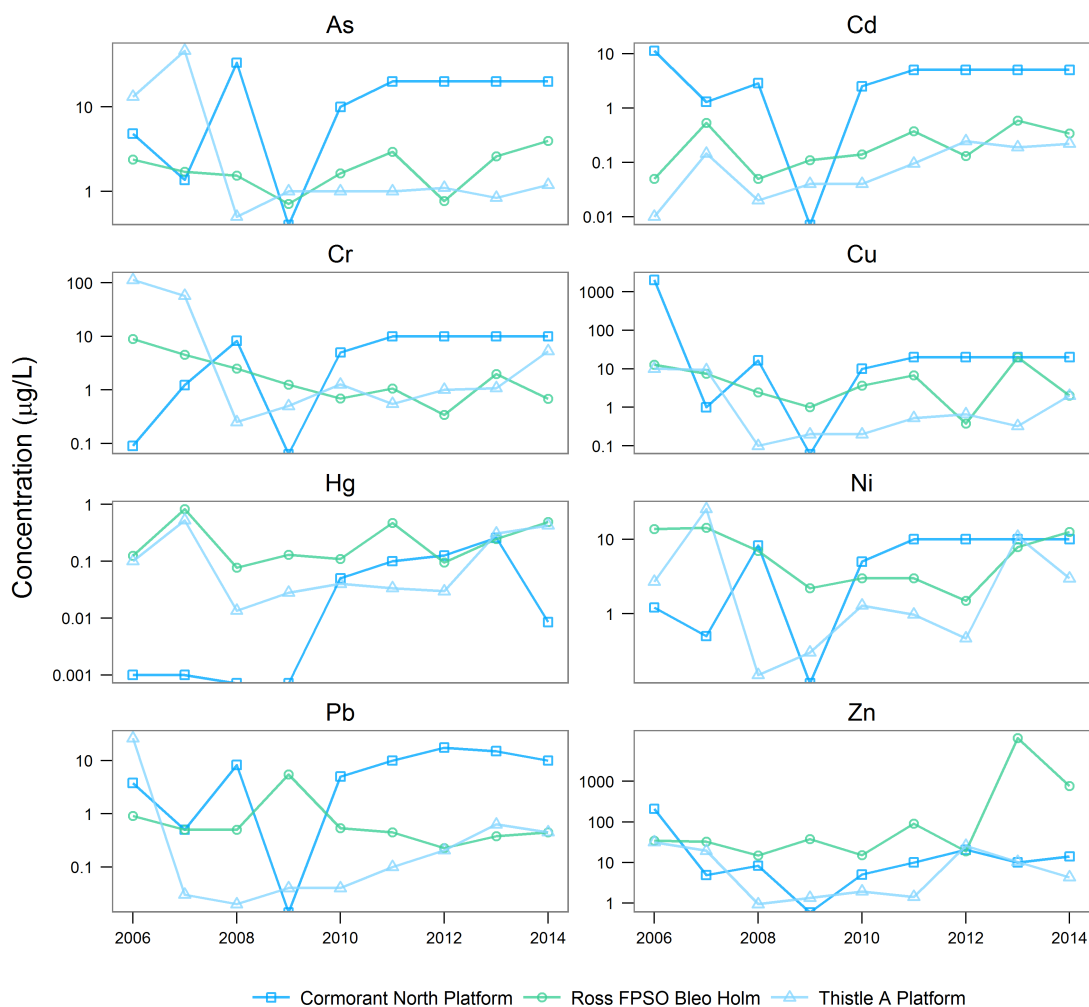
Figure 5.6: *Time series median trace metal concentrations for Ross, Cormorant North and Thistle facilities, for the period 2006 - 2014. Note $\log_{10}$ y-axes.*

The selected facilities are *Ross FPSO*[2] *Bleo Holm*, *Cormorant North Platform* and *Thistle A Platform*. Since the *Captain* field is no longer operations, the *Ross FPSO Bleo Holm* facility is the nearest currently operating platform, and it is assumed that it will most likely be reporting for fields producing from similar reservoir horizons as *Captain*. Since each facility reports bi-annually and from a number of different sampling points on the facility, the median concentrations for each year were again calculated, using the same criteria of produced water volume > 0 m^3. Note that again concentrations in Figure 5.6 are plotted on $\log_{10}$ y-axes since there are large variations in the values.

The *Cormorant North Platform* and *Thistle A Platform* are both located in the Northern North Sea, while *Ross FPSO Bleo Holm* is located in the Moray Firth. The story for these individual facilities is the same as for the wider areas in which they are located: concentrations are relatively constant from 2006 until 2014. Cadmium shows a tenfold increase in concentrations for *Ross FPSO Bleo Holm* and *Thistle A Platform*, and Pb shows an increase for *Thistle A Platform* since 2008. And there is a decrease in median concentrations for Cr at the *Ross FPSO Bleo Holm* facility, Figure 5.6. These are exceptions, however, to the overarching consistency of concentrations for these facilities.

5.3.2 Correlating trace metals with supplementary data

A correlation matrix was produced, Appendix D (Figure D.12), to determine whether any correlations exist between the trace metal EEMS data, and selected other variables. The 8 trace metals were tested against: total hydrocarbons (H/C), reservoir temperature (T), initial reservoir pressure, total dissolved solids (TDS), pH, Ca, Fe, K, Mg, Na, and chlorides. Pearson correlation coefficients were generated for calculated linear regressions on cross-plotted pairs of data. The EEMS data was aggregated into a mean for each reporting facility, spanning the period of 2006 - 2014. Calculating the mean EEMS data was required in order that facility data could be compared with data obtained from the literature for other variables such as pH, TDS, Na, etc., of which there is usually only a single value published per field. Field data was matched with facility data based on similarity of names, however it is acknowledged firstly that an EEMS facility may be reporting mixed fluids from a number of fields, and secondly that the field data may have changed since measurements were taken during exploration or initial production.

The strongest correlations, with Pearson correlation coefficients ranging between 0.70 and 0.98 were determined to be between TDS and the major elements reported in the literature (Ca, Fe, K, Mg, Na, Cl). This is of no surprise since TDS is the sum of, among others, major elements in solution. Subsequently, there are strong correlations between these elements, with correlation coefficients ranging between 0.63 and 0.81 for Fe, K, Mg and Na. Calcium correlates poorly with other major elements. Sodium and Cl are the most strongly correlated pair of elements (R^2 = 0.96), Figure 5.7a, which is to be expected given that formation waters in the North Sea basin are dominated by NaCl brines.

TDS also correlations well with pH, Figure 5.7b, with an R^2 of 0.84 and showing a negative trend. There is a north-to-south increase in salinity in UK North Sea fields, with the gas fields of the Southern North Sea having the lowest pH's and highest salinities. The low pH values may be indicative of CO_2 content in gas fields. Using available literature data on % volume CO_2 concentrations, a moderate correlation (R^2 = 0.60) between decreasing CO_2 and increasing pH is apparent. Increased CO_2 could lead to increasing TDS, however the high TDS formation waters of the Southern North Sea are most likely the result of dissolution the regional Zechstein evaporites than from large scale dissolution of the reservoirs from CO_2 entrainment. Therefore, while pH and TDS correlate well, they are probably coincidentally correlated and not co-dependent.

The trace metal data from EEMS does not correlate strongly with any of the supplemental data used from the literature, Figure D.12. Lead and Zn appear to correlate well with Cd, Figures 5.7c and 5.7d, but only for the Southern North Sea facilities. Again, correlation is not causation and with no strongly identifiable relationship to Cd of any other variable considered, it could be simple coincidence that these

---

[2]Floating Production Storage and Offloading

elements correlate. No Southern North Sea rock samples were used in the batch experiments, which may have established experimentally some relationship between these elements and a process which may mobilise them. Future experimental work should consider using core samples from the Southern North Sea to try and determine which metal mobilisation processes exist.
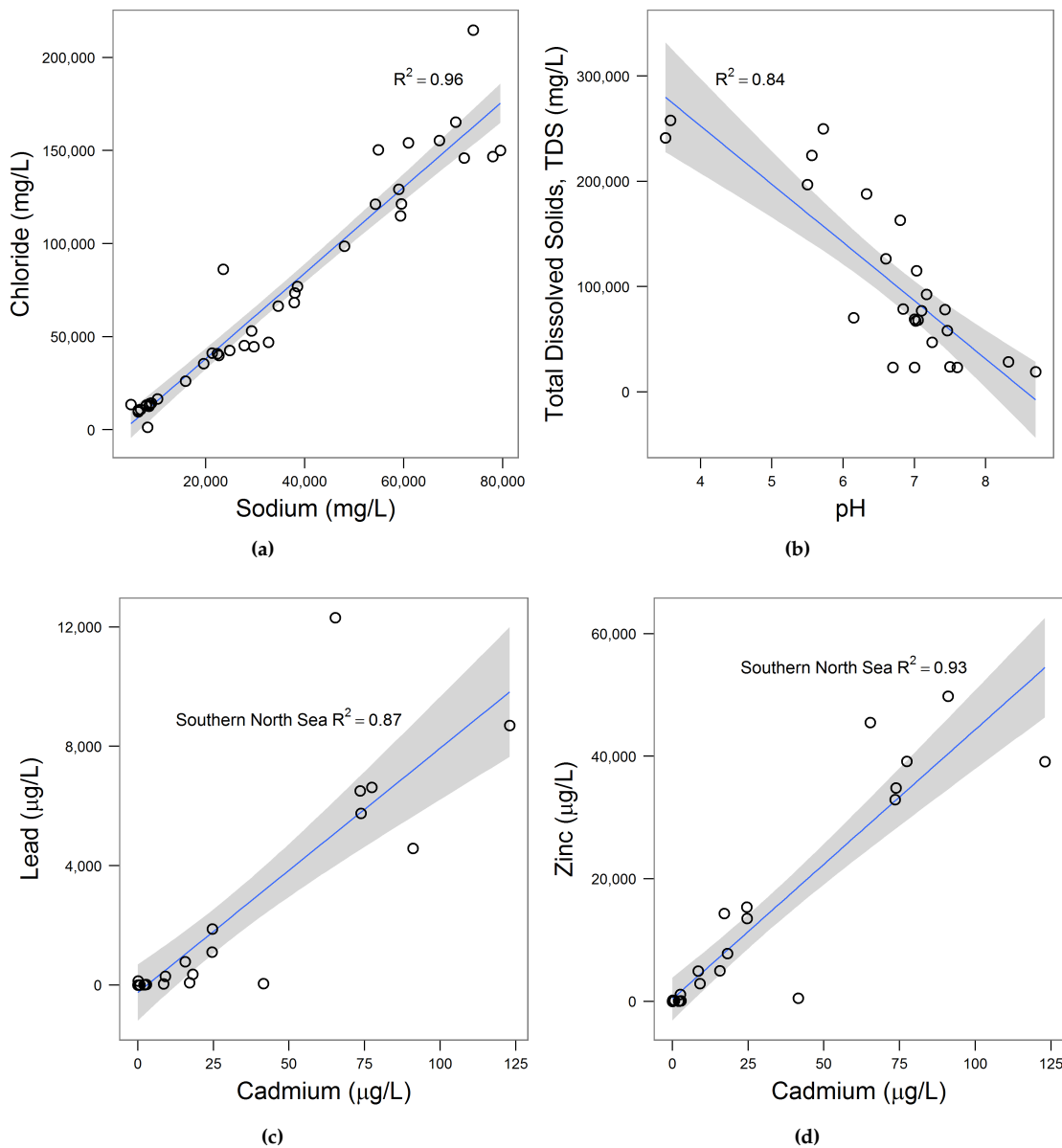
Figure 5.7: *Crossplots of UK North Sea literature well data. Linear regression (line) and standard error (shaded areas) plotted, with associated R^2 value. (a) Na and Cl concentrations (mg/L) (b) pH and TDS concentrations (mg/L) (c) Cd and Pb concentrations (d) Cd and Zn concentrations (μg/L).*

5.3.3 Comparison with batch experiment data

The concentration data for the 8 trace metals of interest can be compared between the EEMS dataset and the batch experiments carried out for this thesis. By comparing the experimental data of leached trace metals from North Sea reservoir sandstones with produced waters, the experimental data can be put into the context of UK North Sea activities operating under existing environmental guidelines. How the experimental data compares could inform on decisions to be made with regard to future environmental regulations for offshore UK CO_2 storage.
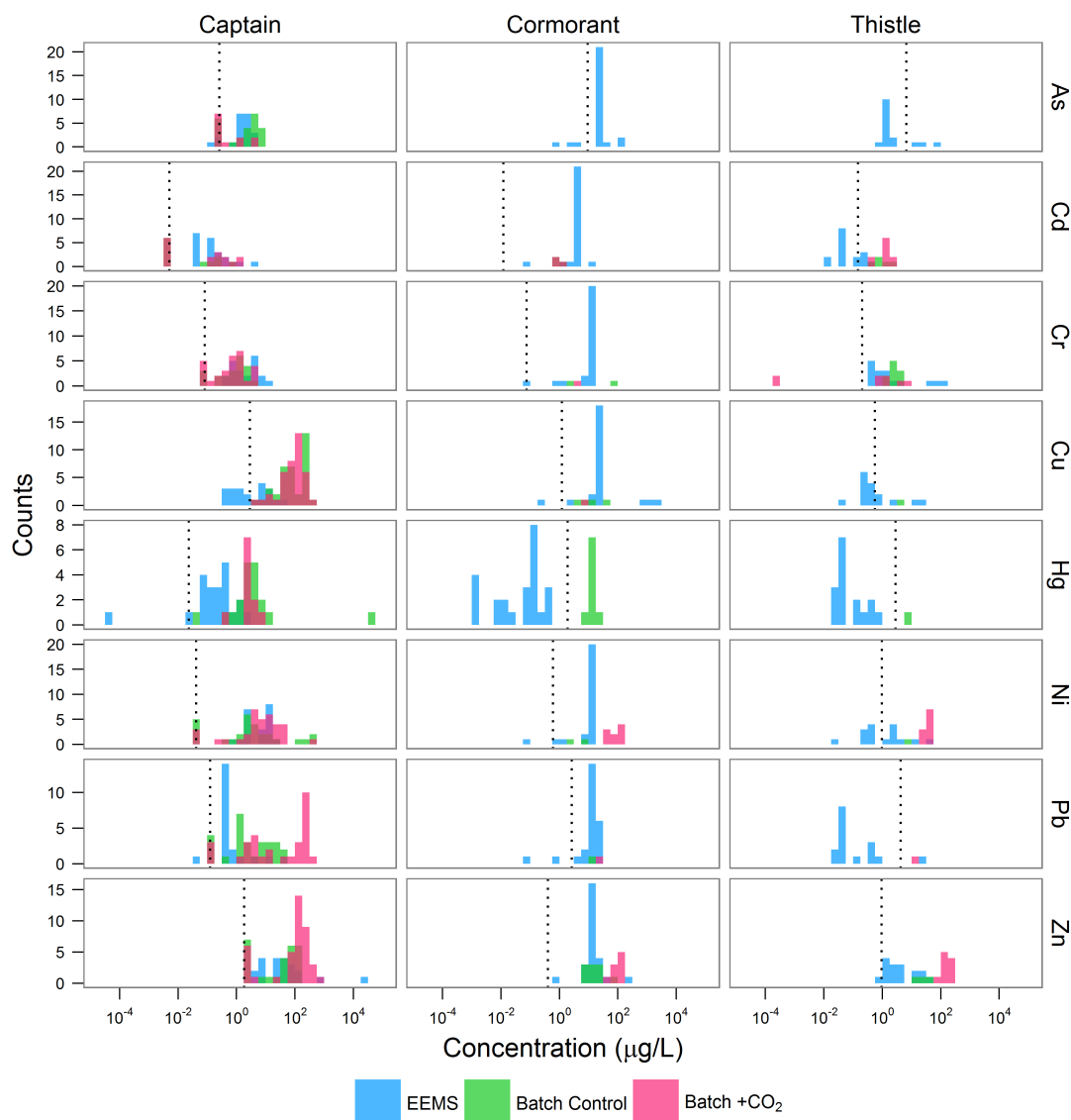
Figure 5.8: *Batch experiment concentration data for Captain, Cormorant and Thistle samples (μg/L) compared with data submitted to EEMS for the equivalent reporting facilities, plotted as histograms. Note log_{10} x-axes. Dotted vertical lines denote analytical detection limits for the experimental values.*

The experimental data and the EEMS data are plotted as histograms in Figure 5.8, divided by field (as per Figure 5.6) and by trace metal. The experimental data has also been split by control and $+CO_2$ results. Since there is, again, a very wide range of values over several orders of magnitude, the histograms are plotted on log_{10} x-axes and therefore necessitates the exclusion of zero values. Zero values in the experimental data referred to concentrations less than the analytical detection limit (LOD, Chapter 2)

and so these detection limits are marked as dotted lines in the plots. Detection limits are not published with the EEMS dataset.

Due to few samples taken for the *Cormorant* and *Thistle* experiments, combined with many samples below analytical detection limits, there are few data to compare with the *Cormorant North Platform* and *Thistle A Platform* EEMS data, Figure 5.8. There are significantly more data, however, for the *Captain* experiments to compare with the *Ross FPSO Bleo Holm* facility, as all experimental data collected for the experiment were used (samples *SA7* and *SA10*, grain and chip sample sizes).

Data show again that elements such as Ni, Pb and Zn are higher in concentrations for the $+CO_2$ experiments than for the controls, as already discussed in Chapter 3 (North Sea). Looking at the *Captain* data, Figure 5.8, all control and $+CO_2$ batch concentrations of As, Cd, Cr and Ni lie within the range of concentrations reported to EEMS. For Pb and Zn, the $+CO_2$ concentrations lie above the EEMS range, with the control data being within the range. Copper and Hg exceed the EEMS range for both control and $+CO_2$ experiments. For *Cormorant*, batch concentrations of As, Cd, Cu, Pb and Zn do not exceed EEMS, with Cr and Hg exceeding with the control data, and Ni exceeding for the $+CO_2$ experiments. And with *Thistle*, the experimental values exceeding EEMS are both control and $+CO_2$ Cr data, Hg control, and Zn $+CO_2$ data, Figure 5.8.

This is summarised in Table 5.3, where ✗ denotes non-exceedance of the EEMS data range by batch experiment data, ✓ denotes batch experiment concentrations exceed EEMS, and '< LOD' denotes where batch values were not recorded above the analytical detection limit.

Element	Captain		Cormorant		Thistle	
	Control	$+CO_2$	Control	$+CO_2$	Control	$+CO_2$
As	✗	✗	< LOD	< LOD	< LOD	< LOD
Cd	✗	✗	✗	< LOD	✓	✓
Cr	✗	✗	✓	✗	✗	✗
Cu	✓	✓	✗	✗	✗	< LOD
Hg	✓	✓	✓	< LOD	✓	< LOD
Ni	✗	✗	✗	✓	✗	✗
Pb	✗	✓	✗	✗	< LOD	✗
Zn	✗	✓	✗	✗	✗	✓

Table 5.3: *Summary of batch experiment trace metal concentrations exceeding the EEMS data for each field considered.*

Batch experiment Hg concentrations are consistently elevated above the EEMS concentrations, and Hg falls below detection limits only for the $+CO_2$ experiments. This is most likely a symptom of the Hg washout issue described in the Methods (Section 2.5.2.2). Hg concentrations leached during the batch experiments are most likely much lower than recorded.

Aside from Hg, no single element appears to be consistently leaching during the batch experiments in concentrations which exceed those reported by individual EEMS reporting facilities. Zinc concentrations do exceed EEMS for the $+CO_2$ experiments for *Captain* and *Thistle*, while the control data remains within the EEMS range. This could be an indication that, if CO_2 were to be injected into these fields, that produced waters during the storage operations would contain higher concentrations of Zn than would normally be produced. Field experiments carried out by Kharaka *et al.* (2006); Peter *et al.* (2012); Trautz *et al.* (2013) appeared to show, however, that the effect of CO_2 injection can be short lived in terms of increasing concentrations of dissolved constituents. Therefore, while concentrations may exceed regular, or historic, oil and gas activities then this may only be a temporary effect and of little long-term concern.

If the batch experiment data, including *Field X*, is aggregated by all the control and $+CO_2$ concentrations, then a comparison can be made with the whole EEMS dataset. This will give an indication of how the batch experiments' data overall compares with produced waters for the whole UK North Sea area.

These data are shown in Figure 5.9 as box-and-whisker plots, subdividing the data by trace metal, with concentrations plotted on $\log_{10}$ axes. The median ($\tilde{x}$) and number of values (n) are tabulated in Table

5.4, and are calculated based on all values > 0 to remain consistent with the exclusion of 0 values when plotting data on a logarithmic axis for the box-and-whisker diagram. The maximum predicted no-effect concentrations ($PNEC_{max}$) were also calculated from the sum of maximum average seawater background concentrations and the OSPAR PNEC values (Tables 1.3 and 1.4 of the Introduction, respectively), and added to Figure 5.9. The calculated $PNEC_{max}$ values are given in Table 5.4. $PNEC_{max}$ is an indication of the maximum concentrations of these metals which should be overboarded into the North Sea, based on broad global seawater composition.
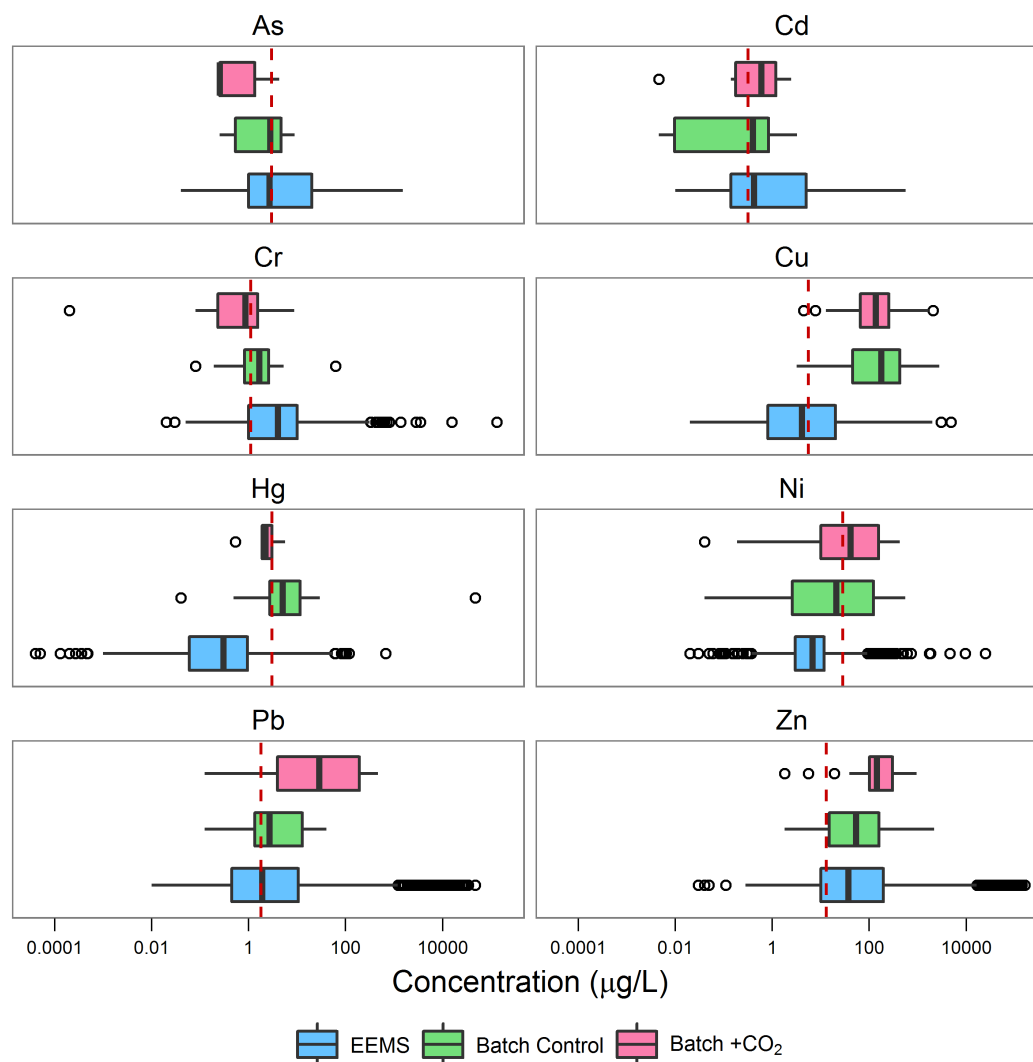
Figure 5.9: *Box-and-whisker plot of aggregated batch experiment concentration data for Captain, Cormorant, Thistle and Field X samples (µg/L) compared with all data submitted to EEMS. Box shows median value, lower and upper quartiles (interquartile range, IQR). Whiskers are 1.5×IQR. Open circles are outlier values > 1.5×IQR. White diamond gives mean value. Note x-axes are $\log_{10}$ scale. Dashed line denotes estimated maximum predicted no effect concentrations ($PNEC_{max}$). Median, n and $PNEC_{max}$ values given in Table 5.4.*

Median concentration values of both control and +CO₂ experimental data are greater than the median EEMS values for 5 of the 8 trace metals considered: Cu, Hg, Ni, Pb and Zn. Medians are the same, or less, for As, Cd and Cr. +CO₂ medians are also slightly higher than the controls in most cases, indicating some effect of CO_2 in mobilising these elements, but the range of concentration values of the experimental results do not exceed the upper range of EEMS values. The exception is a single Hg outlier for the control experiments, which can be attributed to the ICP-MS washout problem.

As shown in Figure 5.3, the distribution of metals concentrations by UKCS area tends to be for lower concentrations in the Northern areas of the North Sea (Northern North Sea to Central North Sea), and higher concentrations in the Southern North Sea. Given that the samples used in the batch experiments were from the Moray Firth and Northern North Sea areas, it would be expected that concentrations remained within the range since, firstly, concentrations would be expected to be at the lower end of the range (Figure 5.3), and secondly they do not significantly exceed individual fields' concentrations (Figure 5.8). If a sample from the Southern North Sea had been used in the batch experiments, it might be expected that batch concentrations would range further towards the upper end of the EEMS values, and may even exceed them. However, without data this is speculation only.

The comparison of EEMS and experimental data with $PNEC_{max}$ (Figure 5.9, Table 5.4) shows that median data in half of the EEMS cases is higher than $PNEC_{max}$ (Cd, Cr, Pb, Zn), although not significantly so. Median experimental values, both control and $+CO_2$, are higher than $PNEC_{max}$ in most cases, Figure 5.9. Copper, Pb and Zn are significantly so for the $+CO_2$ data being, respectively, 25, 17 and 10 times higher than $PNEC_{max}$. Therefore, while the overall range of concentrations of the batch experiments does not exceed the EEMS data, the median values are higher than EEMS and exceed the calculated $PNEC_{max}$ value more often.

Caution should be taken when interpreting this result, however. As described in the Introduction (Section 1.2.7), the PNEC (or $PNEC_{max}$ here) should be compared with a modelled predicted concentration in the environment (PEC) in order to determine whether mitigation of production water trace metal loads is desirable. The PEC will be site specific, and does not depend on concentrations alone. The EEMS data also do not reveal whether the water has been treated prior to disposal, although the DECC guidance (Department of Energy & Climate Change, 2014) does stipulate that sampling occurs at the final stage of produced water handling, therefore it would not be unreasonable to assume that some treatment for trace metals has occurred in many instances. Clearly this differs from the experimental data, where samples are untreated.

The conclusion drawn here is that with weak CO_2 acid leaching, batch experiments were not able to mobilise concentrations of the 8 trace metals of interest in sufficient concentrations to exceed the total EEMS range for the UK North Sea, however median concentrations are often higher than EEMS and exceed OSPAR recommendations for produced waters. Based on this assessment, produced waters from CO_2 storage and CO_2-EOR may require treatment for trace metal loads before disposal in the North Sea, in order for concentrations to remain comparable to current offshore UK hydrocarbon activity. Whether this treatment is additional to existing operations is not clear, however.

Chemical	EEMS		Control		$+CO_2$		$PNEC_{max}$[†]
	$\tilde{x}$	n	$\tilde{x}$	n	$\tilde{x}$	n	
As	2.7	1,845	2.8	24	0.26	12	3.0
Cd	0.42	1,817	0.42	22	0.59	31	0.32
Cr	4	1,851	1.6	33	0.86	38	1.1
Cu	4.1	1,850	180	59	140	53	5.6
Hg	0.3	1,841	5	29	2.2	11	3.05
Ni	6.7	1,843	21	53	41	80	28.6
Pb	1.9	1,833	2.7	28	30	32	1.8
Zn	37	1,872	53	56	140	79	13

Table 5.4: *Median ($\tilde{x}$) concentrations (μg/L) of all EEMS and all North Sea control and $+CO_2$ batch experiment data, and number of samples (n) used in calculation. Zero values removed from calculation to remain consistent with box-and-whisker plot, Figure 5.9. [‡]Estimated maximum predicted no effect concentration (PNEC), calculated from OSPAR PNEC guidelines (Table 1.4) and maximum background concentrations from literature (Table 1.3).*

5.4   Conclusions

- Data submitted to EEMS from 2006 to 2014 show that concentrations of 8 trace metals (As, Cd, Cr, Cu, Hg, Ni, Pb and Zn) in produced waters are generally highest from reservoirs in the Southern North Sea.

- Median concentration values show large variations with time across all UKCS areas, but without any apparent trends between 2006 and 2014, with the possible exception of Cd.

- Trace metal concentrations do not correlate with any other of the supplementary data (pH, temperature, pressure, various cations and anions), although there are strong correlations between Cd and Pb, and Cd and Zn for the Southern North Sea.

- Batch experiment trace metal concentrations for *Captain*, *Cormorant* and *Thistle* lie mostly within the ranges of the equivalent reporting facilities, although there are exceptions with the addition of CO_2 including Cu, Pb and Zn.

- Taking into account the whole EEMS dataset, batch experiment concentrations are within the EEMS ranges for all metals, except a single anomalous Hg value attributable to analytical problems.

- However, median batch experiment concentrations are higher for the most part than median EEMS values, and exceed OSPAR guidance on trace metals in most cases, particularly for Cu, Pb and Zn.

- Batch experiments with weak CO_2-acid leaching showed that concentrations of the 8 trace metals could be elevated, on average, above current offshore UK hydrocarbon activities, therefore some mitigation may be required in the form of produced water treatment. Such mitigation should be assessed on a case-by-case basis, using a risk-based approach, as recommended by OSPAR.

Conclusions

6.1 Summary Conclusion Statement

A series of CO_2-water-rock batch experiments and sequential extraction procedures (SEP) were undertaken on sandstone samples to determine: i) the mobility in solution of a suite of 8 trace metals (arsenic, cadmium, chromium, copper, lead, mercury, nickel, zinc) under enhanced dissolved CO_2 conditions, and ii) the susceptibility of defined mineral groups to CO_2 leaching of trace metals. These experiments were carried out to in order to better understand potential trace metal mobility in future offshore CO_2 storage sites, and therefore the environmental impacts of offshore carbon capture and storage (CCS) compared with current oil and gas activities. Experimental trace metal data was compared with data from natural CO_2-driven cold water springs in Utah, USA, and with production water data from UK offshore oil and gas facilities.

This thesis concludes that the mobility of 8 trace metals of interest is, overall, low with concentrations leached by weak CO_2-acid solution from sandstones often lower than analytical detection limits. For the majority of these metals, where concentrations are detected, their susceptibility to CO_2 leaching is uncertain. Notable frequent exceptions are nickel and zinc, which appear to be linked to the dissolution of carbonate minerals, mostly calcite. The presence of other trace metals in solution may be due to the dissolution of calcite and feldspars, but also due to desorption from mineral surfaces, particularly clays. In the context of existing North Sea oil and gas activities, trace metal concentrations leached in batch experiments are within the total range of North Sea produced water trace metal loads, however on average CO_2-leached trace metal concentrations are higher than oil and gas data and occasionally exceed international recommendations. Therefore, some mitigation of trace metals may be required in future offshore CO_2 storage operations, prior to disposal at sea, in order to minimise their environmental impact.

This work is novel in that it is the first study to attempt to quantify leaching of metals during offshore CO_2 storage, and compare with existing offshore hydrocarbon activities. As such, the results of this work are applicable to an applied CCS audience, such as regulators looking to legislate for future offshore CO_2 storage. The work is also applicable to a more general CCS audience and a wider geochemistry audience, who seek to further understand CO_2-water-rock interactions, particularly in the context of environmental trace metal mobilisation, but also more generally in terms of weathering of siliciclastic rocks.

6.2   Main Thesis Conclusions

The conclusions of the preceding data and discussion chapters are summarised at the end of each chapter:

- Chapter 3. North Sea. Page 120;

- Chapter 4. Utah. Page 177;

- Chapter 5. Environmental and Emissions Monitoring System (EEMS). Page 198.

The main conclusions of these chapters, and of the thesis, are as follows. The addition of CO_2 to batch experiment flasks containing NaCl brines and sandstones reduces pH to values of between 5 and 7, and which is buffered by mineral dissolution, evident in increasing alkalinity.

Under the experimental conditions mobility of the 8 trace metals of interest (As, Cd, Cr, Cu, Hg, Pb), determined from their concentrations, was low in most cases. Nickel and Zn are the most common exceptions, being readily mobilised in North Sea sandstones with increased pCO_2. The trace metals of interest tend to be concentrated in mineral phases which are classified as immobile under enhanced CO_2 conditions, as determined by the sequential extraction procedure. This would generally confirm their lack of mobility under the batch experiment conditions.

Metals such as Ca, Ba, Mg, Mn and Sr were readily mobilised with increased pCO_2, with analysis determining that calcite dissolution is the dominant release mechanism for these elements. In the case of the Utah experiments, carbonate minerals likely precipitated during the control period, which then redissolved on bubbling CO_2. Some feldspar dissolution was also noted, from correlations between increased Si, K and Li, however this was a weaker control on overall metal mobility. Little correlation exists between major and trace metal concentrations, with the exceptions of Ni and Zn - and occasionally Cu - suggesting mineral dissolution (rather than desorption) is the primary mechanism for the mobility of Ni and Zn, and therefore carbonate dissolution is the primary source of these two metals. Where feldspars are more abundant, however, their dissolution may also contribute to Cu and Zn mobility.

Where elevated trace metal concentrations do not correlate with major elements, there may be some component of ion exchange/desorption, however this is not as significant as dissolution of calcite. Predictions of mobilised concentrations based on the SEP is, however, difficult with no particular relationship between apparent mobility and actual leached concentrations.

Data from the UK North Sea oil and gas industry (EEMS) from 2006 - 2014 shows no particular trends with time for the 8 trace metals of interest, although concentrations tend to be highest from reservoirs in the Southern North Sea. Not only this, but trace metal concentrations do not correlate with other data available for the UK North Sea (pH, temperature, pressure, selection of cations and anions).

Putting the batch experiment data in the context of existing offshore activities, batch experiment trace metal concentrations for the North Sea sandstones tested lie mostly within the ranges of the equivalent reporting facilities, although there are exceptions with the addition of CO_2 including Cu, Pb and Zn. However, these exceptions disappear when considering the whole North Sea dataset.

Median batch experiment concentrations are, however, mostly higher than median North Sea values, and exceed environmental guidance in most cases, particularly for Cu, Pb and Zn. Some mitigation may be required in the form of produced water treatment in future CO_2 storage or CO_2-EOR projects to minimise their environmental impact. Such mitigation should be assessed on a case-by-case basis, using a risk-based approach, as recommended by international guidance.

6.3 Application of This Work to Others

The relevance of this work should be considered in the wider scientific context with respect to:

- direct application of the results and conclusions, for example within a regulatory context such as future legislation for offshore produced waters in the UK;

- a global CCS audience of researchers seeking to replicate this work, perhaps with other offshore basins beyond the North Sea;

- a broader research audience examining rock-water interactions and weathering.

6.3.1 Applied CCS audience

For an applied CCS audience, such as a regulator, consideration would be given to issues such as the difference in reaction rates and scale between experiment outlined in this thesis and potential CO_2 storage reservoirs. Batch experiments, while useful, produce rates of reactions several orders of magnitude higher than in-situ reactions (e.g. Kampman *et al.* 2009; Mickler *et al.* 2013; Wigley *et al.* 2013b). This can be due to the increase in reactive surface areas from disaggregation of the samples, unrealistic water:rock ratios which may lead to an under saturation of mineral species and far-from-equilibrium conditions, and a high CO_2 content which might not be achieved in the subsurface. Batch reaction experiments may, therefore, not be realistic compared with what would actually happen in the subsurface (e.g. Malmström *et al.* 2000; Mickler *et al.* 2013; Yang *et al.* 2015). The batch experiments presented here also did not account for reactive transport within the reservoir, and therefore did not contribute to our understanding of this, which is currently considered to be poor (Lions *et al.*, 2014).

Considering the issue of scaling results of batch experiments up to reservoir scale, clearly the sample selection used in the experiment is considerably smaller than the volume of rock present in the reservoir. For example, Mickler *et al.* (2013) indicate that the difference in reacted reservoir mass between their push-pull field experiment and batch experiment is in the order of 10^9:1, while Malmström *et al.* (2000) indicates even larger discrepancy of up to 10^{11}:1. This would therefore account neither for heterogeneities within the reservoir, but also may place a higher significance on the 'nugget' effect (Chapter 3, pp. 62) in the batch experiment by not averaging this out across a much larger volume of material. Comparing field and batch results, Mickler *et al.* (2013) observed contradictory results where small changes of concentrations were found. Since the batch experiments carried out for the thesis have no direct comparison with a field experiment, and would be prohibitively expensive to do so, the data from the experiments must in all likelihood be taken as 'worst case' by regulators.

Another consideration for regulator could be the difference in potential impact between the extraction of brines for pressure relief in a CO_2 storage reservoir, and the extraction of brines during CO_2-EOR. In the first case the extracted brines are likely to be from areas of the reservoir where the CO_2 plume, or CO_2-enriched waters have yet to reach. The extraction and disposal of CO_2 or CO_2-enriched fluids during CO_2 storage is, of course, undesirable and would be avoided. This by default would mitigate the production of reservoir brines with potentially enhanced metal loads. On the other hand, production of CO_2-enriched reservoir fluids during CO_2-EOR would be a routine operation, and therefore far more likely in this scenario that reservoir brines with potentially enhanced metal loads are discharged into the offshore environment. Regulators may need to make provision for both 'normal' CO_2 storage and CO_2-EOR, in terms of their likelihood to impact the environment.

6.3.2 Global CCS audience

The importance of this study has been to determine for the first time the potential for UK North Sea reservoirs to leach trace metals in the context of CO_2 storage. The methods and conclusions are similar

to a significant body of work already carried out in determining the potential impacts of CO_2 on metal mobility with respect to onshore storage, and the possible effects on drinking water quality (see Introduction, Chapter 1 for a review). The novelty of this study has been to examine the offshore context of CO_2 storage.

The conclusions of the thesis are broadly similar to the existing body of work on onshore storage issues. That is, the effect of minor carbonate content in the rock is significant on fluid chemistry, with the simultaneous release of alkalinity with Ca, Mg, Mn and Sr indicative of carbonate dissolution. This holds true in this study regardless of detected carbonate content. Indeed, in reporting on the results of batch experiments, Yang *et al.* (2015) showed that despite the apparent absence of carbonates in the samples (below X-ray diffraction (XRD) detection limits), carbonate dissolution was readily detectable and significantly influenced the batch fluid chemistry. This is the same conclusion reached in this thesis.

Silicate dissolution is also noted to occur, from trends in Si and K in this study's experimental results, but as a lesser effect than carbonate dissolution. This is also noted in other studies; silicate dissolution rates are slower than carbonate and have less of an effect on the fluid chemistry (e.g. Mickler *et al.* 2013; Yang *et al.* 2015). It is therefore important to note that even minor traces of carbonate, which may not be detected by commonly deployed methods, have a strong potential to influence fluid chemistry. Therefore, any trace metals of concern associated with carbonates (e.g. Pb and Zn) could be readily mobilised from these minerals. A sequential extraction procedure (SEP) may therefore be more useful in this regard than XRD analysis to determine the presence of carbonates.

Noting this, the SEP allows a characteristion of which metals are contained in broad categories of the rock/reservoir. It allows for more definitive statements to be made about where, for example, trace metals such as Pb and Zn are bound rather than making assumptions. For example, Yang *et al.* (2015) assume that As and Pb are strongly adsorbed to clays, due to their theoretical properties. However, this study shows that this may not necessarily be true, depending on the rock considered, with these metals often significantly lower in concentrations (or below detection limits) than contained in other fractions of the rock. The SEP is also useful in categorising what could, or could not, be particularly susceptible to mobilisation with CO_2. Despite the benefits of increased detail characterisation of the samples, the particular SEP undertaken for this thesis was complicated and time consuming, and often produced contradictory or inconsistent results when compared with the batch experiments. A simplified and more refined SEP, for example by grouping oxides, sulphides and silicates together, may be as valuable but cheaper and easier to carry out. The batch experiments, however, were a simple and inexpensive way of gathering data for potential metal release from sandstones, and could be used to demonstrate the worst case for metal release in these rocks.

The batch experiments didn't generate many clear trends in trace metal mobility, with the exceptions of Ni and Zn in most cases. The relative immobility of the remainder of the trace elements is perhaps not that surprising, give then the samples used predominantly comprised of silicates (and mostly of quartz) and as such were largely unreactive within the experiments. Samples of rock from more reactive, or geochemically 'interesting' reservoirs (e.g. carbonates and younger reservoirs) might allow for the determination of the potential trace metal loads from much more extreme reservoirs. Again, these could provide worst case scenarios for storage options, and particularly with respect to offshore storage.

6.3.3 Non-CCS audience

A broader geochemistry audience may find this study relevant to their research. For example, the batch experimental technique used here could be applied to questions of weathering rates in elevated CO_2 palaeo environments, when pCO_2 was higher than at the present day (Rothman, 2002; Royer, 2006). Other, modern, high pCO_2 environments could also include natural CO_2 seeps, although the application of the experiments is limited since the surface CO_2 seepage often results in precipitation, rather than dissolution of minerals (i.e. travertines, see Burnside *et al.* 2009 for example).

The batch experiments are also relevant to near surface water-rock interactions where pressures are not a factor, with specific application to environmental contamination. The use of the Tessier *et al.* (1979) method in determining metal mobility from North Sea sandstones is also novel, with most researchers applying the method to soils outwith the context of CO_2 storage. Researchers seeking to investigate potential environmental impacts from rock dissolution could find the outcomes of this study of interest, in that the extraction appears to work well and provide good data.

In terms of general weathering and equilibrium processes, the batch experiments were dominated by carbonate dissolution and its effect on fluid chemistry. Cation release rates were not calculated for this study, however they were calculated using the *Captain* data as part of the Masters study undertaken previously (Carruthers, 2011). Calculated release rates of Ca at the end of the batch experiments with CO_2 averaged $5.6 \times 10^{-1} \pm 2.0 \times 10^{-1}$ mmol/l/hr, which is comparable to a value of 3.2×10^{-1} mmol/l/hr published by Mickler *et al.* (2013) (their supplementary material, Table S3). Beyond this effect, desorption was considered as a possible mechanism for metal mobility, as a function of pH. Here, the pristine point of zero net proton charge (PZNPC) at a determined or estimated pH value (pH_{PZNPC}) is an indicator of the likelihood of a mineral to adsorb or desorb cations and anions. At pH values higher than pH_{PZNPC} then cations are likely to displace ions on surface of particles, releasing cations of interest into solution. If one considers feldspars, which are perhaps a likely source of desorbed cations into solution in these batch experiments, pH_{PZNPC} values given by Langmuir (1997) are between 5.2 and 6.8, although there is some uncertainty over these (Brantley and Stillings, 1996). Experimental pH values largely cluster at pH values between 5 and 7 (Figure 3.31, pp. 109) and so one would expect desorption from feldspars surfaces to be low. Desorption from kaolinite would occur above pH 4.6, while for silica it occurs above pH 1 - 3 (quartz) and 3.5 (amorphous) (Langmuir, 1997). Given that metal release from the experiments does not appear to be strongly controlled by pH would suggest that either the effect is too small to quantify, or that pH_{PZNPC} values may need to be recalculated from this data, if possible.

6.4   Further Work

The main limitation of this study was not being able to conduct batch experiments at reservoir pressures. The influence of pressure was briefly explored within the data chapters (Chapters 3 & 4), comparing experimental results from this thesis with published literature, and drawing the conclusion that the effect of pressure has less influence than bulk composition of the rock. pH values from this study's experiments were consistent with published literature using pressurised batch experiments, and the conclusions drawn with respect to calcite dominating fluid chemistry are also broadly similar to other work. However, in terms of the confidence which the results here are interpreted more widely by industry and the public, it is considered that these audiences may focus on 'what if' style of reasoning. Therefore, simulating reservoir conditions as closely as possible would reduce uncertainty and increase confidence in the collected data, particularly with respect to the trace metals considered in this thesis.

Also, while experiments were carried out on a total of 10 sandstone samples, they were mostly highly weathered and largely composed of unreactive minerals (mostly quartz) under the conditions of the experiments. The thesis did not explore the use of more 'interesting' rocks, such as carbonates or volcanoclastic sediments, which might have more abundant reactive minerals capable of leaching the trace metals of interest.

Furthermore, little consideration was given to modelling the results of the experiments, and exploring in more detail the possible mechanisms of release beyond simple correlations of data. Therefore, future work would include:

- The use of pressurised batch containers, for example such as those outlined by Kaszuba *et al.* (2013), Lu *et al.* (2014), and Purser *et al.* (2014) to reproduce reservoir conditions with supercritical CO_2, and using rocks already examined for this study to compare the results of increased pCO_2. This would seek to determine whether increased experimental pressures significantly affect the mobility of the elements of interest. This may involve applying to use equipment held elsewhere (i.e. British Geological Survey), or by constructing bespoke equipment;

- Appropriating this equipment to examine rocks with a higher potential to leach the trace metals of interest, particularly rocks which have not undergone significant burial and diagenesis and are relatively young, or which are carbonates and therefore particularly reactive to CO_2-saturated waters;

- The SEP would be refined by aggregating the final three steps (oxide, sulphide, silicates) into a single step, focusing the method on the most reactive species to weak-CO_2 acid leaching;

- Build a geochemical model through collaboration with other academics, to replicate the experimental data and allow more detailed assessment to be made of processes influencing trace metal mobility. Modelling could answer questions on the predictability of metal release, or allow limited data to be extrapolated or scaled up from experimental to reservoir scales.

Bibliography

(1993). Memoir of the Geological Society London No. 14.

(2003). Memoir of the Geological Society London No. 20.

(2005). The Offshore Petroleum Activities (Oil Pollution Prevention and Control) Regulations 2005.

(2008). The Energy Act 2008.

(2011). The Offshore Petroleum Activities (Oil Pollution Prevention and Control) (Amendment) Regulations 2011.

Antonelli, S. (2010). *Evaluating the poential of the Captain Sandstone for geological CO_2 storage*. Unpublished, The University of Edinburgh.

Assayag, N., Matter, J., Ader, M., Goldberg, D., and Agrinier, P. (2009). Water-rock interactions during a CO_2 injection field-test: Implications on host rock dissolution and alteration effects. *Chemical Geology*, 265(1-2):227–235.

Balls, P. W. (1985). Trace Metals in the Northern North Sea. *Marine Pollution Bulletin*, 16(5):203–207.

Beck, J. W., Edwards, R. L., Ito, E., Taylor, F. W., Recy, J., Rougerie, F., Joannot, P., and Henin, C. (1992). Sea-surface temperature from coral skeletal strontium/calcium ratios. *Science (New York, N.Y.)*, 257(5070):644–647.

Beiras, R., Bellas, J., Fernández, N., Lorenzo, J. I., and Cobelo-García, A. (2003). Assessment of coastal marine pollution in Galicia (NW Iberian Peninsula); metal concentrations in seawater, sediments and mussels (*Mytilus galloprovincialis*) versus embryo-larval bioassays using *Paracentrotus lividus* and *Ciona intestinali*. *Marine environmental research*, 56(4):531–53.

Blackford, J. C., Torres, R., Cazanave, P., and Artioli, Y. (2013). Modelling dispersion of CO_2 plumes in sea water as an aid to monitoring and understanding ecological impact. *Energy Procedia*, 37:3379–3386.

Blossom, N. (2006). Copper in the Ocean Environment. Technical report, American Chemet Corporation, American Chemet Corporation.

Blunt, M., Fayers, F. J., and Orr Jr., F. M. (1993). Carbon dioxide in enhanced oil recovery. *Energy Conversion and Management*, 34(9):1197–1204.

Brantley, S. L. and Stillings, L. (1996). Feldspar dissolution at 25°C and low pH. *American Journal of Science*, 296:101–127.

British Geological Survey (1990). The geology of the Moray Firth.

Brown, A. M., Milne, A. D., and Kay, A. (2003). The Thistle Field, Blocks 211/18a, 211/19a, UK North Sea. *Geological Society, London, Memoirs*, 20(1):383–392.

Bruland, K. W., Knauer, G. A., and Martin, J. H. (1978). Zinc in north-east Pacific water. *Nature*, 271:741–743.

Burnside, N. M., Dockrill, B., Shipton, Z. K., and Ellam, R. M. (2009). Dating and Constraining Leakage Rates from a Natural Analogue for CO_2 Storage - The Little Grand Wash and Salt Wash Fault. *2nd International Conference on Fault and Top Seals - From Pore to Basin Scale*, (September 2009).

Busch, A., Kampman, N., Hangx, S., Snippe, J., Bickle, M., Bertier, P., Chapman, H., Spiers, C., Pijnenburg, R., Samuelson, J., Evans, J., Maskell, A., Nicholl, J., Pipich, V., Di, Z., Rother, G., and Schaller, M. (2014). The Green River Natural Analogue as A Field Laboratory To Study the Long-term Fate of CO_2 in the subsurface. *Energy Procedia*, 63(0):2821–2830.

Cahill, A. G. and Jakobsen, R. (2013). Hydro-geochemical impact of CO_2 leakage from geological storage on shallow potable aquifers: A field scale pilot experiment. *International Journal of Greenhouse Gas Control*, 19:678–688.

Cahill, A. G., Jakobsen, R., Mathiesen, T. B., and Jensen, C. K. (2013). Risks attributable to water quality changes in shallow potable aquifers from geological carbon sequestration leakage into sediments of variable carbonate content. *International Journal of Greenhouse Gas Control*, 19:117–125.

Carruthers, K. (2011). *Using batch experiments to quantify the potential of North Sea saline aquifers to leach contaminants upon injection of CO₂*. Unpublished, The University of Edinburgh.

Chadwick, A., Arts, R., Bernstone, C., May, F., Thibeau, S., and Zweigel, P. (2008). Best Practice for the Storage of CO_2 in Saline Aquifers. Observations and guidelines from the SACS and CO2STORE projects. Technical report.

Deer, W., Howie, R., and Zussman, J. (1992). *An introduction to the rock-forming minerals*. 2nd edition.

Department of Energy & Climate Change (2014). Methodology for the Sampling and Analysis of Produced Water.

Department of Energy & Climate Change (2015). Oil and gas: field data. https://www.gov.uk/oil-and-gas-uk-field-data Accessed: 2015-11-27.

Dockrill, B. and Shipton, Z. K. (2010). Structural controls on leakage from a natural CO_2 geologic storage site: Central Utah, U.S.A. *Journal of Structural Geology*, 32(11):1768–1782.

Eisler, R. and Hennekey, R. J. (1977). Acute Toxicities of Cd^{2+}, Cr^{+6}, Hg^{2+}, Ni^{2+} and Zn^{2+} to Estuarine Macrofauna. *Environmental Contamination and Toxicology*, 6:315–323.

Engel, D. W. and Fowler, B. a. (1979). Factors influencing cadmium accumulation and its toxicity to marine organisms. *Environmental health perspectives*, 28:81–88.

European Parliament (2000). Directive 2000/60/EC of the European Parliament and of the Council of 23 October 2000 establishing a framework for Community action in the field of water policy. *Official Journal of the European Union*.

European Parliament (2006). Directive 2006/11/EC of the European Parliament and of the Council of 15 February 2006 on pollution caused by certain dangerous substances discharged into the aquatic environment of the Community. *Official Journal of the European Union*, (2455):52–59.

Fattorini, D., Alonso-Hernandez, C. M., Diaz-Asencio, M., Munoz-Caravaca, A., Pannacciulli, F. G., Tangherlini, M., and Regoli, F. (2004). Chemical speciation of arsenic in different marine organisms: Importance in monitoring studies. *Marine Environmental Research*, 58(2-5):845–50.

Ferreira, A. C., Costa, A. C., and Korn, M. D. G. (2004). Preliminary evaluation of the cadmium concentration in seawater of the Salvador City, Brazil. *Microchemical Journal*, 78(1):77–83.

Fischer, S., Liebscher, A., and Wandrey, M. (2010). CO_2–brine–rock interaction — First results of long-term exposure experiments at in situ P–T conditions of the Ketzin CO_2 reservoir. *Chemie der Erde - Geochemistry*, 70:155–164.

Florence, T. M., Stauber, J. L., and Ahsanullah, M. (1994). Toxicity of nickel ores to marine organisms. *The Science of the total environment*, 148(2-3):139–55.

Francesconi, K. A. and Edmonds, J. S. (1996). Arsenic and Marine Organisms. *Advances in Inorganic Chemistry*, 44:147–189.

Freifeld, B. M. (2005). The U-tube: A novel system for acquiring borehole fluid samples from a deep geologic CO_2 sequestration experiment. *Journal of Geophysical Research*, 110(B10):1–10.

Gill, R., Ramsey, M. H., Walsh, J. N., Thirlwall, M. F., Rowland, A. P., Fitton, G., Parry, S. J., Mattey, D. P., Jarvis, K. E., Jocham, K. P., Brown, L., Shimizu, N., Lewis, C. A., and Ingram, G. A. (1997). *Modern Analytical Geochemistry: An Introduction to Quantitative Chemical Analysis Techniques for Earth, Environmental and Materials Scientists*. Addison Wesley Longman Limited, Harlow.

GISTEMP Team (2015). GISS Surface Temperature Analysis (GISTEMP).

González, J. A. and del C. Ruiz, M. (2006). Bleaching of kaolins and clays by chlorination of iron and titanium. *Applied Clay Science*, 33:219–229.

Gupta, N., Sass, B., and Ickes, J. (2000). Technical Progress Report, February 2000 to September 2000: Experimental evaluation of chemical sequestration of carbon dioxide in deep aquifer media - Phase II. Technical report, Batelle Memorial Institute, Columbus, Ohio.

Guthrie, R. K., Davis, E. M., Cherry, D. S., and Murray, H. E. (1979). Biomagnification of heavy metals by organisms in a marine microcosm. *Bulletin of environmental contamination and toxicology*, 21(1-2):53–61.

Haszeldine, R. S., Quinn, O., England, G., Wilkinson, M., Shipton, Z. K., Evans, J. P., Heath, J., Crossey, L., Ballentine, C. J., and Graham, C. M. (2005). Natural geochemical analogues for carbon dioxide storage in deep geological porous reservoirs, a United Kingdom perspective. *Oil and Gas Science and Technology*, 60(1):33–49.

Heath, J. E., Lachmar, T. E., Evans, J. P., Kolesar, P. T., and Williams, A. P. (2009). Hydrogeochemical characterization of leaking, carbon dioxide-charged fault zones in east-central Utah, with implications for geologic carbon storage. *Geophysical Monograph Series*, 183:147–158.

Hem, J. D. (1985). Study and Interpretation of the Chemical Characteristics of Natural Water, 3rd ed. U.S. Geological Survey Water-Supply Paper 2254.

Humez, P., Lagneau, V., Lions, J., and Negrel, P. (2013). Assessing the potential consequences of CO_2 leakage to freshwater resources: A batch-reaction experiment towards an isotopic tracing tool. *Applied Geochemistry*, 30(July 2012):178–190.

Huq, F., Blum, P., Marks, M. A. W., Nowak, M., Haderlein, S. B., and Grathwohl, P. (2012). Chemical changes in fluid composition due to CO_2 injection in the Altmark gas field: preliminary results from batch experiments. *Environmental Earth Sciences*, 67(2):385–394.

Intergovernmental Panel on Climate Change (2005). *Special Report on Carbon Dioxide Capture and Storage*. Cambridge University Press, New York.

Intergovernmental Panel on Climate Change (2014). Climate Change 2014 Synthesis Report Summary Chapter for Policymakers. Technical report.

Kampman, N., Bickle, M., Becker, J., Assayag, N., and Chapman, H. (2009). Feldspar dissolution kinetics and Gibbs free energy dependence in a CO_2-enriched groundwater system, Green River, Utah. *Earth and Planetary Science Letters*, 284(3-4):473–488.

Kampman, N., Bickle, M., Maskell, A., Chapman, H., Evans, J., Purser, G., Zhou, Z., Schaller, M., Gattacceca, J., Bertier, P., Chen, F., Turchyn, A., Assayag, N., Rochelle, C., Ballentine, C., and Busch, A. (2014). Drilling and sampling a natural CO_2 reservoir: Implications for fluid flow and CO_2-fluid–rock reactions during CO_2 migration through the overburden. *Chemical Geology*, 369:51–82.

Kampman, N., Burnside, N. M., Shipton, Z. K., Chapman, H. J., Nicholl, J. A., Ellam, R. M., and Bickle, M. J. (2012). Pulses of carbon dioxide emissions from intracrustal faults following climatic warming. *Nature Geoscience*, 5(5):352–358.

Kaszuba, J., Yardley, B., and Andreani, M. (2013). Experimental Perspectives of Mineral Dissolution and Precipitation due to Carbon Dioxide-Water-Rock Interactions. *Reviews in Mineralogy and Geochemistry*, 77(1):153–188.

Kaszuba, J. P., Janecky, D. R., and Snow, M. G. (2003). Carbon dioxide reaction processes in a model brine aquifer at 200°C and 200 bars: implications for geologic sequestration of carbon. *Applied Geochemistry*, 18(7):1065–1080.

Kaszuba, J. P., Janecky, D. R., and Snow, M. G. (2005). Experimental evaluation of mixed fluid reactions between supercritical carbon dioxide and NaCl brine: Relevance to the integrity of a geologic carbon repository. *Chemical Geology*, 217(3-4):277–293.

Kay, M. A. (2001). *Physico-Chemical Mechanisms of Fault Sealing: An Experimental Study*. PhD thesis, University of Edinburgh.

Kharaka, Y., Cole, D., Hovorka, S., Gunter, W., Knauss, K., and Freifeld, B. (2006). Gas-water-rock interactions in Frio Formation following CO_2 injection: Implications for the storage of greenhouse gases in sedimentary basins. *Geology*, 34(7):577.

Kharaka, Y. and Hanor, J. (2007). Deep fluids in the continents: 1. Sedimentary basins. In Drever, J., editor, *Surface and Ground Water, Weathering and Soils. Treatise on Geochemistry 5.* Elsevier, San Diego.

Kharaka, Y. K., Thordsen, J. J., Kakouros, E., Ambats, G., Herkelrath, W. N., Beers, S. R., Birkholzer, J. T., Apps, J. a., Spycher, N. F., Zheng, L., Trautz, R. C., Rauch, H. W., and Gullickson, K. S. (2010). Changes in the chemistry of shallow groundwater related to the 2008 injection of CO_2 at the ZERT field site, Bozeman, Montana. *Environmental Earth Sciences*, 60(2):273–284.

Kirsch, K., Navarre-Sitchler, A. K., Wunsch, A., and McCray, J. E. (2014). Metal Release from Sandstones under Experimentally and Numerically Simulated CO_2 Leakage Conditions. *Environmental science & technology*, 48(3):1436–1442.

Kirste, D., Haese, R., Boreham, C., and Schacht, U. (2014). Evolution of formation water chemistry and geochemical modelling of the CO2CRC Otway Site residual gas saturation test. *Energy Procedia*, 63:2894–2902.

Kjöller, C., Weibel, R., Bateman, K., Laier, T., Nielsen, L. H., Frykman, P., and Springer, N. (2011). Geochemical impacts of CO_2 storage in saline aquifers with various mineralogy - Results from laboratory experiments and reactive geochemical modeling. *Energy Procedia*, 4:4724–4731.

Klein, D. H. and Goldberg, E. D. (1970). Mercury in the Marine Environment. *Environmental Science & Technology*, 4(9):765–768.

Kling, G. W., Clark, M. A., Compton, H. R., Devine, J. D., Evans, W. C., Humphrey, A. M., Koenigsberg, E. J., Lockwood, J. P., Tuttle, M. L., and Wagner, G. N. (1987). The 1986 Lake Nyos Gas Disaster in Cameroon, West Africa. *Science*, 236(4798):169–175.

Krüger, M., West, J., Frerichs, J., Oppermann, B., Dictor, M. C., Jouliand, C., Jones, D., Coombs, P., Green, K., Pearce, J., May, F., and Möller, I. (2009). Ecosystem effects of elevated CO_2 concentrations on microbial populations at a terrestrial CO_2 vent at Laacher See, Germany. *Energy Procedia*, 1(1):1933–1939.

Langmuir, D. (1997). *Aqueous Environmental Geochemistry*. Prentice Hall, Inc., Upper Saddle River, New Jersey.

Laslett, R. E. (1995). Concentrations of Dissolved and Suspended Particulate Cd, Cu, Mn, Ni, Pb and Zn in Surface Waters Around the Coasts of England and Wales and in Adjacent Seas. *Estuarine, Coastal and Shelf Science*, 40:67–85.

Lima, V. D., Einloft, S., Ketzer, J. a. M., Jullien, M., Bildstein, O., and Petronin, J.-C. (2011). CO_2 Geological storage in saline aquifers: Paraná Basin caprock and reservoir chemical reactivity. *Energy Procedia*, 4:5377–5384.

Lindeberg, E., Vuillaume, J.-F., and Ghaderi, A. (2009). Determination of the CO_2 storage capacity of the Utsira formation. *Energy Procedia*, 1(1):2777–2784.

Lions, J., Devau, N., De Lary, L., Dupraz, S., Parmentier, M., Gombert, P., and Dictor, M. C. (2014). Potential impacts of leakage from CO_2 geological storage on geochemical processes controlling fresh groundwater quality: A review. *International Journal of Greenhouse Gas Control*, 22:165–175.

Little, M. G. and Jackson, R. B. (2010). Potential impacts of leakage from deep CO_2 geosequestration on overlying freshwater aquifers. *Environmental Science & Technology*, 44(23):9225–32.

Lokhorst, A. (1997). NW European Gas Atlas.

Lu, J., Mickler, P. J., Nicot, J.-P., Yang, C., and Romanak, K. D. (2014). International Journal of Greenhouse Gas Control Geochemical impact of oxygen on siliciclastic carbon storage reservoirs. *International Journal of Greenhouse Gas Control*, 21:214–231.

Lu, J., Partin, J. W., Hovorka, S. D., and Wong, C. (2010). Potential risks to freshwater resources as a result of leakage from CO_2 geological storage: a batch-reaction experiment. *Environmental Earth Sciences*, 60(2):335–348.

Lu, P., Fu, Q., Seyfried, W. E., Hereford, A., and Zhu, C. (2011). Navajo Sandstone–brine–CO_2 interaction: implications for geological carbon sequestration. *Environmental Earth Sciences*, 62(1):101–118.

Malmström, M. E., Destouni, G., Banwart, S. A., and Strömberg, B. H. E. (2000). Resolving the Scale-Dependence of Mineral Weathering Rates. *Environmental Science and Technology*, 34(7):1375–1378.

Maskall, J. E. and Thornton, I. (1998). Chemical Partioning of Heavy Metals in Soils, Clays and Rocks at Historical lead Smelting Sites. *Water, Air, and Soil Pollution*, 108:391–409.

Matsunaga, K., Konishi, S., and Nishimura, M. (1979). Possible errors caused prior to measurement of mercury in natural waters with special reference to seawater. *Environmental Science & Technology*, 13(1):63–65.

Mayo, A. L., Morris, T. H., Peltier, S., Petersen, E. C., Payne, K., Holman, L. S., Tingey, D., Fogel, T., Black, B. J., and Gibbs, T. D. (2003). Active and inactive groundwater flow systems: Evidence from a stratified, mountainous terrain. *Geological Society of America Bulletin*, 115(12):1456.

Mearns, A. J., Oshida, P. S., Sherwood, M. J., Young, D. R., and Reish, D. J. (1976). Chromium effects on coastal organisms. *Journal - Water Pollution Control Federation*, 48(8):1929–1939.

Mickler, P. J., Yang, C., Scanlon, B. R., Reedy, R., and Lu, J. (2013). Potential impacts of CO_2 leakage on groundwater chemistry from laboratory batch experiments and field push-pull tests. *Environmental Science and Technology*, 47:10694–10702.

Morse W., J. and Mackenzie T., F. (1990). Chapter 5 Composition and Source of Shoal-Water Carbonate Sediments. *Developments in Sedimentology*, Volume 48:179–239.

Moss, B., Barson, D., Rakhit, K., Dennis, H., and Swarbrick, R. (2003). Formation pore pressures and formation waters. In Evans, D., Graham, C., Armour, A., and Bathurst, P., editors, *The Millennium Atlas: Petroleum Geology of the Central and Northern North Sea*, chapter 18. The Geological Society of London.

Neal, P. R., Cinar, Y., and Allinson, W. G. (2011). The economics of pressure-relief with CO_2 injection. *Energy Procedia*, 4:4215–4220.

Neff, J. M. (1997). Ecotoxicology of arsenic in the marine environment. *Environmental Toxicology and Chemistry*, 16(5):917–927.

OSPAR Commission (2010). Overview assessment of the implementation of OSPAR Recommendation 2001/1 for the management of produced water from offshore installations.

OSPAR Commission (2012a). OSPAR 12/22/1, Annex 18. OSPAR Recommendation 2012/5 for a risk-based approach to the Management of Produced Water Discharges from Offshore Installations.

OSPAR Commission (2012b). OSPAR 12/22/1, Annex 19. OSPAR Guidelines in support of Recommendation 2012/5 for a Risk-based Approach to the Management of Produced Water Discharges from Offshore Installations (OSPAR Agreement: 2012-7).

Paterson, L., Boreham, C., Bunch, M., Dance, T., Ennis-King, J., Freifeld, B., Haese, R., Jenkins, C., LaForce, T., Raab, M., Singh, R., Stalker, L., and Zhang, Y. (2013). Overview of the CO2CRC Otway Residual Saturation And Dissolution Test. *Energy Procedia*, 37:6140–6148.

Pearce, J. M., Holloway, S., Wacker, H., Nelis, M. K., Rochelle, C., and Bateman, K. (1996). Natural occurrences as analogues for the geological disposal of carbon dioxide. *Energy Conversion and Management*, 37(6-8):1123–1128.

Peter, A., Lamert, H., Beyer, M., Hornbruch, G., Heinrich, B., Schulz, A., Geistlinger, H., Schreiber, B., Dietrich, P., Werban, U., Vogt, C., Richnow, H.-H., Groß mann, J., and Dahmke, A. (2012). Investigation of the geochemical impact of CO_2 on shallow groundwater: design and implementation of a CO_2 injection test in Northeast Germany. *Environmental Earth Sciences*, 67(2):335–349.

Phillips, D. J. H. (1976). The Common Mussel *Mytilus edulis* as an Indicator of Pollution by Zinc, Cadmium, Lead and Copper. I. Effects of Environmental Variables on Uptake of Metals. *Marine Biology*, 38:59–69.

Phillips, D. J. H. (1990). Arsenic in aquatic organisms: a review, emphasizing chemical speciation. *Aquatic Toxicology*, 16:151–186.

Pipe, R., Coles, J., Carissan, F., and Ramanathan, K. (1999). Copper induced immunomodulation in the marine mussel, *Mytilus edulis*. *Aquatic Toxicology*, 46(1):43–54.

Preston, A., Jefferies, D. F., Dutton, J. W. R., Harvey, B. R., and K, S. A. (1972). British Isles coastal waters: The concentrations of selected heavy metals in sea water, suspended matter and biological indicators - A pilot survey. *Environmental Pollution*, 3(1):69–82.

Pudlo, D., Reitenbach, V., Albrecht, D., Ganzer, L., Gernert, U., Wienand, J., Kohlhepp, B., and Gaupp, R. (2012). The impact of diagenetic fluid–rock reactions on Rotliegend sandstone composition and petrophysical properties (Altmark area, central Germany). *Environmental Earth Sciences*, 67(2):369–384.

Purser, G., Rochelle, C., Rushton, J., Pearce, J., and Wagner., D. (2014). An Experimental and Analogue Study of Iron Release from Red Sandstones. *Energy Procedia*, 63:3268–3274.

Rao, C. R. M., Sahuquillo, A., and Lopez Sanchez, J. F. (2008). A Review of the Different Methods Applied in Environmental Geochemistry For Single and Sequential Extraction of Trace Elements in Soils and Related Materials. *Water, Air, and Soil Pollution*, 189(1-4):291–333.

Ray, S. (1986). Bioaccumulation of cadmium in marine organisms. *Experientia. Supplementum*, 50:65–75.

Renzoni, A., Zino, F., and Franchi, E. (1998). Mercury levels along the food chain and risk for exposed populations. *Environmental Research*, 77(2):68–72.

Roberts, J. J., Wood, R. A., and Haszeldine, R. S. (2011). Assessing the health risks of natural CO_2 seeps in Italy. *Proceedings of the National Academy of Sciences*, 108(40):16545–16548.

Rosenbauer, R. J., Koksalan, T., and Palandri, J. L. (2005). Experimental investigation of CO_2-brine-rock interactions at elevated temperature and pressure: Implications for CO_2 sequestration in deep-saline aquifers. *Fuel Processing Technology*, 86:1581–1597.

Rothman, D. H. (2002). Atmospheric carbon dioxide levels for the last 500 million years. *Proceedings of the National Academy of Sciences of the United States of America*, 99(7):4167–4171.

Royer, D. L. (2006). CO_2-forced climate thresholds during the Phanerozoic. *Geochimica et Cosmochimica Acta*, 70(23):5665–5675.

Scottish Carbon Capture & Storage (2011). Progressing Scotland's CO_2 storage opportunities. Technical report.

Scottish Centre for Carbon Storage (2009). Opportunities for CO_2 Storage around Scotland. Technical report.

Shipton, Z. K., Evans, J. P., Kirschner, D., Kolesar, P. T., Williams, A. P., and Heath, J. (2004). Analysis of CO_2 leakage through 'low-permeability' faults from natural reservoirs in the Colorado Plateau, east-central Utah. *Geological Society, London, Special Publications*, 233(1):43–58.

Shiraki, R. and Dunn, T. L. (2000). Experimental study on water-rock interactions during CO_2 fooding in the Tensleep Formation, Wyoming, USA. *Applied Geochemistry*, 15:265–279.

Siegel, F. R. (1960). The effect of strontium on the aragonite-calcite ratios of Pleistocene corals. *Journal of Sedimentary Petrology*, 30(2):297–304.

Smith, J. V. and Brown, W. L. (1988). *Feldspar Minerals Volume 1: Crystal Structures, Physical, Chemical, and Microtextural Properties*. Springer-Verlag Berlin Heidelberg, 2nd edition.

Smyth, R. C., Hovorka, S. D., Lu, J., Romanak, K. D., Partin, J. W., Wong, C., and Yang, C. (2009). Assessing risk to fresh water resources from long term CO_2 injection–laboratory and field studies. *Energy Procedia*, 1(1):1957–1964.

Spangler, L. E. (1992). Records of Wells in Sandstone and Alluvial Aquifers and Chemical Data for Water From Selected Wells in the Navajo Aquifer in the Vicinity of the Greater Aneth Oil Field, San Juan County, Utah. Technical report, U.S. Geological Survey.

Stallard, R. and Edmond, J. (1983). Geochemistry of the Amazon 2. The influence of geology and weathering environment on the dissolved load. *Journal of Geophysical Research*, 88(C14):9671–9688.

Taylor, D., Maddock, B. G., and Mance, G. (1985). The acute toxicity of nine 'grey list' metals (arsenic, boron, chromium, copper, lead, nickel, tin, vanadium and zinc) to two marine fish species: dab (*Limanda limanda*) and grey mullet (*Chelon labrosus*). *Aquatic Toxicology*, 7:135–144.

Taylor, D. J. and Dietvorst, J. P. a. (1991). The Cormorant Field, Blocks 211/21a, 211/26a, UK North Sea. *Geological Society, London, Memoirs*, 14(1):73–82.

Terzi, K., Aggelopoulos, C. a., Bountas, I., and Tsakiroglou, C. D. (2014). Effects of carbon dioxide on the mobilization of metals from aquifers. *Environmental Science and Technology*, 48:4386–4394.

Tessier, A., Campbell, P. G. C., and Bisson, M. (1979). Sequential Extraction Procedure for the Speciation of Particulate Trace Metals. *Analytical Chemistry*, 51(7):844–851.

Trautz, R. C., Pugh, J. D., Varadharajan, C., Zheng, L., Bianchi, M., Nico, P. S., Spycher, N. F., Newell, D. L., Esposito, R. A., Wu, Y., Dafflon, B., Hubbard, S. S., and Birkholzer, J. T. (2013). Effect of Dissolved CO_2 on a Shallow Groundwater System: A Controlled Release Field Experiment. *Environmental science & technology*.

Ullah, H., Noreen, S., Fozia, Rehman, A., Waseem, A., Zubair, S., Adnan, M., and Ahmad, I. (2013). Comparative study of heavy metals content in cosmetic products of different countries marketed in Khyber Pakhtunkhwa, Pakistan. *Arabian Journal of Chemistry*.

Vandecasteele, C. and Block, C. B. (1993). *Modern Methods for Trace Element Determination*. John Wiley & Sons Ltd., Chichester.

Vanegas, C., Espina, S., Botello, a. V., and Villanueva, S. (1997). Acute toxicity and synergism of cadmium and zinc in white shrimp, Penaeus setiferus, juveniles. *Bulletin of Environmental Contamination and Toxicology*, 58(1):87–92.

Varadharajan, C., Tinnacher, R. M., Pugh, J. D., Trautz, R. C., Zheng, L., Spycher, N. F., Birkholzer, J. T., Castillo-Michel, H., Esposito, R. a., and Nico, P. S. (2013). A laboratory study of the initial effects of dissolved carbon dioxide (CO_2) on metal release from shallow sediments. *International Journal of Greenhouse Gas Control*, 19:183–211.

Wanamaker Jr, A. D., Kreutz, K. J., Wilson, T., Borns Jr, H. W., Introne, D. S., and Feindel, S. (2008). Experimentally determined Mg/Ca and Sr/Ca ratios in juvenile bivalve calcite for *Mytilus edulis*: implications for paleotemperature reconstructions. *Geo-Marine Letters*, 28(5-6):359–368.

Wandrey, M., Fischer, S., Zemke, K., Liebscher, A., Scherf, A.-K., Vieth-Hillebrand, A., Zettlitzer, M., and Würdemann, H. (2011). Monitoring petrophysical, mineralogical, geochemical and microbiological effects of CO_2 exposure — Results of long-term experiments under in situ conditions. *Energy Procedia*, 4(0):3644–3650.

Warren, E. A. and Smalley, P. C. (1994). North Sea Formation Waters Atlas. *Memoir of the Geological Society London*, 15.

Widdicombe, S., Dashfield, S., McNeill, C., Needham, H., Beesley, A., McEvoy, A., Øxnevad, S., Clarke, K., and Berge, J. (2009). Effects of CO_2 induced seawater acidification on infaunal diversity and sediment nutrient fluxes. *Marine Ecology Progress Series*, 379(2008):59–75.

Wigand, M., Carey, J., Schütt, H., Spangenberg, E., and Erzinger, J. (2008). Geochemical effects of CO_2 sequestration in sandstones under simulated in situ conditions of deep saline aquifers. *Applied Geochemistry*, 23(9):2735–2745.

Wigley, M., Dubacq, B., Kampman, N., and Bickle, M. (2013a). Controls of sluggish, CO_2-promoted, hematite and K-feldspar dissolution kinetics in sandstones. *Earth and Planetary Science Letters*, 362:76–87.

Wigley, M., Kampman, N., Chapman, H. J., Dubacq, B., and Bickle, M. J. (2013b). In situ redeposition of trace metals mobilized by CO_2-charged brines. *Geochemistry, Geophysics, Geosystems*, 14(5):1321–1332.

Wigley, M., Kampman, N., Dubacq, B., and Bickle, M. (2012). Fluid-mineral reactions and trace metal mobilization in an exhumed natural CO_2 reservoir, Green River, Utah. *Geology*, 40(6):555–558.

Wilkinson, M., Gilfillan, S. M. V., Haszeldine, R. S., and Ballentine, C. J. (2009). Plumbing the Depths: Testing Natural Tracers of Subsurface CO_2 Origin and Migration, Utah. In Grobe, M., Pashin, J. C., and Dodge, R. L., editors, *Carbon Dioxide Sequestration in Geological Media-State of the Science. AAPG Studies in Geology*, volume 69, pages 619–634.

Yamamoto, M., Abe, T., Kuwabara, J., Komura, K., Ueno, K., and Takizawa, Y. (1994). Polonium-210 and Lead-210 in marine organisms: Intake levels for Japanese. *Journal of Radioanalytical and Nuclear Chemistry*, 178(1):81–90.

Yang, C., Hovorka, S. D., Treviño, R. H., and Delgado-Alonso, J. (2015). Integrated Framework for Assessing Impacts of CO_2 Leakage on Groundwater Quality and Monitoring-Network Efficiency: Case Study at a CO_2 Enhanced Oil Recovery Site. *Environmental Science and Technology*, 49:8887–8898.

Appendices

MSc Experimental Method

A.1 MSc Experimental Methodology

The following text has been copied directly from the Experiment Methodology chapter of the Carruthers (2011) thesis submitted for a Masters qualification at the University of Edinburgh, and describes the batch experiment undertaken on samples of the Captain Sandstone. Data and analysis presented in Chapter 3 (North Sea). Only the sections relevant to this thesis were copied, with minor editing for formatting.

A.1.1 Materials preparation

Small hand specimens of the Captain Sandstone had been previously collected by Sara Antonelli in 2010; *SA1 - 10*. Thin sections were prepared from all samples, with XRD carried out on five of the samples (Antonelli, 2010), Table A.1.

Sample	Core number	Depth (ft)	Thin section	XRD	Oil Staining
SA1	13/22a-2	3137.65	✓	✓	
SA2	13/22a-2	3112.4	✓		✓
SA3	13/30a-4	6365.5	✓		
SA4	13/30a-4	6382	✓	✓	
SA5	13/30a-4	6448	✓		
SA6	13/30a-4	6451	✓	✓	
SA7	13/24a-4	5316.5	✓		✓
SA8	13/24a-4	5371	✓	✓	
SA9	13/24a-4	5416	✓		
SA10	13/24a-4	5432	✓	✓	

Table A.1: *Analytical methods undertaken by Antonelli (2010) denoted by ✓ on samples collected during her study. Highlighted samples SA7 and SA10 were used for the experimental work in this study.*

Following analysis by Antonelli (2010), the remaining sample materials had been stored in polythene bags and boxed for approximately one year. The two samples, *SA7* and *SA10* were selected for the experimental work to compare the effect of an oil-stained sample versus a 'clean' sample. On visual and olfactory evidence, sample *SA7* was noted to contain hydrocarbons, while *SA10* appeared to be hydrocarbon free.

Samples *SA7* and *SA10* were broken up by hand into 'chip' and 'grain' particle sizes, to determine whether surface area would affect the results of the experiment. 'Chip' dimensions averaged $0.97 \times 0.86 \times 0.72$ cm (± 0.01 cm) (*SA7*) and $1.07 \times 0.88 \times 0.70$ cm (± 0.01 cm) (*SA10*), measured by digital caliper. 'Grain' size was determined using a particle size analyser; L230 (VSM Plus) with a quoted relative standard deviation of 1% or better. The mean grain size diameter of *SA10* was determined to be 220 ± 2 µm.

Grain size analysis of *SA7* was not carried out due to the presence of hydrocarbons and therefore mean grain size of *SA7* was assumed to be equivalent to *SA10*.

The sample density of *SA10* was crudely determined by adding 1.28 ± 0.01 g of *SA10* chips to a 5 mL measuring cylinder containing deionised (D.I.) water. The volume change was measured at 0.55 ± 0.05 mL. The density of *SA10* is therefore 2.33 ± 0.21 g/cm^3.

The 'chip' and 'grain' samples of *SA7* and *SA10* were weighed out to ensure approximately equal weights of sample in each batch. Weights are given in Table A.2, below.

The saline solution used during the experiment was made up from 13.50 ± 0.01 g of Fisherbrand 'SLR' grade sodium chloride (NaCl) solid reagent per 1,000 mL of 11 mΩ/cm high purity water (from a Milli-Q water system) to give a 13,500 ppm NaCl solution representative of reservoir conditions.

Sample	Batch	Chip (g)	Grain (g)
SA7	CO_2	3.36	2.75
	Non-CO_2	3.17	2.75
SA10	CO_2	3.36	2.64
	Non-CO_2	3.18	2.85

Table A.2: *Batch experiment sample weights in grams.*

A.1.2 Experimental setup

All glassware and sampling bottles were soaked overnight in 10% nitric acid, prior to being rinsed with tap water and 11 mΩ/cm D.I. water. Glassware was wrapped in aluminium foil and dried at 450°C for four hours to destroy any residual organic material, and left wrapped in foil until the experiment was set up.

The experimental setup comprised of five sets of flasks, which were subjected to CO_2 flow, and five sets of beakers which had no CO_2 flow and acted as the experimental controls.

A.1.2.1 Non-CO_2 control beakers

Five glass beakers, *B1 - B5*, were each filled with 250 mL of 13,500 ppm NaCl solution and placed in a water bath set to a temperature of 58 ± 1°C, determined as representative of reservoir conditions. Non-PVC cling film covered each beaker to reduce evaporation of the solution.

A.1.2.2 +CO_2 flasks

The CO_2 flow batch experiment was set up in a fume cupboard and comprised five 250 mL three-neck flasks, *F1 - F5*, which were each sat on glass fibre wool on a Fisherbrand 150 W heating mantle. The flasks were fitted with a glass water cooled coil condenser and loosely fitted stopper to reduce evaporation, a thermometer, and a hollow glass rod for gaseous CO_2 flow, Figure A.1.

Figure A.1: *CO_2 batch experimental setup, comprising (left-to-right) flasks F1 - F5 set on heating mantles set to 58°C, each with glass condensing coil, thermometer, glass CO_2 feed rod and rubber CO_2 feed tubing from a vapour withdrawal CO_2 bottle.*

CO_2 gas was fed through rubber tubing from a BOC supplied vapour withdrawal CO_2 bottle with attached regulator and needle valve. 250 mL of 13,500 ppm NaCl solution was added to each flask and warmed to approximately $58 \pm 1°C$.

A.1.2.3 Commencement of the experiment

Once solution temperatures had stabilised at approximately $58 \pm 1°C$, rock samples were added to the flasks and beakers in the configuration noted in Table A.3. Each CO_2 flask had an equivalent non-CO_2 control beaker. The samples were agitated as little as possible when added to the batches, and were not deliberately agitated at any time throughout the duration of the experiment. Despite minimal disturbance of the chip samples, individual grains were observed to detach from the chips during the experiment.

Batch Name	Sample	Sample Type	CO_2 Flow
B1	None	-	No
B2	SA7	Chip	
B3	SA7	Grain	
B4	SA10	Chip	↓
B5	SA10	Grain	
F1	None	-	Yes
F2	SA7	Chip	
F3	SA7	Grain	
F4	SA10	Chip	↓
F5	SA10	Grain	

Table A.3: *Experimental configuration of non-CO_2 and +CO_2 batches. Batches B1 and F1 contain no rock samples and act as the overall experimental controls.*

The commencement of CO_2 flow was taken as the start of the experiment: 0 hrs, Day 1. CO_2 was supplied to the flasks *F1 - F5*, with Hoffman tubing clamps used to control CO_2 flow through the tubing. Flow rate was not measured, however the saline solutions were oversaturated with respect to CO_2 as bubbles escaped from the solution at the tip of the glass rod.

A.1.2.4 CO_2 flow issues

CO_2 flow to the flasks was not constant for the duration of the experiment. The CO_2 bottle emptied a total of four times on Days 3, 11, 22, and 26, later attributed to a faulty regulator. A problem with replenishing CO_2 meant that there was no CO_2 flow during Days 3 - 8, while a leaking tube prohibited flow during Days 11 and 12.

A.1.3 Sampling and analysis

The first fluid sampling and measurements were taken at 4 hrs, Day 1. The last sampling and measurements were taken at 689.5 hrs, Day 30, with the experiment ended at this time.

A.1.3.1 pH measurements

pH was measured on Days 1 - 7 with a Hanna HI98128 pH meter, calibrated with HI7007 (pH 7.01) and HI7004 (pH 4.01) buffer solutions and is accurate to ± 0.05 pH. From each batch container, 5 mL of water was removed by pipettor to a clean beaker and immediately measured for pH.

Due to pH measurements being temperature dependent (Langmuir, 1997), pH values rose continuously as the water sample cooled and the pH meter corrected for the temperature change, making accurate and consistent readings difficult. 5 mL of sample was also not sufficient to obtain as accurate a result as possible.

Thus, for the remainder of the experiment (Days 9 - 11, 13, 14, 16, 22 and 30), pH measurements were taken with a Hanna HI9025 pH meter, calibrated with the above buffer solutions and accurate to $\pm$ 0.01 pH. The change in meter reduced the sampled volume to 2 mL, which was transferred to a vial and allowed to cool to room temperature before taking measurements. This method produced more reliable results.

A.1.3.2 Alkalinity measurements

Alkalinity was measured using a Palintest Photometer 7100, accurate to $\pm$ 5 mg/L. Measurements were taken by crushing a Palintest alkophot 'M' reagent tablet in 9 mL[1] of sample water. The photometer was calibrated with a blank before each test, which comprised 9 mL of 13,500 ppm NaCl solution. Bicarbonate and carbonate concentrations in mg/L were recorded on Days 1 - 7, 9, 11, 14, 22, 30, with alkalinity reported as carbonate alkalinity.

A.1.3.3 Metals analysis

On Days 1, 3, 5, 9, 11, 14, 22 and 30, water was drawn from the batch containers to sample for metal cation analysis.

From each batch container, 4 mL of sample was drawn with a pipettor on Days 1, 3 and 5, reducing to 3.5 ml for the remaining days. This was transferred directly to a disposable syringe and passed through a disposable 0.22 μm Millipore filter. The filtered sample was then sub-sampled into individual Teflon bottles as follows: a) 0.5 mL of sample, diluted with 9.5 mL of 11 mΩ/cm D.I. water (20 $\times$ dilution factor) and acidified with 2% (200 μL) of Aristar grade 69% nitric acid; b) 2.5 mL of sample acidified with 2% (50 μL) nitric acid. The samples were then refrigerated until required for analysis.

Water samples were analysed by ICP-MS using an Agilent 7500ce (with octopole reaction system), employing an RF forward power of 1540 W, reflected power of 1 W, argon gas flows of 0.82 L/min and 0.2 L/min for carrier and makeup flows, respectively, and nickel skimmer and sample cones, with a Micro mist nebuliser and peristaltic pump providing a solution uptake rate of approximately 1.2 mL/min. The instrument was operated in spectrum multi-tune acquisition mode and three replicate runs per sample were employed.

The instrument was calibrated with a Merck multi-element standard (ICP Multi-element standard solution VI CertiPUR®) for all metals listed in Table A.4 except Sb and Ti, which were calibrated with Spex Certiprep 1,000 ppm ICPMS standards, and Hg which was calibrated a BDH 'SpectrosoL' 1,000 ppm solution. Calibration was checked with Standard Reference Material® (SRM) 1643e and instrument drift corrected for with a Spex Certiprep internal standard containing Indium ([115]In).

Analytical uncertainties at two standard deviations ($2s$) were in the range $\pm$ 6 - 35%, calculated from repeat analysis (n = 6) of SRM1643e. Hg, Ti and U are absent from SRM1643e, and are therefore taken as $\pm$ 15% based upon the mean of the other metals' uncertainties, Table A.4.

Analytical limits of detection (LOD's) were calculated for each element by analysing ten blank D.I. samples and using the method outlined in Vandecasteele and Block (1993), with the 95% student t-test value of 2.26 used, Table A.4.

A.1.3.4 X-ray diffraction

X-Ray diffraction (XRD) analysis was previously carried out on sample *SA10* by Antonelli (2010), however this data was not obtained for *SA7*.

A sample of *SA7* was ground with acetone in an agate mortar and pestle, transferred to a glass slide and bulk mineral analysis was carried out using a Bruker D8-Advance X-ray Diffractometer, employing

---

[1]Palintest sample tubes are marked with a 10ml measuring line, however accurate measuring of volumes with a pipettor required only 9ml of sample to fill the tube to the 10ml line. This was considered sufficient for the purposes of the test, as the reagents were designed to be used with the volume of water that reached the mark on the tube.

Metal	Symbol	Sampled Days			Detection Limit (µg/L)	Analytical Uncertainty (%)
		1, 3, 5	9, 11, 14	22, 30		
Aluminium	Al	✓	✓	✓	3.78	± 28
Antimony	Sb	✓		✓	0.004	± 6
Arsenic	As	✓	✓	✓	0.19	± 18
Barium	Ba	✓	✓	✓	0.28	± 7
Cadmium	Cd	✓	✓	✓	0.004	± 10
Calcium	Ca	✓	✓	✓	97.6	± 12
Cobalt	Co	✓		✓	0.05	± 8
Copper	Cu	✓	✓	✓	2.17	± 19
Chromium	Cr	✓	✓	✓	0.06	± 19
Iron	Fe	✓	✓	✓	1.07	± 20
Lead	Pb	✓	✓	✓	0.09	± 10
Magnesium	Mg	✓	✓	✓	0.86	± 18
Manganese	Mn	✓	✓	✓	0.05	± 14
Mercury	Hg	✓	✓	✓	0.02	± 15
Nickel	Ni	✓	✓	✓	0.03	± 10
Potassium	K	✓	✓	✓	10.6	± 23
Selenium	Se	✓		✓	89.7	± 14
Sodium	Na	✓	✓	✓	0.08	± 35
Titanium	Ti	✓	✓	✓	0.54	± 15
Uranium	U	✓	✓	✓	0.0006	± 15
Vanadium	V	✓	✓	✓	0.02	± 17
Zinc	Zn	✓	✓	✓	1.36	± 27

Table A.4: *Summary of metal cation analysis carried out by ICPMS, denoted by ✓. Analytical limit of detection (LOD) calculated: (2.26 × [std. deviation of 10 D.I. samples]) / [slope of D.I. sample calibration line]. Analytical uncertainties calculated from repeat (n = 6) analysis of SRM1643e, Hg, Ti and U taken as ± 15%.*

a 2-theta (2θ) configuration, with X-rays generated by a Cu-anode X-ray tube operating at 40 kV, and a tube current of 40 mA.

Diffracted X-rays were detected using a Sol-X energy dispersive detector, scanning from 2° to 60° 2θ at a scan rate of 0.01°/second and the resultant diffractograms compared with the 2008 issue of the International Centre for Diffraction Data (ICDD) diffractogram database library using the EVA analysis package. The detection limit for crystalline phases is approximately 1 wt.%.

Due to the small amount of sample available for *SA7*, repeat analysis for instrumental precision was not carried out. The results of the *SA10* precision analysis can be found in Antonelli's thesis.

The clay fraction of the sample was not obtained due to the hydrocarbon contamination of *SA7*. There was insufficient time to carry out Soxhlet extraction to remove hydrocarbons, and the subsequent clay separation.

A.1.4   General comments

- Following sampling and measurement for pH and alkalinity, these water samples were discarded; water was not replenished in any batch container following sampling. This ensured that measured metal concentrations were true concentrations, and were not changed by dilution effects. The exception to this was flask *F1*. Due to the water volume in the flask being unexpectedly low (estimated at 30 - 50 mL) on Day 17, compared with the other flasks, 150 mL of 13,500 ppm NaCl was added to ensure that there was sufficient water to complete the experiment.

- As samples were drawn from the CO_2 batch flasks and therefore the volumes of water remaining reduced, the temperature controller on each heating mantle was turned down to maintain as constant a temperature as was possible. The temperatures measured throughout the experiment are summarised in Table A.5, below.

- Flasks were set up in a fume cupboard and there was an issue with water temperatures rising when the sash was raised in order to work in the cupboard. Temperatures rose in the order of 5-10°C during the time taken to measure and sample from the flasks, Table A.5. This was probably

due to cooler air being drawn in over the heating mantles when the sash was open, causing the heating element to turn on and overheating the water.

Batch	Temperature Range (°C)
F1	54.0 - 63.0
F2	53.5 - 58.5
F3	50.0 - 68.0
F4	56.0 - 64.0
F5	57.0 - 63.0
B1	55.0 - 58.0
B2	55.0 - 58.0
B3	55.0 - 58.0
B4	55.0 - 58.0
B5	55.0 - 58.0

Table A.5: *Temperature range of batch experiments. All temperatures are $\pm$ 1°C.*

Dilution Correction Method

During the batch experiments for *Cormorant* and *Thistle*, the batch brines in two flasks were topped up with fresh solutions due to volumes running too low to continue the experiment. For the *Field X* batch experiments, fresh brine was added back to the batch vessels after each sampling for analysis, to maintain a constant volume through the experiment. By diluting the batch fluids, concentrations are reset to a new level, and require a mathematical correction to be applied to give the concentrations which would have been measured if the dilution had not been performed.

The following dilution correction, taken from Kay (2001), was applied to *Cormorant*, *Thistle* and *Field X* samples listed in Table B.1. There are three stages:

$$C_s = C_{to} \times \frac{V_s}{V_d} \tag{B.1}$$

where C_{to} is the last known 'real' concentration, C_s is the concentration of C_{to} after dilution, V_s is the volume in the flask after sampling, and V_d is the volume after dilution back to the original 'pre-sampling' volume. C_s is then applied to:

$$dC_{t+n} = C_{t+1} - C_s \tag{B.2}$$

where dC_{t+n} is the concentration correction factor and C_{t+1} is the concentration at time $t+1$. Finally

$$C_R = C_{to} + dC_{t+n} \tag{B.3}$$

where C_R is the corrected concentration using the last known 'real' concentration (C_{to}) and the concentration factor (dC_{t+n}).

This correction was applied to the following samples:

Cormorant	Thistle	Field X
F2 17/06/12 (Day 7)	F4 25/06/12 (Day 15)	All Flasks
F2 19/06/12 (Day 9)		06/02/13 - 27/02/15
F2 21/06/12 (Day 11)		Day 1 - Day 22
F2 25/06/12 (Day 15)		

Table B.1: *Batch experiment samples corrected using the dilution correction method given in Kay (2001).*

Experimental Data

Please refer to the Microsoft Excel files (.xlsx) provided on the enclosed disc (inside back cover) for the following data:

File	Enclosed Data
`Batch_Experiment_data_KC_Dec15.xlsx`	Batch experiment geochemistry: Captain (SA7, SA10) Cormorant Thistle Field X (8518, 8579) Utah (Entrada S1 & S2, Wingate S3, Navajo S4)
`SEP_data_KC_Dec15.xlsx`	Sequential Extraction Procedure data: Captain (SA7) Cormorant Thistle Utah (Entrada S1 & S2, Wingate S3, Navajo S4 & S5)

Table C.1: *File locations for enclosed electronic thesis data.*

Correlation Matrices

D.1   North Sea Batch Experiment Data
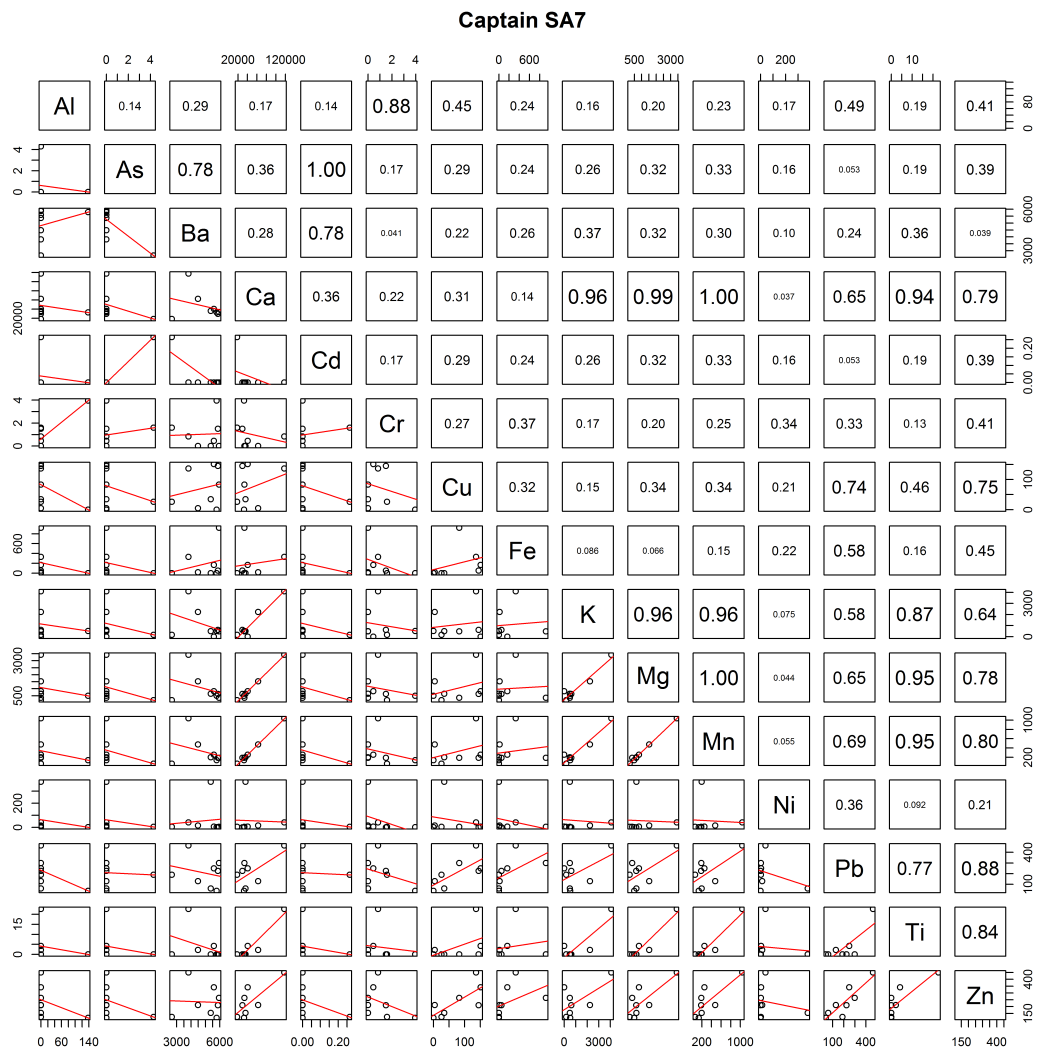
Figure D.1: *Correlation matrix for Captain SA7 elements.*
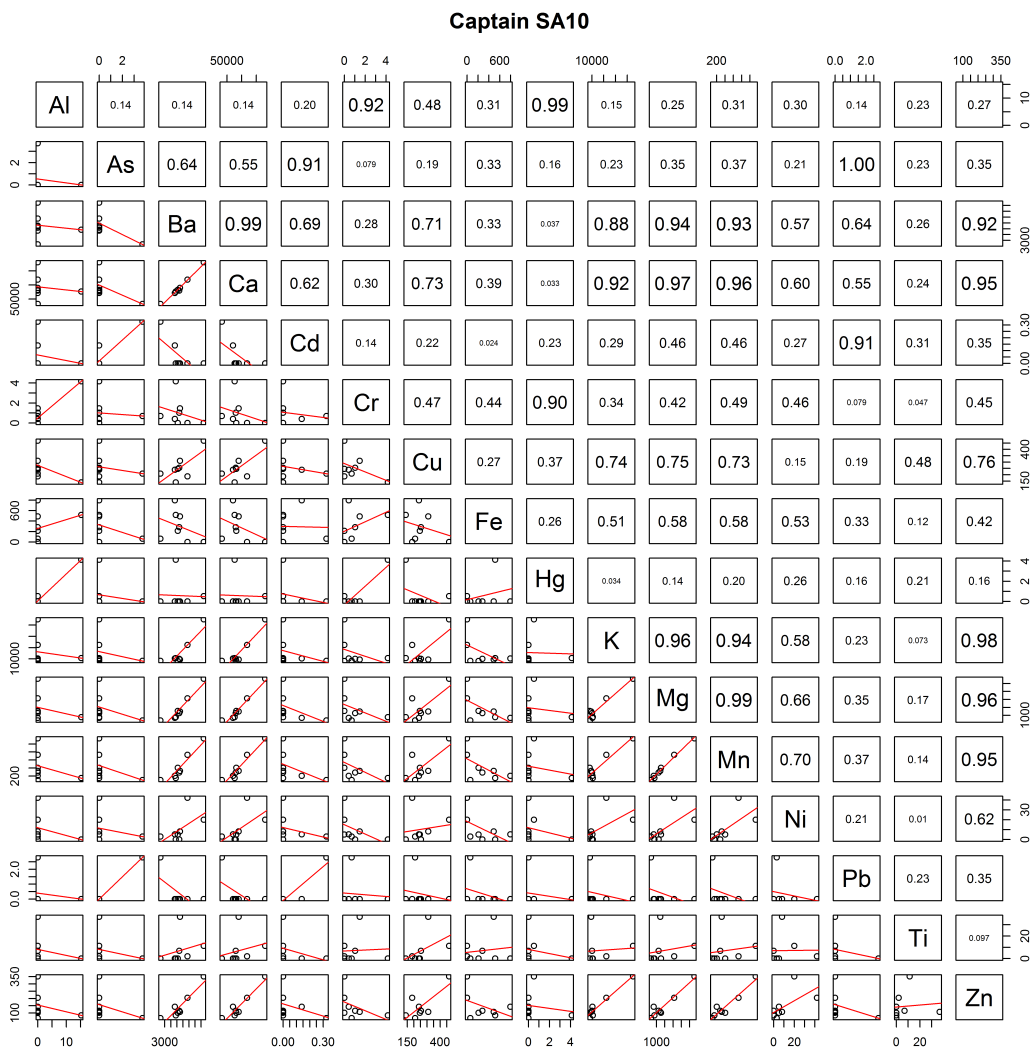
Figure D.2: *Correlation matrix for Captain SA10 elements.*
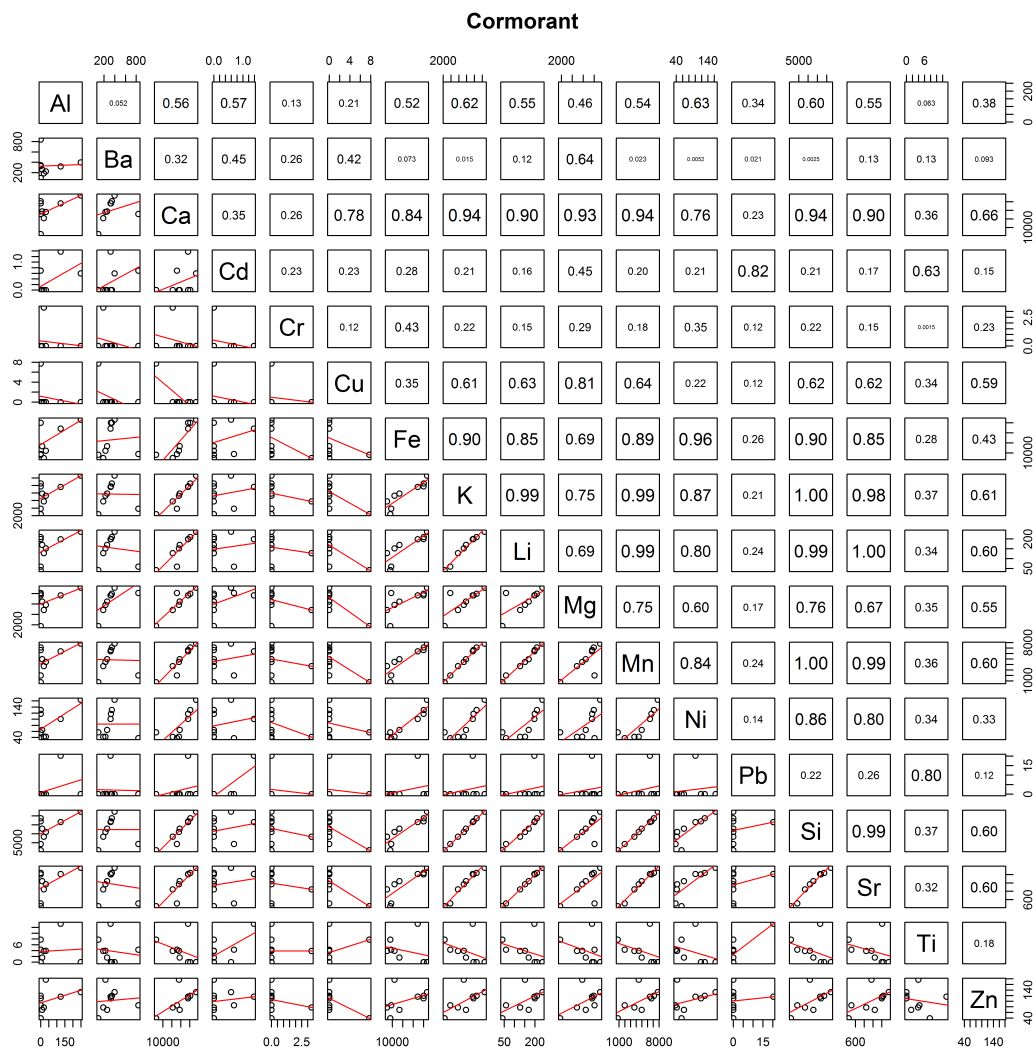
Figure D.3: *Correlation matrix for Cormorant elements.*
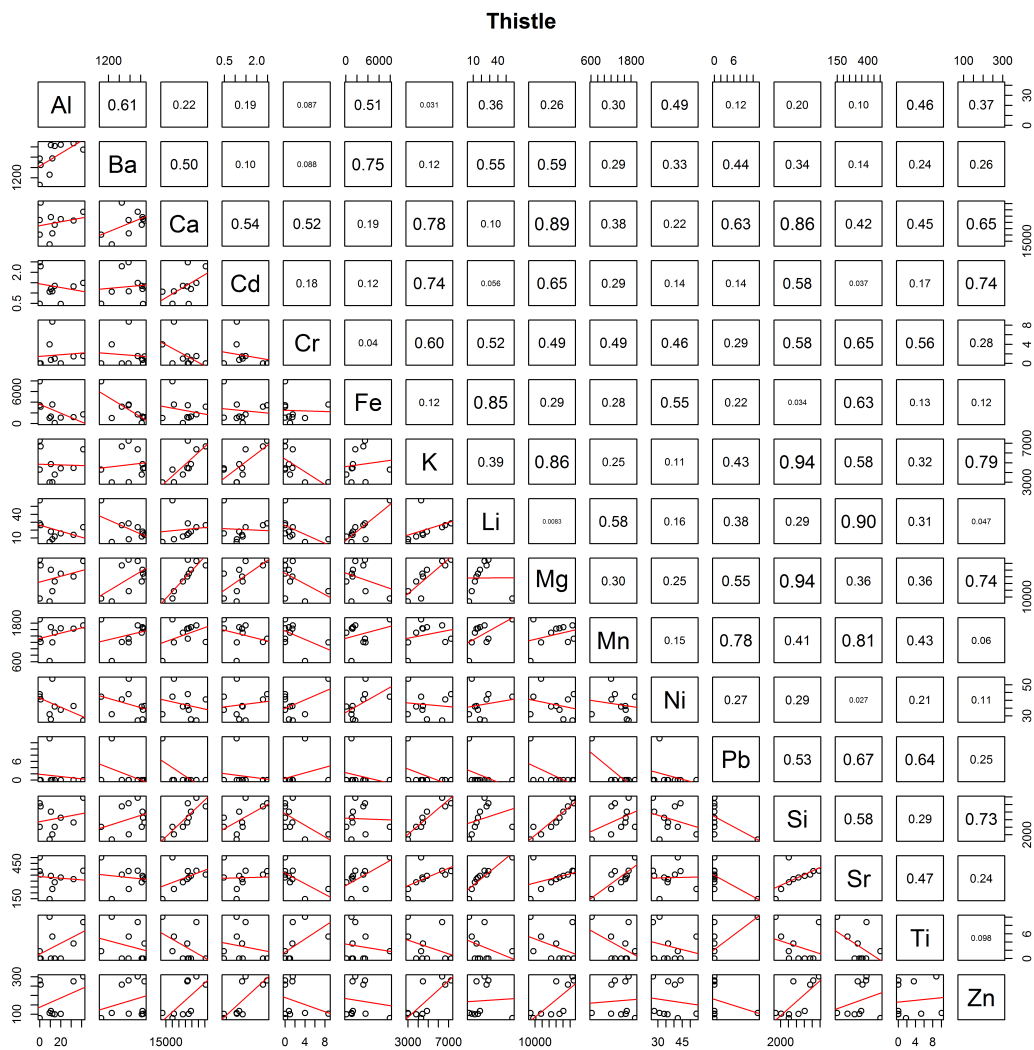
Figure D.4: *Correlation matrix for Thistle elements.*
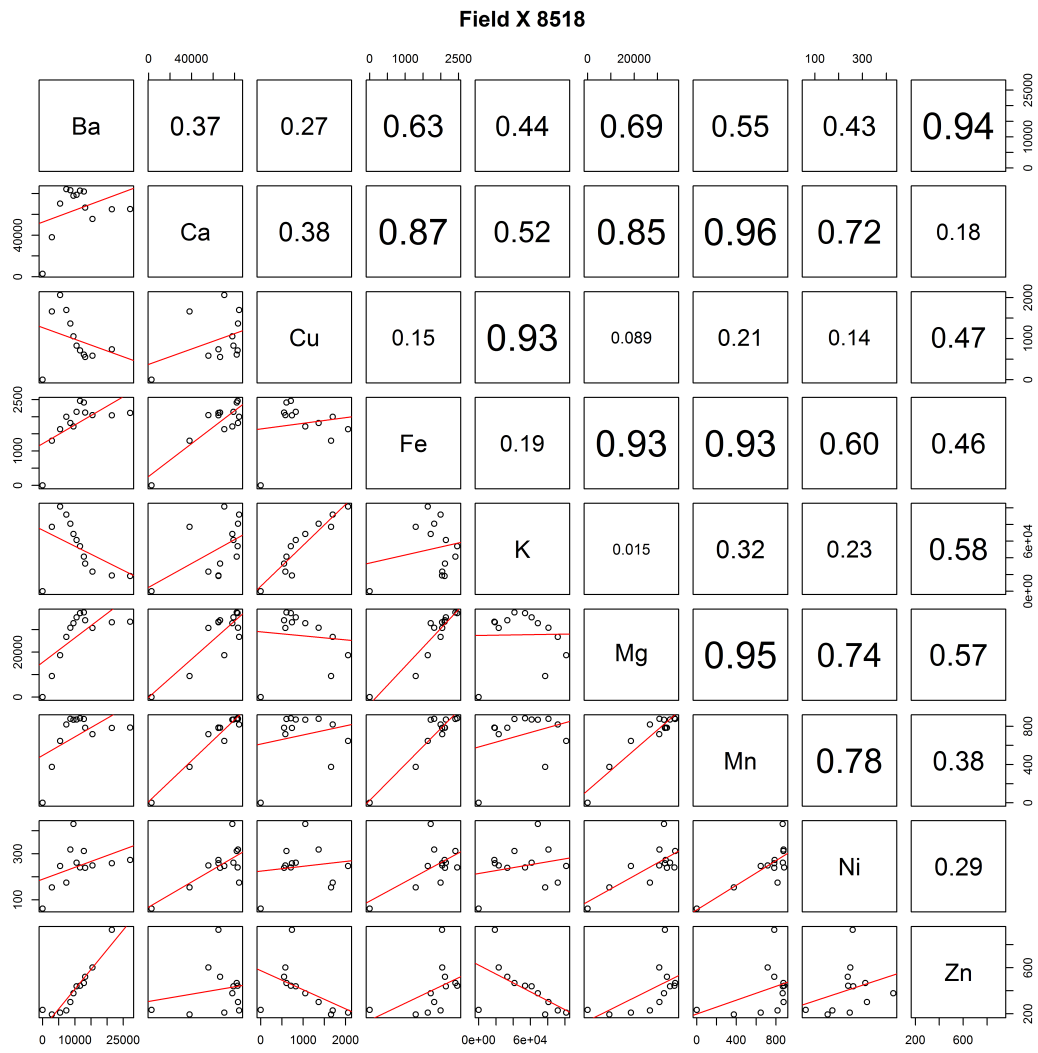
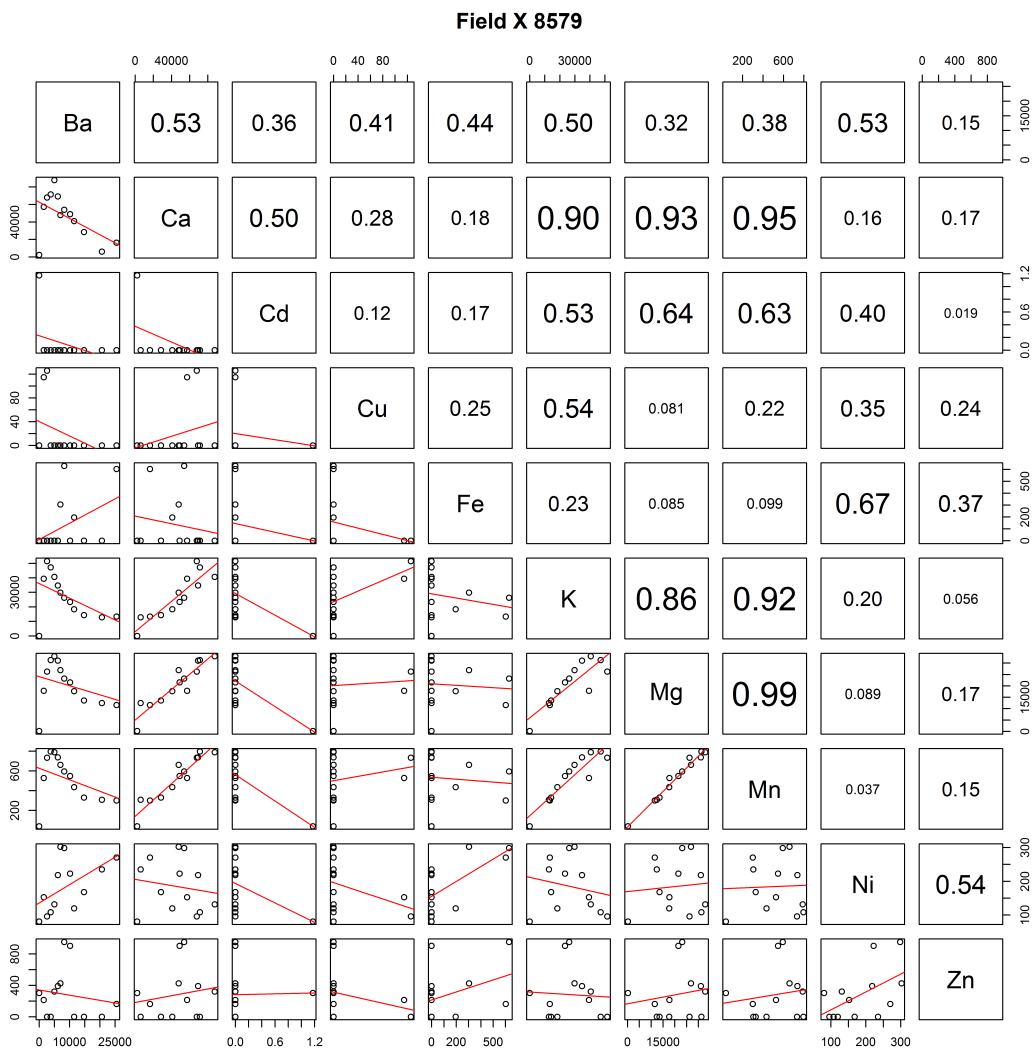**Figure D.5:** *Correlation matrix for Field X 8518 elements.*

Figure D.6: *Correlation matrix for Field X 8579 elements.*

D.2 Utah Field Data

Figure D.7: *Correlation matrix for Green River Springs.*

D.3   Utah Batch Experiment Data
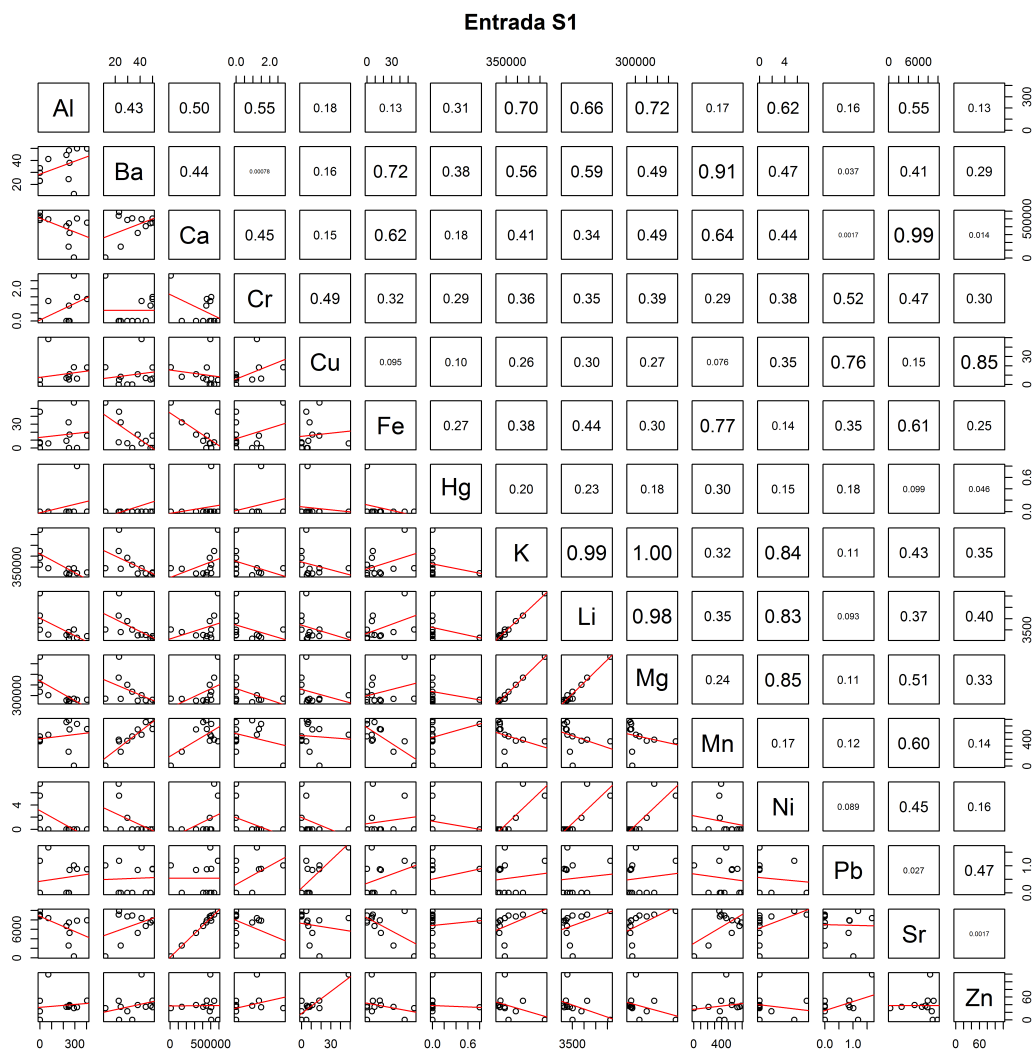
Figure D.8: *Correlation matrix for Entrada S1 elements.*
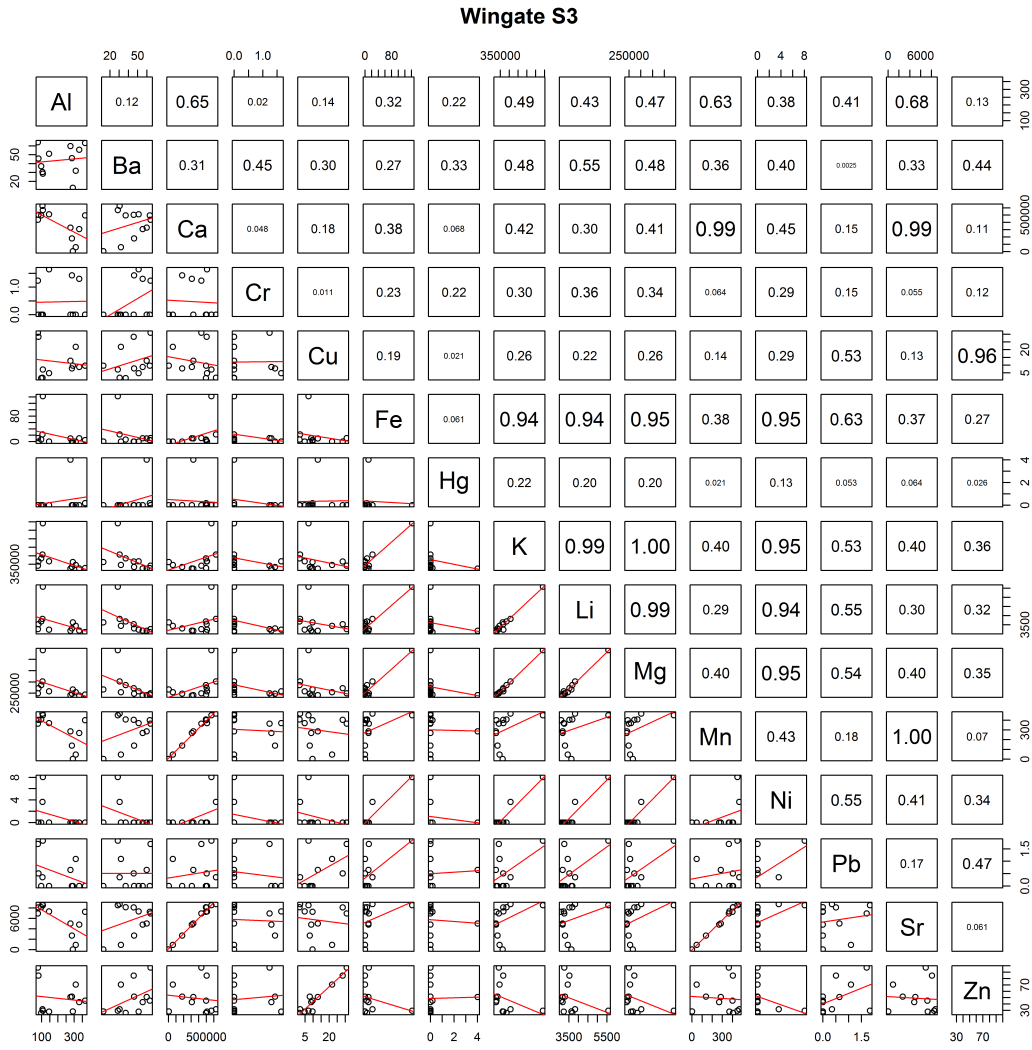
Figure D.9: *Correlation matrix for Entrada S2 elements.*

Figure D.10: *Correlation matrix for Wingate S3 elements.*
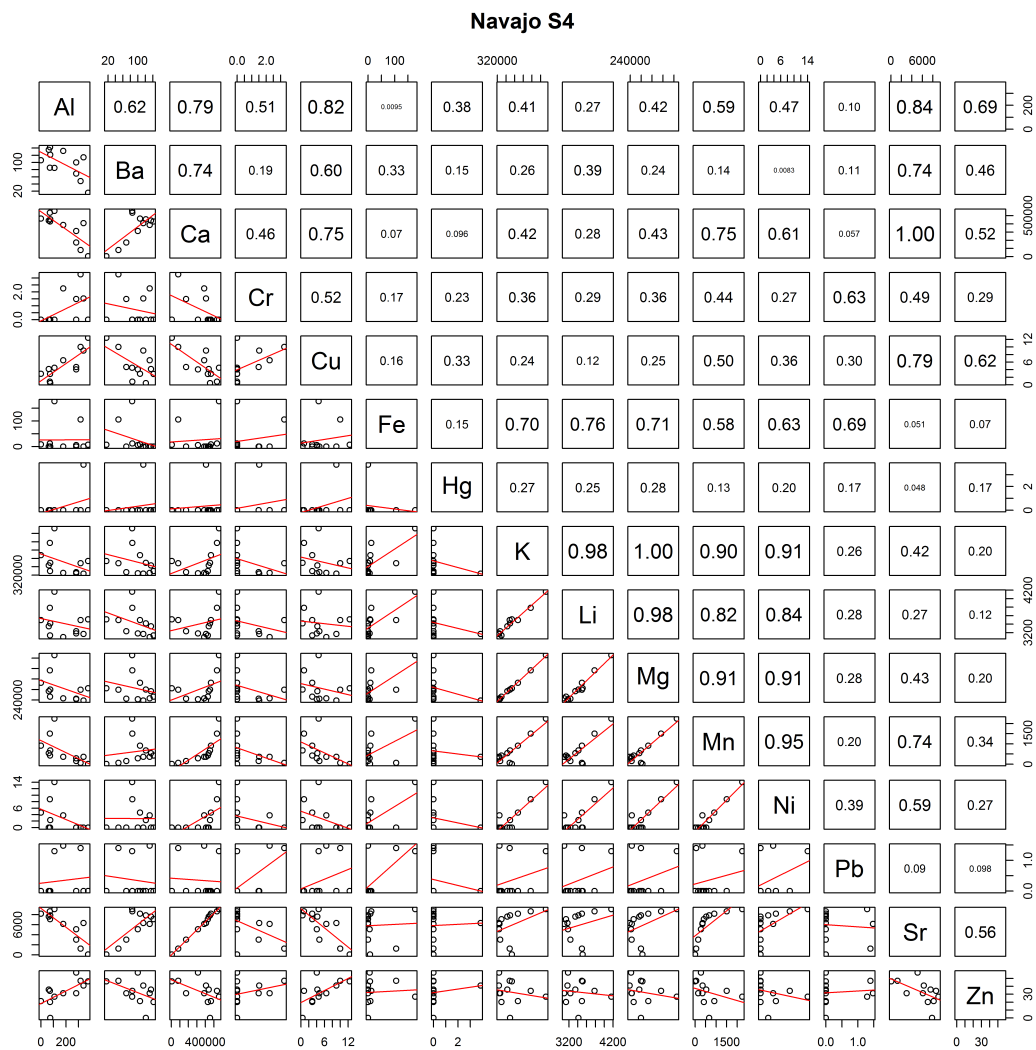
Figure D.11: *Correlation matrix for Navajo S4 elements.*

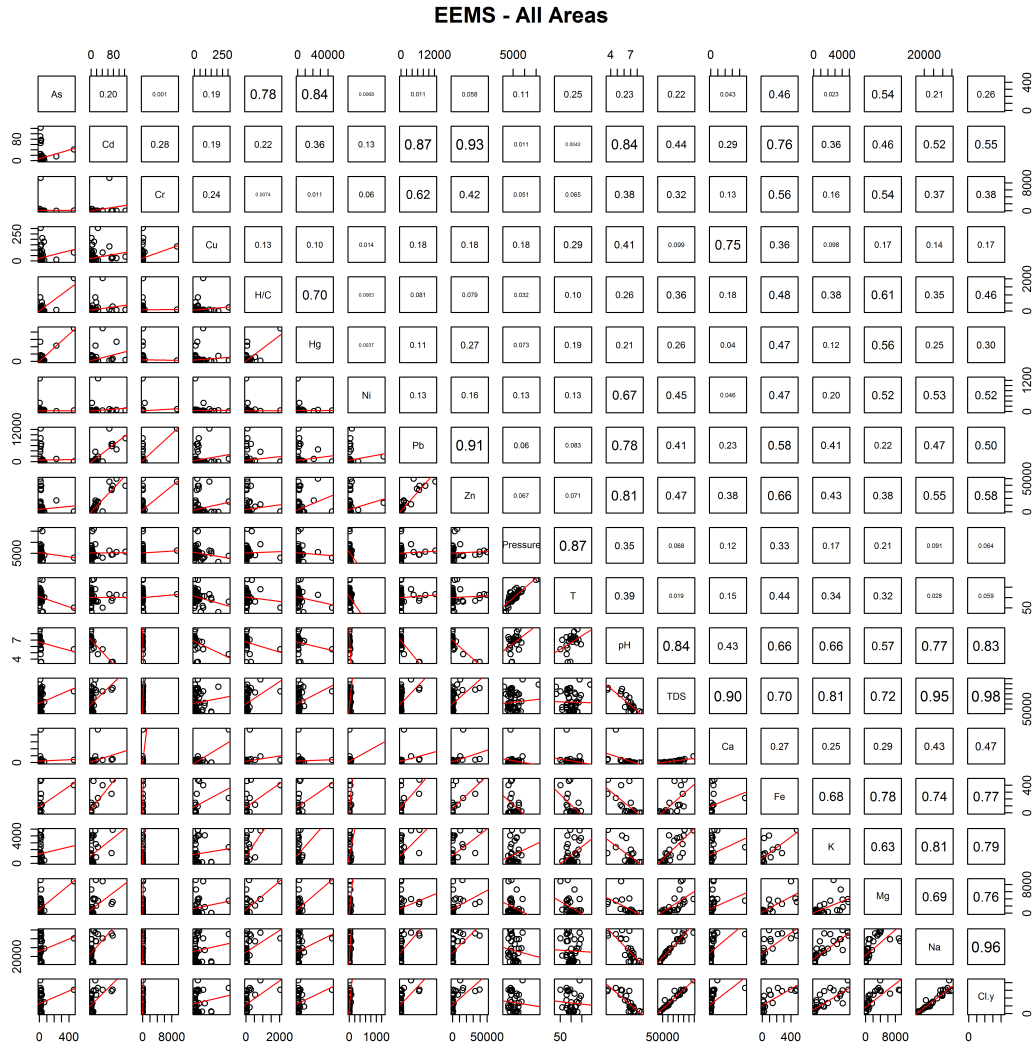## D.4 Emissions and Environmental Monitoring System (EEMS)

Figure D.12: *Correlation matrix for EEMS and North Sea literature data.*